University of Nottingham
UK | CHINA | MALAYSIA

MONASH University

NanoBRET to probe ligand-receptor and receptor-receptor interactions in living cells

Diana C. Alcobia, BSc. M.Sc.

Thesis submitted to the University of Nottingham and Monash University for the degree of Doctor of Philosophy

SEPTEMBER 2018

This thesis is entirely the candidate's own work. The candidate was enrolled in a joint PhD Programme with both University of Nottingham, at the Cell Signalling and Pharmacology Department, in Nottingham, UK, and with Monash University, at the Monash Institute of Pharmaceutical Sciences (MIPS) and the Drug Discovery Biology Department, Melbourne, Australia. The experiments described in this thesis were performed by the author between October 2014 and August 2018. Experiments performed between September 2016 and September 2017 were conducted at Monash University (MIPS). No part of the material has been submitted previously for a degree or any other qualification at any university.

Chapter 6 contains one set of data acquired by Dr. Alexandra Ziegler, a postdoctoral research member from Dr. Erica Sloan's laboratory at Monash University.

Publications arising from this thesis

Papers

- **Alcobia, D.C.**, Kilpatrick, L.E., Peach C. *et al*. (2018) Complex formation between VEGFR2 and two GS protein-coupled receptors. Nature Chem Biol. *(under submission)*
- **Alcobia, D.C.**, Ziegler, A.I., Kondrashov, A. *et al.* (2018) Visualising ligand-binding to a GPCR *in vivo* using nanoBRET. iScience *6,* 280-288
- Peach C., Mignone V.W., Arruda M.A., **Alcobia D.C.** *et al.* (2018) Molecular pharmacology of VEGF-A isoforms: Binding and signalling at VEGFR2. *International Journal of Molecular Science* 19, 2-27
- Kilpatrick, L.E., Friedman-Ohana, R., **Alcobia, D.C.** *et al.* (2017) Real-time analysis of the binding of fluorescent $VEGF_{165}$a to VEGFR2 in living cells: effect of receptor tyrosine kinase inhibitors and fate of internalized agonist-receptor complexes. Biochemical Pharmacology *136*, 62-75

Abstract

Increasing evidence has revealed the role of G protein-coupled receptors (GPCRs) in the regulation of signalling responses via complex cross-talk mechanisms with the receptor tyrosine kinase (RTK) family of transmembrane receptors. Vascular endothelial growth factor-a (VEGFa) mediates cancer angiogenesis via binding to its cognate VEGF receptor 2 (VEGFR2). The two class A GPCRs, adenosine A_{2A} receptors and β_2-adrenoceptors, have also been intimately involved in cancer angiogenesis, and their activation can contribute to cancer progression and invasion. However, the molecular mechanisms involved in the cross-talk between these receptor families are not well understood.

Using a NanoLuc-based bioluminescence resonance energy transfer (NanoBRET) methodology, we reveal a novel mechanism in which VEGFR2 can associate with either of these Gs-coupled GPCRs to form oligomeric complexes in living cells. We also demonstrated that VEGF-stimulated VEGFR2 can induce a switch from a transient to a more stable interaction between β_2AR and the adaptor protein β-arrestin-2, which may have an impact in endosomal signalling.

The pharmacological inhibition of β_2-adrenoceptor (β_2AR) signalling, using selective β_2AR antagonists (or β-blockers), represents a potential therapeutic approach for the treatment of triple-negative breast cancer variant, which has limited treatment options. This study demonstrated the novel application of NanoBRET technology to probe specific β-blocker-β_2-adrenoceptor engagement in a pre-clinical *in vivo* model of triple-negative breast cancer. This novel methodology will allow a strong correlation between drug-target engagement and mediated physiological response.

Acknowledgements

I would like to thank both the University of Nottingham and Monash University for the fantastic opportunity to undertake my PhD with these two excellent institutions, located in opposite sides of the World. It was a really great opportunity to spend one whole year in Australia to learn and perform science with very well-known scientists in the GPCR field, and to explore Australia and New Zealand.

I specially thank my supervisors Professor Stephen J. Hill and the Associate Professor Jeanette Woolard, from the University of Nottingham, for all their amazing support, advice and guidance throughout my PhD. Their help and advice really contributed to my overall success as a PhD student, as well as a person and to my exposure in the scientific society.

I also thank all the postdocs, PhD students, and members of staff from the Cell Signalling and COMPARE departments, at the University of Nottingham, for their friendship and incredible team-work. A special thank you to Dr Laura Kilpatrick, who was deeply involved in this project and contributed to its great success, and for her friendship. Also, to Jackie Glenn for her support and friendship.

I also thank my supervisor Assistant Professor Erica Sloan and all Sloan's lab members, at Monash University, for their support and guidance during my time at the Monash Institute of Pharmacological Sciences (MIPS). A special thank you to the PhD student Aeson Chang, who became a great friend and has given me great support during my time in Australia.

Finally, I want to thank my other half, Tiago, who has been on my side for a long time, and to whom I got secretly married during my time in Australia, and to my parents and sister, who live back home in Portugal, but were always there when I needed them the most.

Abbreviations

2-ME – 2-mercaptoethanol

AR – adenosine receptor (A_1, A_{2A} or A_3)

BRET – Bioluminescence Resonance Energy Transfer

BRET max – maximal BRET signal

BSA – bovine serum albumin

CA200647 (or CAXAC) – adenosine A_3 fluorescent Xanthine Amine Congener (XAC) analog

cDNA – complementary DNA

CGP 12177-TMR - bordifluoropyrromethane-tetramethylrhodamine-(±)CGP 12177

CGP 20712A - 1-[2-((3-Carbamoyl-4-hydroxy)phenoxy)ethylamino]-3- [4-(1-methyl-4-trifluoromethyl-2-imidazolyl)phenoxy]-2- propanolmethanesulfonate

CGP12177 - 4-[3-[(1,1-Dimethylethyl)amino]2-hydroxypropoxy]-1,3- dihydro-2*H* benzimidazol-2-one

D – diffusion coefficient

ddH2O – double-distilled water

DMEM - dulbecco's modified Eagle's medium

DMSO - dimethyl sulphoxide

DPCPX – 8-Cyclopentyl-1,3-dipropylxanthine

DTT – dithiothreitol [(-)-1,4-DITHIO-L-THREITOL]

EC_{50} – concentration at which half the system maximal response occurs

ERK – extracellular-signal-regulated kinase

FCS – fluorescence correlation spectroscopy

GPCR – G protein-coupled Receptor

GRKs – G protein-coupled receptor kinases

HBSS – HEPES or Hanks buffered saline solution

HEK 293T – human Embryonic kidney 293 cells

IC_{50} – concentration to inhibit 50% binding of a ligand

ICI 118551 – (-)-1-[2,3-(Dihydro-7-methyl-1*H*-inden-4-yl)oxy]-3-[(1-methylethyl)amino]-2 butanol

Isoprenaline – 4-[1-Hydroxy-2-[(1-methylethyl)amino]ethyl]-1,2-benzenediol hydrochloride

K_D – dissociation constant, concentration at which half the receptors are occupied

k_{off} - dissociation rate constant

k_{on} - association rate constant

LB – luria-Bertani broth

MDA-231 – MDA-MB-231^{HM} , highly metastatic (HM) or triple-negative human breast cancer cell line

MRS1220 – *N*-[9-Chloro-2-(2-furanyl)[1,2,4]-triazolo[1,5-*c*]quinazolin-5-yl]benzene acetamide

N – particle number

Nb-80-GFP – nanobody-80-tagged with green fluorescent protein (GFP)

Nluc – nanoLuc luciferase

PBS – phosphate buffered saline

PCH – photon counting histogram

PFA – paraformaldehyde

Propranolol-BY630/650 – propranolol-βalanine-βalanine-X-BODIPY-630/650

Propranolol- (*RS*)-1-[(1-methylethyl)amino]-3-(1-napthalenyloxy)-2-propanol

PSB36 – 1-Butyl-8-(hexahydro-2,5-methanopentalen-3a(1*H*)-yl)-3,7-dihydro-3-(3-hydroxypropyl)-1*H*-purine-2,6-dione

RT – residence time

RTK – receptor Tyrosine Kinase

SCH58261 – 2-(2-Furanyl)-7-(2-phenylethyl)-7*H*-pyrazolo[4,3-*e*][1,2,4]triazolo[1,5-*c*]pyrimidin-5-amine

SIM – structured Illumination Microscopy

TAMRA – 5-carboxy-tetramethylrhodamine N-succinimidyl ester

T_D – diffusion time

TMR – tetramethyl-rhodamine

VEGFR2 – vascular endothelial growth factor receptor 2

$VEGF_{165}$a-TMR – vascular endothelial growth factor $_{165}$a with tetramethyl-rhodamine fluorophores at a single cysteine N-terminal residue

βAR – β-adrenergic receptor (β_1AR or β_2AR)

ε – molecular brightness measured as counts per molecule per second ($cpms^{-1}$)

Table of Contents

Abstract III

Acknowledgements IV

Abbreviations V

Chapter 1: General Introduction 1

1.1. G protein-coupled receptors superfamily 1

1.1.1. GPCR activation 3

1.1.2. G-protein dependent signalling 5

1.1.3. GPCR desensitisation, internalisation and endocytosis 7

1.1.4. Role of GRKs and β-arrestins in GPCR trafficking and mitogenic signalling 10

1.2. β_2-adrenoceptors 12

1.2.1. β_2-adrenoceptors structure 12

1.2.2. β_2-adrenoceptors signalling and trafficking 13

1.2.3. β_2-adrenoceptor oligomerisation 15

1.2.4. β_2-adrenoceptors in angiogenesis and tumour development 16

1.3. Adenosine receptors 18

1.3.1. Adenosine receptors structure 18

1.3.2. Adenosine receptors signalling and trafficking 19

1.3.3. Adenosine 20

1.3.4. Adenosine receptors oligomerisation 23

1.3.5. Adenosine A_{2A} receptor in angiogenesis and tumour development 23

1.4. Receptor Tyrosine kinase superfamily 25

1.4.1. RTK classic activation model 25

1.4.2. RTK trafficking 26

1.5. VEGFR family 28

1.5.1. VEGFR2 activation 28

1.5.2. VEGFa isoforms family 29

1.5.3. VEGFR2 canonical signalling 30

1.5.4. VEGFR2 trafficking and endocytic signalling 34

1.6. GPCR-RTK crosstalk 35

1.6.1. Transactivation mechanisms 36

1.6.2. Bidirectional cross-talk 40

1.7. NanoBRET to probe ligand-receptor and receptor-receptor interactions 42

1.7.1. NanoBRET to investigate ligand-receptor binding pharmacology 42

1.7.2. BRET to investigate GPCR-RTK oligomerisation 43

1.8. Thesis Aims 45

Chapter 2: Materials and Methods 46

2.1. Materials 46

2.2. Molecular biology 47

2.3. Cell culture 61
2.3.1. Generation of new stable or transient cell lines 62
2.4. Fluorescence Correlation Spectroscopy (FCS) 64
2.4.1. Calibration 66
2.4.2. Solution-based experiments using $VEGF_{165}$a-TMR and TAMRA fluorescent ligands 68
2.4.3. Solution-based experiments using $VEGF_{165}$a-TMR ligand treated with the reducing agents 2-mercaptoethanol (2-ME) or dithiothreitol (DTT) 69
2.4.4. FCS Data Analysis 70
2.5. NanoBRET-based *in vitro* assays 73
2.5.1. Saturation and competition binding assays to investigate ligand-receptor interaction under equilibrium conditions 73
2.5.2. Kinetic binding assay to investigate ligand-receptor interaction under non-equilibrium conditions 79
2.5.3. Saturation binding assay to investigate receptor-receptor interactions 80
2.5.4. Investigation of the effects of subtype selective ligands on heterodimer complex formation 83
2.5.5. Investigation of potential cooperativity across putative (GPCR-VEGFR2) heterodimer interface 84
2.5.6. β-arrestin-2 recruitment assay 85
2.5.7. Nanobody-80 recruitment assays 88
2.5.8. NanoBRET-based *in vitro* assays data analysis 90
2.6. Cell imaging 93
2.6.1. Confocal imaging using Zeiss 710 93
2.6.2. Confocal imaging using a plate reader ULTRA ImageXpress 93
2.6.3. Confocal imaging using Leica SP8 94
2.6.4. Wide-field luminescence imaging 94
2.6.5. Super-resolution Structured illumination microscopy 95
2.7. Breast cancer animal model 97
2.7.1 Bioluminescence *in vivo* imaging to track tumour growth and metastasis 98
2.7.2 NanoBRET to investigate ligand-receptor target engagement *in vivo* 99
2.7.3. In vivo NanoBRET imaging data analysis 101
Chapter 3: Characterisation of a fluorescently labelled $VEGF_{165}$a ligand in solution using Fluorescence Correlation Spectroscopy 103
3.1. Introduction 103
3.2. Brief materials and methods 104
3.3. Results 107
3.4. Discussion and Conclusion 120
Chapter 4: Characterisation of two different class A GPCRs and VEGFR2 at the level of ligand binding using NanoBRET 123
4.1. Introduction 123
4.2. Brief materials and methods 126

4.3. Results 128
4.4. Discussion and Conclusion 149
Chapter 5: NanoBRET to investigate *in vitro* receptor-receptor interactions and the functional properties of β_2AR-VEGFR2 oligomeric complex in HEK 293T cells. 153
5.1. Introduction 153
5.2. Brief materials and methods 155
5.3. Results 159
5.3. Discussion and Conclusion 178
Chapter 6: Visualising ligand-binding to β_2-adrenergic receptor *in vivo* using NanoBRET 181
6.1. Introduction 181
6.2. Brief materials and methods 183
6.3. Results 185
6.4. Discussion and Conclusion 197
Chapter 7: General Discussion 200
References 206

Chapter 1: General Introduction

G protein-coupled receptors (GPCRs) and receptor tyrosine kinases (RTKs) are the major superfamilies of transmembrane receptors present in eukaryotic cells (Cattaneo et al., 2014). Two decades ago, these two different transmembrane receptor families were thought to function in a separate and independent manner (Liebmann and Böhmer, 2000). Nowadays, we know that complex cross-communication mechanisms can occur between these receptor families that contribute to both physiological and pathological conditions (Delcourt et al., 2007; Köse, 2017; Pyne and Pyne, 2011). Vascular endothelial growth factor receptor 2 (VEGFR2), a member of the RTK family, is the major mediator of VEGF-driven responses in endothelial cells, including permeability changes, proliferation, migration and angiogenesis. The latter is a process involved the formation of new blood vessels from pre-existing vasculature (Simons et al., 2016). Vascular endothelial growth factor (VEGF) and its cognate receptor (VEGFR2) are key players in tumour-induced angiogenesis and tumour cell invasion and are therefore widely targeted in cancer therapy (Niu and Chen, 2010). Increasing evidence has suggested a role for adenosine receptors and β_2-adrenoceptors, two Class A GPCR members, in promoting angiogenesis via the release of VEGF in response to local hypoxia and neoplasia (Hill et al., 2014; Ryzhov et al., 2014). However, there is a lack of understanding regarding the molecular mechanisms by which signalling from VEGFR2 and these two Class A GPCRs may cross-talk. This chapter will introduce the GPCR and RTK families, with a focus on the two class A GPCRs, adenosine A_{2A} receptor and β_2-adrenoceptors, as well as on the class IV RTK, VEGFR2. Recent advances on RTK-GPCR oligomerisation will be also presented.

1.1. G protein-coupled receptors superfamily

G protein-coupled receptors (GPCR) comprise the largest family of transmembrane receptors and are the most diverse group of membrane-binding proteins present in eukaryotic organisms (Lefkowitz, 2007). GPCRs

respond to a wide range of stimuli including odorants, ions, photons, small neurotransmitters, large peptides and hormones. Thus, this receptor superfamily is involved in many different diseases, such as neurological, cardiovascular, immunological and infectious diseases (Calebiro and Godbole, 2018; Capote et al., 2015; Magalhaes et al., 2012).

GPCRs are encoded by more than 800 genes in the human genome (Klaasse et al., 2008), and nearly a third of the pharmaceuticals available on the market have been developed to target members of this family of receptors (Kimple et al., 2011). All GPCRs share the same typical structural motifs of seven membrane-spanning α-helices, and for this reason can be also described as seven-transmembrane (7-TM) domain receptors (Alexander et al., 2017) (Figure 1.1). According to the International Union of Basic and Clinical Pharmacology (IUPHAR), and on the basis of sequence homology, GPCRs have been divided into three different classes. Class A GPCR (or rhodopsin-like family) is the largest family of GPCRs, containing approximately 700 receptors, including the rhodopsin, adenosine and adrenergic receptors (Franco et al., 2016). Class B (or secretin family) have a large globular N-terminal domain and extracellular loops which are essential for their activation. Examples of GPCRs belonging to this family are the corticotropin-releasing factor (CRF) and glucagon-related peptide I (GLP-I) (Miller et al., 2014). The Class C family is characterised by a large N-terminal extracellular orthosteric ligand binding domain, that resembles a Venus flytrap. Members of the family C include the metabotropic glutamate (mGlu), γ-aminobutyric acid B ($GABA_B$) and Ca^{2+}-sensing receptors (Wu et al., 2014). This family of GPCRs form obligate dimers to function (Gurevich and Gurevich, 2008).

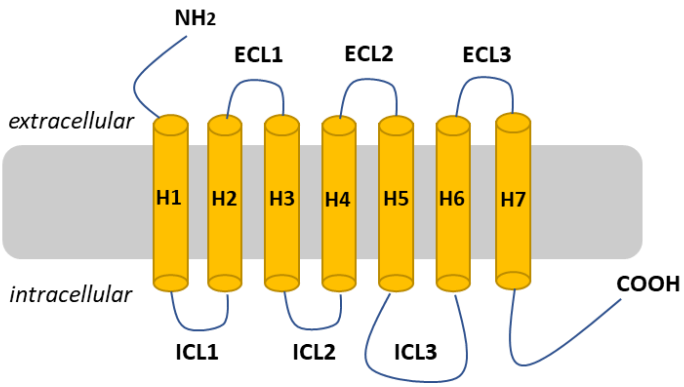

Figure 1.1. Generic representation of 7-transmembrane receptors (7-TMR) structure. The different receptor domains (α-helixes 1-7 also nominated as transmembrane domains (TM) 1-7) are connected via 3 extracellular (ECL) and 3 intracellular (ICL) loops. The C-terminus is the docking site for accessory proteins, containing phosphorylation and palmitoylation sites that are relevant for the regulation of receptor desensitisation and internalisation (Klaasse et al., 2008). The third intracellular loop (ICL3) and the C-terminus are involved in G-protein coupling, G protein-coupled receptor kinases (GRKs) and binding of β-arrestins (Reiter and Lefkowitz, 2006). Recent evidence revealed that β-arrestins can adopt two different conformations, a 'tail' or a 'tail and core' conformations. These studies suggested that β-arrestins can interact with the GPCR only at the C-terminus ('tail' conformation) or interact simultaneously with the C-terminus and intracellular domains of the receptor ('tail and core' conformation), which seem to regulate downstream signalling (Eichel et al., 2018; Ranjan et al., 2017; Thomsen et al., 2016).

1.1.1. GPCR activation

GPCRs do not have intrinsic activity like other transmembrane receptors, such as receptor tyrosine kinases, they require intracellular partners that serve as canonical transducer proteins, the heterotrimeric G-protein family. Based on structural studies, the mode of GPCR activation occurs by the following steps (Figure 1.2.): (1) agonist ligand binds to the receptor inducing conformational changes in critical domains of the 7-transmembrane helix pocket; (2) these changes induce additional conformational changes in the intracellular domains of the receptor, and consequent activation via receptor interaction with heterotrimeric guanine nucleotide binding G-proteins; (3) receptor activation promotes nucleotide GDP to GTP exchange within the Gα-subunit which leads

to the dissociation of the heterotrimeric complex, where both the GTP-bound Gα-subunit and the βγ complex are released (Bologna et al., 2017; George et al., 2016; Kimple et al., 2011; Weis and Kobilka, 2018) Both GTP-Gα and Gβγ are then able to activate different effectors and 'second' messengers to promote downstream signalling physiological responses (George et al., 2016; Khan et al., 2013). Recent evidence showed that GPCRs can also be activated in the absence of ligands, where G-proteins can form non-functional interactions with receptors which become 'primed' for activation (Gupte et al., 2017; Wootten et al., 2018). Substantial evidence has shown that different ligands can induce distinct receptor conformations, and that these conformations can lead to specific signals to promote different subset of signalling events, also known as biased signalling (Bologna et al., 2017; Lane et al., 2017; Wootten et al., 2018). Biased ligands are now being explored as potential therapeutics to target GPCRs (Rominger et al., 2014).

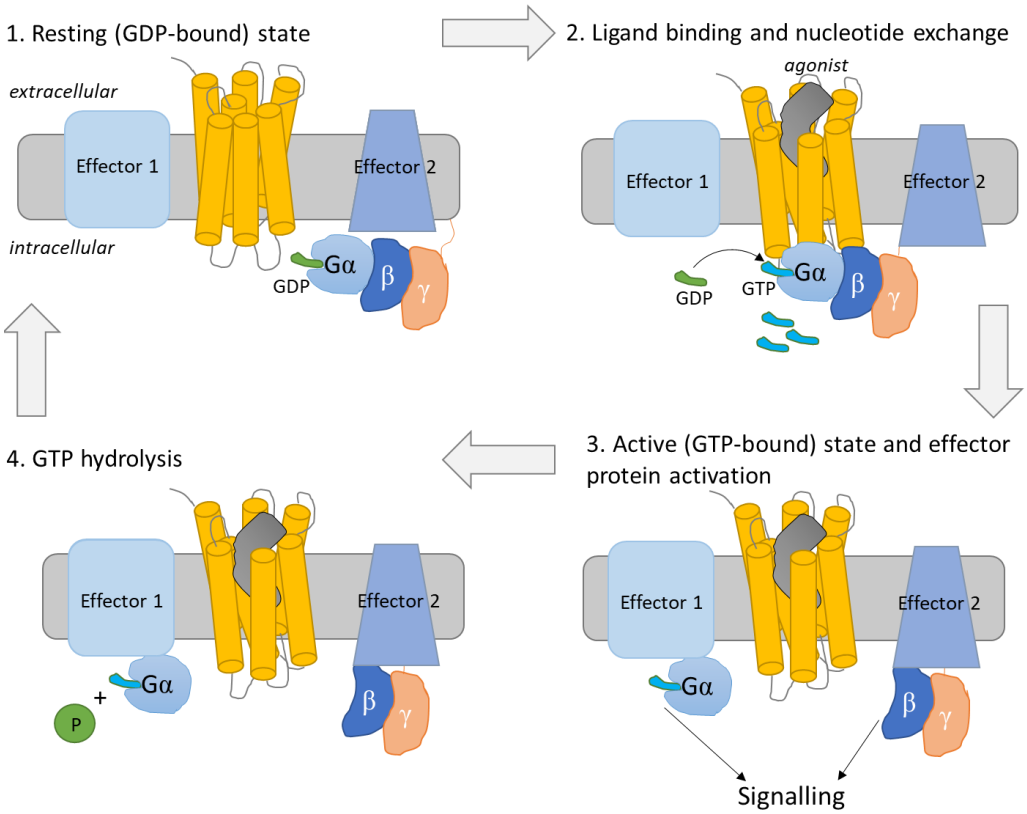

Figure 1.2. Heterotrimeric G protein cycle. In the 'resting' state G proteins exist as an attached αβγ trimer complex. Upon ligand-binding (agonist) to the G protein-coupled receptor, a

nucleotide exchange occurs with a release of guanosine-diphosphate (GDP) and binding of guanosine-triphosphate (GTP) to the Gα-subunit. A conformational change results in the dissociation of the GTP-bound α-subunit from the Gβγ subunits, and a consequent activation of the G protein. Gα subunit then binds and stimulates different enzyme cascades, via activation of different protein effectors (Effector 1). Other enzymes can also interact with the βγ subunits, such as β-arrestins, to further modulate the signal (Effector 2). The hydrolysis of GTP to GDP, via intrinsic guanosine triphosphatase (GTPase) activity of Gα subunit, leads to the re-association of the Gαβγ trimer complex and the signalling is then terminated (Kimple et al., 2011; Magalhaes et al., 2012).

1.1.2. G-protein dependent signalling

The canonical GPCR signalling is initiated by activation of the heterotrimeric G-protein family (Bologna et al., 2017; Halls et al., 2005). GPCRs regulate a wide variety of cellular processes by coupling to different G proteins (Alexander et al., 2017; Milligan and Kostenis, 2006). The heteromeric G-protein family is formed by 3 subunits: Gα, Gβ and Gγ subunits. 16Gα, 5Gβ and 13Gγ subunits have been identified so far (Wootten et al., 2018), which can be present in a variety of combinations of heterotrimeric complexes to promote different functions in different cell types. The Gα subunit is divided into 4 sub-families based on gene sequence homology ($G\alpha_s$/$G\alpha_{olf}$, $G\alpha_{i1/2/3/o}$, $G\alpha_{q/11/14/15}$ and $G_{12/13}$) which are conserved in the animal kingdom (Milligan and Kostenis, 2006). A brief description of the role of Gα and Gβγ subunits is provided in Table 1.1. Gαs and Gαi proteins activate or inactivate adenylate cyclase (AC), respectively, and stimulation or inhibition of intracellular cyclic adenosine monophosphate (cAMP) production. cAMP is a central second messenger that regulates multiple downstream responses, including mitogenic signalling (Borland et al., 2009). Gαq proteins can activate different PLC isoforms that regulate intracellular calcium stores (Luttrell, 2006). $G\alpha_{12/13}$ proteins can induce signalling that promote changes in the cytoskeleton (McCudden et al., 2005). Gβγ subunits can also interact with intracellular or membrane effectors to regulate downstream signalling upon their release from Gα-subunit. This

dimeric complex can promote activation of multiple kinase enzymes (including, PI3K, c-Src, JNK and ERK) and ion channels (Khan et al., 2013).

Table 1.1. The role of Gα and Gβγ subunits in cellular activity.

Type	Activity	References
Gαs	Stimulate adenylate cyclase (AC) pathway, cAMP production and PKA activation. PKA activation can lead to EPAC/ERK signalling.	(Hildebrandt, 1983; Borland et al., 2009; Fredholm et al., 2011)
Gαi	Inhibit AC pathways and cAMP production.	(Hildebrandt, 1983; Fredholm et al., 2011; Khan et al., 2013)
Gαq	Regulate phospholipase Cβ (PLCβ) activity and intracellular calcium release	(Hildebrandt, 1983; McCudden et al., 2005; Luttrell, 2006)
Gα12/13	Regulate cell processes by activation of RhoGEFs/Rho signalling	(Hildebrandt, 1983; Hamm, 1998; Luttrell, 2006)
Gβγ	Regulates PLC-β_2, PLC-β_3, AC, c-Src and phosphoinositide-3-kinase-γ (PI3K-γ) activity. Acts as a guanine nucleotide dissociation inhibitor (GDI), inhibiting the release of GDP from Gα subunit. Regulates ion channels. GRK/β-arrestin recruitment MAPK cascade, JNK and p38 MAPK activation	(McCudden et al., 2005; Luttrell, 2006; Smrcka, 2008; Khan et al., 2013)

Abbreviations: Gαi - pertussis toxin sensitive G-protein, Gαs - pertussis toxin insensitive G-protein, AC - adenylate cyclase, cAMP - cyclic adenosine monophosphate; EPAC – exchange protein directly activated by cAMP; extracellular signal-regulated kinase 1/2; PLC – phospholipase; RhoGEF - Rho guanine nucleotide exchange factor; cSrc – non-receptor tyrosine kinase; GRK – GPCR kinase; MAPK – mitogen-activated protein kinases; JNK – c-Jun N-terminal kinase.

1.1.3. GPCR desensitisation, internalisation and endocytosis

GPCR desensitisation and internalisation can be mediated by three families of regulatory proteins: G protein-coupled receptor kinases (GRKs), arrestins, and second-messenger-dependent protein kinases (Smith and Rajagopal, 2016).

β-arrestins belong to the arrestin family which is composed of four members, arrestin 1, 2, 3 and 4 (Luttrell and Lefkowitz, 2002) . β-arrestin-1 and -2 (also denominated as arrestin-2 and -3, respectively) have been identified due to their sequence homology with the visual arrestin (arrestin-1) (Attramadal et al., 1992). The name arrestin has derived from the ability of arrestin-1 to 'arrest' rhodopsin signalling in the retina (Shenoy and Lefkowitz, 2003). β-arrestin-1 and -2 share 78% sequence homology and can be expressed ubiquitously in different tissues (Attramadal et al., 1992). β-arrestins were first identified for their ability to desensitise agonist-induced β_2-adrenoceptors signalling (Lohse et al., 1990). GPCR desensitisation can occur after a prolonged or repeated exposure of ligand, leading to signalling termination (Luttrell and Lefkowitz, 2002; Shenoy and Lefkowitz, 2003). Nowadays, it is known that these proteins not only promote receptor desensitisation but are also key players in intracellular signalling promoted from different intracellular compartments (Calebiro and Godbole, 2018). Intracellular signalling has been subject of intensive investigation (Calebiro and Godbole, 2018; Eichel and von Zastrow, 2018; Ellisdon and Halls, 2016) .

Classical GPCR internalisation (by homologous desensitisation) is mediated after ligand-induced activation of GPCR leading to the dissociation of α and βγ subunits, and βγ-subunit-induced recruitment of GRKs to the agonist-occupied receptor (Figure 1.3.) (Magalhaes et al., 2012). The GRK family is composed by 7 members (GRK 1-7) (Ribas et al., 2007). These kinases phosphorylate key serine threonine residues located in the third intracellular loop and/or C-terminus of the GPCR receptor that promote rapid recruitment of β-arrestins to the phosphorylated receptor (Kelly et al., 2008; Klaasse et al., 2008; Komolov and Benovic, 2018). β-arrestin can then promote receptor desensitisation (by

sterically hindering further G protein coupling to the receptor, resulting in downregulation of G-protein-mediated signalling) and internalisation of the receptor via clathrin-dependent or -independent mechanisms (Doherty and McMahon, 2009; Eichel et al., 2018). Most GPCRs undergo clathrin-mediated internalisation, where GPCRs are recruited to clathrin coated pits (CCPs) by interacting with key proteins including, clathrin heavy chain and clathrin adapter protein (AP2) (Calebiro and Godbole, 2018; Laporte et al., 1999). These are then detached from the plasma membrane in a process involving the small GTPase dynamin (Doherty and McMahon, 2009). After internalisation, and depending on the receptor and cell type, receptors can undergo endocytosis to endosomes that express the small GTPase rab5 protein (rab5-positive endosomes or early endosomes). From there, GPCRs can either be targeted for degradation in lysosomes, or undergo fast or slow recycling to the plasma membrane (Eichel and von Zastrow, 2018; Sorkin and Von Zastrow, 2009).

GPCRs have been broadly divided into 'Class A' or 'Class B' receptors (Figure 1.3.), according to their transient or more stable interaction with β-arrestins, respectively (Smith and Rajagopal, 2016). 'Class A' GPCRs, such as β_2-adrenoceptors, engage with β-arrestin in a transient complex, resulting in rapid dissociation and fast recycling to the plasma. On the other hand, 'Class B' GPCRs, such as vasopressin type 2 receptor (V_2R) form stable interactions with β-arrestin inducing sustained internalisation into late endosomes (rab7-positive), which then can either be slowly recycled back to the plasma membrane or undergo degradation in lysosomes (Shenoy and Lefkowitz, 2003; Smith and Rajagopal, 2016). Recent studies using FlAsh-based β-arrestin 2 sensors demonstrated distinct conformational signatures that seem to be related to the higher (Class B) or lower (Class A) affinity for β-arrestin (Lee et al., 2016; Nuber et al., 2016).

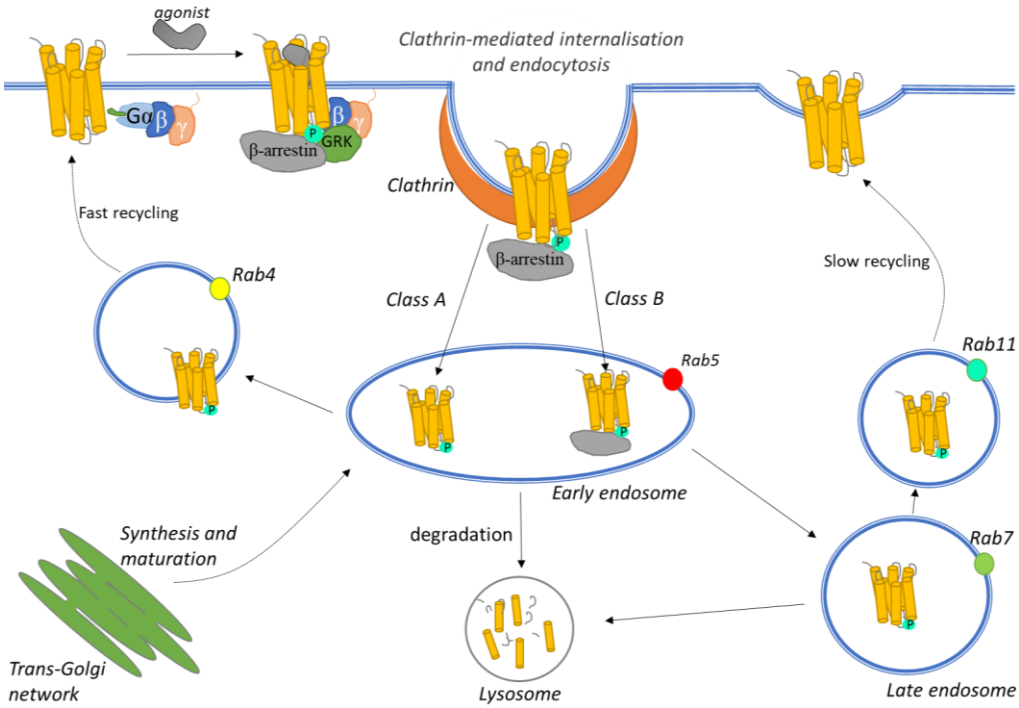

Figure 1.3. Homologous model of GPCR desensitisation, internalisation and recycling or degradation. GPCR regulation is described by a mechanism in which an agonist-activated receptor gets phosphorylated at key serine and/or threonine residues from the intracellular C-terminal domain and/or intracellular loop 3 (IL3), by members of the G protein-coupled receptor kinases (GRKs) (Ribas et al., 2007). Once the GPCR is phosphorylated, β-arrestin protein is rapidly recruited to the phosphorylated receptor localised at the plasma membrane, leading to receptor desentisation. β-arrestin may also interact with the heavy chain of clathrin, with β_2-adaptin subunit of the clathrin adaptor protein AP-2, and with phosphoinositides, which direct the phosphorylated GPCR to punctate clathrin-coated pits (orange). GPCRs are internalised with the contribution of GTPase dynamin, a protein that constrains the neck of the clathrin-coated vesicle, forming a spiral around it, and breaks its association to the cell surface, leading to GPCR sequestration into the intracellular space (Ferreira et al., 2012). Class A receptors, such as β_2-adrenoreceptors (β_2AR), recruit β-arrestin 2, which promote receptor traffic to clathrin-coated pits. The receptor is then directed to rab5-positive endosomes (early endosomes) and rapidly recycled back to the plasma membrane (in rab4-positive endosomes) (Sorkin and Von Zastrow, 2009). Class B receptors, such as angiotensin type 1A receptor ($AT_{1A}R$) recruit both β-arrestin 1 and 2 (Magalhaes et al., 2012). These receptors internalise with the β-arrestin forming a stable complex with it in early endosomes, which can then move to later endosomes (rab7-positive) and be slowly recycled to the plasma membrane (Cahill et al., 2017; Eichel et al., 2018). Receptors may also be targeted to lysosomes for degradation (Magalhaes et al., 2012). Receptors are synthesised in the Trans-Golgi network (TGN) and maturation can

occur in early endosomes before receptors are made available at the plasma membrane (Sorkin and Von Zastrow, 2009).

1.1.4. Role of GRKs and β-arrestins in GPCR trafficking and mitogenic signalling

GRKs and β-arrestins function is not limited to GPCR desensitisation and internalisation (Calebiro and Godbole, 2018). Intensive investigation showed evidence for the role of β-arrestins as important scaffold molecules to promote GPCR spatial-temporal regulated signalling from different cellular compartments, including plasma membrane (PM) and intracellular membrane compartments, such as endosomes and Golgi apparatus (Calebiro and Godbole, 2018; Eichel and von Zastrow, 2018; Halls et al., 2016; Irannejad et al., 2013). β-arrestins work as 'rheostats' to regulate GPCR trafficking, endocytosis, recycling and intracellular signalling (Gutkind and Kostenis, 2018).

The first evidence of β-arrestin interaction with signalling proteins was in 1999 by Lefkowitz group (Luttrell et al., 1999), who found that β-arrestin interacts with the proto-oncogene Src (c-Src). β-arrestin-targeted c-Src is then recruited to agonist-occupied receptor, ultimately leading to the activation of extracellular signal-regulated kinase (ERK1/2) (Luttrell et al., 1999). β-arrestins also scaffold multiple kinases of other MAP kinase pathways, including c-Jun amino-terminal kinase (JNK), p38-MAPK, raf, MEK-1, as well as Akt, which play essential roles in cell proliferation, survival and migration (Kumari et al., 2016; Li et al., 2014; Luttrell et al., 2001; Nuber et al., 2016).

Recent structural and functional studies showed that β-arrestin-GPCR complex can activate different pools of downstream signalling depending on their location within the cell, and depending on the duration and/or stability of their interaction (Calebiro and Godbole, 2018; Ellisdon and Halls, 2016; Ranjan et al., 2017). Five different patterns of internalisation-dependent signalling activation have been described so far:

(1) For 'Class A' GPCRs (i.e. β2-adrenoceptors) β-arrestin interacts as a transient complex with the activated GPCR at the plasma membrane, inducing receptor internalisation and rapid ERK1/2 signalling activation from early endosomes (Eichel et al., 2016; Ranjan et al., 2016).

(2) In contrast to 'Class A', 'Class B' GPCRs (i.e. $AT_{1A}R$) form a stable complex with β-arrestins to undergo sustained endocytosis leading to a sustained ERK1/2 signalling from different intracellular compartments (Calebiro et al., 2013; Irannejad et al., 2013; Laporte et al., 1999; Thomsen et al., 2016).

(3) A novel mechanism has been reported for β_1-adrenoceptors which remains at the plasma membrane upon rapid interaction and activation of β-arrestin which then undergoes endocytosis to promote ERK1/2 signalling in endosomes (Ranjan et al., 2016).

(4) A fourth pattern has also been recently reported in which G proteins can associate with receptors localised in endocytic compartments, including endosomes (Irannejad et al., 2013) or in the Golgi apparatus (Godbole et al., 2017; Irannejad et al., 2017), to promote receptor activation and downstream signalling by forming a megacomplex with active-GPCR-β-arrestin-G-protein (Cahill et al., 2017; Eichel and von Zastrow, 2018; Thomsen et al., 2016).

(5) GPCRs can also mediate signalling via direct-interaction and transactivation of members of the receptor tyrosine kinase family (RTKs) to promote signalling (Balthasar et al., 2008; Chaplin et al., 2017; Daub, 1996; Maudsley, 2000). This latest mechanism will be described in more detail towards the end of this chapter. Even though studies have reported the role of GPCR-RTK oligomerisation in mitogenic signalling and biological responses (Cattaneo et al., 2014; Pyne and Pyne, 2011), none of these studies have provided evidence showing GPCR-RTK complexes localised in endosomes.

In this project we were interested in investigating possible molecular interactions between the two Class A GPCRs, adenosine A_{2A} and β_2-

adrenergic receptors, and the receptor tyrosine kinase VEGFR2 by investigating complex oligomerisation and intracellular trafficking.

1.2. β_2-adrenoceptors

Beta-adrenoceptors (βARs) are class A GPCRs that mediate central and peripheral actions of the catecholamines, noradrenaline and adrenaline, produced by the adrenal gland and released from sympathetic nerves into the blood stream during a fight-or-flight or stress response (Bers and Despa, 2009). Beta-adrenoceptors (βARs) play critical roles in the control of blood pressure and myocardial contractile rate and force, and in a variety of metabolic and central nervous system (CNS) functions. Agonists and antagonists for these receptors have shown therapeutic actions in a variety of different diseases, such as congestive heart failure, hypertension, ischaemia, asthma, depression, and cancer (Capote et al., 2015; Firouzabadi et al., 2017; Hulsurkar et al., 2017).

Three different β-adrenergic subtypes have been identified: β_1, β_2 and β_3, which are predominantly expressed (but not exclusively) in the heart (Capote et al., 2015), vascular and non-vascular smooth muscle (Mercier et al., 2002) and adipose tissue (Harms et al., 1974), respectively.

1.2.1. β_2-adrenoceptors structure

The β_2-adrenoceptor is a typical 7-TM GPCR with a more unstable conformation compared to rhodopsin (Bang and Choi, 2015). The first inactive crystal structures were obtained in 2007 using an inverse agonist, carazol, and with the unstable intracellular loop 3 (IL3) replaced by a T4 lysozyme (Cherezov et al., 2007; Rasmussen et al., 2007). Other inactive β_2AR structures were later reported using the partial inverse agonist, timolol, or the antagonist alprenolol (Hanson et al., 2008; Wacker et al., 2010). In 2011, two active structures of β_2AR were determine using the high affinity agonist (BI-157107) and stabilised with the nanobody 80 (Nb-80, a Gs mimetic) (Rasmussen et al., 2011a) or Gs protein bound to β_2AR intracellular domains (Rasmussen et al., 2011b). These

studies demonstrated that β_2AR can form a highly engaged complex with Gs, which involves interactions with both C- and N-terminal domains of the Gα-subunit with the transmembrane domains TM5 and TM6, and the intracellular loop 2 (IL2) of the β_2AR (Rasmussen et al., 2011b). Comparison between inactive and active structures showed that only small changes occur on the extracellular side of the receptor, but large conformational changes can be observed in the intracellular side (Zhou et al., 2017). Key interactions between residues within the TM5 induces rearrangements of hydrophobic interactions that result in the cytoplasmic end of TM6 to swing outward. Outward movement of TM6 is the largest change in the cytoplasmatic domains of β_2AR and other class A GPCRs, such as adenosine A_{2A} receptor (Carpenter and Lebon, 2017). TM6 movement is accompanied by the outward movement of the C-terminus of TM5, and slight inward arrangement of TM3 and TM7 where the nanobody-80 and Gs protein interact (Zhou et al., 2017).

1.2.2. β_2-adrenoceptors signalling and trafficking

β_2AR action is mainly mediated by the Gαs protein, which stimulates adenylate cyclase, leading to cAMP production. cAMP can promote activation of PKA activity, which in turn phosphorylates key downstream regulatory proteins involved in the control of smooth muscle tone (Lymperopoulos and Negussie, 2013). PKA can also bind to β_2AR and phosphorylate the receptor at serine residues on position 261 and 262 on the third intracellular loop, and positions 345 and 346 on the C-terminus, which lead to a rapid desensitisation of β_2AR-induced stimulation of adenylate cyclase (classically known as heterologous desensitisation) (Baker, 2003; Yuan et al., 1994). β_2AR can interact with members of the GRK family that promote rapid and transient association of the receptor with β-arrestin 2, resulting in receptor desensitisation and internalisation (Nuber et al., 2016). β_2AR can interact with GRK2, which phosphorylates the receptor at specific amino acids localised in the receptor C-terminus (Komolov and Benovic, 2018; Krasel et al., 2008). The non-selective β-

adrenoceptor agonist isoprenaline and the inverse agonist, carvedilol, can induce β-arrestin-mediated ERK activation that requires β_2AR phosphorylation by GRK6 (Jean-Charles et al., 2017; Nobles et al., 2012). β_2AR phosphorylation by GRK2 and GRK6 is also necessary for efficient desensitisation of cAMP signalling (Jean-Charles et al., 2017). Activation of mitogenic signalling by β_2AR was also shown to be induced via a GRK5/6-β-arrestin-dependent and G-protein-independent mechanism (Shenoy et al., 2006). Mapping of GRK phosphorylation sites of activated β_2AR revealed specific phosphorylation 'barcodes' (Nobles et al., 2012). These phosphorylation 'barcodes' are thought to contribute to signalling bias induced by different ligands (Jean-Charles et al., 2017; Wang et al., 2018; Wootten et al., 2018).

β_2AR is a prototypical 'Class A' GPCR that interacts transiently with both β-arrestin 1 and 2 leading to receptor desensitisation. β_2AR internalisation to early endosomes is mediated via clathrin coated vesicles, followed by rapid recycling to the plasma membrane (Cahill et al., 2017; Drake et al., 2006; O'Hayre et al., 2017). A recent study using small-interference RNA (siRNA) and genomic approaches (including TALEN and CRISPR/Cas9) to knockdown β-arrestin 1 or 2 showed that β_2AR internalisation is mainly mediated by β-arrestin 2 and not by β-arrestin 1 (O'Hayre et al., 2017). Recent structural studies revealed that β-arrestin 1 can interact with β_2AR at two points of contact, including the C-terminus or 'tail' and the receptor transmembrane domain or 'core' but this interaction is unstable which is thought to contribute to the rapid dissociation of β-arrestins from β_2AR (Cahill et al., 2017; Ranjan et al., 2016; Thomsen et al., 2016). Some studies showed that the transient association between β_2AR and β-arrestins can result in transient ERK activation from early endosomes (Cahill et al., 2017; Kumari et al., 2016). However, O'Hayre and colleges reported that agonist stimulation of β-arrestin-'less' HEK 293 cells (using β-arrestin 1 and 2 KO cells) did not result in a decrease in ERK phosphorylation, but rather an increase of ERK activation at 5min (which showed to be mediated by a Gβγ-c-Src-Sos-Raf pathway) (O'Hayre et al., 2017).

Recent studies using β_2AV_2R chimera (formed by β_2AR with the C-tail of a 'Class B' GPCR, V_2R) showed that agonist stimulated β_2AV_2R could promote cAMP signalling from endosomes, which is not observed for β_2AR (Kumari et al., 2016; Thomsen et al., 2016). Structural analysis using cryo-electron microscopy (cryo-EM) revealed that β_2AV_2R chimera bound to β-arrestin 1 could be in two distinct conformations. In one conformation, β-arrestin 1 was partially engaged with β_2AV_2R, by creating points of contact with the receptor C-terminus (tail conformation), whereas in the other conformation β-arrestin 1 showed to fully engage with β_2AV_2R, by binding to both C-terminus and intracellular domains of the receptor (tail and core conformation). These studies also revealed that the 'tail' conformation could accommodate the Gs protein (Cahill et al., 2017; Kumari et al., 2016). Using a truncated β_2AV_2R chimera lacking the 3rd intracellular loop (hence defective to create core-β-arrestin 1 contacts) led to the recruitment of β-arrestin 1 and agonist-induced sustained ERK activation from endosomes (Kumari et al., 2016). These studies suggest the formation of mega-complexes in endocytic compartments where both β-arrestins and G-proteins can interact directly with the receptor to promote intracellular signalling (Cahill et al., 2017; Ranjan et al., 2016, 2017; Thomsen et al., 2016). These new mechanisms may contribute to the high degree of spatial control and complexity of signalling promoted by GPCRs (Eichel and von Zastrow, 2018).

1.2.3. β_2-adrenoceptor oligomerisation

The first evidence for the existence of β_2-adrenoceptor homodimers was acquired using immune-affinity chromatography and transmission electron microscopy in mammalian lung (Fraser et al., 1987; Wnorowski and Jozwiak, 2014). Experiments using co-immunoprecipitation and western blot assays with differential epitope tags demonstrated further evidence supporting β_2AR dimerization (Hebert et al., 1996). β_2R dimerization was later reported using biophysical approaches including BRET (Angers et al., 2000) and FRET (Fung et al., 2009). The latter study showed that binding of an inverse agonist (ICI

118551) but not the full agonist (isoprenaline) induced formation of higher-order oligomers, whereas addition of Gs protein to the system resulted in oligomer destabilisation (Fung et al., 2009). These findings suggest that β_2AR oligomers may constitute the inactive form of the receptor (Wnorowski and Jozwiak, 2014). A more recent study from Calebiro's group applied a single-molecule tracking approach, using total internal reflection fluorescence microscopy (TIRF-M) combined with SNAP-tag labelled receptors, to monitor spatial and temporal organisation of receptors (Calebiro et al., 2013). This study showed that at lower receptor densities, β_2ARs are in a dynamic equilibrium as monomers and dimers, whereas at higher receptor densities these receptors could be present as a mixer of monomers, dimers and higher order oligomers (Calebiro and Sungkaworn, 2017; Calebiro et al., 2013). Their study also suggested that β_2ARs oligomerisation may occur on cycles of rapid binding and transient interaction between highly dynamic protomers (Calebiro et al., 2013). β_2-adrenoceptors can also interact with other GPCRs to form heteromeric interactions, which are reviewed in (Ferré et al., 2014; Wnorowski and Jozwiak, 2014). These receptors can also form oligomeric complexes with members of the receptor tyrosine kinase (RTK) family to mediate biological responses (Kim et al., 2008; Mandic et al., 2014; Maudsley, 2000).

1.2.4. β_2-adrenoceptors in angiogenesis and tumour development

Angiogenesis is a process promoted by endothelial cells (ECs) to promote the formation of blood vessels from pre-existing ones (Carmeliet and Jain, 2011). This process includes the proliferation and migration of ECs, which is controlled by ERK/MAPK and Akt signalling pathways, which are mainly mediated by the vascular endothelial growth factor (VEGF) and VEGF receptor 2 (VEGFR2) signalling axis (Peach et al., 2018a). Pathological angiogenesis is associated to tumour development, which occurs due to an intimate cross-talk between tumour cells and ECs (Claesson-Welsh and Welsh, 2013). This cross-talk results in the formation of a disorganised and leaky vascular network surrounding the tumour cells, providing a source of nutrients and oxygen for tumour growth, as

well as a route of escape for tumour cells to evade other sites (metastasis) (Hanahan and Weinberg, 2011; Shibuya, 2013).

Chronic stress and consequent high levels of circulating adrenaline (or locally release noradrenaline from sympathetic nerve endings) have been linked to tumour-induced angiogenesis and accelerate metastasis in pre-clinical models via activation of β-adrenoceptors (Chang et al., 2016; Hulsurkar et al., 2017; Le et al., 2016). Clinical and pre-clinical evidence showed that β-adrenoceptor antagonists (clinically known as β-blockers to treat cardiovascular disease) have a therapeutic effect in different tumour types, including breast (Melhem-Bertrandt et al., 2011; Sloan et al., 2010), pancreatic (Chang et al., 2015), prostate (Braadland et al., 2015) and ovarian (Thaker et al., 2006; Watkins et al., 2015) cancers. Activation of the β_2AR signalling axis has been implicated in a more invasive breast cancer phenotype demonstrated using *in vitro* and *in vivo* models of breast cancer (Chang et al., 2016; Creed et al., 2015; Sloan et al., 2010). The β_2AR-selective agonist formoterol, but not the β1-selective agonist xamoterol, induced formation of invapodia in breast cancer cells, which is an essential process for tumour cell invasion (Creed et al., 2015). Using a small-hairpin RNA (shRNA) approach to silence β_2AR gene via RNA interference (iRNA) in a highly metastatic breast cancer cell line (MDA-MB-231HM) resulted in reduced cell invasion and attenuated stress-enhanced metastasis in an orthotopic mouse model (Chang et al., 2016). Moreover, β_2AR overexpression in a low metastatic breast cancer model (MCF-7) resulted in the increase in invapodia formation (Chang et al., 2016). β_2AR is the predominant βAR subtype expressed in endothelial cells and evidence exists showing that β_2AR activation can mediate angiogenesis via the release of growth factors, including VEGF (Garg et al., 2017; Howell et al., 1988; Lemmens et al., 2017). Therefore, the action of beta-blockers and reduced metastasis may be, in part, associated with the cross-talk between cancer cells and ECs. However, the exact molecular mechanisms behind β_2AR activation and angiogenesis are not well understood. The better understanding of these mechanisms may unveil novel targets for cancer treatment.

1.3. Adenosine receptors

Adenosine receptors belong to the Class A or rhodopsin-like GPCR family. There are four different adenosine receptor subtypes, A_1, A_{2A}, A_{2B} and A_3, which have been identified and characterised pharmacologically using a variety of agonists and antagonists in different mammalian cells (Fredholm et al., 2011; Gao et al., 2004; Guo et al., 2016a; Ranganathan et al., 2015). These receptors are ubiquitously expressed throughout the human body and contribute to a wide range of physiological and pathological conditions including, cardiovascular and neurodegenerative diseases, anti-inflammatory, immunosuppressive and angiogenic effects, as well as cancer growth (Borea et al., 2016, 2017; Gomes et al., 2011; Jespers et al., 2018; Sepúlveda et al., 2016).

1.3.1. Adenosine receptors structure

Adenosine A_{2A} receptor subtype is one of the most stable GPCRs and, therefore, several crystal structures have been determined for this receptor in an inactive state bound to inverse agonists (Doré et al., 2011; Hanson et al., 2008; Sun et al., 2017). Some of these structures revealed an allosteric site (a site that is topographically distinct from the orthosteric binding site) (Sun et al., 2017). Recent crystal structures of the adenosine A_1 receptor have been determined in complex with xanthine antagonists (Cheng et al., 2017; Glukhova et al., 2017). Moreover, active intermediate states for adenosine A_{2A}R bound to different agonists (adenosine, NECA and the selective A_{2A}AR agonist CGS21680) have also been determined (Lebon et al., 2012, 2015), as well as the fully active state bound to an agonist and coupled to an engineered minimal G protein (mini-G protein) (Carpenter and Lebon, 2017; Carpenter et al., 2016; García-Nafría et al., 2018). These structures were important to determine the inactive to intermediate and active states, which revealed an essential role of G protein to stabilise the full active state of a GPCR (Jespers et al., 2018).

1.3.2. Adenosine receptors signalling and trafficking

Adenosine A_1 and A_{2A} receptor subtypes are expressed in the cardiovascular system and have critical roles in myocardial coronary blood flow regulation and oxygen consumption (Zhou et al., 2013). These are also expressed in the brain where they play a role in regulation of neurotransmitters release, including dopamine and glutamate (Gomes et al., 2011). The adenosine A_{2A}, as well as, A_{2B} and A_3 receptor subtypes are expressed in the periphery and contribute to processes such as inflammation and immune responses (Hatfield and Sitkovsky, 2016; Schulte and Fredholm, 2000; Sun et al., 2006). Adenosine receptor subtypes A_1, A_{2A} and A_{2B} are highly homologous (80-95% similarity) and conserved among animal species, whereas A_3 is less conserved among different species (Antonioli et al., 2008).

Adenosine A_1 and A_3 receptors can couple to Gαi resulting in the inhibition of adenylate cyclase and decrease in cAMP levels, whereas adenosine A_{2A} and A_{2B} receptor subtypes couple to Gαs subunit promoting activation of AC and cAMP accumulation (Figure 1.4.) (Alexander et al., 2017; Fredholm et al., 2011; Schulte and Fredholm, 2000). Adenosine A_{2B} receptors can also activate phospholipase C (PLC) and mobilise calcium stores in cardiac fibroblasts, via coupling to the Gαq protein (Klinger et al., 2002; Ryzhov et al., 2009). All the different adenosine receptor subtypes can promote mitogen-activated protein kinases (MAPK) signalling regulation, including extracellular signal-regulated kinases 1/2 (ERK1/2), c-Jun-N-terminal kinase 1/2 (JNK1/2) and p38-MAPK, which play a role in cell proliferation, growth and survival (Kim et al., 2013; Schulte and Fredholm, 2000, 2003; Stoddart et al., 2014).

The adenosine receptor subtypes A_{2A}, A_{2B} and A_3 were all shown to desensitise rapidly upon agonist stimulation (Klaasse et al., 2008). These receptors can be phosphorylated by GRKs which then lead to the recruitment of β-arrestins, followed by sequestration of the receptor from the plasma membrane by internalisation via clathrin coated pits (Stoddart et al., 2015b; Trincavelli et al., 2000). On the other hand, adenosine A_1 receptor undergoes much slower desensitisation and internalisation (Klaasse et al., 2008).

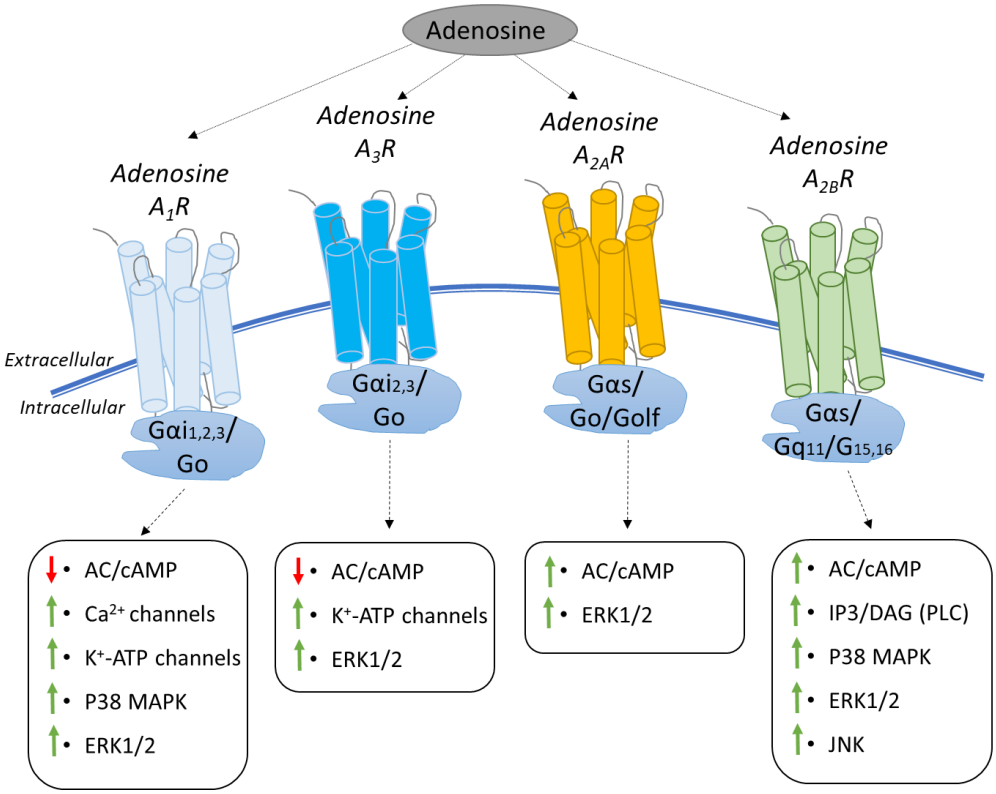

Figure 1.4. Adenosine binding to G protein-coupling adenosine receptor subtypes, and downstream effectors. Extracellular adenosine can bind to stimulate the four different adenosine receptor subtypes. Adenosine subtypes can either inhibit (A_1R and A_3R) or stimulate ($A_{2A}R$ and $A_{2B}R$) adenylate cyclase (AC), resulting in either inhibition or stimulation of cAMP production, respectively (Schulte and Fredholm, 2000). The activation of adenosine A_1 and A_3 receptors may also stimulate the release of calcium ions (Ca^{2+}) from intracellular stores and activation of potassium (K^+)-ATP channels, mediated via Gβγ complex (Verzijl and IJzerman, 2011). All receptor subtypes activate MAPK signalling pathways which may include activation of ERK1/2, JNK and/or p38 MAPK, reviewed in (Antonioli et al., 2013; Borea et al., 2016; Gessi et al., 2011).

1.3.3. Adenosine

Adenosine is the natural agonist for the different adenosine receptors (Antonioli et al., 2014). This endogenous purine nucleoside binds with higher-affinity to A_1 and A_{2A} receptors, and with lower affinity to A_{2B} and A_3 receptors (Poulsen and Quinn, 1998). Adenosine plays a central role in energy metabolism, being released from almost all cell types of the human body in response to cell damage, hypoxia, ischaemia and shear stress (Borea et al.,

2017; Merighi et al., 2001). It is produced both intracellular and extracellularly by the activity of a series of enzymes that maintain the extracellular adenosine concentrations at a range of 30 to 200nM, under normoxic conditions (Sheth et al., 2014). Adenosine is formed in the extracellular space by the breakdown of adenosine triphosphate (ATP) and adenosine monophosphate (AMP), by the ectoenzymes apyrase (CD39) and 5'-nucleotidase (CD73), respectively (Figure 1.5.). On the other hand, intracellular adenosine production depends on AMP hydrolysis by an intracellular CD73 or the S-adenosylhomocysteine hydrolase (SAH) (Antonioli et al., 2014). Adenosine concentration is maintained under equilibrium by the action of nucleoside transporters (NTs) located at the cell and via the action of intracellular and extracellular localised adenosine deaminase (ADA) which converts adenosine to inosine, and adenosine kinase (ADK) which converts adenosine to AMP (Antonioli et al., 2008, 2014).

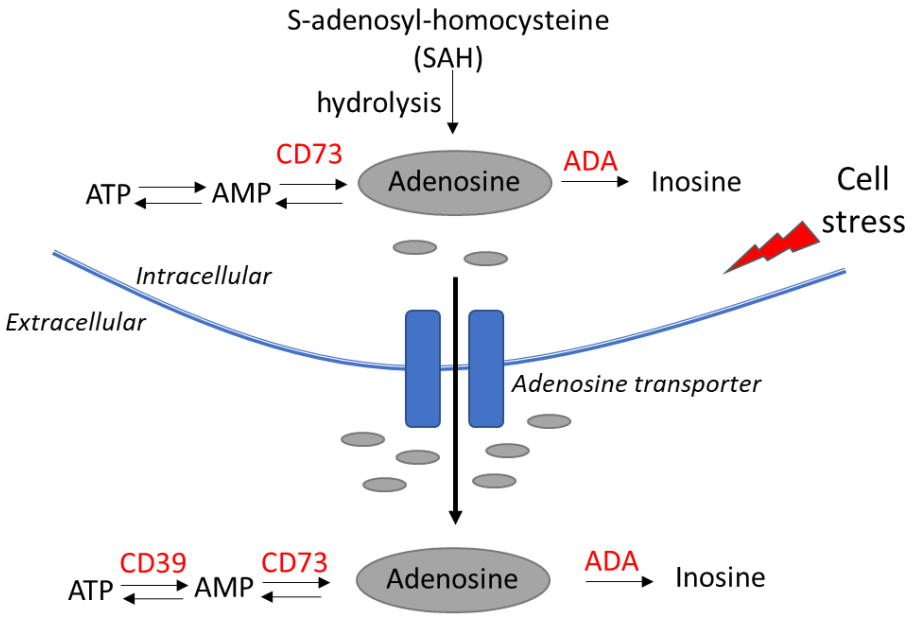

Figure 1.5. Adenosine metabolism. Intracellular adenosine levels are dependent on the hydrolysis of AMP, by 5'-nucleotidase (5'-NT) or hydrolysis of S-adenosyl-homocysteine (SAH). Extracellular adenosine is produced by the breakdown of adenosine 5' mono-, di- or triphosphates triphosphate (AMP, ADP, ATP), through a series of ectoenzymes, including including 5'-nucleotidase (CD73) and apyrase (CD39). Inosine is a product of adenosine deamination, by the action of the enzyme adenosine deaminase (Antonioli et al., 2014).

The intracellular dephosphorylation of ATP as a source of adenosine constitutes the major pathway under hypoxic/ischaemic conditions, which is generated during events of high metabolic demand (Borea et al., 2017; Gessi, 2009). Adenosine levels increase to µM levels during conditions involving high metabolic and/or oxygen demand, which can contribute to different pathological conditions including vascular deficiency, pain, inflammation and cancer (Adair, 2005; Antonioli et al., 2013; Borea et al., 2016). Chronic accumulation of adenosine in the tumour environment and stroma can contribute to immunosuppressive processes that protects the cancer cells from the immune cell system, as well as angiogenesis and matrix remodelling that contribute to tumour growth and invasion (Antonioli et al., 2013; Auchampach, 2007; Sitkovsky et al., 2008; Spychala, 2000). Several tumours show altered adenosine metabolism to enhance adenosine production and/or

reduce its degradation, which result in a 'protective adenosine halo' that contributes to tumour growth and development (Antonioli et al., 2013).

1.3.4. Adenosine receptors oligomerisation

The first evidence for adenosine receptor homodimers was observed for A_1 receptor, which were found in the brain cortex using immunoprecipitation and immunoblotting techniques (Ciruela et al., 1995). Much later, another study revealed the presence of A_1R higher-order oligomers at the plasma membrane, using fluorescence correlation spectroscopy (FCS) and bimolecular fluorescence complementation (BiFC) approaches (Briddon et al., 2008). Adenosine A_{2A} receptors can also form homodimers/oligomeric structures at the plasma membrane which was demonstrated using fluorescence or bioluminescence resonance energy transfer techniques, FRET or BRET, respectively (Canals et al., 2004; Vidi et al., 2008). Adenosine A_3 receptor homodimers have also been reported to have negative cooperativity across their dimer interface, at the level of ligand binding (Corriden et al., 2014; May et al., 2011). No evidence has yet been reported for adenosine A_{2B} receptor interactions.

Adenosine receptors can also interact with other GPCRs to form heteromeric interactions, which are reviewed in (Ferré et al., 2014; Porzionato et al., 2018). These receptors can also form oligomeric complexes with members of the RTK family to promote neuroprotective responses (Flajolet et al., 2008; Xie et al., 2009).

1.3.5. Adenosine A_{2A} receptor in angiogenesis and tumour development

All adenosine subtypes have been implicated in the control of the pro-angiogenic factor VEGF expression (Clark et al., 2007; Du et al., 2015; Merighi

et al., 2006). However, the adenosine A_{2A} and A_{2B} receptors seem to play a dominant role in regulating pro-angiogenic processes (Auchampach, 2007; Feoktistov et al., 2004). In human, porcine and rat endothelial cells, stimulation of A_{2A}R can mediate cell proliferation/migration and synthesis of pro-angiogenic factors, including VEGF (Feoktistov et al., 2002, 2004; Grant et al., 1999). Feoktistov's group found that hypoxia can induce the expression of adenosine receptors evoking a switch towards an "angiogenic phenotype" (Feoktistov et al., 2004). In this study, they showed using both human umbilical vein endothelial (HUVECs) and bronchial smooth muscle (BMSCs) cell lines, that hypoxia can induce a decrease in adenosine A_{2A}R expression (predominantly expressed in normoxic cells), leading to an increase in A_{2B}R expression, which is coincident with the upregulation of VEGF mRNA. Adenosine A_{2A} agonists were shown to promote wound-healing via increasing microvessel formation (Desai et al., 2005; Montesinos et al., 2015). The role of adenosine A_{2A}R in angiogenesis and wound-healing was also confirmed using A_{2A} knockout mice (Montesinos et al., 2002).

Signalling mediated via adenosine A_{2A}R has been implicated in different pro-tumoural processes, including immunosuppression of immune system against cancer cells, angiogenic stimulation and promotion of cancer cell migration (Antonioli et al., 2013; Borea et al., 2017). Adenosine A_{2A}R activation has been associated with the increase in cell growth and proliferation for different cancer cell types, including melanoma, breast and lung carcinoma cell lines (Gessi et al., 2017). In the same study, it was shown that these processes were regulated via a PLC-PKCδ-MAPK signalling mechanism, which could be reversed by the treatment with adenosine A_{2A}R antagonist ZM41384 (Gessi et al., 2017). A_{2A}R-gene deficient mice showed strong anti-tumour immunity, rejection of established tumours and prolonged survival (Ohta et al., 2006; Young et al., 2016). Targeting A_{2A}R has shown great potential for cancer immunotherapy (Allard et al., 2017; Antonioli et al., 2013; Borea et al., 2016). However, the exact molecular mechanisms behind A_{2A} action, particularly in regulation of VEGF-induced angiogenesis need further investigation.

1.4. Receptor Tyrosine kinase superfamily

Receptor tyrosine kinases (RTKs) have intrinsic kinase activity and are the second major transmembrane receptor family, after GPCRs (Hubbard and Miller, 2008). These receptors have been classified into 20 classes, with at least 58 members identified so far, that share a conserved architecture (Lemmon and Schlessinger, 2010). The first RTK discovered was the Class I epidermal growth factor receptor (EGFR) which was first found to be directly mutated in different types of cancer in humans and is, therefore, designated as the prototypical RTK (Gschwind et al., 2004). RTKs act as receptors for growth factors, hormones, cytokines and other signalling molecules (Lemmon and Schlessinger, 2010). These receptors display a similar molecular structure with a single transmembrane helix, an extracellular binding domain, carrying seven immunoglobulin (Ig)-like domains, and a cytosolic lobe with intrinsic tyrosine kinase activity (Figure 1.6.) (Stuttfeld and Ballmer-Hofer, 2009).

1.4.1. RTK classic activation model

Most inactive RTK are present as monomers, and dimeric RTK ligands may induce RTK activation via a dimerization process (Lemmon and Schlessinger, 2010), with an exception for the insulin receptor and the closely related insulin growth factor-like 1 (IGF-1) receptor, which are expressed as pre-existing disulphide-linked dimers (Smith and Milligan, 2010). The traditional model of RTK activation follows three steps: 1) ligand-mediated dimerization of receptor monomers, 2) conformational changes in the receptor extracellular domain (ECD), and 3) auto- or trans-phosphorylation and signalling transduction (Schlessinger, 2014). It is believed that specific conformation and orientation of the intracellular kinase domains can determine specificity of signalling activation (Manni et al., 2014a).

The traditional model of RTK activation involves ligand-induced receptor homo- or hetero-dimerization, which stabilises the interaction between the two

receptor monomers (Stuttfeld and Ballmer-Hofer, 2009). However, an increasing number of studies have shown that RTKs can also form higher-order oligomers (or clusters) in the absence of ligand, which is well-reported for the ErbB receptor family (Abulrob et al., 2010; Casaletto and McClatchey, 2013). It has been postulated that these receptor clusters may be active or 'primed' for ligand-induced activation (Casaletto and McClatchey, 2013; Szabó et al., 2010).

1.4.2. RTK trafficking

RTKs can undergo constitutive internalisation in the absence of ligand or be internalised upon ligand-binding and receptor activation (Miaczynska, 2013). RTKs typically undergo rapid internalisation upon ligand binding (Goh and Sorkin, 2013). The earlier idea that ligand-stimulated RTK localised on the plasma membrane was signalling competent is changing. Nowadays, it is accepted for many RTKs that receptor internalisation and endocytosis is required for full response duration and, in some cases, for signal amplification (Miaczynska, 2013).

Following internalisation, similar to GPCRs, RTKs can also undergo endocytosis to different intracellular compartments (Figure 1.6.). Recent evidence in the field of endocytosis discovered that internalisation can occur via different plasma membrane structures, for example clathrin-coated vesicles, caveoli, macropinocytosis and other clathrin- and dynamin-independent mechanisms (Conner and Schmid 2003; Mayor and Pagano 2007; Howes et al. 2010; McMahon and Boucrot 2011).

RTK internalisation and trafficking differs for different receptor types, ligand availability, cell type, among other factors (Miaczynska, 2013). Similar to other transmembrane proteins, including GPCRs, the active receptor undergoes internalisation and endocytosis, via either clathrin-dependent or -independent mechanisms (Sorkin and Von Zastrow, 2009). Vesicles then move the receptor to early endosomal compartments (rab5-positive endosomes) (Sorkin and Von

Zastrow, 2009). The receptors can then be either targeted for lysosomal degradation, or be recycled back to the plasma membrane (Simons, 2012). Lysosomal degradation ultimately leads to signalling termination, whereas recycling allows sustained signalling, after receptor re-activation (Simons et al., 2016). Receptor targeted for degradation move from early endosomes to late endosomes which is characterised by a 'rab conversion mechanism' in which the receptor moves from rab5 to rab7-positive endosomes (Figure 1.6.) (Rink et al., 2005). Fast RTK recycling is mediated by rab4-positive endosomes, whereas slow recycling occurs via rab11-positive endosomes (Jones et al., 2006; Jopling et al., 2011).

RTK intracellular membrane trafficking, recycling and degradation have a great impact on signalling regulation, response duration, amplification and specificity (Berger and Ballmer-Hofer, 2011; Sorkin and Von Zastrow, 2009). However, the mechanisms involved in RTK trafficking and signalling fate, for different RTK families in different cellular and tissue environments, have been poorly explored and need further investigation.

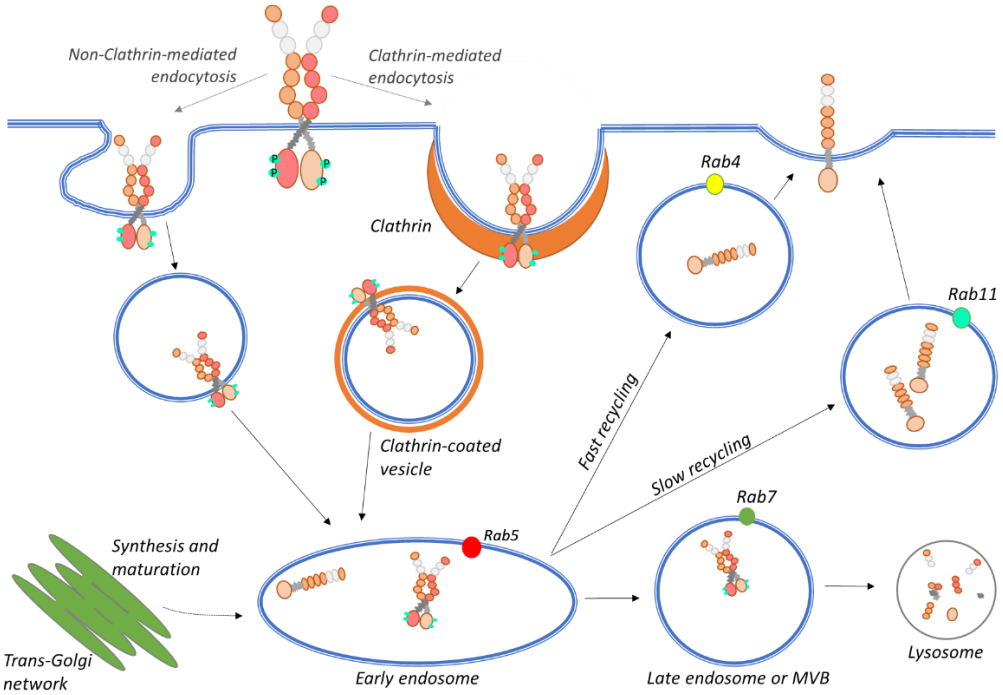

Figure 1.6. Schematic representation RTK endocytosis and trafficking. Ligand-bound or unbound active-RTK can undergo rapid internalisation via clathrin-dependent or -independent mechanisms. Internalised RTK is then moved into early endosomes (or rab5-positive

endosomes). Depending on the receptor and/or cellular context, the receptor can be targeted for degradation in lysosomes (characterised by a 'rab conversion' process where receptor moves from early rab5-positive endosomes to rab7-positive late endosomes) (Rink et al., 2005). Instead of being targeted for degradation, the receptor can be recycled back to the plasma membrane via a fast recycling mechanism (by rab4-positive endosomes) or via a slow recycling mechanism (by rab11-positive endosomes). Receptors are synthesised in the Trans-Golgi network (TGN) and maturation can occur in early endosomes before receptors are made available at the plasma membrane (Goh and Sorkin, 2013; Miaczynska, 2013; Sorkin and Von Zastrow, 2009).

1.5. VEGFR family

VEGFR2 (also known as KDR [kinase insert domain receptor] in the human and Flk1 [fetal liver kinase 1] in the mouse) is a class IV RTK glycoprotein with a size of 210-230 kDa (Koch et al., 2011). It is as a member of the VEGFR family which consists of 3 members: VEGFR1, VEGFR2 and VEGFR3. VEGFR2 is mainly expressed in endothelial cells, playing a major role in angiogenesis and vasculogenesis (Peach et al., 2018a; Simons et al., 2016). VEGFR1 is not only expressed in endothelial cells but also in hematopoietic stem cells and inflammatory cells, playing a role in chemotaxis (Ferrara et al., 2003). VEGFR3 is predominantly expressed in lymphatic vessels and is a major mediator of lymphagiogenesis (Olsson et al., 2006). VEGFR2-triggered angiogenesis is one of the hallmarks of cancer development and invasion of secondary tumour sites (metastasis) (Claesson-Welsh and Welsh, 2013; Fontanella et al., 2014; Hanahan and Weinberg, 2011).

1.5.1. VEGFR2 activation

VEGFR2 has a typical RTK structure with an extracellular (EC) domain formed by seven immunoglobulin (Ig) homology domains (D1-D7), a transmembrane (TM) domain, and an intracellular kinase domain (Figure 1.7.) (Stuttfeld and Ballmer-Hofer, 2009). Homodimeric-ligands bind to EC region between the Ig-domains D2 and D3 leading to a conformational switch and receptor

dimerization by lateral diffusion (Sarabipour et al., 2016). VEGFR2 can be activated by VEGFa isoforms, and by processed forms of VEGF-C and VEGF-D isoforms (Olsson et al., 2006).

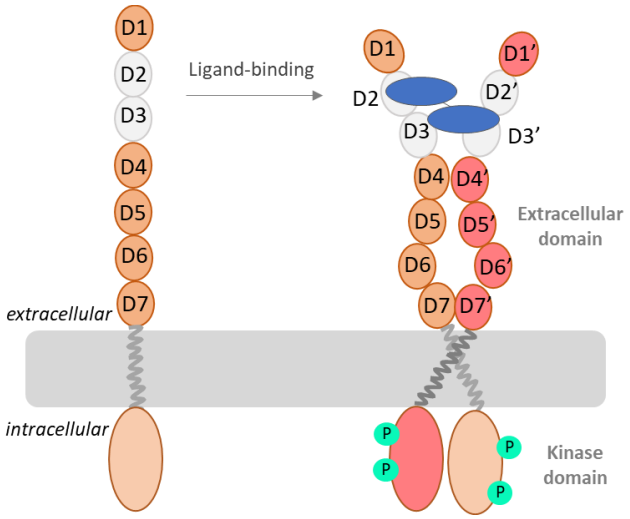

Figure 1.7. Structure and activation of VEGFR2. In active dimers, homotypic receptor-receptor contacts between domains D4 and D7 were shown to be critical for efficient ligand-induced VEGFR2 phosphorylation. Dimeric ligand induces conformational changes in the receptor and consequent activation of the intracellular kinase domain (Sarabipour et al., 2016).

1.5.2. VEGFa isoforms family

VEGFa family of ligands is formed by different isoforms as a result of alternative gene splicing (Figure 1.8.) (Peach et al., 2018a; Bates et al. 2018). VEGF-A pre-mRNA can be alternatively spliced at exon 8, whereby proximal splice site selection results in the prototypical pro-angiogenic VEGFxxxa isoforms and distal splice site selection generates the anti-angiogenic VEGFxxxb isoforms, i.e. $VEGF_{165}b$ (Bates et al. 2018). These isoforms resulting from alternative splicing have different amino acid lengths, and the ones with longer lengths contain additional sequences that enable their interaction with VEGFR2 co-receptors, such as neuropilin-1 (NRP-1) and heparan sulfate proteoglycans (Peach et al., 2018a). All isoforms exhibit similar binding affinity at VEGFR2 (Peach et al., 2018b). However, their interaction or lack of interaction with VEGFR2 co-receptors and other matrix-binding proteins is thought to be involved in their

differential regulation of VEGFR2 activity (Fearnley et al., 2016; Peach et al., 2018a, 2018b).

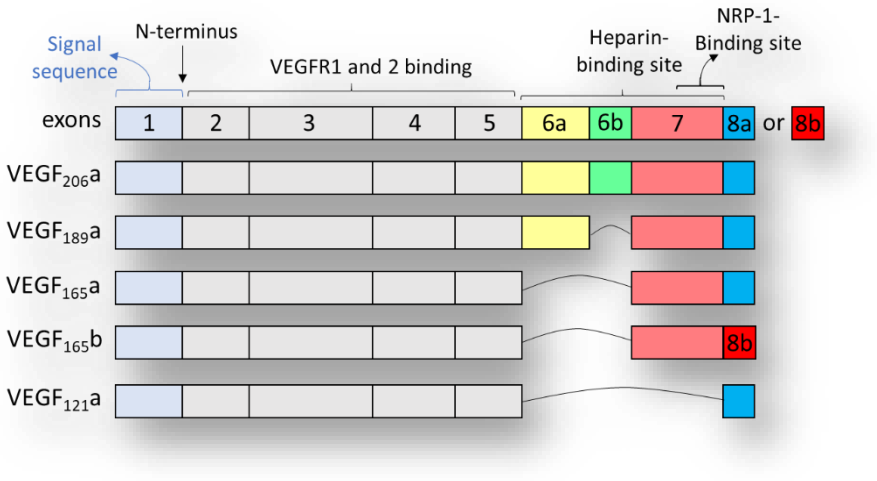

Figure 1.8. Schematic representation of VEGFa isoforms. VEGF isoforms are originated by alternative gene splicing. VEGF structure is formed by eight exons with different amino acid lengths ($VEGF_{xxx}a$) (i.e. $VEGF_{165}a$ has 165 amino acids). Isoforms with lower lengths lack residues that enable their interaction with components of the extracellular matrix (ECM), which is the case for $VEGF_{121}a$ isoform. Longer size isoforms (such as $VEGF_{206}a$) have higher ability to interact with the ECM. Proximal splicing at exon 8 results in the prototypical $VEGF_{xxx}a$ isoforms, whereas distal splicing originates $VEGF_{xxx}b$ isoforms. $VEGF_{xxx}a$ isoforms are the major mediators of vascular permeability, cell proliferation, survival migration, and angiogenesis (Olsson et al., 2006; Shibuya, 2013). On the contrary, $VEGF_{xxx}b$ isoforms have been described as anti-angiogenic (Nowak et al., 2008; Woolard et al., 2004; Ye et al., 2016)

1.5.3. VEGFR2 canonical signalling

As some RTK family members, VEGFR2 can be activated by a dimeric ligand (Sarabipour et al., 2016). The VEGF ligand can bind in a cis or trans position to the VEGFR2, for example by binding to heparan sulfate in the same cell (cis) or to heparan sulfate localised in adjacent cells (trans). VEGF ligand binding to VEGFR2 induces receptor homo- or heterodimerisation (Jakobsson, 2006; Manni et al., 2014b). The ligand-induced conformational change of the receptor leads to an exposure of ATP-binding sites in the C-terminus that can be auto- or trans-phosphorylated in specific intracellular tyrosine residues to

mediate VEGF-induced responses (Koch et al., 2011). VEGF can induce endothelial cell (EC) proliferation, migration, survival and vascular permeability, which are processes that contribute to vasculogenesis and angiogenesis (Figure 1.9.) (Domigan et al., 2014; Koch et al., 2011; Peach et al., 2018a).

Phosphorylation of VEGFR2 tyrosine 1175 (Tyr1175) residue creates docking sites for PLCγ and the adaptor proteins SHB (SH2-domain adaptor protein B) and SCH (Src adaptor protein) (Holmqvist et al., 2004). PLCγ cleaves PIP2 (phosphatidylinositol-4,5-bisphosphate) into DAG (diacylglycerol) or IP3 (inositol trisphosphate). IP3 can diffuse to the endoplasmic reticulum (ER) to activate Ca^{2+} intracellular stores (Lemmon and Schlessinger, 2010). The increase in calcium ions can activate calcineurin which dephosphorylates and activates NFAT transcription factor (Schweighofer et al., 2009). DAG can activate PKC (protein kinase C), which in turn activates PKD (protein kinase D), leading to activation of the transcription factor CREB (cAMP-response-element-binding protein).

Tyr1175 phosphorylation also recruits Grb2 (growth factor-bound protein 2), which in turn recruits Sos (son of sevenless) to VEGFR2 (Kroll and Waltenberger, 1997), and activation of Ras/Raf/MEK/ERK mitogenic cascade (Meadows et al., 2001). The efficacy and duration of the ERK signal transduction is regulated by the scaffolding protein kinase suppressor Ras (KSR) (Schlessinger, 2014). These pathways are important for endothelial cell proliferation (Olsson et al., 2006). The adaptor protein SHB can activate FAK (focal adhesion kinase) that promotes focal adhesion turnover, being important to EC attachment and migration (Holmqvist et al., 2004). Docking sites for Grb2 can also bind the p38 subunit of PI3K, that phosphorylates PIP2 to PIP3 (phosphatidylinositol 3,4,5-trisphosphate), and in turn activates the small GTPase Rac, resulting in membrane ruffle formation and cell motility (Laramé et al., 2007). PIP3 can also induce PKB (also known as Akt) activation though PDK1/2 (phosphoinositide-dependent kinase 1/2). Akt phosphorylates BAD (Blc-(B-cell-lymphoma)-2-associated-death promoter) and caspase-9

inducing cell survival, via inhibition of apoptotic activity (Datta et al., 1999). AKT activation can also lead to nitric oxide (NO) production that mediates endothelial cell permeability (Di Lorenzo et al., 2014).

Phosphorylation of Tyr1214 residue allows the recruitment of NCK, which ultimately leads to the activation of p38MAPK, a key player in actin reorganisation and cell motility (Lamalice et al., 2006).

Phosphorylation of Tyr1054 and Tyr1059 is important for kinase activity, and their phosphorylation is regulated via phosphorylation of Tyr801 residue (Koch et al., 2011). Tyr1059 can activate Src kinase that in turn phosphorylates other VEGFR2 kinase residues involved in cell proliferation and migration (Zeng et al., 2001).

Tyr951 is a docking site for SH2-domain containing TSAD (T-cell-specific adaptor molecule) which can form a complex with Src kinase to mediate actin reorganisation and migration (Matsumoto et al., 2005). VEGF can induce permeability through Src-mediated VE-Cadherin (or cadherin-5) phosphorylation and internalisation, in which endocytosis of VE-Cadherin is mediated by beta-arrestin2 (Gavard and Gutkind, 2006).

These signalling pathways undergo extensive cross-talk [reviewed in (Simons et al., 2016)], and are now known to be activated not only from the plasma membrane, but also from intracellular compartments, such as endosomes (Berger and Ballmer-Hofer, 2011; Casaletto and McClatchey, 2013; Peach et al., 2018a).

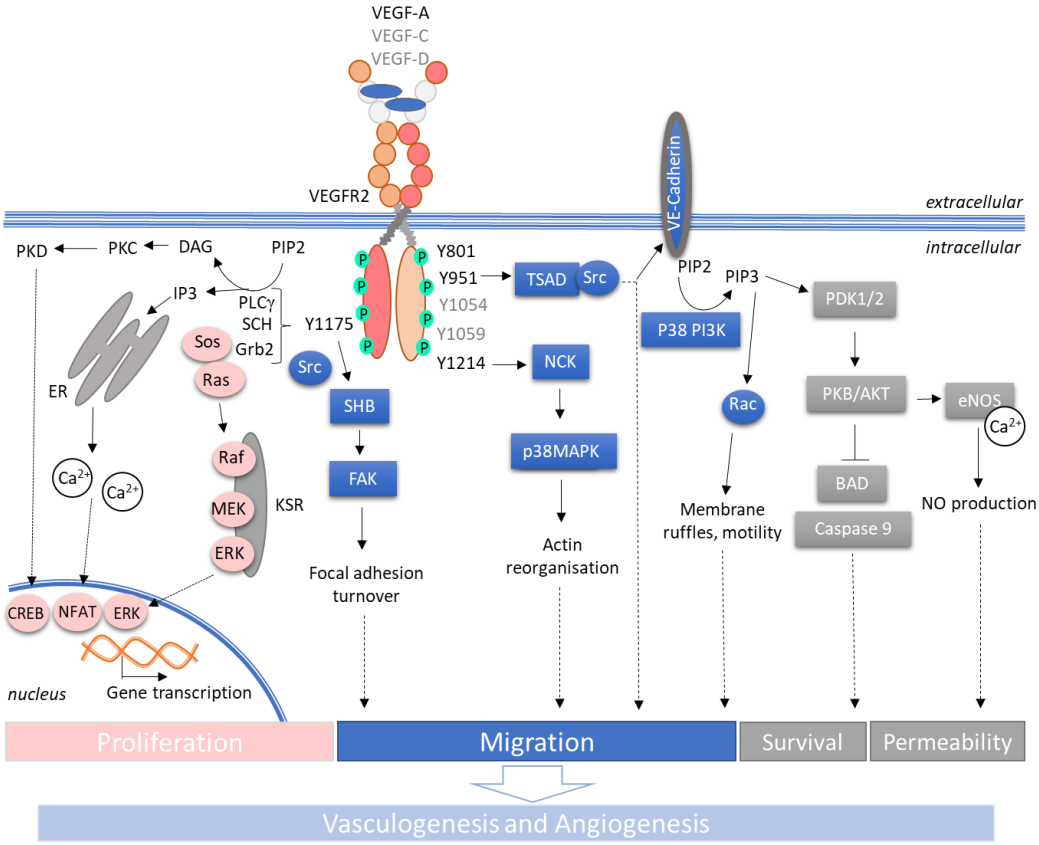

Figure 1.9. Schematic of VEGFR2 canonical signalling. VEGFR2 canonical signalling is promoted upon ligand binding to Ig-like domains D2 and D3. Ligand binding to VEGFR2 induces conformational changes and the activation of specific residues with kinase activity. Phosphorylation of tyrosine residues 1175 (Tyr1175) mediates most processes involved in endothelial cell (EC) proliferation. Activation of Tyr1175 residues can also promote cell attachment and motility, via activation of FAK (focal adhesion kinase), or cell survival via activation of PI3K/AKT pathway, and nitric oxide (NO) production important for endothelial cell permeability. Activation of Tyr1214 residues results in processes mediating actin reorganisation and cell motility. Tyr1054 and Tyr1059 are important for tyrosine activity, which is regulated by phosphorylated of Tyr801 residue. Finally, Tyr951 can induce activation of TSAD-Src complex, an important mediator of action reorganisation and migration. Src kinase can also activate VE-Cadherin to promote cell junction permeability (Peach et al., 2018a; Simons, 2012). Abbreviations: PIP2 (phosphatidylinositol-4,5-bisphosphate); DAG (diacylglycerol); PKC (protein kinase C); CREB (cAMP-response-element-binding protein); PLCγ (phospholipase Cγ); SCH (Src adaptor protein); Grb2 (growth factor-bound protein 2); Sos (son of sevenless); Ras (non-tyrosine kinase receptor Ras); Raf (rapidly accelerated fibrosarcoma); MEK (mitogen-activated protein kinase); KSR (protein kinase suppressor Ras); ERK (extracellular signal-regulated kinase); IP3 (inositol trisphosphate); NFAT (nuclear factor of activated T-cells); Src (proto-oncogene tyrosine kinase); PKD (protein kinase D); SHB (SH2-domain adaptor protein B); FAK (focal adhesion kinase); TSAD (T-cell-specific adaptor molecule); NCK (non-catalytic

region of tyrosine kinase adaptor protein); p38MAPK; p38 PI3K (p38 subunit of phosphoinositide 3 kinase); PIP3 (phosphatidylinositol 3,4,5-trisphosphate); PDK1/2 (phosphoinositide-dependent kinase 1/2); PKB (protein kinase B); BAD (Blc-2 associated death promoter); eNOS (endothelial Nitric oxide synthase); NO (nitric oxide).

1.5.4. VEGFR2 trafficking and endocytic signalling

VEGFR2 signalling was thought to be mediated solely from the plasma membrane (Galperin and Sorkin, 2008). However, increasing evidence has challenged this idea and has demonstrated the importance of VEGFR2 endocytosis and trafficking in signalling regulation (Galperin and Sorkin, 2008; Sorkin and Von Zastrow, 2009).

VEGFR2 undergoes rapid endocytosis upon ligand binding, and endosomal signalling is important to achieve sufficient signalling duration (Berger and Ballmer-Hofer, 2011; Goh and Sorkin, 2013; Sorkin and Von Zastrow, 2002). Ligand-unbound receptor (inactive or with low level of activity) can be constitutively internalised and rapidly recycled back to the plasma membrane (Jopling et al., 2011; Simons, 2012). Both constitutive and ligand-bound receptors undergo clathrin and dynamin-dependent internalisation that direct the receptor to early endosomal compartments, that contain rab-5 and EEA1 (early endosomal antigen 1) proteins (Simons, 2012).

In HUVECs, a ligand-unstimulated pool of VEGFR2 undergoes constitutive endocytosis into rab-4-positive endosomes that are rapidly recycled back to cell surface (Gampel et al., 2006). VEGFR2 endocytic signalling can be regulated by different effectors, one of them is the protein tyrosine phosphatase 1B (PTP1B) that phosphorylates VEGFR2 located in endosomes, resulting in a decrease in ERK1/2 signalling (Lanahan et al., 2014). VEGFR2 can either be directed to Rab-7 late endosomes to be degraded in lysosomes, or recycled back to plasma membrane, via rab-11 endosomes (slow recycling) (Simons, 2012).

A recent paper revealed that VEGFR2 constitutive internalisation plays a role in protecting VEGFR2 against proteolytic cleavage (shedding) (Basagiannis and

Christoforidis, 2016). This constitutive internalisation was shown to be mediated via a clathrin-dependent manner, as interference with clathrin, dynamic or Rab-5 function led to a dramatic increase in VEGFR2 shedding (Basagiannis and Christoforidis, 2016). $VEGF_{165}$a-driven VEGFR2 activation and internalisation in HUVECs occurs mainly via macropinocytosis, whereas clathrin-mediated VEGFR2 internalisation does not seem to contribute for VEGFR2 function (Basagiannis et al., 2016). This group showed that $VEGF_{165}$a-induced VEGFR2 macropinocytosis is crucial for signalling and endothelial functions both *in vitro* and *in vivo*, including angiogenesis (Basagiannis et al., 2016). However, VEGFR2 endocytic route may differ in different cell types, for different VEGF isoforms, as well as interactions with co-receptors (including NRP-1) or other matrix-binding proteins (Basagiannis et al., 2016; Berger and Ballmer-Hofer, 2011; Krilleke et al., 2009; Peach et al., 2018a).

Understanding VEGFR2 signalling dynamics and regulation via interaction with other proteins, including GPCRs, is important to identify novel therapeutic targets (Pyne and Pyne, 2011; Sorkin and Von Zastrow, 2009).

1.6. GPCR-RTK crosstalk

Two decades ago, it was believed that GPCR and RTK followed distinct and independent signalling pathways that eventually converged in a common downstream effector (Cattaneo et al., 2014; Liebmann and Böhmer, 2000). A large body of evidence revealed a complex signalling network between these receptor families for the tight regulation of different biological processes for cellular homeostasis (George et al., 2013; Pyne and Pyne, 2011).

Receptor 'cross-talk' can be defined as synergic interactions between two receptors, which lead to an amplification and/or a negative regulation of responses within the same cell, resulting in a 'fine-tuning' of cellular function (Barnes, 2006). Elucidating cross-talk mechanisms between cell-surface receptors can contribute to a better understanding of human disease, and to

generate specific therapeutic agents that will target these specific interactions, in a conformational and spatial-dependent manner (Köse, 2017).

It has become clear that GPCRs and RTKs collaborate with each other to promote cell growth, survival, proliferation, migration, and more recently to promote angiogenesis and tumour spread (metastasis) (Bergelin et al., 2010; Flajolet et al., 2008; Köse, 2017; Sysa-Shah et al., 2016). These cellular functions may be associated with their role in targeting MAPK signalling cascades, playing a role in the activation and regulation of ERK1/2, Jun amino-terminal kinase and p38MAPK pathways (Liebmann and Böhmer, 2000; Oligny-Longpre et al., 2012; Shenoy et al., 2006; Wetzker and Böhmer, 2003). GPCR-RTK cross-talk can be mediated by different transactivation mechanisms which will be described in the following section (Chaplin et al., 2017).

1.6.1. Transactivation mechanisms

GPCR-RTK cross-talk was first reported by Ullrich group in the early 90s, who showed that GPCR agonists, including angiotensin II (Ang-II), bradykinin, lysophosphatidic acid (LPA), dopamine and endothelin (ET-1) agonists, could induce mitogenic responses, via activation (known as 'transactivation') of the RTK family (Daub et al., 1997; Prenzel et al., 1999). These responses could be mediated via RTK-ligand dependent or independent mechanisms (Cattaneo et al., 2014). GPCR-induced RTK transactivation, via a RTK ligand-independent mechanism could result in rapid phosphorylation of the RTK, and in the activation of downstream signalling to promote cell proliferation, migration and survival (Daub, 1996; Lebman and Spiegel, 2008; Schäfer et al., 2004a).These effects could be inhibited with the use of GPCR antagonists (Daub, 1996; Schäfer et al., 2004b, 2004a).

Taking into consideration numerous studies, three major GPCR-RTK cross-talk mechanisms have been proposed: (1) GPCR activation of RTK by shedding of heparin-binding-epidermal growth factor (HB-EGF), promoted by matrix metalloproteases (MMPs), and consequent RTK activation; (2) GPCR activation

of RTK via intracellular signalling (c-Src, PKC, β-arrestin, ROS, Ca^{2+}) leading to the autophosphorylation and activation of the RTK, and (3) GPCR-RTK receptors oligomerization. Given that in mechanism (1) the signal crosses the plasma membrane three times before signalling activation, this mechanism is also described as triple membrane passing signal (TMPS) pathway. Mechanisms (2) is promoted in a ligand-independent manner, in which GPCR activation induces autophosphorylation of the RTK (Cattaneo et al., 2014; George et al., 2013). For mechanism (3) to occur, both GPCR and the RTK need to be associated in a complex platform (Delcourt et al., 2007; Liebmann, 2011; Pyne and Pyne, 2011). For example, the GPCRs, β_2-adrenoceptor (Kim et al., 2008; Maudsley, 2000), somatostatin receptors (Watt et al., 2009) and chemokine receptor CXCR7 (Kallifatidis et al., 2016) can form complexes and transactivate EGFR. Several other examples of GPCR-RTK association for downstream signalling regulation have been reported (Table 1.2.).

Table 1.2. Evidence for GPCR/RTK complex formation.

Stimuli	GPCR/RTK	Methodology	Cell type/Physiology	References
PDGF/S1P	**S1P1/PDGFR-β**	Co-IP	Airway smooth muscle cells – cell proliferation and migration HEK293	(Waters et al., 2003, 2005, 2006) (Alderton et al., 2001)
VEGF/S1P	**$S1P_1$/VEGFR2**	Co-IP	Follicular thyroid carcinoma ML-1 cells – cell migration and proliferation	(Balthasar et al., 2008; Bergelin et al., 2010)
S1P	**$S1P_1$ and $S1P_3$/Flk-1**	Co-IP and PLA	Mouse embryonic stem cell proliferation	(Park et al., 2016; Ryu et al., 2014)
SST/EGF	**SSTR1, SSTR5/EGFR2, Erb2**	photobleaching FRET (pbFRET)	Breast cancer cell lines – regulation of mitogenic signalling and cell proliferation.	(Kharmate et al., 2011; Watt et al., 2009)
CPA (Adenosine A_1 agonist)	**A_1R/EGFR**	Co-IP	Cultured primary cortical neurons – neuroprotective effect	(Xie et al., 2009)
CGS21680 (adenosine A_{2A}R-agonist) and aFGF	**A_{2A}R/PDGFR-1β**	GS-pulldown and Co-IP	PC12 cells Differentiation and neurite extension, spine morphology, cortical-striatal plasticity	(Flajolet et al., 2008)
Ki16425 (protean agonist)	**LPA1/ TrkA**	Co-IP	Lung epithelial cells – migration and proliferation	(Moughal et al., 2006; Nan et al., 2016)
Kisspeptin-10 (endogenous KISS1R ligand)	**KISS1R (GPR-54)/ EGFR**	Co-IP and FRET	Breast cancer cells MDA-231 and Hs578T – increased cell motility and invasion	(Köse, 2017; Zajac et al., 2011)

Table 1.2. Continue

Stimuli	GPCR/RTK	Methodology	Cell type/Physiology	References
Isoprenaline (agonist)	**β_1AR/EGFR**	Co-IP and FRET	HEK293 and U2 sarcoma cells and human heart tissue – cardioprotection	(Tilley et al., 2009)
Insulin	**β_2AR/IGF-1**	Co-IP, BRET^2 and bioinformatic analysis	Mouse heart and HEK293 cells – cardiac contractibility dysfunction (diabetic cardiomyopathy)	(Fu et al., 2014; Mandic et al., 2014)
Isoprenaline and 17-PTP (EP-1 agonist)	**β_2AR/EP-1R**	Co-IP and BRET	HEK293 Airway smooth muscle cells – reduced bronchodilation	(Barnes, 2006; Mcgraw et al., 2006)
Isoprenaline, carvedilol (inverse-agonist)	**β_2AR/Erb2 and EGFR**	Co-IP	Mouse heart, COS-7 and HEK293 cells – mitogenic signalling activation and cardioprotective affect	(Kim et al., 2008; Maudsley, 2000; Negro et al., 2006; Sysa-Shah et al., 2016)
-	**Neuraminidase 1 receptor (Neu-1) / EGFR**	co-IP	Xenograft mouse pancreatic cancer model – tumour growth and invasion	(Gilmour et al., 2013)
oxotremorine-M	**M_1R / PDGFR1**	PLA	mouse hippocampus and cerebral cortex – neurite outgrowth	(Di Liberto et al., 2017)
5-HT1A/FGF2	**5-HT1AR / FGFR**	Co-IP, PLA and FRET	PC12 and primary hippocampal culture – neurite outgrowth. Anti-depressant effect in vivo (using forced swim test with rats)	(Borroto-escuela et al., 2015; Borroto-Escuela et al., 2012, 2013a)

Abbreviations: Co-IP (co-immunoprecipitation), BRET/FRET (Bioluminescence or Fluorescence Resonance Energy Transfer), S1P$_1$ (sphingosine 1 phosphate receptor 1), PDGFR (platelet derived growth factor receptor), PLA (proximity ligation assay), FGFR (fibroblast growth factor receptor), M$_1$R (muscarinic receptor 1), SSTR (somatostatin receptor), EP-1R (prostaglandin receptor 1), 5-HT1AR (serotonin 1A receptor), HEK293 (human embryonic kidney), TrkA (tropomyosin receptor kinase A), LPA-1R (lysophosphatidic acid receptor 1).

1.6.2. Bidirectional cross-talk

Increasing studies have reported a novel mechanism of bidirectional cross-talk, in which the GPCR can induce RTKs transactivation and, reciprocally, the GPCR can be transactivated by cytokines and RTK ligands (Delcourt et al., 2007; Sysa-Shah et al., 2016). First evidence showing that GPCR could also be transactivated by RTKs were obtained with the use of molecules that disrupt GPCR signalling promoted by RTK ligands (i.e. Pertussis toxin, which inhibits Gi-coupling, and the C-terminal domain of GRK2, which sequesters Gβγ proteins) (Delcourt et al., 2007). This was demonstrated for the insulin and IGF-1 receptors which were shown to associate with Gαi and Gβγ proteins to promote ERK pathway and mitogenesis (Hallak et al., 2000). Other studies showed evidence that RTKs can also associate with pertussis-insensitive Gαs protein. For example, agonist stimulated EGFR have been shown to activate Gαs protein to increase its ability to stimulate AC (Poppleton et al., 1996). However, there is no evidence that ligand-RTK receptor activation can induce GDP-GTP exchange that promote G-protein activation (Delcourt et al., 2007). One possibility that has been proposed for RTK-induced GPCR signalling is via the use of constitutively active G-proteins (Waters et al., 2006).

β-arrestins were also found to associate with different RTKs, including EGFR, insulin and IGF-1 receptors (Mandic et al., 2014; Maudsley, 2000; Povsic et al., 2003). β-arrestin coupling to IGF-1R is involved in the clathrin-mediated endocytosis of IGF-1R, and to promote mitotic and anti-apoptotic signalling (Delcourt et al., 2007; Oligny-Longpre et al., 2012).

Two different factors can contribute to the accumulation of extracellular GPCR ligand upon RTK activation: transcriptional upregulation and enzymatic activity. A transcriptional dependent mechanism was found for the Gαi-coupled chemokine receptor CCR5 by IGF-1R (Mira et al., 2001). Activation of IGF-1R leads to the upregulation of RANTES, the natural CCR5 ligand, promoting chemotaxis of MCF-7 human carcinoma cells. An example of enzymatic activity was demonstrated for the sphingosine phosphate receptor 1 ($S1P_1$) (previously

known as EDG-1 receptor), which can be transactivated by different RTK ligands including PDGF, VEGFa, and IGF-1 to induce cell motility and migration (Bergelin et al., 2010; Long et al., 2006; Ryu et al., 2014). The endogenous ligand for $S1P_1$ receptor is the sphingosine 1 phosphate (S1P). S1P cellular concentration is regulated by sphingosine kinase SphK1 which promotes S1P synthesis, whereas S1P phosphatases promote S1P degradation. (Balthasar et al., 2008). Exposure of cells to growth factors induces SphK1 enzyme activation and translocation to the plasma membrane, which then leads to an enhanced synthesis and secretion of S1P, and consequent $S1P_1$ activation (Bergelin et al., 2010). The physical association via complex oligomerisation between $S1P_1R$ and VEGFR2 has been reported and contribute to ML-1 thyroid carcinoma cell migration (Bergelin et al., 2010). In this study a bidirectional cross-talk mechanism was reported, in which S1P-induced ERK1/2 phosphorylation was sensitive to VEGFR2 inhibition, and VEGFa-induced ERK1/2 phosphorylation was sensitive to pertussis toxin (PTX) treatment or silencing of $S1P_1R$ using small interfering (siRNA) (Balthasar et al., 2008; Bergelin et al., 2010).

Signalling mediated via VEGFR2 is well-known to promote tumour angiogenesis and invasion (Simons et al., 2016). Adenosine receptors and β_2-adrenoceptor activation is known to promote VEGFa expression in endothelial cells and also in different tumour types (Antonioli et al., 2013; Chen et al., 2014; Desai et al., 2005; O'Leary et al., 2015). The pharmaceutical inhibition of β_2-adrenoceptor, using beta-blockers can treat infantile haemangioma and angioblastomas patients (Chow et al., 2015; Pan et al., 2015), and showed promising therapeutic effects in different malignant vascularised tumours (Chang et al., 2015; Hulsurkar et al., 2017; Sloan et al., 2010). However, the cross-talk mechanisms between VEGFR2 and the class A GPCRs adenosine receptors and β_2-adrenoceptors are not well understood.

This project was focused on the investigation of potential VEGFR2-GPCR oligomerisation using a proximity-based methodology, bioluminescence resonance energy transfer (BRET) with the super bright luciferase NanoLuc (therefore denominated as NanoBRET).

1.7. NanoBRET to probe ligand-receptor and receptor-receptor interactions

1.7.1. NanoBRET to investigate ligand-receptor binding pharmacology

When developing a new drug, pharmacological properties such as strength (affinity), duration (k_{on} and k_{off}) and specificity of the binding of that drug to a desired receptor, are important parameters to be measured (Kenakin, 2017). NanoBRET technology has been applied with great success in our lab, and now by other groups, to measure real-time ligand-receptor binding kinetics in whole living cells, using a combination of fluorescently-labelled and unlabelled ligands (Stoddart et al., 2015a, 2018). For these experiments, the receptor is fused at the N-terminus with NanoLuc luciferase (BRET donor), whereas fluorescently-labelled ligands act as BRET acceptors. NanoLuc (Nluc) luciferase is a small (19kDa) and very bright luminescent molecule, isolated and modified from the deep sea shrimp *Olophorus gracilirostris* (England et al., 2016; Hall et al., 2012). This luciferase covers a broad emission spectrum, bringing high sensitivity to reporter gene assays and other bioluminescent assays, including BRET (England et al., 2016). It uses a novel coelenterazine analogue, furimazine, as its substrate, which gets oxidised to form furimamide, resulting in an emission of a glow-type luminescence (Kim and Grailhe, 2016). Due to the fact that it is a secreted protein, Nluc luciferase can be positioned at the N-terminus of transmembrane receptors without effecting receptor trafficking to the cell surface (Stoddart et al., 2018).

NanoBRET technology has been successfully applied to investigate ligand-receptor binding pharmacology for different GPCRs including, the adenosine A_1 and A_3, adrenergic receptors β_1 and β_2, and the angiotensin receptor-1 (AT-1) (Soave et al., 2016; Stoddart et al., 2015a). More recently, this methodology was extended to study VEGFR2 and its co-receptor neuropilin-1 (NRP-1) pharmacology (Kilpatrick et al., 2017; Peach et al., 2018b; Stoddart et al., 2018).

Different live-cell NanoBRET assays are used to investigate ligand-receptor pharmacology including: saturation and competition assays, performed under equilibrium conditions to determine labelled and unlabelled ligands binding affinity (K_D or IC_{50}), respectively, and kinetics binding assay, performed under non-equilibrium conditions, to determine ligand association (k_{on}) and dissociation (k_{off}) rate constants (Kilpatrick et al., 2017; Peach et al., 2018b; Stoddart et al., 2018).

Methodologies that can monitor specific drug-receptor interactions in living animals are still lacking (Durham and Blanco, 2015). In this study was also proposed the application of NanoBRET to monitor drug-β_2-adrenoceptor engagement *in vivo*, using a pre-clinical model of breast cancer (Alcobia et al., 2018).

1.7.2. BRET to investigate GPCR-RTK oligomerisation

Most evidence supporting GPCR-RTK association is based on traditional biochemical approaches, such as co-immunoprecipitation (co-IP). These techniques were initially used to characterise GPCR-RTK interaction and function (Guo et al., 2017). However, the invasive nature of these approaches leads to the disruption of the cellular environment and, therefore, may not represent existent interactions, particularly for transient interactions (Briddon et al., 2008; Ellisdon and Halls, 2016).

Proximity-based biophysical approaches, such as Fluorescence or Bioluminescence resonance energy transfer (FRET/BRET) have been extensively applied in the GPCR field to investigate GPCR-GPCR interactions, and to better understand the protein-protein interactions occurring within the GPCR oligomer (Briddon et al., 2008; Gandía et al., 2008). BRET has been demonstrated to be a powerful biophysical tool to investigate direct GPCR-RTK associations in whole cells and at real-time (Borroto-Escuela et al., 2013b). In these studies, the investigation of receptor-receptor association was

performed using one receptor protomer fused at the C-terminal tail with a luciferase donor, typically renilla luciferase (Rluc), and the other protomer fused at its C-terminal with a fluorescent acceptor (i.e. green/yellow fluorescent proteins - GFP or YFP) (Borroto-Escuela et al., 2013b; Mandic et al., 2014; Mcgraw et al., 2006). Once these receptors are in close proximity (at a distance <10nm) and at the right orientation, the luminescent donor can excite the fluorescent acceptor, and receptor-receptor association is measured as BRET ratios (fluorescence acceptor emission divided by luminescent donor emission). The ratiometric property of BRET measurements allows protein-protein interactions to be determined using different expression levels of receptors, and is also independent on cell number (Stoddart et al., 2018). The advantage of BRET relative to FRET is that in BRET assays an external light source for donor excitation is not required, which minimises auto-fluorescence and/or photobleaching of the fluorophore (Siddiqui et al., 2013). BRET has also the advantage of the absence of light contamination, being able to detect smaller variations in BRET signals due to low background signal (Siddiqui et al., 2013).

As mentioned in the previous section, our lab has developed the NanoBRET-based system which uses the super bright and secreted NanoLuc luciferase to monitor specific ligand-receptor interactions (Stoddart et al., 2018). One of the aims of this project was to develop a NanoBRET-based assay to monitor receptor-receptor interactions and to investigate potential molecular association between VEGFR2 and the two class A GPCRs adenosine and β_2-adrenergic receptors.

1.8. Thesis Aims

The primary aim of this thesis was to investigate the molecular interactions between VEGFR2 and the two Class A GPCRs, adenosine receptors and β_2-adrenoceptors.

During this project the following key questions were addressed:

- Can NanoBRET be used as an approach to investigate ligand binding pharmacology for the human full-length VEGFR2, using a newly developed $VEGF_{165}$a homodimeric peptide fluorescent ligand?
- Can NanoBRET system be used to measure direct receptor-receptor interaction?
- Does cross-talk between VEGFR2 and the adenosine or β_2-adrenergic receptors occur via a mechanism involving VEGFR2-GPCR oligomerisation?
- Can NanoBRET be applied to measure ligand-receptor pharmacology in a physiologically relevant system (e.g. cancer cell model)?
- And finally, could NanoBRET be applied to monitor ligand-receptor engagement in living animals?

Chapter 2: Materials and Methods

2.1. Materials

i) Molecular Biology:

pcDNA3.1zeo(+) DNA vector and One Shot® Top 10F' chemically competent cells were purchased from Invitrogen (Paisley, UK). Restriction enzymes (BamHI, BglII, Xho I and XbaI), and respective buffers, T4 DNA ligase, Pfu DNA polymerase (and respective 10x buffer), 1kb DNA ladder, and Pureyield™ Plasmid Miniprep System were purchased from Promega (Southampton, UK). The forward (5'- CCAAGATCTCTGCCGCCCTCCATCTCAGC-3') and reverse (5'-TGGTCTAGACTAGTCATCAGGCCTCTCTTCTGG-3') oligonucleotide primers used for A_1R PCR reaction (lab catalogue number 57 and 58, respectively), and T7 forward (5'-TAATACGACTCACTATAGGG-3') and BGHR reverse (5'-TAGAAGGCACAGTCGAGG-3') primers used for pcDNA3.1 constructs sequencing, were all synthesised by Eurogentec (Southampton, UK). The GenElute™ gel extraction, PCR purification and miniprep and maxiprep kits were bought from Sigma Aldrich (Gillingham, UK). DNA sequencing was performed by the DNA sequencing laboratory, at School of Life Sciences, University of Nottingham (UK).

ii) Cell and animal models

HEK 293T cells were purchased from Invitrogen (Paisley, UK). HEK 293T cells stably expressing Nluc-VEGFR2 were a gift from Matt Roberts (Promega, Madison, WI). The highly metastatic variant of the MDA-MB-231 triple-negative human breast cell line (MDA-MB-231^{HM}; MDA-231) was a kind gift from Dr. Zhou Ou, Fudan University Shanghai Cancer Center (China) (Chang et al., 2016). A mouse low metastatic adenocarcinoma cell line (66cl4), was a gift from R. Anderson (Peter MacCallum Cancer Centre, Melbourne, Australia) (Pon et al., 2016). Female BALB/c nu/nu immune-compromised mice (7-week-old) were from University of Adelaide (Australia).

iii) Fluorescent and non-fluorescent ligands:

SNAP-Tag Surface substrate Alexa Fluor 647 (catalogue number S9137) and 488 (catalogue number S9129S) were purchased from New England Biolabs (Hitchen, UK). Halo-tag membrane impermeable Alexa F488 (catalogue number G1001) and AF660 (catalogue number G8471) were purchased from Promega (Southampton, UK). $VEGF_{165}a$ ligand was from R&D Systems. H33342, protease-free bovine serum albumin (BSA), and Isoproterenol hydrochloride (Isoprenaline) were from Sigma-Aldrich. NECA, MRS1220, DPCPX, PSB36, ICI 118551 hydrochloride and CGP12177) dihydrochloride and SCH58261 compounds were purchased from Tocris (Bristol, UK). CA200645 and propranolol-β-Ala-β-Ala-X-BODIPY630/650 were purchased from CellAura Technologies Ltd (Nottingham, UK). BODIPY-CGP12177-TMR was purchased from Molecular Probes (Oregon, USA). $VEGF_{165}a$-TMR ligand was a gift from Matt Robers (Promega Corporation, Madison, Wisconsin, USA).

iv) Other materials and reagents

Dulbecco's modified eagle's medium (DMEM), optimal minimum essential medium (Opti-MEM), Phosphate-buffered saline (PBS), blastocidin, ampicillin and G418 (neomycin) antibiotics were bought from Sigma-Aldrich, UK. Lipofectamine 2000 was purchased from Life Technologies, UK. All cell culture plasticware were bought from Fisher Scientific (Loughborough, UK). 5-Carboxy-tetramethylrhodamine N-succinimidyl ester (TAMRA, catalogue number 53048), 2-mercaptoethanol (2-ME, catalogue number M6250) and (-)-1,4-DITHIO-L-THREITOL (DTT, catalogue number D9760) were purchased from Sigma-Aldrich. Rhodamine 6G (R6G) and zeocin antibiotic were purchased from Invitrogen (Paisley, UK). Nano-Glo™Luciferase substrate (furimazine) was bought from Promega (UK or Australia)

2.2. Molecular biology

A summary of all constructs used is provided in Table 2.1. The lentiviral construct pSIN-IRES/BSD encoding β_2AR-Nluc or Nanobody-80-GFP (Nb-80-

GFP), were a gift from Dr. Alexander Kondrashov, Wolfson Centre for Stem Cells, Tissue Engineering & Modelling (STEM), Centre for Biomolecular Sciences, at the University of Nottingham, UK. The construct encoding β-arrestin2-Venus-YFP was a gift from Dr. Kevin D. G. Pfleger and Dr. Carl W. White, from University of Western Australia (Nedlands, Australia).

Table 2.1. Constructs used for the study.

Host vector	N or C-terminal tag	cDNA insert	Bacterial Resistance	Mammalian resistance	Construct made by:
pcDNA3.1(+)	empty	empty	Ampicillin	Zeocin	Invitrogen
pcDNA3.1(+)	N-terminal SNAP	empty	Ampicillin	Zeocin	*Alcobia D.C.
pcDNA3.1(+)	N-terminal SNAP	A_1R	Ampicillin	Zeocin	*Alcobia D.C.
pcDNA3.1(+)	N-terminal Nluc	A_1R	Ampicillin	G418	Stoddart L. (1)
pcDNA3.1(+)	N-terminal SNAP	$A_{2A}AR$	Ampicillin	G418	*Groenewoud N. J.
pcDNA3.1(+)	N-terminal Nluc	$A_{2A}AR$	Ampicillin	G418	
pcDNA3.1(+)	N-terminal SNAP	A_3R	Ampicillin	Zeocin	*Alcobia, DC
pcDNA3.1(+)	N-terminal Nluc	A_3R	Ampicillin	G418	*Stoddart L. (1)
pF-SNnk	N-terminal Nluc	VEGFR2	Kanamycin	G418	Promega (2)
pF-SNnk	C-terminal Nluc	VEGFR2	Ampicillin	G418	Promega
pFN21A	N-terminal Halo	VEGFR2	Ampicillin	G418	Promega (2)
pcDNA3.1(+)	N-terminal SNAP	β_2AR	Ampicillin	G418	*Soave M.
pF-SNnk	N-terminal Nluc	β_2AR	Ampicillin	G418	Promega (1)
pF-SNnk	C-terminal Nluc	β_2AR	Kanamycin	G418	Promega
pSIN-IRES	N-terminal Nluc	β_2AR	Ampicillin	Blastocidin	Kondrashov A.
pcDNA3	C-terminal-Venus-YFP	β-arrestin2	Ampicillin	G418	Pfleger K. D. G. (3)
pSIN-IRES	N-terminal-GFP	Nb-80	Ampicillin	Blastocidin	Kondrashov A.

*cDNA constructs made in our lab.

N or C-terminal – tag fused at the N or C-terminal of the receptor; SNAP – SNAP-Tag; Nluc – NanoLuc luciferase; Halo – Halo-Tag; cDNA – complementary DNA; Venus-YFP – variant of yellow fluorescent protein; GFP – green fluorescent protein; A_1R, $A_{2A}AR$, A_3R – Adenosine receptor A_1, $A_{2A}AR$ or A_3, respectively; β_2AR – β-adrenergic receptor 2; G428 – neomycin antibiotic.

(1) (Stoddart et al., 2015a)
(2) (Kilpatrick et al., 2017)
(3) (Kocan et al., 2008)

Here will be provided a detailed description of the generation of pcDNA3.1/zeocin constructs encoding SNAP-tag alone or fused in frame at the

N-terminus of adenosine A_1 or A_3 receptors. The initial strategy to investigate molecular interactions between adenosine receptor subtypes A_1 or A_3 and VEGFR2, was to stably co-transfect these receptors in a HEK 293T cell line. To enable selective co-selection of these receptors in these cells, the receptors had to be expressed from vectors with different antibiotic selection. N-terminal Nluc-VEGFR2 was generated by Promega in a pcDNA3.1/neo vector, which is resistant to neomycin (G418) in mammalian cells. Therefore, cDNA constructs encoding N-terminal-SNAP-tagged-A_1 or -A_3 receptors were generated in a pcDNA3.1/zeo vector, which has resistance to zeocin antibiotic in mammalian cells. SNAP-tag is a 20kDa mutated version of the human DNA repair protein O6-alkylguanine transferase (hAGT) that can covalently bind commercially available substrates with a fluorophore. We firstly generated a sigSNAP-pcDNA3.1/zeo construct to which we then ligated the adenosine A_1 or A_3-encoding DNA genes (*ADORA1* or *ADORA3* genes, respectively).

A schematic representation of the generation of a sigSNAP-pcDNA3.1/zeo, sigSNAP-A3-pcDNA3.1/zeo or sigSNAP-A1-pcDNA3.1/zeo constructs is represented in Figures 2.1 and 2.2. Detailed methodology of the different steps to generate these constructs will be provided in the following sections. Briefly, the sigSNAP-pcDNA3.1/zeo vector was generated after digestion of sigSNAP DNA region (by KpnI and BamHI restriction enzymes) from an available sigSNAP-A_3R-pcDNA3.1/neo construct (Stoddart et al., 2015a) (Figure 2.1.). The NEB cutter tool (New England BioLabs) was used to identify restriction enzymes to use for digestion of the SNAP-Tag DNA region (540bp, 180 amino acids). This tool was also used to determine restriction enzymes for A_1R and A_3R DNA region digestion. This sigSNAP region contains a start Kozac consensus sequence (sig) with an ATG initiation codon (GCACCATG), which facilitates initiation of SNAP-Tag translation. Restriction enzymes recognise and bind to a specific sequence of nucleotides (restriction site), cleaving the DNA into specific fragments. The digested sigSNAP region, as well as, digested pcDNA3.1/zeo vector were separated onto an agarose gel using electrophoresis and purified using a gel purification kit. The purified insert and vector were then ligated as

will be described below. The A_3R DNA region was then digested from the same initial sigSNAP-A3R-pcDNA3.1/neo construct (using BamHI and XhoI restriction enzymes), separated by gel electrophoresis, purified, and then ligated with digested sigSNAP-pcDNA3.1/zeo vector, generating the sigSNAP-A3R-pcDNA3.1/zeo cDNA construct (Figure 2.1.).

To generate the sigSNAP-A1R-pcDNA3.1\zeo construct, we used an available sigSNAP-A1R-pcDNA3.1\neo construct (made by Hanna Chilvers, a previous student from our lab) (Figure 2.2.). This construct had an initiation codon (methionine, ATG) between the SNAP-Tag region and the A_1R DNA region, which can result in the transcription and translation of SNAP-Tag or A_1 receptor proteins alone, instead of the full-length SNAP-tagged-A1 receptor protein. A polymerase chain reaction (PCR), was performed to replace the ATG codon for a leucine (CTG), as well as to incorporate BglII and XbaI restriction sites at the beginning and end of the A_1R DNA region, respectively. Since BglII and BamHI restriction enzymes form stretches of single-stranded DNA that are complementary to each other, the A_1R DNA insert could then be ligated with BamHI/XbaI digested sigSNAP-pcDNA3.1/zeo vector (Figure 2.2.). All these details will be provided in the following sections.

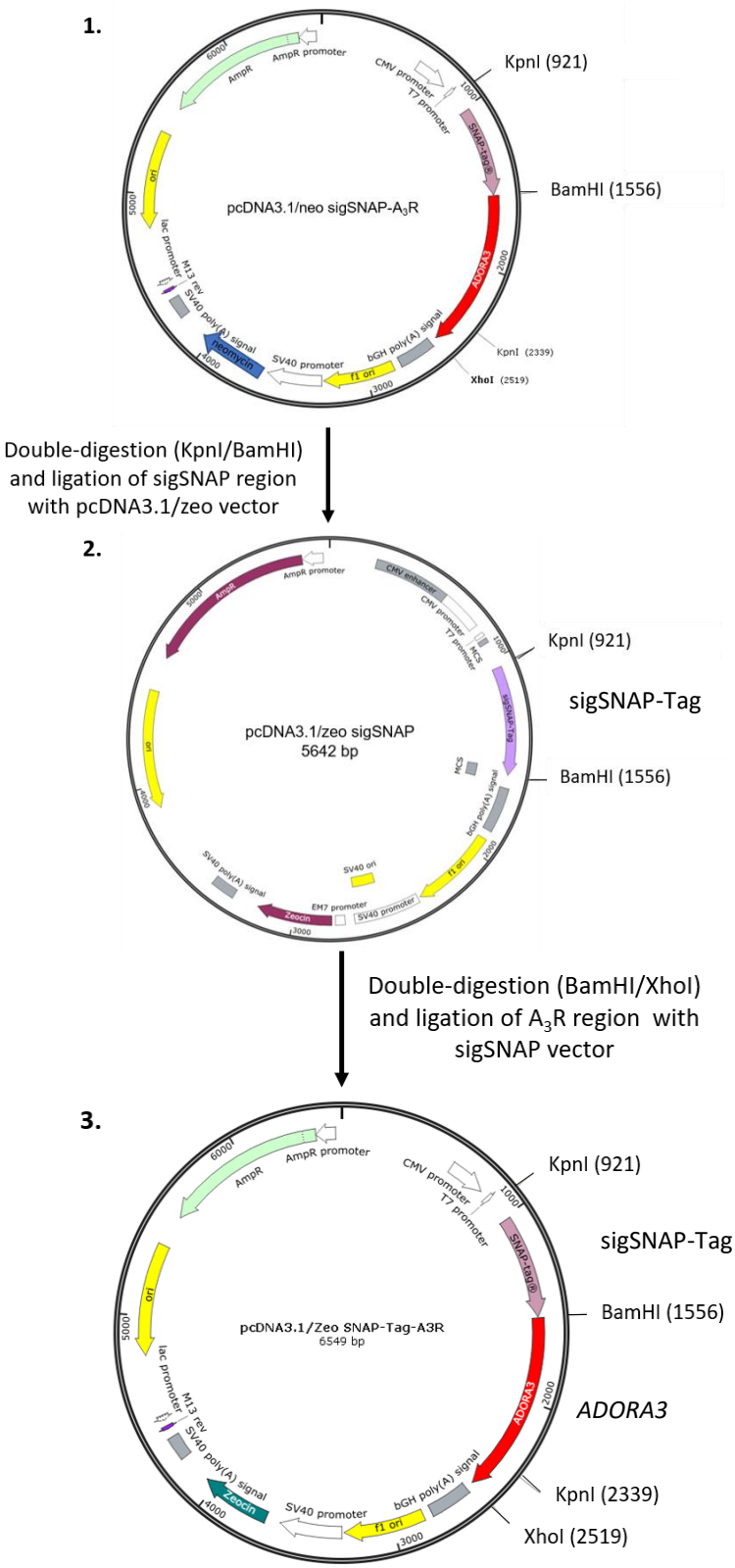

Figure 2.1. Schematic for generation of sigSNAP-A_3-pcDNA3.1/zeo cDNA construct (3). A sigSNAP-pcDNA3.1/zeo (2) was firstly generated after double-digestion of sigSNAP region, using KpnI/BamHI restriction enzymes (from an available sigSNAP-A3 pcDNA3.1/neo vector (1)), and ligated with a pcDNA3.1/zeo vector (previously digested using same enzymes). A_3R DNA region from vector (1) (digested by BamHI/XhoI) was then ligated to the sig-SNAP-pcDNA3.1/zeo vector (2) (digested by same enzymes).

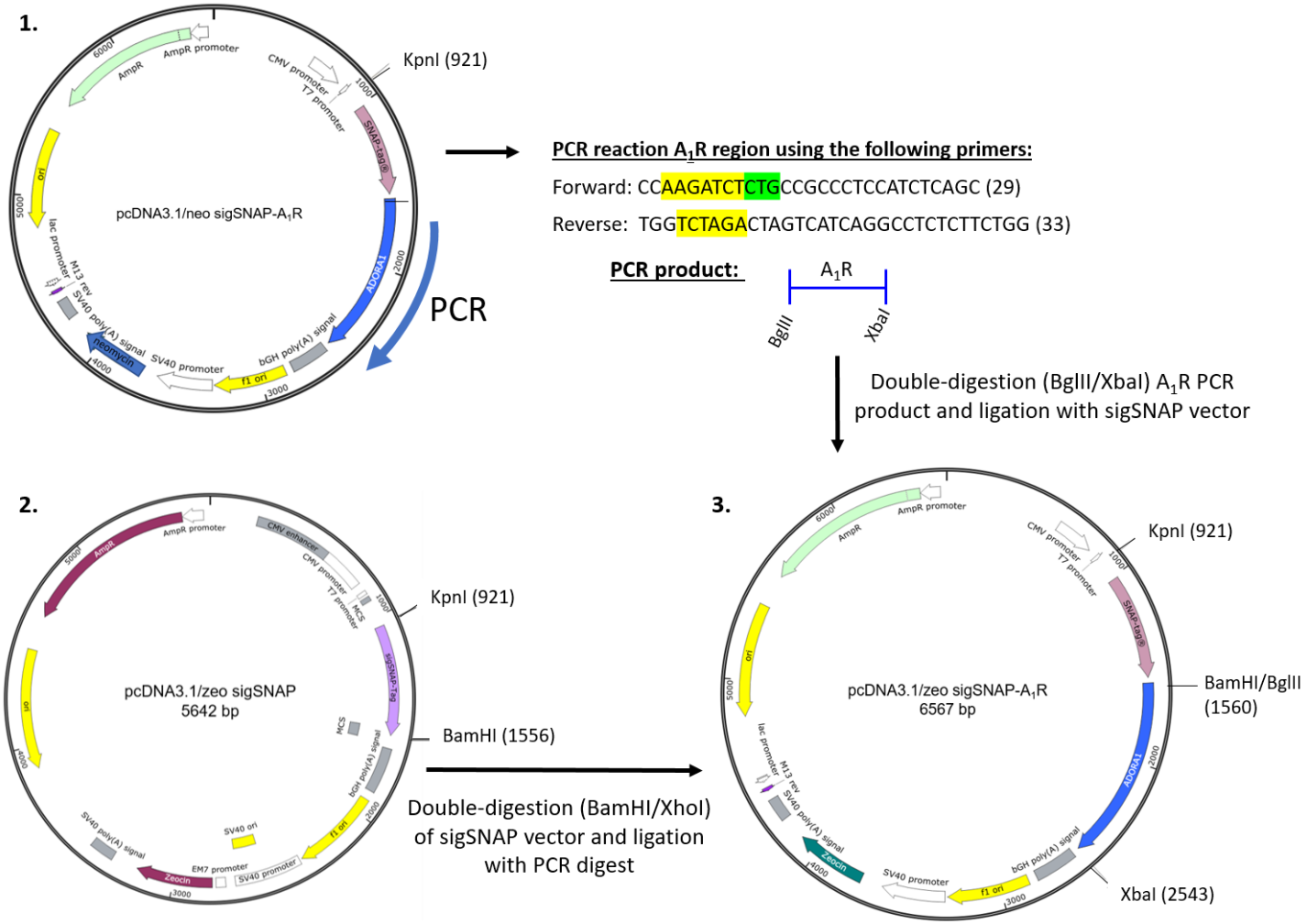

Figure 2.2. Schematic for generation of sigSNAP-A_1R pcDNA3.1/zeo cDNA construct (3). Firstly, we performed a PCR reaction to modify the A_1R region from an available sigSNAP-A_1R-pcDNA3.1/neo vector (1). The PCR reaction was performed to incorporate BglII and XbaI restriction sites (highlighted in yellow) to the beginning and end of the A_1R region, respectively, as well as, to replace an initiation codon (ATG) for a leucine (CTG, highlighted in green). PCR products were then digested using bglII and XbaI restriction enzymes and ligated with sig-SNAP-pcDNA3.1/zeo vector (2) (previously digested with BamHI/XbaI enzymes.

Digestion reactions

Restriction enzymes are used to cut DNA fragments into specific regions. In this study double digests were used, using two different restriction enzymes, to remove or to open specific DNA regions. The sigSNAP DNA region was digested using KpnI and BamHI restriction enzymes to ligate with a pcDNA3.1/zeo vector, digested using the same enzymes. The A_3R DNA region was digested using BamHI and XhoI restriction enzymes and ligated with the sigSNAP-pcDNA3.1/zeo vector, previously digested using the same enzymes. Finally, the A_1R DNA region, which was subcloned using PCR, was digested using BglII and XbaI enzymes, and ligated in a digested sigSNAP-pcDNA3.1/zeo vector, using BamHI and XbaI enzymes.

Digestion reactions were prepared in 0.5mL sterile eppendofs by adding 4µL of 10x buffer multicore (Promega; for KpnI/BamHI digest), or 4µL of 10x Buffer D (Promega; for BamHI/XhoI or BamHI/XbaI and BglII/XbaI digests), together with 1µL of each respective restriction enzyme and, 2µL DNA added immediately before reaction. Digestion reactions were incubated for 2h at 37^{o}C, followed by heat inactivation for 20min at 65^{o}C. Heat inactivation at 65^{o}C stops restriction endonucleases action, which have an optimal incubation temperature at 37^{o}C.

i) Gel Electrophoresis

Gel electrophoresis is a technique that applies an electric current to move and separate the DNA loaded on a gel matrix. DNA fragments with greater size move slower across the gel matrix, whereas lower size DNA moves faster through the gel. This technique was used to isolate the digested products (sigSNAP, A_3R and A_1R DNA regions, and digested vectors pcDNA3.1/zeo and sigSNAP-pcDNA3.1/zeo).

Agarose gel matrix was prepared by diluting 350mg agarose in 35mL 1xTAE buffer (diluted from 50x TAE buffer, containing 242g TRIS base, 100mL EDTA and 57.1mL acetic acid). The mixture was heated from 1min using a microwave

(~700W), and once it cooled down, but still in its liquid form, 3.5µL ethidium bromide was added and mixed. Ethidium bromide is a DNA intercalating agent that enables DNA visualisation under UV light. Liquid gel was placed in a proper recipient with a comb to generate wells where DNA would be loaded. DNA samples were prepared by mixing 40µL DNA with 8µL 6x sample buffer (Promega). Sample buffer contains glycerol to increase DNA density, and bromophenol blue to enable sample visualisation when loading the DNA into the gel matrix wells. 10µL 1kb DNA ladder (Promega), which is a molecular weight marker, was also loaded in the gel alongside the loaded DNA samples, to visualise DNA fragment size. Samples were run on the agarose gel using a horizontal electrophoresis Bio-Rad system at 80V for 30min. Gel containing the separated DNA bands was visualised under UV light, and bands were quickly excised to avoid DNA damage due to UV light. DNA present in those bands was then purified using a GenElute^{TM} Clean-Up kit, following manufacturer's instructions. In Figure 2.3. are displayed pictures of the different gels after extraction of digested DNA bands for (a) sigSNAP DNA region (540bp), (b) A3R DNA region (957bp), pcDNA3.1/zeo vector (5015bp), and (c) A1R PCR product (978bp). Unfortunately, pictures were only taken after band extraction, observed bands were bright and showed expected molecular size.

Gel extracted DNA inserts and respective vectors were then purified, ligated and transformed in E.coli competent cells, as will be described in the following sections. To confirm presence of inserts in transformed bacteria, purified DNA extracted from different bacteria colonies was digested using respective restriction enzymes. For this purpose, lower DNA amounts were used. DNA samples were prepared in 0.5mL sterile microcentrifuge tubes containing 12µL digested DNA mixed with 2µL sample buffer, which were loaded in 1% agarose gel, together with 1kb ladder loaded alongside DNA samples. DNA was then separated by electrophoresis (at 100V, 20min,) and visualised under UV light.

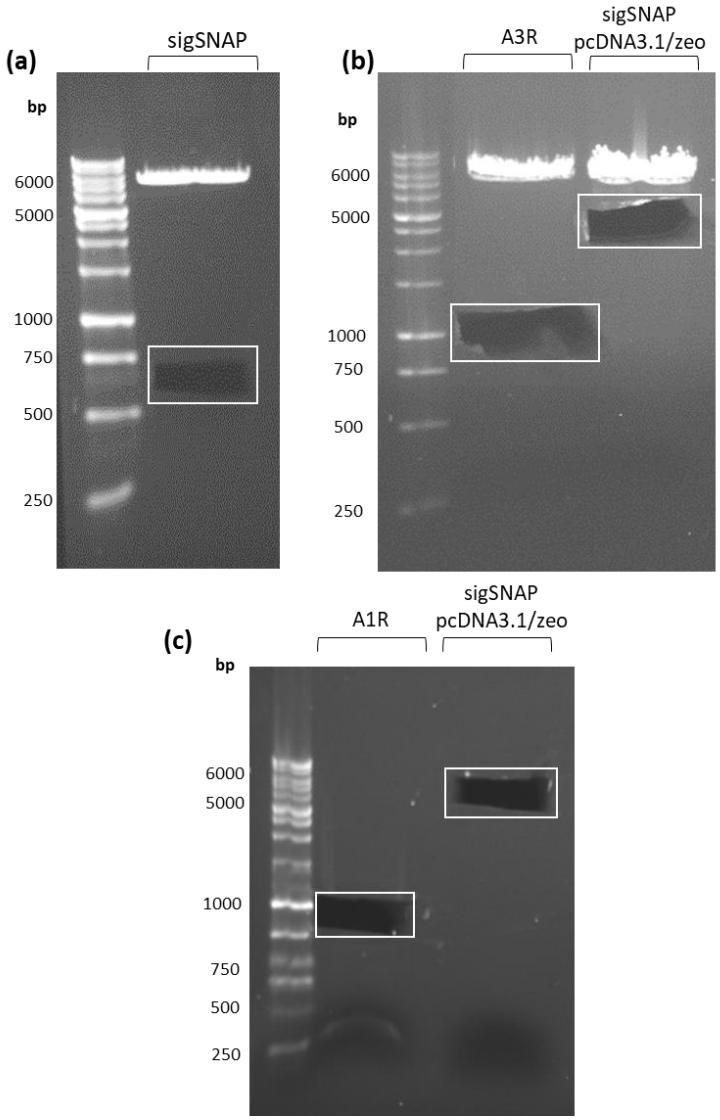

Figure 2.3. Pictures of electrophoresis agarose gels after band excision. (a) sigSNAP DNA fragment was separated by electrophoresis after digestion of sigSNAP-pcDNA3.1/neo vector using KpnI and BamHI restriction enzymes. **(b)** digested A_3R DNA region, from a sigSNAP-A3-pcDNA3.1/neo vector, and sigSNAP-pcDNA3.1/zeo, using BamHI and XhoI restriction enzymes. And **(c)** digested A_1R DNA region (by BglII/XbaI restriction enzymes) after PCR, using sigSNAP-A1-pcDNA3.1/neo vector as PCR DNA template. On the right of this gel picture is an excised band with digested sigSNAP-pcDNA3.1/zeo with BamHI and XbaI restriction enzymes. Band size in base pairs (bp) was determined using a 1kb ladder. Gel was run at 80V for 30min. Bands were visualised and excised using a small blade while under UV light.

ii) Ligation

Ligation reactions were performed to ligate digested sigSNAP DNA region in digested pcDNA3.1/zeo vector, and digested A_3R or A_1R DNA regions in digested sigSNAP-pcDNA3.1/zeo vector (Figures 2.1. and 2.2.). Ligation reactions were prepared in 0.5mL sterile microcentrifuge tubes by adding 1µL ligase buffer (Promega), 7µL DNA insert (or 7µL double distilled H_2O in negative control), 1µL vector and 1µL T4 DNA ligase (Promega). These were incubated overnight for 16h at 16^oC. Negative control containing vector and no insert was used to check for re-ligation of vector without the insert.

iii) Polymerase chain reaction

As mentioned earlier, sigSNAP-A_1R-pcDNA3.1/zeo vector was generated from an available sigSNAP-A1R-pcDNA3.1/neo vector made in our lab. Polymerase chain reaction (PCR) is a technique used to amplify a single copy of DNA strand by several orders of magnitude. PCR was performed using the forward and reverse primers displayed in Table 2.2. These primers were used to change a methionine (ATG) start codon to a leucine (CTG), as well as, to incorporate BglII and XbaI restriction sites at each far end of the A_1R DNA region. These primers are complementary to each of the ends of the sequence to be amplified.

Table 2.2. Sequences of the forward and reverse primers used in the polymerase chain reaction and respective melting temperatures (Tm). These primers were used to incorporate BglII (forward primer) and XbaI restriction site (reverse primer) at each far end of the A_1R coding region (highlighted in yellow). Forward primer also replaced the start codon (ATG) for a CTG codon (highlighted in green).

Primers	Sequence (5'-3')	Tm (^oC)
Forward (57)	CCAAGATCTCTGCCGCCCTCCATCTCAGC (29)	62.1

Reverse (58)	TGGTCTAGACTAGTCATCAGGCCTCTCTTCTGG (33)	60.6

Five different PCR reactions were prepared in sterile 0.2 mL single thin wall PCR tubes, to which were added 5µL 10x Reaction Buffer, 5µL deoxyribonucleotides triphosphate (dNTPs), 1µL of forward and reverse primers, 0.5µL of cDNA (or double-distilled water (ddH_2O) in negative control), and 1µL of Pfu DNA polymerase was added only at the end before reaction. ddH_2O was also added for a final volume of 50µL per reaction. Negative control without DNA was used to check for contamination with foreign DNA. DNA was diluted to a final concentration of 100ng/µL and primers were diluted using a 1:2 dilution in ddH_2O, for a final 1:50 dilution in reaction. PCR programme used is indicated in Table 2.3. The first PCR step was an initial denaturation of DNA template at 95°C, for 5min, to separate the double-stranded DNA. This was followed by 29 cycles of denaturing, annealing of complementary primers (using calculated annealing temperature at 55°C), followed by primer extension (elongation), to amplify generated DNA strand into multiple copies. The last step was the final elongation for 10min at 72°C. DNA was then stored at 4°C.

Table 2.3. Programme used for polymerase chain reaction (PCR). PCR reaction was performed *using a* Master gradient thermo-cycler (Eppendorf).

Number of cycles	Stage	T (°C)	Time (min.)
1	Initial denaturing	95	5
29	Denaturing	95	1
	Annealing	55	1
	Elongation	72	3
1	Final elongation	72	10

iv) Transformation in E.coli competent cells

DNA ligations of sigSNAP-A_1R or -A_3R in sigSNAP-pcDNA3.1/zeo vector were transformed in E.coli competent Top10F' cells. Negative control ligation, containing vector with no insert, was also transformed in these cells.

Firstly, agar plates were prepared using 35g/L Luria-Bertani (LB) broth with agar (Lennox) diluted in ddH_2O and autoclaved. Once LB agar decreased temperature to around 37^oC, 50µg/mL ampicillin selection antibiotic was added, and agar was poured into Petri dishes to solidify. These were then used or stored at 4^oC. 20g/L LB broth without agar was also prepared in ddH_2O, autoclaved and stored at room temperature.

For competent cells transformation, 25µL Top10F' cells were added in 0.5µL sterile microcentrifuge tubes together with 1µL ligated DNA (sigSNAP-pcDNA3.1/zeo, sigSNAP-A_1R-pcDNA3.1/zeo or sig-A_3R-pcDNA3.1/zeo vectors), or negative control ligation. The microcentrifuge tubes were then incubated on ice for 30min, followed by heat shock at 42^oC for 30sec, and incubated on ice for 2min. Competent E.coli cells have the capacity to incorporate and replicate high molecular weight exogenous DNA. The 30min incubation on ice allows the bacterial membrane to stabilize, while the heat shock changes the fluidity of the bacterial membrane allowing the incorporation of the exogenous DNA. After incubation on ice, 250µL of LB broth was added to microcentrifuge tubes containing transformed bacteria and incubated under agitation for 1h, at 37^oC. This incubation allows the transformed bacteria to replicate. After incubation, 200µL of transformed bacteria (with DNA ligation or ligation negative control), were spread, using a plate spreader, onto different agar plates. Agar plates with bacteria were incubated upside down overnight, at 37^oC. On the following day, random individual colonies were picked and placed in different universals containing 5mL LB broth with 5µL ampicillin (50 µg/mL). Universals were incubated at 37^oC under agitation overnight. On the next day, bacterial DNA was isolated and purified using GenElute^{TM} HP Plasmid miniprep system, following manufacturer's instructions.

To confirm successful ligation of insert and vector in the different DNA minipreps, these were digested using restriction enzymes. The sigSNAP DNA region in pcDNA3.1/zeo vector was confirmed after digestion with kpnI/BamHI restriction enzymes, to confirm the presence of A_3R DNA region in sigSNAP-pcDNA3.1/zeo vector, BamHI/XhoI enzymes were used, whereas, for sigSNAP-A_1R DNA region in pcDNA3.1/zeo vector, digestion was performed using KpnI and XbaI restriction enzymes. The digested DNA was then run on an agarose gel, using electrophoresis, and visualised under UV light. Figure 2.4. displays pictures of the different gels for screening of DNA minipreps for (a) sigSNAP-pcDNA3.1/zeo, (b) sigSNAP-A_3R-pcDNA3.1/zeo and (c) sigSNAP-A_1R-pcDNA3.1/zeo. Colonies positive for insert (indicated with a white square in Figure 2.4.a and 2.4.b, or with an arrow in Figure 2.4.c were sent for sequencing to confirm correct DNA sequence.

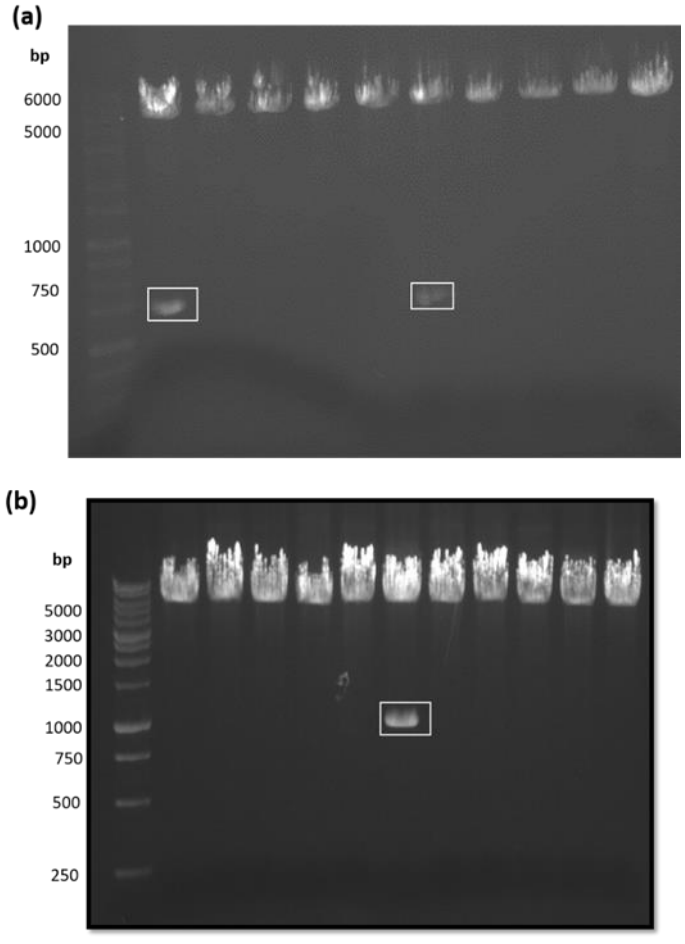

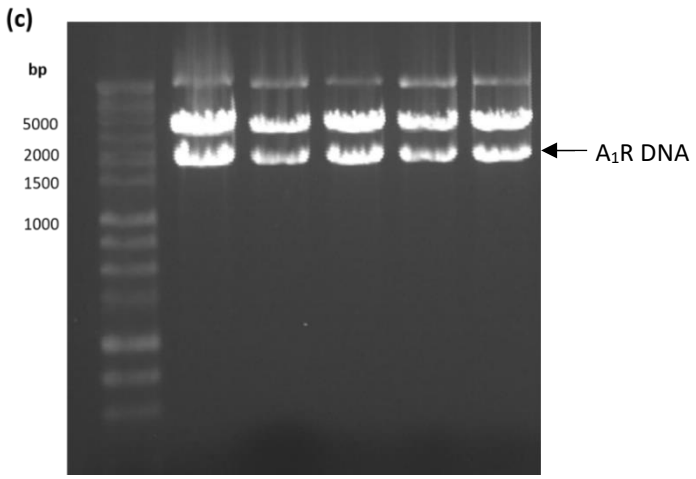

Figure 2.4. Pictures of agarose gels to confirm successful ligation. (a) DNA minipreps of transformed colonies with sigSNAP-pcDNA3.1/zeo ligation, were digested using kpnI/BamHI enzymes and ran on a gel. Two out of ten colonies contained sigSNAP DNA (white square, 540bp). These were sent for sequencing **(b)** DNA minipreps of transformed colonies with sigSNAP-A_3R-pcDNA3.1/zeo ligation, were digested using BamHI/XhoI enzymes and ran on a gel. One out of eleven colonies contained A_3R DNA (white square, 957bp). Finally, **(c)** DNA minipreps of transformed colonies with sigSNAP-A_1R-pcDNA3.1/zeo ligation, were digested using kpnI/BglII enzymes and ran on a gel. All of the colonies contained sigSNAP-A_1R DNA insert (1621bp), and only two DNA minipreps were chosen for sequencing.

v) DNA Sequencing

The concentration of DNA minipreps, containing the insert, was measured using a NanoDrop™ 2000 spectrophotometer (Thermo-Fisher). DNA was diluted to a final concentration of 100ng/µL in ddH_2O, and 20µL were sent for sequencing. Sequencing was performed by the DNA sequencing laboratory, at School of Life Sciences, University of Nottingham (UK), using the forward and reverse primers displayed in Table 2.4.

Sequencing results were analysed using the SnapGene® Viewer 2.5, to confirm the correct open reading frame and the presence of an initiation and stop

codon (see sequencing results in Appendix 1). The presence of a leucine CTG, instead of an initiation codon between the SNAP-Tag and A_1 or A_3 receptor-encoding regions was also confirmed. Sequence alignment was performed using the NCBI Blast® tool, to confirm presence of desired genes.

Table 2.4. Primers used for sequencing.

Primers	Sequence (5'-3')
Forward (T7)	TAATACGACTCACTATAGGG (20)
Reverse (BGH)	TAGAAGGCACAGTCGAGG (18)

2.3. Cell culture

Human Embryonic kidney 293T (HEK 293T) cells were used for most *in vitro* studies. A human highly metastatic (triple-negative) adenocarcinoma cancer parental cell line (MDA-231), or stably transfected to express N-terminally-tagged-Nluc-β_2-adrenoceptor (MDA-231 Nluc-β_2AR) were used for *in vitro* pharmacological characterisation (shown in Chapter 4), and MDA-231 Nluc-β_2AR cell line was also used for *in vivo* studies (showed in Chapter 6). A mouse low metastatic adenocarcinoma cell line (66cl4) was stably transfected to express N-terminally-tagged Nluc-β_2-adrenoceptor and pharmacologically characterised using *in vitro* studies (showed in Chapter 4). In Table 2.5. are the growth media used for the different cell lines used.

Table 2.5. Condition media used for the different cell lines

Cell line	Condition media supplemented with 10% fetal bovine serum (FBS)	Catalogue number and Supplier (UK)
HEK 293T	Dulbecco's modified Eagle's medium (DMEM), containing glutamine	(D6429) Sigma-Aldrich, UK
MDA-231	Dulbecco's modified Eagle's medium (DMEM) Glutamax	(10569010) Thermo Fisher, UK
66cl4	Minimum essential medium (MEM) alpha	(12571063) Thermo Fisher, UK

Cells were passaged at around 80% confluency to avoid cell stress and cell detachment. The media was firstly removed and 1mL Phosphate buffered saline (PBS) was used to wash any residual fetal bovine serum (FBS), which deactivates trypsin. Cells were then detached from flask using 1mL trypsin (0.25% w/v). Trypsin is a serine protease that acts by hydrolysing proteins involved in cell adherence, facilitating cell detachment from the culture flask. 10mL of culture medium (Table 2.5.) was then added to collect detached cells and these were centrifuged for 5min at 1000rpm. Cells were then resuspended in 10mL media and passaged to a new T75 flask using the required dilution ratio, typically 1:5 to 1:20 ratios. For experiments, 100µL cell suspension was placed onto a haemocytometer and the number of cells, within a 1mm^2 area, was counted (25x0.04mm^2 squares). The average number of cells was multiplied by 10000 to calculate the number of cells present in 1mL. This cell suspension was then resuspended in an appropriate amount of media to give the required cell density. Prior to seeding of HEK 293T cells into 96-well plates, these were coated with poly-D-lysine (10µg/mL in ddH_2O, filter sterilised using 0.2µm filter and a 20mL syringe). Poly-D-lysine was left for 20min and washed with PBS before seeding the cells.

2.3.1. Generation of new stable or transient cell lines

HEK 293T cells were stably transfected with a SNAP-A_1R or SNAP-A_3R pcDNA3.1 cDNA construct, earlier described in this chapter, using Lipofectamine 2000 (Life Technologies, UK) transfection reagent. Before transfection, cells were seeded into T25 flasks until 80-90% confluency. Lipofectamine 2000 was used following manufacturer's instructions. 48h after transfection, 250µg/mL zeocin antibiotic was added to T25 containing cells for colonies selection. Media containing antibiotic was replaced every 2/3 days until there was aconsiderable amount of cell death. Once small colonies started to be observed, zeocin concentration was reduced to 25µg/mL for selection maintenance.

Human triple-negative MDA-MB-231^{HM} and mouse low metastatic 66cl4 adenocarcinoma cells, were stably transfected with the lentiviral construct pSIN-IRES-Nluc-β_2AR (Table 2.1.). Cells were seeded into T25 flasks, until 80-90% confluency and stably transfected using Fugene HD reagent, following manufacturer's instructions. 48h after transfection, 20 μg/mL blasticidin (Invitrogen, UK) were added for selection, and media containing antibiotic was replaced every 2/3 days. After a considerable amount of cell death, and when colonies started to be observed, the concentration of antibiotic for selection was reduced to 5 μg/mL.

HEK 293T were also stably transfected with the lentiviral construct pSIN-IRES-Nb-80-GFP (Table 2.1.) using Fugene, as previously described.

Transiently transfected HEK 293T cells were used for some receptor-ligand binding studies, and for all receptor-receptor interaction studies (in Chapters 4 and 5). Before transient transfection, HEK 293T cells were seeded, at 12000 cells/well, into poly-D-lysine coated Greiner white U-bottom 96 well plates (Thermo Scientific, UK), and left overnight at 37^{o}C/5%CO_2. On the next day, cells were transiently transfected with Fugene reagent, using a 3:1 Fugene:cDNA ratio. The amounts of cDNA used are described later in NanoBRET assays section 2.5.

Generated cell lines, at different cell passages, were frozen down and placed into liquid nitrogen for long-term storage. For freezing down the cells, these were resuspended in 1mL FBS serum supplemented with 10% dimethyl sulfoxide (DMSO) and placed in cryovials. The cryovials were placed in a Mr Frosty^{TM} (Thermo-Fisher), containing 100% Isopropyl alcohol, which allows the slow freezing process of the cells, avoiding membrane disruption and cell death. These containers were placed in a freezer at -80^{o}C, before long-term storage of the cryovials in liquid nitrogen at -180^{o}C.

2.4. Fluorescence Correlation Spectroscopy (FCS)

Fluorescence Correlation Spectroscopy (FCS) is a single-photon counting technique that is highly sensitive to detect small changes in fluorescence intensity (Gherbi et al., 2018). This high sensitivity is achieved due to the generation of a small Gaussian-shaped detection volume (~0.25 fl) where these intensity fluorescence fluctuations are measured at a sub-microsecond temporal resolution (Briddon and Hill, 2007). This small detection volume is created by focusing a laser to a diffraction limited spot, using a high aperture number objective, which creates lateral resolution, and a fixed confocal pinhole of one Airy unit, creating axis resolution (Briddon et al., 2010). As a simple explanation, fluorescently-labelled molecules in solution can freely diffuse in and out of the detection volume, due to Brownian motions (Figure 2.5.a). When fluctuating molecules cross the small detection volume, these are excited by a laser, at a specific wavelength, and fluctuations in fluorescence intensity can be recorded in a time-correlated manner. The autocorrelation curve (Figure 2.5.c) is derived from an autocorrelation function (Figure 2.5.b), which is explained in further detail in the FCS analysis section 2.4.4. from this chapter.

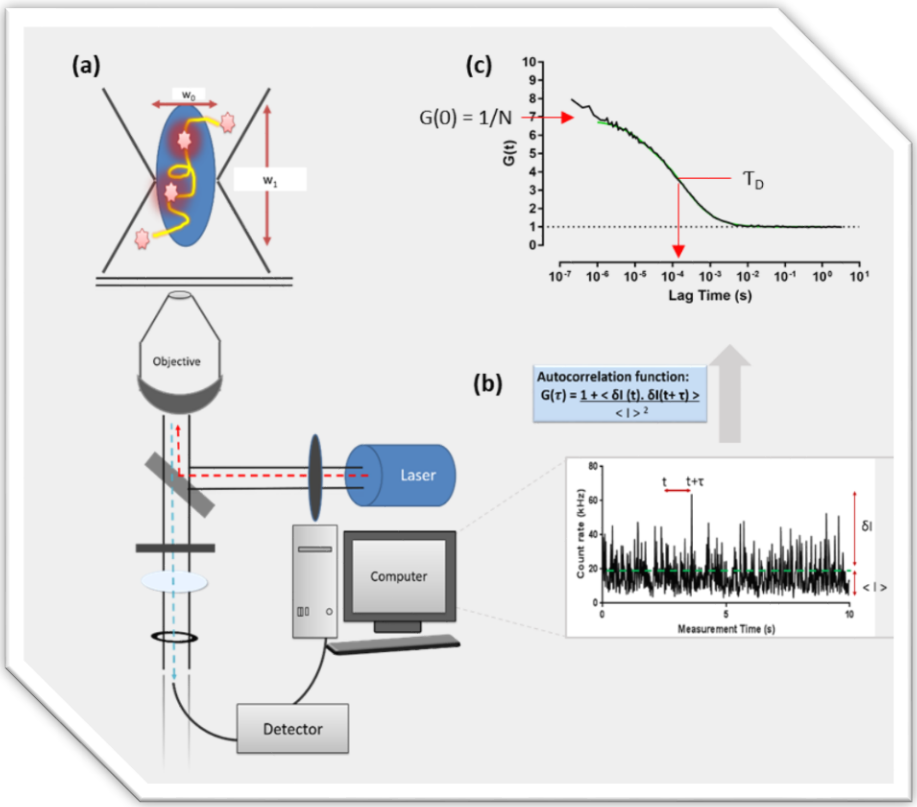

Figure 2.5. Schematic representation of the basic components of a single-channel FCS microscope. (a) Example of fluctuations in intensity recorded during a typical FCS experiment, in a small gaussian-shaped confocal volume, and microscope set up, with measurements in fluorescence intensity. **(c)** General form of the autocorrelation function G(t), which is obtained using the autocorrelation function shown in the blue box **(b)**. w_0 is the waist of the confocal volume and w_1 is the height of the detection volume; G(0) is the autocorrelation function at time zero seconds; N is the average particle number; τ_D is the diffusion time or dwell time; finally, I is intensity.

FCS was used in this study to investigate the concentration in solution and the homodimeric structure of a fluorescently-labelled vascular endothelial growth factor ligand, $VEGF_{165}$a-TMR, (Kilpatrick et al., 2017) in Chapter 3. For these experiments, a LSM510 NLO Confocor 3 fluorescent microscope fitted with a c-Apochromat 40x NA 1.2 water immersion objective lens (Zeiss, Germany) was used.

2.4.1. Calibration

In FCS measurements, calibration is a necessary task which enables the determination of the Gaussian-shaped confocal detection volume, as well as the structural parameter (SP), which are determined using a reference dye (rhodamine-6G, or R6G) (Briddon and Hill, 2007). This step is a pre-requisite to determine correct diffusion coefficients and particle number, which are then used to calculate the concentration of fluorescence species (see FCS analysis section 2.4.4. from this chapter for further details)

Calibration was performed using Rhodamine 6G (R6G), which has a diffusion coefficient described in the literature as D_{R6G}= 2.8x$10^{-10}$$m^2s^{-1}$ (Briddon et al., 2010). R6G dilutions at 1µM and 20nM were prepared from a 1mM R6G stock, previously diluted in 100% ethanol. These were diluted in fluorescent-free high-performance liquid chromatography (HPLC)-grade water (Chromasolv®; Sigma- Aldrich,UK) to avoid background fluorescence. 200µL of 1µM and 20nM R6G dilutions were placed in a coverglass 8 well-plate (Nunc Lab-Tek, Thermo Fisher Scientific, UK) which is scratch and distortion free. The plate was placed on the microscope stage and centred on the well containing the 1µM R6G dilution.

A reflection beampath was used to position the detection volume into the calibration volume. The reflected laser light from the top surface of the coverslip was used to determine the focal position in z plane. Once reflection was found, the focal position was set 200µm upwards into the solution. This z plane position 200µm above well cover-glass at was used for all measurements.

An Argon laser set to 50% output and a diode-pumped solid state (DPSS) 561-10 laser line (with excitation at 556-566 nm) were used for calibration with 1µM and 20nM R6G. Pinhole diameter was set to one Airy unit. A 488 laser line beampath (with a 580nm longpass emission filter) was firstly selected for calibration procedure, using 1µM R6G. This calibration is a necessary step for optimization of pinhole and system alignment. The laser power was adjusted to obtain a count rate of 250KHz, with Acousto-optic tunable filters (AOTF) set

to 1. The pinhole position was also optimised in the x and y planes, and correction collar was adjusted to ensure maximal count rate. The optimization of system alignment and count rate will give a best indication of good signal to noise (S:N) for the system.

The objective was then positioned under the well containing 20nM R6G solution, and the laser power was adjusted to obtain ~100 counts per molecule (CPM). 10 consecutive 10 second reads were taken to obtain autocorrelation curves and respective parameters, including count rate (CR), counts per molecule (CPM), diffusion coefficient (D) and particle number (N). Autocorrelation parameters were recorded for each experiment.

The same measurements were taken using the 561nm laser line beampath. This beampath was used in calibration with R6G because it corresponds to the excitation and emission wavelengths of the fluorophore used in this study, a Tetramethyl-rhodamine fluorophore (TMR) with $\lambda_{excitation}$=543nm and $\lambda_{emission}$=578nm. 10x10 seconds reads were taken using maximum laser power (100%) and AOTF at 100. Autocorrelation parameters obtained using this laser line were used to calculate confocal volume and described in FCS data analysis section 2.4.4. below.

1x60sec measurements were also taken using the fluorescent fluorophore 5-carboxy-tetramethylrhodamine N-succinimidyl ester (TAMRA, Sigma-Aldrich) diluted at 10nM in fluorescent-free high-performance liquid chromatography (HPLC)-grade water. These TAMRA FCS readings were used to determine the first order correction used in the photon counting histogram (PCH) analysis, explained below in data analysis section 2.4.4.).

For laser power optimisation, single measurements of $VEGF_{165}$a-TMR at 2nM and 10nM concentrations, prepared in HBSS buffer without BSA were taken, using a range of increasing laser powers (Figure 2.6.). Laser power optimisation is essential to avoid spot photobleaching of the fluorophore, and to guaranty a

signal strong enough to achieve good signal to noise. The laser power used for all experiments was 20%, corresponding to 0.394 kW/cm^2.

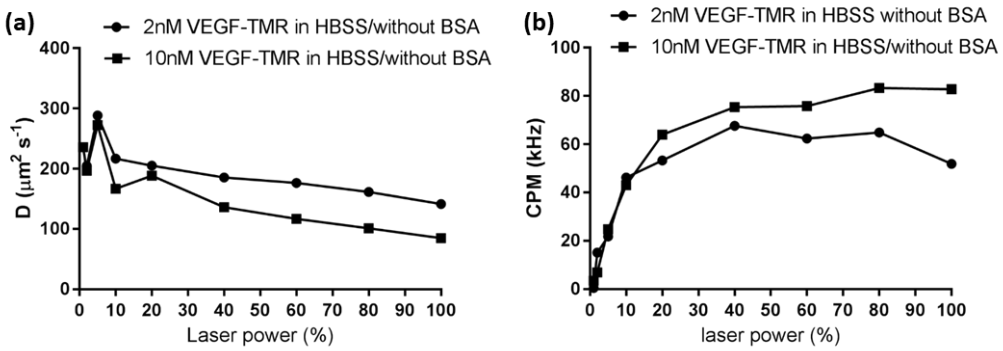

Figure 2.6. FCS laser power optimisation. 2nM and 10nM of $VEGF_{165}$a-TMR in HBSS buffer without BSA were used to identify optimal laser power, that would provide the best signal to noise (S:N) for the experiments. These solutions were prepared on 8-well coverglass chambers and immediately placed on the stage of a Zeiss LSM510 NLO Confocor 3, at 22^{o}C, to record fluctuations in fluorescence intensity, in a small confocal volume. Using autocorrelation analysis, (a) diffusion coefficient and (b) counts per molecule (CPM) data were collected. These are representative data from three independent experiments.

2.4.2. Solution-based experiments using $VEGF_{165}$a-TMR and TAMRA fluorescent ligands

Solution-based experiments were performed using $VEGF_{165}$a-TMR, which was synthesised as a dimer formed by two $VEGF_{165a}$ molecules and each molecule containing a tetramethyl-rhodamine (TMR) fluorophore (see Kilpatrick *et al.*, 2017 for synthesis details). For autocorrelation and PCH analysis, a range of $VEGF_{165}$a-TMR fluorescent ligand concentrations (1.25 - 10nM) were prepared in physiological solution using 1x HEPES's Buffered Salt Solution (HBSS; 25mM HEPES, 10mM glucose, 146mM NaCl, 5mM KCl, 1mM $MgSO_4$, 2mM sodium pyruvate, 1.3mM $CaCl_2$; pH 7.45), supplemented with 1.8g/L glucose, with or without 0.1% protease-free bovine serum albumin (0.1% BSA, Sigma-Aldrich, UK). 200μL of each dilution was added to Nunc Labtech 8-well chambered coverglass (Thermo Fisher, UK). $VEGF_{165}$a-TMR dilutions without BSA in solution were added to one plate, and dilutions in vehicle containing BSA were added to a different plate. The aliquots were only prepared and added to the

plate right before the confocal readings, to minimise binding of fluorescent ligand to plastic and glass in microcentrifuge tubes and plate. Plates were read using the 561m laser line beampath, with the laser power set to 20% (AOTF=10), corresponding to 0.394 kW/cm^2. The row to row scanning setting was selected, with 7 repetitions of 2 counts per 10sec reads, corresponding to a total scanning time of 21 min, at 22^{o}C. 10x10 second reads were taken using a range of laser powers (1-100%) for laser power optimisation, to identify optimal laser power.

Solution-based experiments were also performed using TAMRA fluorophore (5-Carboxy-tetramethylrhodamine N-succimidyl ester, Sigma-Aldrich, UK), which was used a control to confirm the dimeric and double-labelling structure of the $VEGF_{165}$a-TMR ligand. The technique was executed as described earlier for the $VEGF_{165}$a-TMR ligand readings, using the same concentration range and FCS settings. 10x10sec reads, using different laser powers, were also taken to verify optimal laser power.

2.4.3. Solution-based experiments using $VEGF_{165}$a-TMR ligand treated with the reducing agents 2-mercaptoethanol (2-ME) or dithiothreitol (DTT)

FCS experiments were performed using the same range of $VEGF_{165}$a-TMR ligand as mentioned earlier. $VEGF_{165}$a-TMR aliquots were prepared in HBSS buffer, containing 0.1% BSA and either 1mM 2-mercaptoethanol (2-ME; M3148, Sigma-Aldrich), or 1nM or 10mM dithiotreitol (DTT; (-)-1,4-DITHIO-L-THREITOL, Sigma-Aldrich), and incubated for 30min., at 37^{o}C, before readings. Both 2-ME and DTT are potent reducing agents that reduce disulphide bonds that are formed between thiol groups of cysteine residues in proteins (Chang, 1997). These reducing agents were used to separate the two $VEGF_{165}$a molecules that form the $VEGF_{165}$a-TMR homodimer, which would theoretically result in the separation of TMR fluorophores initially bound at the end of each $VEGF_{165}$a molecule. Experiments were performed using the same settings and conditions mentioned in previous sections.

2.4.4. FCS Data Analysis

i) Autocorrelation analysis

Autocorrelation analysis, which measures fluctuations in fluorescence intensity in a time-correlated manner, was performed using the Zeiss Zen2010 software (Jena, Germany).

Emitted fluorescence within the confocal detection volume were captured by the objective, passed through a dichroic mirror (using an appropriate band pass filter) and recorded over-time. These recordings were then analysed using the Zeiss Zen2010 software to calculate the autocorrelation function G(τ), which represents the time dependence decay in fluorescence fluctuation intensity using the equation 1:

Equation 1: $G(t) = 1 + \frac{<\delta I(t).\delta I\ (t+\tau)>}{<I^2>}$

This autocorrelation function compares the size of a fluctuation in intensity (δI) from fluctuations at a time (t+τ) later, with the mean fluorescence intensity ($< I >$). The autocorrelation curve is derived from the whole range of τ values, which are normalised to the square of the mean intensity measured ($< I >^2$) (Figure 2.5.). The resulting autocorrelation curves represent fluctuations in fluorescence intensity as a function of particle number and diffusion time. The average diffusion time of a fluorescent molecule to travel across the confocal volume (τ_D) is calculated from the mid-point of the autocorrelation curve. The Diffusion coefficient (D) from fluorescent-tagged molecule of interest is calculated using equation 2:

(Equation 2): D = $\frac{{w_0}^2}{4*\tau_D}$, where w_0 is the waist of the confocal volume and τ_D is the average diffusion time.

The amplitude of the autocorrelation function at time zero G(0) is inversely related to the average particle number (N): N = $\frac{1}{G(0)}$.

The autocorrelation curves obtained from calibration using R6G and TAMRA in water solution, TAMRA and $VEGF_{165}$a-TMR in buffer with or without BSA, were fitted using the Zeiss 2010 Software (Zeiss Germany), using the one component 3D diffusion model. The structural parameter is a value that is extremely sensitive to correct calibration, as it corresponds to the ratio of the height to waist radius of the confocal volume (Briddon et al., 2010). Since the 561m beampath was used for calibration using R6G, and the ideal structural parameter (SP) for this laser line is 6, SP was set to 6 for autocorrelation curves fitting. Structural parameter (set to 6) and average diffusion times (τ_D) obtained from calibration autocorrelation curves using R6G (with 561nm laser line) were then used to calculate the detected confocal volume (using equations described in Box 1). Calculated confocal volume and average particle number (N) (obtained from autocorrelation curves of TAMRA and $VEGF_{165}$a-TMR readings) were then used to calculate the concentration of fluorescent species in solution (Box 1) (Briddon et al., 2010).

Box 1: Data analysis to calculate free fluorescent ligand concentration in solution:

1. The radius of the detection volume $(\boldsymbol{w_0}) = \sqrt{\boldsymbol{4 \times \tau_D \times D}}$, where D is the Diffusion Coefficient of a reference fluorophore; D(R6G)= $2.8X10^{-10}m^2s^{-1}$. And τ_D is the diffusion time representing halfway point decay of the autocorrelation function, G(τ).
2. The half-height of the detection volume $(\boldsymbol{w_1}) = \boldsymbol{w_0} \times \boldsymbol{SP}$
3. The detection volume is calculated as: $\boldsymbol{V = \pi^{3/2} \text{ x } w_0^2 \text{ x } w_1}$.
4. The concentration of fluorescent particles in solution is then calculated as:

$\boldsymbol{C(M) = \frac{1}{V} \text{ x } \frac{N}{NA}}$, where N is the particle number, which is equal to the inverse of G(0), as shown in the autocorrelation curve represented above, V is the confocal detection volume, and NA is the Avogadro constant $6x10^{23}$ mol^{-1}.

All data were fit using a simple one-component, free 3D Brownian diffusion model, with a pre-exponential to include any photo-physical phenomena, such as a triple state formation, using the following equation:

$$G(\tau) = 1 + AN^{-1} \cdot \left(1 + \frac{\tau}{\tau_D}\right)^{-1} (1 + \tau/(S^2\tau_D)^{-1/2} \ ,$$

Where: $A = 1 + (T\tau . e^{-\frac{\tau}{t\tau}})(1 - T\tau)^{-1}$

$T\tau = triplet\ state$

$t\tau = triple\ relaxation\ time$

N = particle number

S = structural parameter

ii) Photon Counting Histogram (PCH) analysis

Autocorrelation analysis separates fluctuation in fluorescence intensity in a time-correlated manner (Briddon et al., 2018). The fluctuations in fluorescence intensity recorder during FCS analysis can be used to generate photon counting histograms. PCH analysis separates those fluctuations in intensity in separate binning times, measuring the frequency of photons emitted at a specific time. Therefore, PCH analysis can provide quantitative information about the number of fluorescent molecules and the number of photons per molecule (Herrick-Davis et al., 2012). PCH analysis uses a 3D Gaussian approximation of the laser bin profile and super-Poisson statistics to predict the molecular brightness (ε) of the fluorescent molecule being measured. Molecular brightness (ε) refers to the counts of photons per second per molecule (cpm s^{-1}) and is calculated by the following equation:

$\varepsilon = k/N$, where k =photon count rate (in kHz) and N = average number of molecules.

Histograms were generated using the Zeiss 2010 Software, and the bin time of 20µs was chosen for this analysis. This bin time was chosen because it is less than the diffusion or dwell time of the fluorescent ligands species (208 ± 5µs for $VEGF_{165}$a-TMR). And, it is also long enough to exclude more rapid time-dependent fluctuations that result from photo-physical events of the

fluorophore. All data were fitted to a one-component model. First order correction of 0.5 was obtained from calibration data using TAMRA 60sec measurements, with concentration and molecular brightness parameters allowed to be free. Therefore, PCH analysis for TAMRA and $VEGF_{165}a$ in HBSS buffer measurements were performed with first order correction set to 0.5, with concentration and molecular brightness allowed to be free. First order correction accounts for deviation from a Gaussian detection volume.

2.5. NanoBRET-based *in vitro* assays

2.5.1. Saturation and competition binding assays to investigate ligand-receptor interaction under equilibrium conditions

The NanoBRET ligand binding assay is a quantitative method, that uses the novel NanoLuc-luciferase (Nluc), to monitor receptor-ligand binding interactions in live cells and in real-time (Stoddart et al., 2015a, 2018). Nluc is a small 19kDa luciferase isolated and modified from the deep-sea shrimp, *Oplophorus gracilirostris*. This luciferase uses furimazine as a substrate, converting furimazine into furimamide by an oxidising reaction, resulting in very bright glow type luminescence (Hall et al., 2012). It is about 150-fold more luminescent then Renilla Luciferase (Rluc; *Renilla reniformis*) or firefly luciferase (Fluc; *Photinus Pyralis*), and its luminescence output lasts longer and is more stable than the mentioned luciferases. Nluc luminescence can cover a broad emission spectrum, with an emission maximum of 460 nm.

These assays rely on the principle of non-radiative energy transfer between a bioluminescent donor and a fluorescently-labelled acceptor, also known as bioluminescence resonance energy transfer (BRET) (Stoddart et al., 2018). For this purpose, we have used a NanoLuc-tagged receptor (luminescent donor) that excites a fluorescent ligand bound to the receptor (fluorescent acceptor), if in close proximity (<10 nm), represented in Figure 2.7.

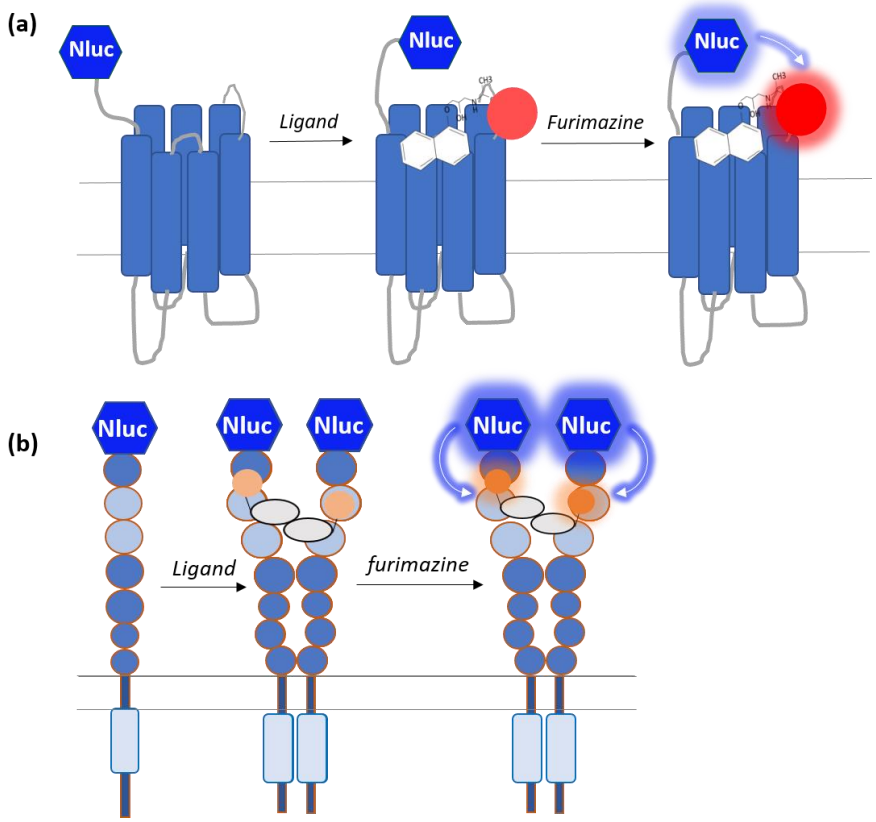

Figure 2.7. Schematic representation of NanoBRET assays to investigate dynamic ligand-receptor interactions for (a) class A GPCRs and (b) VEGFR2.

For ligand-receptor binding assays, a receptor of interest fused with a NanoLuc-luciferase (BRET donor), and a fluorescently-labelled ligand (BRET acceptor) were used. After furimazine treatment, which is a substrate for NanoLuc, this luciferase produces a glow type luminescence. When the NanoLuc is in close proximity with the fluorescent ligand (<10nm), bioluminescence resonance energy transfer occurs between the NanoLuc and the fluorescent ligand, leading to an increase in the energy state of the fluorophore and consequent fluorescence emission. The emission from both NanoLuc and fluorescence ligand were measured in these studies using a PHERAstar or CLARIOstar plate readers and also a whole-animal in vivo system (IVIS Lumina II), and data are expressed as BRET ratios calculated as fluorescence emission divided by luminescence emission.

A saturation binding assay was used to determine receptor affinity (i.e. the dissociation constant (K_D) of the fluorescent ligand). K_D values represent the concentration of ligand required for half-maximal occupancy of the receptor (Stoddart et al., 2018). High-affinity of a ligand to its receptor results from greater intermolecular forces between the two, while low-affinity results from lower intermolecular force between the ligand and its receptor. To define level

of non-specific binding, a high concentration of a competing non-fluorescent ligand was used.

The competition binding assay can be applied to determine the concentration of competing ligands (agonist or antagonist) needed to inhibit 50% of the specific binding of the fluorescent ligand (IC_{50}). The IC_{50} values obtained using this assay do not give a direct indication of receptor-ligand affinity. The Cheng Prusoff equation is used to convert IC_{50} values to an absolute inhibition constant (Ki) (Stoddart et al., 2012), as shown in data analysis section 2.5.8.

HEK 293T cells stably/transiently transfected to express full length human A_3R, $A_{2A}R$, β_1AR, β_2AR or VEGFR2 tagged at the N-terminus with NanoLuc luciferase, were used for saturation and competition binding experiments in chapter 4. MDA-231 cells stably transfected with Nluc-β_2AR (N-terminal-tagged-β_2AR with NanoLuc) fused in a lentiviral construct (pSIN-Nluc- β_2AR-IRES/BSD), were used to investigate ligand-receptor binding kinetics in chapter 4, and for *in vivo* ligand-receptor engagement in chapter 6.

For both saturation and competition binding experiments, cells were seeded into poly-D-lysine (10 µg/mL) coated white flat bottom 96 well Greiner plates (Bio One, UK), and incubated for 24h at 37°C/5%CO_2. For $A_{2A}R$ studies, HEK 293 cells were seeded into poly-D-lysine pre-coated 96-well white plate, and transiently transfected, 24 hours after seeding, with 0.1 µg/well Nluc-$A_{2A}R$ cDNA construct, using a 3:1 Fugene:cDNA ratio and Opti-MEM media, following manufacturer's instructions. Figure 2.8. represents the plate layout used for the saturation binding assay, while Figure 2.9. represents the plate layout used for the competition binding assay. Before each assay, complete media (DMEM/10% FBS) was aspirated and cells were washed with 100µL pre-heated HBSS at 37°C and incubated with 90µL HBSS. Cells were then incubated with 10µL of fluorescent ligand and 10µL non-fluorescent antagonist 10µL buffer, in respective wells, with a final volume of 100µL per well. All ligands were prepared in microcentrifuge tubes at 10x their final desired concentration. Fluorescent, non-fluorescent ligands, and respective concentrations used, are

summarised in Table 2.6. and 2.7. $VEGF_{165}$a-TMR and $VEGF_{165}$a ligands were prepared in HBSS buffer supplemented with 0.1% protease-free BSA, in order to keep ligands in solution. Cells treated with respective ligands were incubated for 1h at 37°C/without CO_2. Carbonate-based buffers, such as HEPES buffer, become acidic in the presence of CO_2, hence, for our experiments we incubated cells without CO_2 to maintain pH levels. Cells were then incubated with 10µL of 10µM furimazine substrate, at room temperature and in the dark, for 5 min before reading on a plate reader, allowing the equilibration of the luminescence reaction. Luminescent and fluorescent emissions were sequentially measured using a PHERAstar FS plate reader (BMG LabTech, Ortenberg, Germany) using 460nm emission (80nm bandpass) and >610nm (longpass) filters. Raw BRET ratios were calculated by dividing the >610nm emission by the 460nm emission.

For Nluc-β_2AR MDA-231 cell line characterisation, a CLARIOstar (BMG LABTECH, Australia) plate reader was used, as well the whole-animal bioluminescence imaging system (IVIS Lumina II, Perkin Elmer, USA), data showed in chapter 4 and 6. For assays using the CLARIOstar plate reader, fluorescence and luminescence sequential readings were taken, with filtered light emission collected at 685nm/100nm bandpass (acceptor) and at 460nm/80nm bandpass (donor). With raw BRET ratios calculated as fluorescence emission divided by luminescence emission.

For the IVIS Lumina II system, light was collected at 660nm/20nm bandpass (BRET acceptor; 30sec exposure time) and using open channel (BRET donor, 1sec exposure time). Fluorescence/Luminescence ratios were calculated from data collected using ROIs (using a grid tool provided by the Living Image Software, Perkin Elmer, USA).

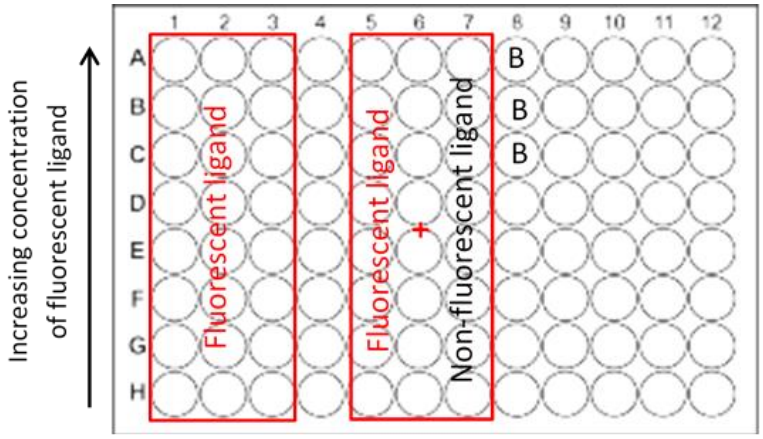

Figure 2.8. Representation of the plate layout for NanoBRET saturation binding assay. 10µL of increasing concentrations of fluorescent ligand were added to columns 1 to 3. 10µL fluorescent ligand plus high concentration of a competing non-fluorescent ligand were added to wells from columns 5 to 7, to define the level of fluorescent ligand non-specific binding. (B) represents basal, where cells were treated with furimazine substrate only. Plate was incubated with ligands for 60min at 37°C/without CO_2. After incubation, 10µL furimazine (10µM) were added to each well, incubated for 5min in the dark and readings were taken using a PHERAstar plate reader with 460nm emission (80nm bandpass) and >610nm (longpass) filter settings. Measurements were performed in triplicate wells.

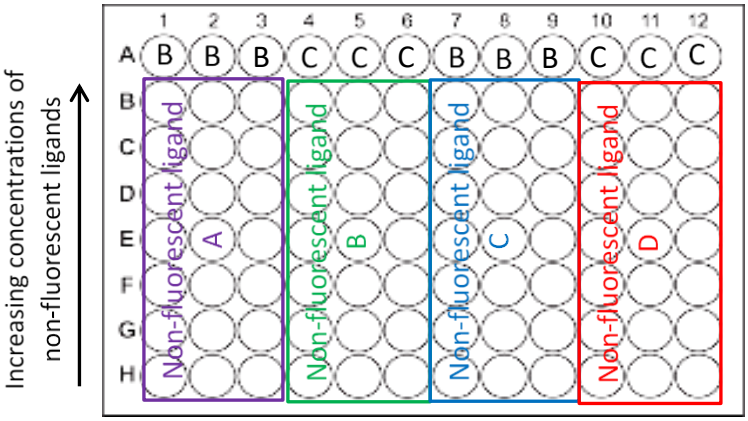

Figure 2.9. Representation of the plate layout for NanoBRET competition binding assay. 10µL of a fixed concentration (measured K_D concentration from saturation binding assay) of fluorescent ligand was added to all wells indicated in the coloured boxes. Fluorescent ligand alone was also added to (C) (positive control). 10µL of increasing concentrations of different non-fluorescent ligands were added as shown in figure. (B) is the basal luminescence, where cells were treated with furimazine substrate only. Plate was incubated with ligands for 60min at 37°C/without CO_2. All mentioned wells were incubated with 10µM furimazine before readings using same settings as above. Measurements were performed in triplicate wells.

Table 2.6. Fluorescent, non-fluorescent ligands and respective concentrations used for saturation binding assay

Saturation Binding Assay				
Receptor	Fluorescent ligand	Conc. used (nM)	Non-fluorescent ligand	Conc. used (μM)
Nluc-A_3R / HEK	CA200645	5 to 500	MRS1220	10
Nluc-A_{2A}R /HEK	CA200645	5 to 500	SCH58261	10
Nluc-β_2AR/ HEK	CGP12177-TMR	10 to 500	propranolol	10
Nluc-β_2AR/HEK	propranolol-(β-Ala)-X-BY630	10 to 200	propranolol	10
Nluc-β_2AR (pSIN)/MDA-231 and 66cl4	propranolol-(β-Ala)-X-BY630	2.5 to 200	propranolol	10
Nluc-VEGFR2/ HEK	$VEGF_{165}$a-TMR	0.1 to 10	$VEGF_{165}$a	10 (nM)

Table 2.7. Fluorescent, non-fluorescent ligands and respective concentrations used for competition binding assay

Competition Binding Assay				
Receptor/cell line	Fluorescent ligand	Conc. used (nM)	Non-fluorescent ligand	Log conc. used (M)
Nluc-A_{2A}R / HEK	CA200645	25	SCH58261	-5 to -11
Nluc-A_3R / HEK	CA200645	100	MRS1220	-5 to -11
			DPCPX	-5 to -11
			PSB36	-5 to -11
			NECA	-5 to -11
Nluc-β_2AR /HEK	CGP12177-TMR	50	ICI118551	-5 to -11
			isoprenaline	-4 to -10
			propranolol	-5 to -11
			CGP12177	-5 to -11
Nluc-β_2AR / HEK	propranolol-(β-Ala)-X-BY630	25	ICI118551	-5 to -11
			isoprenaline	-4 to -10
			propranolol	-5 to -11
			CGP20712A	-5 to -11
Nluc-β_2AR (pSIN)/ MDA-231	propranolol-(β-Ala)-X-BY630	25	ICI118551	-5 to -11
			isoprenaline	-4 to -10
			propranolol	-5 to -11
			CGP20712A	-5 to -11
			carvedilol	-5 to -11
Nluc-VEGFR2/ HEK	$VEGF_{165}$a-TMR	3	$VEGF_{165}$a	-8 to -11

2.5.2. Kinetic binding assay to investigate ligand-receptor interaction under non-equilibrium conditions

Saturation and competition binding assays are performed under equilibrium conditions. These equilibrium conditions are only achieved in closed systems, such as cells, while rarely met when considering a complex *in vivo* system (Guo et al., 2016a). Using a kinetics binding assay, we can determine fluorescent ligand association (k_{on}) and dissociation (k_{off}) rate constants, dissociation constant (K_D) and residence time (RT), which can be described as the period of time that a ligand occupies its receptor ($RT=1/k_{off}$). The equilibrium dissociation constant is calculated as $K_D=k_{off}/k_{on}$. In kinetics binding assay, these parameters are obtained under dynamic conditions, and are believed to predict more accurately *in vivo* pharmacological activity than parameters obtained under equilibrium condition.

For this purpose, MDA-231 Nluc-β_2AR cells were seeded into white flat bottom 96-well Isoplates (Perkin Elmer, Australia), and incubated for 24h at 37^{o}C/5% CO_2. Figure 2.10. represents the plate layout used. For this assay, media was removed from wells and replaced with 50µL of 10µM furimazine substrate prepared in HBSS buffer. Cells were then incubated with substrate at 37^{o}C/without CO_2 for 15 min, to allow luminescence signal equilibrium. Labelled ligand was prepared beforehand in a compound plate 2x more concentrated than desired final concentration. Unlabelled ligand was prepared in an microcentrifuge tubes10x more concentrated than the desired concentration in the well. After incubation, 10µL of unlabelled ligands or HBSS buffer were added to respective wells, 40µL of fluorescent ligand were then quickly added using a multi-channel pipette. Fluorescence and luminescence sequential readings were immediately taken after fluorescent ligand treatment with measurements taken every 2 min over a time-course of 60min. Data were collected using a CLARIOstar BMG or the IVIS Lumina II system, with fluorescence and luminescence sequential readings taken using the same filter settings as mentioned in the above saturation and competition binding assays.

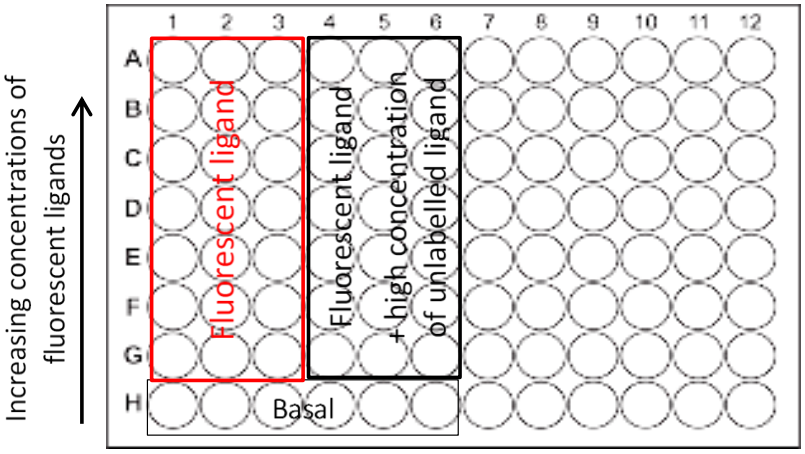

Figure 2.10. Representation of the plate layout for NanoBRET kinetics binding assay. Wells were firstly incubated with 50µL furimazine (10µM) diluted in HBSS buffer and incubated for 15min. After incubation, 10µL high concentration of unlabelled competitor were added to wells in column 4 to 6. While, 10µL HBSS buffer were added to wells from column 1 to 3. 50µL HBSS buffer were added in row H (Basal). 40µL of increasing concentrations of fluorescent ligand were then added to columns 1 to 6. All wells had a final volume of 100µL. Basal represents cells treated with furimazine only, for luminescence background. Immediately after fluorescent ligand treatment, sequential fluorescence and luminescence measurements were taken every 2min, for total time of 60min, at 37°C, using same filter settings as mentioned earlier.

2.5.3. Saturation binding assay to investigate receptor-receptor interactions

To investigate receptor-receptor interactions using BRET, one receptor was fused with a NanoLuc-Luciferase on the N-terminus (BRET donor), and the other receptor was fused with a Halo/SNAP-Tag at the N-terminus (BRET acceptor). If in close proximity (≤ 10nm), and at a favourable conformation, the substrate treated NanoLuc-labelled receptor will excite the fluorophore covalently bound to the Halo/SNAP-Tagged Receptor (Figure 2.11.). Luminescence and fluorescence emissions are then used to calculate BRET ratios.

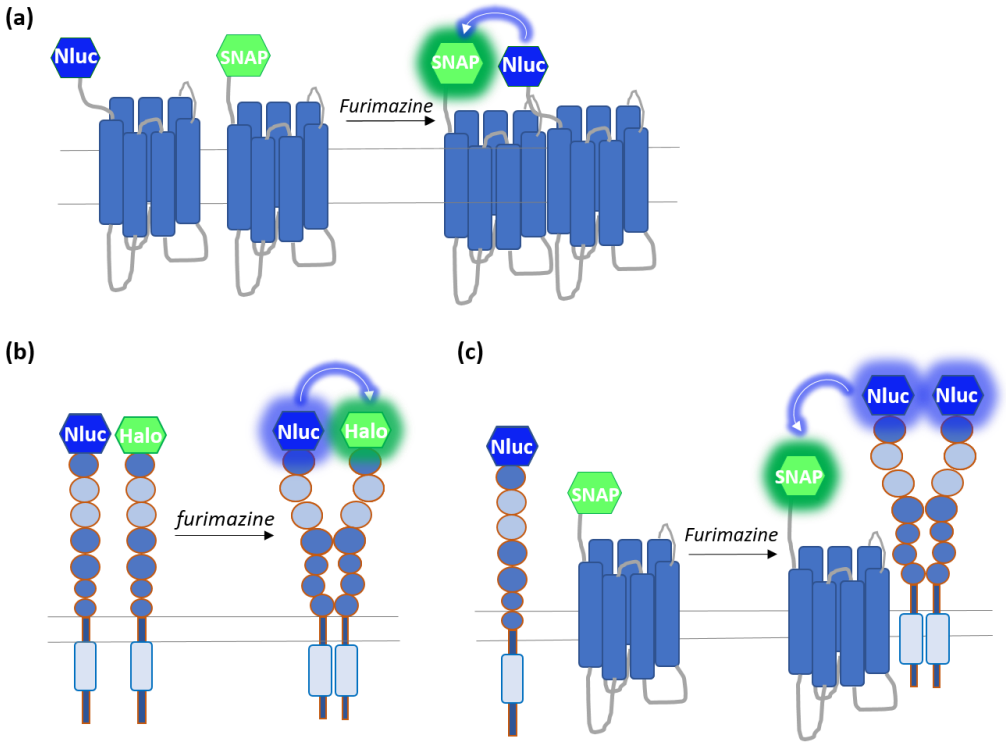

Figure 2.11. Schematic of the use of NanoBRET to investigate receptor-receptor interactions. The receptor donor was fused in frame with a NanoLuc-tag at the N-terminus, while the acceptor was fused with a Halo/SNAP-Tag that can covalently bind exogenously supplied fluorophores. For these experiments, a green-shifted labelled Halo/SNAP-tags substrate (surface Alexa F488) was used. **(a)** Investigation of GPCR-GPCR homodimers **(b)** Investigation of VEGFR2 dimerization; **(c)** investigation of VEGFR2-GPCR heterodimeric complexes.

HEK 293T cells were seeded at 12 000 cells/well into poly-D-lysine coated white flat bottom 96 wells Greiner plates. 24h after these were transiently co-transfected with increasing concentrations of SNAP/Halo-tagged receptor cDNA (0.013 to 0.2 µg/well) and a fixed concentration (0.05 µg/well) of Nluc-tagged receptor cDNA (Table 2.8.). An empty vector vector, pcDNA3.1, was included in transfections to keep the same final cDNA concentration (0.2 µg/well) across the different wells. Transfections were performed using Fugene reagent in Opti-MEM media (3:1 reagent to DNA ratio). Plate layout is represented in Figure 2.12. 24h after transfection, media was aspirated, and duplicate wells were treated with 100µL 0.2µM SNAP/Halo-Tag membrane impermeable Alexa F488 substrates, prepared in serum-free-DMEM. While other duplicate wells containing co-transfected cells were incubated without

acceptor substrate, with 100µL serum-free DMEM, instead. Plates were incubated for 30min at 37°C/5%CO_2. After incubation, cells were washed 3x and incubated with 100µL HBSS. 10µL furimazine at 10µM were then added to all wells, incubated for 5min, at 37°C, in the dark. Sequential luminescent and fluorescent emission measurements were taken using a PHERAstar FS plate reader using 460nm (80nm bandpass; NanoLuc emission) and 535nm (60nm bandpass; SNAP emission) filters. Raw BRET ratios were calculated dividing the 535nm emission (acceptor) by the 460nm emission (donor).

Table 2.8. Combination of cDNA constructs used for Homo- and Hetero-dimers investigation. Donor concentration was kept constant at 0.05 µg/well, while increasing concentrations of acceptor were used (0.013-0.2 µg/well).

Homodimers		Heterodimers	
Donor	**Acceptor**	**Donor**	**Acceptor**
Nluc-A_1R	SNAP-A_1R	**Nluc-VEGFR2**	SNAP-A_1R
Nluc-A_3R	SNAP-A_3R		SNAP-A_3R
Nluc-A_{2A}AR	SNAP-A_{2A}AR		SNAP-A_{2A}AR
Nluc-β_2AR	SNAP-β_2AR		SNAP-β_2AR

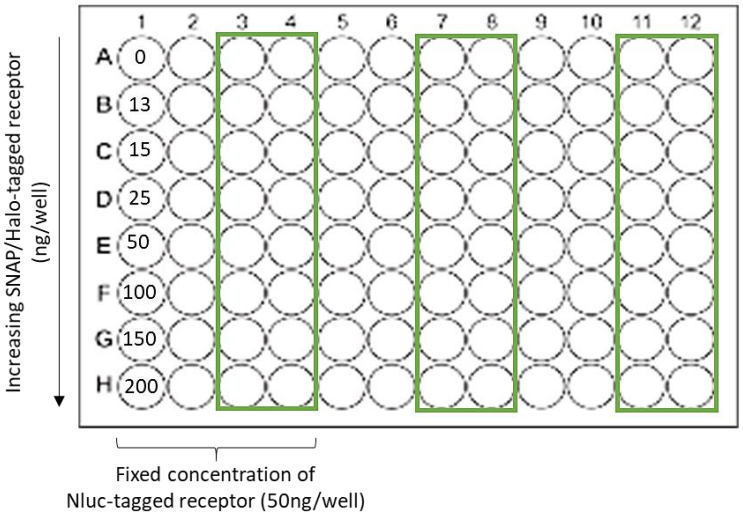

Figure 2.12. Representation of plate layout for NanoBRET saturation assay to investigate receptor-receptor molecular interaction. Cells in wells from column 1 to 4 were transiently co-transfected (3:1 Fugene:cDNA ratio) with both donor and acceptor, or donor alone (row A). Other wells were co-transfected with a different receptor pair. Empty vector (pcDNA3.1) was

added to keep equal cDNA concentration (0.2µg/well) in every well. 24h after transfection, cells in wells with green box were incubated for 30min with 100µL 0.2µM SNAP/Halo-Tag membrane impermeable AF488 substrate, prepared in serum-free DMEM, while other wells were incubated with 100µL serum-free DMEM (background luminescence controls), at 37°C/5%CO_2. Cells were then washed 3x and incubated with 100µL HBSS. Immediately after, 10µL 10µM furimazine were added to all wells containing co-transfected cells and incubated for 5min in the dark. After incubation, fluorescence and luminescence readings were taken using a PHERAstar plate reader with 460nm (80nm bandpass; NanoLuc emission) and 535nm (60nm bandpass; SNAP emission) filters.

2.5.4. Investigation of the effects of subtype selective ligands on heterodimer complex formation.

HEK 293T cells were transiently co-transfected with a 1:2 cDNA (0.05:0.1µg/well) of donor (NLuc-VEGFR2) to acceptor (SNAP-β_2A or -A_{2A} receptor) ratio. Transfection was performed using Fugene and Opti-MEM media with 3:1 Fugene:cDNA ratio. Cells were then left to grow for a further 24h at 37°C/5% CO_2. On the day of the assay, media was aspirated from wells and cells were incubated with 100µL 0.2µM SNAP/Halo-Tag AF488 membrane impermeable substrate, prepared in serum-free DMEM (and incubated for 30min, 37°C). Cells were then washed 3x and incubated with 90µL HBSS buffer and treated with 10µL ligand prepared in HBSS at a concentration 10x more concentrated than desired final concentration in well. Isoprenaline and CGS21680 were prepared at -5M to -8M final concentration in wells, and $VEGF_{165}$a was prepared at -8M to -11M final concentration in well. Treatment was performed using quadruplicate wells. Cells were incubated with ligands for 60min, at 37°C/without CO_2. $VEGF_{165}$a stimulations were performed in HBSS supplemented with 0.1% BSA. For studies using the A2A receptor, 0.5 unit/mL adenosine deaminase (Roche, Basel, Switzerland) was incorporated in the buffer. Adenosine deaminase is an enzyme that can convert adenosine into its related nucleoside, inosine, deactivating endogenously produced adenosine. After incubation, 10µL of furimazine (10µM) were added to every well and incubated for 5min in the dark. Plates were read using a PHERAstar plate

reader, using the same filter settings as previously described for homodimer studies.

2.5.5. Investigation of potential cooperativity across putative (GPCR-VEGFR2) heterodimer interface

The principle of this assay was to use a fluorescent ligand that binds to the Nluc-labelled receptor and investigate whether unlabelled ligands that bind to the receptor pair could interfere with the BRET signal (Figure 2.13.). These observations would indicate whether there was positive/negative cooperativity across the dimer interface.

For this experiment, HEK 293T cells were transiently transfected with a 1:1 ratio of donor (NLuc-VEGFR2, NLuc-β_2A or NLuc-A_{2A} receptor) to acceptor (SNAP-β_2A, SNAP-A_{2A} or Halo-VEGFR2) cDNA constructs (0.05:0.05µg/well) using Fugene (in Opti-MEM using 3:1 Fugene:cDNA ratio). Cells were then left to grow for a further 24h at 37°C/5%CO_2. On the day of the assay, media was aspirated from wells and cells were incubated with 80µL HBSS (pre-heated at 37°C). Cells were treated with 10µL fluorescent ligand ($VEGF_{165}$a-TMR (1 or 2nM); CA200645 (200nM) or BODIPY CGP12177-TMR (15nM)) in the presence or absence of 10µL of increasing concentrations of unlabelled subtype selective ligands (NECA, 0.01nM-10µM; CGS21680, 0.01nM-10µM; ICI 1185511, 0.01nM-10µM; CGP12177, 0.01nM-10µM; or Isoprenaline, 0.1nM-100µM). 10µL HBSS buffer was added to wells incubated with fluorescent ligand only, for a final volume of 100µL per well. Nonspecific binding of fluorescent ligands was defined using a high concentration of unlabelled ligands (10nM $VEGF_{165}$a; 10µM SCH58261 or 10µM propranolol). Ligands were incubated for 60min, at 37°C/without CO_2. HBSS buffer was supplemented with 0.1% BSA, when using $VEGF_{165}$a unlabelled or fluorescently-labelled ligands. After incubation, 10µL of furimazine (10µM) was added to each well, plates were left for 5min, in the dark at 37°C, before readings. Sequential fluorescence/luminescence emission measurements were taken using a PHERAstar FS plate reader, using 460nm (80nm bandpass; NLuc emission) and 610nm (longpass filter; fluorescent ligand

emission) filters. Raw BRET ratios were calculated by dividing 610m emission (acceptor) by 460nm emission (donor).

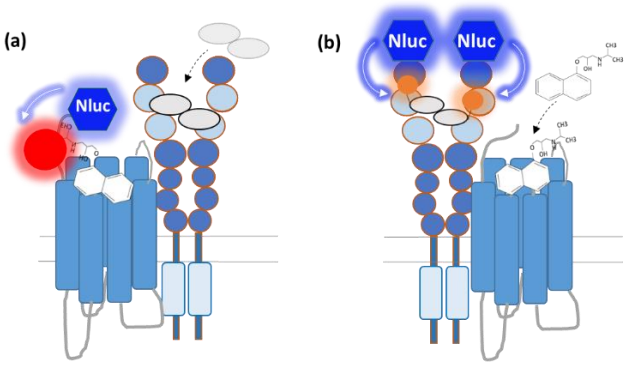

Figure 2.13. Schematic representation of the use of NanoBRET to investigate potential cooperativity effect across dimer interface. (a) HEK 293T cells were transiently co-transfected with 0.05µg/well Nluc-$A_{2A}R$ or Nluc-β_2AR and 0.05µg/well Halo-VEGFR2 and treated with fluorescently labelled adenosine or β-adrenergic fluorescent ligand antagonists and increasing concentrations of unlabelled $VEGF_{165}$a agonist. **(b)** HEK 293T cells were transiently co-transfected with 0.05µg/well Nluc-VEGFR2 and 0.05µg/well SNAP-$A_{2A}R$ or SNAP-β_2AR, and treated with a $VEGF_{165}$a-TMR fluorescent ligand, and increasing concentrations of adenosine or β-adrenergic unlabelled ligands. Ligands were incubated for 60min, at 37°C. Donor and acceptor emissions were measured using a Pherastar plate-reader. And BRET ratios were calculated as acceptor/donor ratios.

2.5.6. β-arrestin-2 recruitment assay

Beta-arrestin-2 (or arrestin-3) are adaptor proteins that are recruited to β_2-adrenoceptor after ligand-stimulation and receptor phosphorylation by G-protein receptor kinases (GRKs) (Reiter and Lefkowitz, 2006). These proteins not only play a role in receptor desensitisation and internalisation, but also act as scaffold proteins for β_2-adrenoceptor-induced signalling from intracellular compartments, including endosomes (Cahill et al., 2017; Shenoy and Lefkowitz, 2003). In this study we used a NanoBRET-based β-arrestin2-YFP recruitment assay to investigate the temporal profile of β-arrestin-2 recruitment for C-terminally-tagged β_2AR with NanoLuc luciferase, in the presence or absence of VEGFR2 (Figure 2.14 a and b).

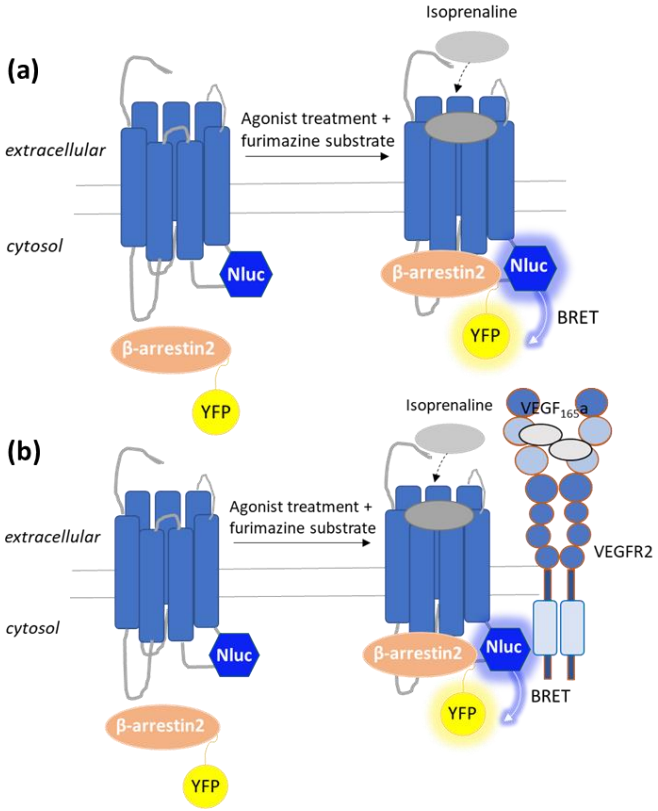

Figure 2.14. Schematic representation of NanoBRET-based assay to measure β-arrestin2-YFP recruitment to stimulated-β_2AR-Nluc. For these experiments, HEK 293T cells were transiently co-transfected with 0.01µg/well of BRET donor (β_2-adrenoceptor tagged at the C-terminal with NanoLuc luciferase), and 0.04µg/well BRET acceptor (β-arrestin2-Venus-YFP), and either 0.04µg/well **(a)** empty vector (pcDNA3.1) or **(b)** Halo-VEGFR2 cDNA. Upon furimazine and isoprenaline (β_2AR selective agonist) treatment, cytosolic β-arrestin2-YFP is recruited to stimulated-β_2AR, inducing receptor internalisation.

For these experiments, HEK 293T cells were seeded at a density of 12000 cells/well into poly-D-lysine coated white flat bottom 96 well plates and incubated for 24h, at 37°C/5%CO_2. Cells were then transiently co-transfected with 0.04µg/well of C-terminal Venus-YFP-β-arrestin2 and Halo-VEGFR2, together with 0.01µg/well of β_2-Nluc cDNA constructs, using Fugene (3:1 Fugene:cDNA ratio), in Opti-MEM media (plate layout is displayed in Figure 2.15.). Venus-YFP is a variant of yellow fluorescent protein (YFP) with faster and more efficient maturation in cells (Nagai et al., 2002), which is suitable to perform BRET (Dacres et al., 2012). On the next day, Opti-MEM media was aspirated and 70/80µL HBSS/0.1%BSA were added to wells. 10µL furimazine at 10µM were added to each well and incubated for 5min, at 37°C, in the dark.

After incubation, sequential fluorescence/luminescence emission measurements were taken for 4 min before ligand treatment, using a PHERAstar FS plate reader. 10µL 10µM isoprenaline plus 10µL 10nM $VEGF_{165}a$ were added in co-treatment conditions, whereas 10µL ligand (isoprenaline or $VEGF_{165}a$) plus 10µL HBSS/BSA were added for single ligand treatment conditions. Continuous readings were taken every 1 min for a total time of 45min, after ligand treatment, using 460nm (80nm bandpass; donor NLuc emission) and 535nm (60nm bandpass; β-arrestin2-Venus-YFP emission) filters. Raw BRET ratios were calculated by dividing the 535nm emission (acceptor) by the 460nm emission (donor). Measurements were performed using triplicate wells.

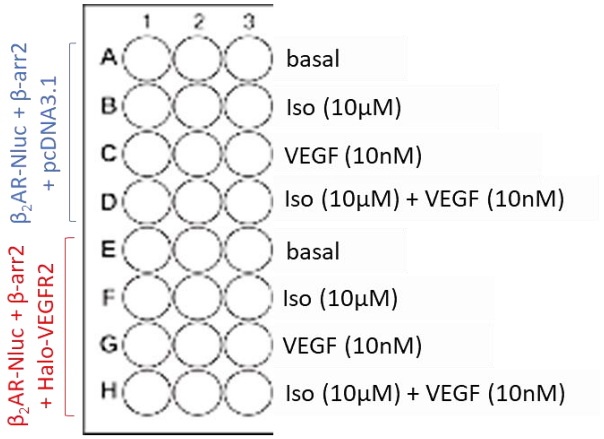

Figure 2.15. Representation of plate layout for NanoBRET-based beta-arrestin2-YFP recruitment to ligand-stimulated-β_2AR-NLuc. Cells in wells from rows A to D were transiently co-transfected (3:1 Fugene:cDNA ratio) with 0.01µg/well **β_2AR-NLuc**, 0.04 µg/well beta-arrestin2-Venus-YFP and 0.04µg/well pcDNA3.1. Cells in wells from rows E to H were transfected with the same conctructs, but instead of pcDNA3.1, these were transfected with 0.04µg/well Halo-VEGFR2 cDNA. 24h after transfection, media was removed and replaced with 1xHBSS (with volumes of 90µL in basal condition, 80µL in single treatment, or 70µL in co-treament conditions). 10µL furimazine substrate (10µM) were added to each well and incubated for 5min, inside the PHERAstar plate-reader at 37°C. After incubation, sequential fluorescence/luminescence readings were taken every minute, using 460nm (80nm bandpass; NanoLuc emission) and 535nm (60nm bandpass; YFP emission) filters. 10µL ligands or vehicle (10µM isoprenaline, 10nM $VEGF_{165}a$) were quickly to respective wells, 4 minutes after initial recordings and further sequential reading were taken for 45min.

2.5.7. Nanobody-80 recruitment assays

For these assays, HEK 293T cells were stably transfected with a lentiviral cDNA construct encoding a Nanobody-80 tagged at the C-terminus with green fluorescent protein (GFP) (pSIN-Nb-80-GFP cDNA construct). Nanobodies are camelid single chain antibody fragments. Nanobody-80 (Nb-80) has G-protein-like properties that bind and stabilises an agonist-activated β_2AR state (Irannejad et al., 2013; Rasmussen et al., 2011a). Nb-80-GFP was used in this study to investigate potential impact of $VEGF_{165}$a-stimulated-VEGFR2 on β_2-adrenoceptor activation status. To investigate this, a NanoBRET-based approach was used to measure Nb-80-GFP recruitment to β_2AR-Nluc, in the absence or presence of $VEGF_{165}$a-stimulated-VEGFR2 (Figure 2.16. a and b). A time-course assay was firstly used to investigate temporal characteristics of Nb-80-GFP recruitment to isoprenaline-stimulated-β_2AR. A isoprenaline concentration response assay, measured at 30min after ligand treatment, was then used to investigate the impact of stimulated-VEGFR2 on β_2AR activation status.

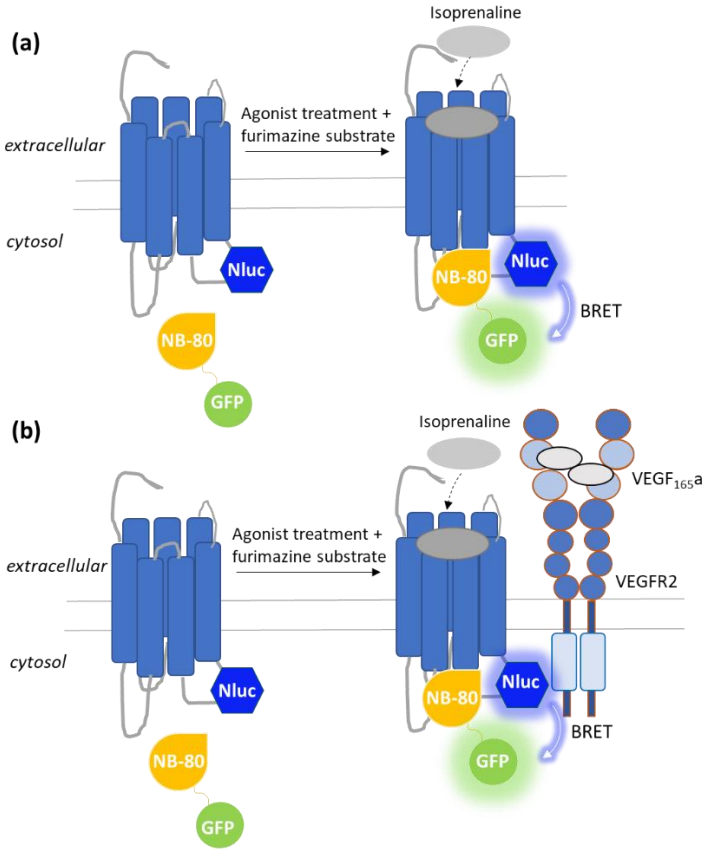

Figure 2.16. Schematic representation of NanoBRET-based assay to measure Nanobody80-GFP recruitment to stimulated-β_2AR-Nluc. For these experiments, HEK 293T cells stably expressing BRET donor (Nb-80-GFP) were transiently co-transfected with 0.025µg/well of BRET donor (β_2-adrenoceptor tagged at the C-terminal with NanoLuc luciferase), and either 0.025µg/well **(a)** empty vector (pcDNA3.1) or **(b)** Halo-VEGFR2 cDNA. Upon furimazine and isoprenaline (β_2AR selective agonist) treatment, cytosolic Nb-80-GFP is recruited to stimulated-β_2AR.

i) Time-course assay

For the Nb-80-GFP recruitment time-course assay, HEK 293T cells stably expressing Nb-80-GFP protein were seeded, at a cell density of 12000 cells/well, into poly-D-lysine coated white flat bottom Greiner 96 well plates and incubated for 24h at 37°C/5%CO_2. Cells were then transiently co-transfected with 0.025µg/well β_2AR-Nluc and 0.025µg/well Halo-VEGFR2 or empty vector (pcDNA3.1), using Fugene in Opti-MEM media. On the day after transfection, media was aspirated from wells and 80µL HBSS/0.1%BSA were

added. 10µL furimazine (10µM) were added to each well, and incubated for 5min, at 37^{o}C, in the dark. After incubation, sequential emission measurements were taken for 5min before ligand treatment, using a PHERAstar plate reader. 10µL Isoprenaline (10µM) and 10µL $VEGF_{165}$a (10nM) were added wells with co-treatment, while in wells with single treatment 10µL ligand were added together with 10µL HBSS/BSA. All wells had a final volume of 100µL. Continuous readings were taken every 1min for a total time of 45min. PHERAstar settings used were the same described in the β-arrestin-2 recruitment assay.

ii) Concentration-response assay

For the concentration-response assay, HEK 293T cells stably expressing Nb-80-GFP cells were co-transfected, as earlier described for the time-course assay. On the day after transfection, Opti-MEM media was aspirated and replaced with 70µL HBSS/0.1%BSA. Cells were then treated with 10µL of increasing concentrations of isoprenaline (0.1nM to 100µM), in the presence or absence of 10µL 100nM ICI 118551 or 10µL 10nM $VEGF_{165}$a; $VEGF_{165}$a treatment was added to cells co-transfected with Halo-VEGFR2, and not added to cells transfected with the empty vector. 20µL HBSS/BSA was added in wells with single treatment, for a final volume of 100µL in each well. Plates were incubated after ligand treatment for 30min at 37^{o}C/without CO_2. After incubation, 10µL 10µM furimazine substrate was added to each well, and incubated for 5min, at 37^{o}C in the dark. Sequential emission measurements were then taken using a PHERAstar FS plate reader, with the same settings used for the β-arrestin-2 recruitment assay.

2.5.8. NanoBRET-based *in vitro* assays data analysis

i) Saturation binding assay for ligand-receptor interaction studies

For the NanoBRET saturation binding assay, increasing concentrations of fluorescent ligand and a fixed high concentration of non-fluorescent antagonist

were used to investigate fluorescent ligand binding affinity (K_D), and the level of ligand specificity for the receptor of interest. The raw BRET ratios obtained from each individual experiment were fitted using a non-linear regression equation shown below, from Graph Pad 6:

$Specific\ binding = \frac{(B_{max} \times A)}{(A+K_D)}$, where A is the concentration of fluorescent ligand, B_{max} is the maximal specific binding, and K_D is the dissociation constant of the fluorescent ligand.

For simplicity and for easier comparison with other studies, dissociation (K_D) values were represented as negative log of the observed dissociation (pK_D).

ii) Competition binding assay for ligand-receptor interaction studies

For the competition binding assay, increasing concentrations of unlabelled ligands and a fixed concentration (measured K_D concentration from saturation binding assay) of the labelled ligand were used. The principal is to compare the concentration of unlabelled compounds needed to inhibit by 50% the specific binding of the labelled ligand (IC_{50}).

The IC_{50} value for each non-labelled ligand was calculated using the following equation fitted to the data using Prism 6:

$\%\ uninhibited\ binding = \frac{(100-NS)}{([A]/IC_{50})+1} + NS$, where [A] is the unlabelled ligand concentration used, IC_{50} is the molar concentration of the non-labelled ligand to generate 50% inhibition of the labelled ligand, while NS accounts for the non-specific binding.

It is important to mention that the IC_{50} values obtained are dependent on the concentration of the labelled ligand used. Therefore, higher concentrations of competing ligand are required to displace high concentrations of labelled ligand. Once the affinity level of the fluorescent ligand is determined (K_D) we can then calculate the inhibition constant (Ki) of the competing ligand using the Cheng Prusoff equation:

$K_i = \frac{IC_{50}}{1+\frac{[L]}{K_d}}$, where [L] is the concentration of labelled ligand and K_D is the dissociation constant of the fluorescent ligand obtained from saturation binding assays.

iii) Kinetics binding assay for ligand-receptor interaction studies

Data obtained for fluorescent ligand binding kinetics, using more than one concentration, were globally fitted to an association kinetics model, which derives a single best-fit estimate for association (k_{on}) and dissociation (k_{off}) rate constants, using the following mono exponential association function:

$Y = Ymax\,.(1 - e^{-K_{obs}.t})$, where $Ymax$ corresponds to the level of binding at infinite time, t is the incubation time and k_{obs} is the rate constant for the observed rate of association. To investigate whether the different concentrations of ligand globally fit to a single mass-action equilibrium interaction, the k_{obs} values obtained were compared at the different concentrations by investigating the linearity of the relationship between them according to the expression:

$k_{obs} = k_{on}\,.L + k_{off}$, where k_{off}, is the dissociation rate constant of the ligand in min^{-1}, and k_{on} is the association rate constant in $M^{-1}\ min^{-1}$. K_D values were calculated from these kinetics parameters using the following equation: $k_D = k_{off}/k_{on}$.

iv) Saturation assay for receptor-receptor interaction studies

Data analysis for receptor-receptor NanoBRET saturation assay was performed using emission measurements through two wavelength windows (donor and acceptor). Baseline-corrected BRET ratios were calculated as shown below:

$Baseline\ corrected\ BRET\ ratio$ = [$(emission\ at\ 535nm)/(emission\ at\ 460nm) - Cf$], where *Cf* corresponds to *(emission at 535nm/emission at 460nm)* from the donor alone.

2.6. Cell imaging

2.6.1. Confocal imaging using Zeiss 710

HEK 293T cells were seeded at 100,000 cells/well on poly-D-lysine pre-coated Nunc Lab-Tek 8 well plates (Thermo-Fisher, UK). After 24h incubation at 37°C/5%CO_2, cells were transiently co-transfected with 0.025µg/well of Halo-VEGFR2, SNAP-β_2A or SNAP-A_{2A} receptor cDNA and let to grown for 24h more. All transfections were performed using Fugene in Opti-MEM media (3:1 reagent:cDNA ratio). On the third day, media was removed, and cells were incubated with 200µL 0.5µM Halo-tag AF660 (68471, Promega Corporation, USA) membrane impermeant ligand, prepared with 0.5µM SNAP-Surface AF488 membrane impermeant ligand (S9129S, New England Bio-Labs) in serum-free media. Cells were incubated with substrates for 30min at 37°C/5% CO_2. Cells were then washed 3x with 180µL HBSS and then stimulated with either 20µL vehicle, 10nM $VEGF_{165}$a, 10µM Isoprenaline or 10µM CGS21680, for 60min at 37°C. For incubation with $VEGF_{165}$a, HBSS was supplemented with 0.1% BSA. Cells were imaged live at 37°C, using a Zeiss LSM710 fitted with a 63x Pan Apochromat oil objective (1.4NA) using Argon488 (SNAP AF488; 496-574nm band pass; 3% power) and/or HeNe excitation (Halo AF660; 621-759nm bandpass; 20% power) using a 488/561/633 beamsplitter with a pinhole diameter of 1 Airy unit. All images were taken at 1024x1024 pixels per frame with 8 averages.

2.6.2. Confocal imaging using a plate reader ULTRA ImageXpress

Confocal imaging using a plate reader (ULTRA ImageXpress, Molecular Devices) was used to confirm protein expression of Halo-VEGFR2, Nb-80-GFP and β-arrestin2-Venus-YFP recruitment assays. Once assay readings were completed, cells were labelled with 100µL SNAP/Halo-tag substrates (at 0.1µM) for 30min, at 37°C/5% CO_2. After incubation, cells were washed 3x with 100µL PBS and fixed using 3% paraformaldehyde (PFA). After fixation, cells were washed and left with 100µL PBS before imaging. Images were captured using a Plan Fluor 40x NA0.6 extra-long working distance objective. Red-shifted fluorophores

were excited at 635 nm and emission collected through a 640-685nm band pass filter, while green-shifted fluorophores were excited at 488nm with emission collected through a 525-550nm band pass filter. Images were exported using MetaXpress software (MetaXpress 2.0, Molecular Devices).

2.6.3. Confocal imaging using Leica SP8

Confocal microscopy was performed using a Leica TCS SP8 inverted scanning microscope with a Zeiss 40x 1.3NA oil immersion HCPL APO CS2 objective lens. MDA-MB-231^{HM} parental or stably expressing Nluc-β_2AR cells were seeded in eight-well coverglass chamber (Ibidi) in 200µL DMEM Glutamax media containing 10% FBS. Prior to imaging, media was replaced with 1x Hank's buffered salt solution (HBSS) (Gibco, Thermo Fisher) pH 7.2-7.4, at 37^{o}C. Cells were incubated for 10min with 200µL Hoechst 33342 nuclear staining (Sigma), prepared in HBSS at 2 µg/mL, and washed twice with 160µL HBSS. Cells were then treated with 20µL propranolol-β-Ala-β-Ala-X-BODIPY630/650 (propranolol-BY630/650), with 20µL unlabelled propranolol, or 20µL HBSS in the respective wells, for a final volume of 200µL per well. Cells were incubated with ligands for 30min, at 37^{o}C. Cells were then washed with 200µL HBSS buffer before imaging, to remove unbound ligand. Nuclear labelling was detected using a 488nm-Argon laser line (455-495nm bandpass), using 3% laser power, and fluorescent ligand labelling was detected using a 633nm-HeNe laser line and a long pass filter, using 5% laser power. Images were exported using ImageJ 1.51 (Fiji, USA) software.

2.6.4. Wide-field luminescence imaging

Bioluminescence imaging was performed using the Olympus LV200 wide-field inverted microscope, equipped with a 60x/1.42NA oil immersion objective lens. MDA-MB-231^{HM} Nluc-β_2AR cells were seeded, at a density of 250 000 cells into a MatTek disk containing a 1µm glass coverslip. Before imaging, media was removed and cells were incubated with 1.6mL HBSS containing 2µL furimazine substrate (~800nM) at 37^{o}C, for 15min. Background luminescence images were taken by capturing sequentially luminescence in the following channels: (1)

open channel (20 sec exposure time); (2) DAPI channel (20 sec exposure time; 420nm longpass filter) and (3) CY5 channel (4 min exposure time; 600/50nm bandpass filter). Cells were then incubated for 30 min with 200µL 50nM propranolol-(β-Ala-β-Ala)-X-BODIPY630/650, and 200µL 10µM ICI 118551 or 200µL HBSS, before images were acquired using the same acquisition sequence. BRET ratio measurements were performed using ImageJ 1.51 (National Institutes of Health, USA) and the time-series analyser V3 plugin.

2.6.5. Super-resolution Structured illumination microscopy

Super-Resolution Structured Illumination Microscopy (SIM) relies on a wide-field microscope setting with a movable diffraction grating (a grid with stripes that can shift and rotate), that has been inserted into the excitation beam path (Wegel et al., 2016). This grid creates light interferences (or patterned illumination), by its superimposition with the sample, which can also be called as Moiré effect (Fig. 2.17, Wegel et al., 2016).

This technique offers more detailed information about the object and higher-resolution imaging compared to a conventional confocal microscope (resolution limit of around 200nm). After z-stack images are acquired, these are reconstructed using a structural illumination analysis processing, available on the equipment software (Zen Black 2012, Zeiss, Germany).

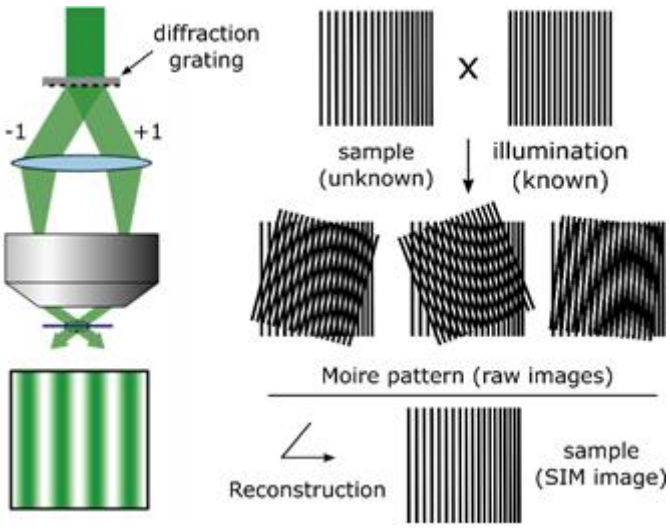

Fig. 2.17. Schematic representation of Moiré effect and the SIM principle. SIM relies on laser-based wide-field microscopy set-up to which a movable diffraction grating has been inserted into the excitation beam path. These laser beams interfere with each other at the focal plane of the objective and create an illumination in stripes (sinusoidal wave). This stripe pattern of light by its superimposition with the sample generates a so-called Moiré effect. For image reconstruction several raw images are collected, each being acquired at different orientation of the structured illumination, which is done by moving the diffraction grating (translation and rotation).

Spatial misalignment between spectrally distinct channels, that result from imaging with different sets of filter cubes, occur during imaging acquisition. To correct this spatial misalignment, a calibration using polystyrene beads coated with multiple fluorophores is needed. Imaging of these beads provide channel alignment parameters that can then be manually or automatically inserted to correct misalignment of acquired and processes images, using the Zen Black software.

Before imaging, HEK 293T cells were seeded at a density of 200,000 cells on poly-D-lysine coated 18x18mm 1.5H coverglasses (474030-9000-000; Zeiss, Germany) in 6-well plate, and cultured for 24h at 37°C/5% CO_2. Cells were transiently co-transfected with Halo-VEGFR2 and SNAP-β_2AR (3µg total cDNA). All transfections were performed using Fugene HD in Opti-MEM media (using 3:1 Fugene:cDNA ratio). Cells were then grown for an additional 24h at 37°C/5% CO_2. On the third day, media was aspirated from cells and coverslips were incubated with 200µL 1µM Halo-Tag surface AF660 membrane impermeant ligand substrate and 1µM SNAP-Surface AF647 membrane impermeant ligand, for 30min at 37°C/5% CO_2 in serum-free DMEM. Substrates were added to parafilm flat on a 6-well plate lid, and coverslips were positioned on top of substrates using twicers, with side containing cells turned down, to be immersed in substrates. After incubation, coverslips were put back in a 6 well plate and washed 3x with 2mL HBSS. 200µL ligands (10nM $VEGF_{165}$a or 10µM Isoprenaline) were added to a new parafilm, and coverslips were incubated with ligands for 60min at 37°C/without CO_2. For $VEGF_{165}$a incubations, HBSS was supplemented with 0.1% BSA. After incubation,

coverslips were put back in 6 well plate and washed with 2mL PBS, followed by fixation with 2mL 3% PFA and incubated for 10min at room temperature. Coverslips were then washed once again with 2mL PBS and mounted onto slides containing 15µL ProLong Glass Antifade Mountant (P36982; Thermo Fisher Scientific, USA) diluted 1:5 in ddH_2O. 2µL TetraSpeck™ microspheres (beads) (0.1µm; T7279, Thermo Fisher Scientific, USA), diluted 1:10 in ddH_2O, were included in each experiment to allow X/Y/Z channel alignment correction in image processing. Slides were left overnight at 4°C.

Imaging was performed using a Zeiss ELYRA PS.1 microscope fitted with a Plan Apochromat 63x/1.4 oil DIC M27 objective and Zeiss Immersol™ 518F (30°C) oil (Zeiss, Germany). Z-stack images of SNAP-β_2AR were acquired using bandpass 495-550 plus longpass 750 filter, at 5% laser power with 150ms exposure time (28µm grating). And, images of Halo-VEGFR2 were acquired using a long-pass 655 filter at 8% laser power with 150ms exposure time (42µm grating). All images were acquired at 1024x1024 frame size over 5 rotations as a Z-stack of 30-40 slices. Images were manually processed with consistent raw scaling between and within experiments (sectioning of 100x83x93; Zen Black 2012, Zeiss, Germany). Channel alignment parameters were defined using spectral beads, which were then manually applied for channel alignment analysis of processed SIM images.

2.7. Breast cancer animal model

Female BALB/c nu/nu immune-compromised mice (7-week-old) (University of Adelaide, Australia) were used in this study. These mice were housed under PC2 barrier conditions on a 12h dark/light cycle and monitored daily. All *in vivo* procedures were carried out at Monash Institute of Pharmaceutical Sciences, according to protocols approved (MIPS.2012.11) by the Monash University Animal Ethics Committee and according to NHMRC guidelines.

For tumour development, mice were injected into the fourth left mammary fat pad with $5x10^5$ MDA-MB-231^{HM} cells stably expressing Nluc-β_2AR (MDA-231 Nluc- β_2AR), using a Hamilton syringe with a 26 1/2G needle. Mice were kept

under 2-3% isoflurane anaesthesia during cells injection. Primary tumours were measured by caliper and volume (mm^3) was calculated using the formula: (length x $width^2$)/2. Tumour development was monitored by caliper measurements and whole-animal bioluminescence imaging (using an IVIS Lumina II Camera System, Perkin Elmer, USA), over a time period of 35 days, after tumour cells injection in mice.

2.7.1 Bioluminescence *in vivo* imaging to track tumour growth and metastasis

The development of solid tumours and metastasis were monitored using bioluminescence imaging. On the day of imaging, mice under 2-3% isoflurane anaesthesia, were injected via the tail vein (i.v.) with furimazine substrate (*circa* 3.7 mg/kg, 100µL in PBS). Whole-animal images were taken 5min after substrate injection using the IVIS Lumina II camera system (open channel; 30 sec exposure time, Figure 2.18.a). Immediately afterwards, images were acquired to the thorax region (metastatic sites), after covering the primary tumour with a small black box to eliminate light contamination from primary tumour (Figure 2.17.b). Images of the thorax region were acquired 10 min after furimazine injection, using luminescence imaging (open channel; 2 min exposure time).

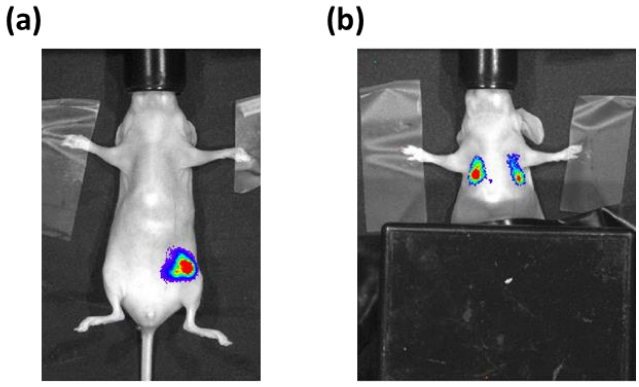

Figure 2.18. Whole-animal bioluminescence imaging using IVIS Lumina II camera system to monitor primary tumour and metastasis development. Mice under 2-3% isoflurane aneathesia were injected via the tail-vein with furimazine substrate (100µL, *circa* 3.7 mg/kg, prepared in PBS) 5 min before imaging. (a) Measurement of luminescence intensity from primary tumour (open channel, 30 sec exposure time). (b) Measurement of luminescence

intensity from thorax region with metastasis is lungs displayed (open channel, 2min exposure time).

2.7.2 NanoBRET to investigate ligand-receptor target engagement *in vivo*

To monitor ligand-receptor engagement *in vivo*, mice kept under 2-3% isoflurane anaesthesia were injected with 0.1 mg/kg propranolol-(β-Ala-β-Ala)-X-630/650 (propranolol-BY630/650; prepared in 50µl PBS) directly into the primary tumour (intratumoral injection; i.t). Non-specific binding was determined by pre-treatment (45min prior to injection of the fluorescent ligand) with 0.3 mg/kg (i.t.; 50µl in PBS) of the selective β_2-adrenoceptor antagonist ICI 118551. Competitive and non-competitive ligands (ICI 118551 at 1 and 10 mg/kg or CGP20712A at 10 mg/kg) were administered via tail-vein injection (i.v. injection, 100µL diluted in PBS).

i) *In vivo* NanoBRET association binding experiments

To measure fluorescent ligand (propranolol-BY630/650) association in living animals, 5 mice were administrated directly into the tumour (intratumoral, i.t. injection) with 0.1 mg/kg propranolol-BY630/650 ligand. Specific binding was investigated by imaging 4 mice pre-administrated with the unlabelled β_2AR-selective antagonist ICI 118551 (i.t. injection, 0.3 mg/kg prepared in 50µL PBS) 45min prior to 0.1 mg/kg propranolol-BY630/650 injection. Furimazine substrate was injected i.v.via the tail-vein (*circa* 3.7 mg/kg in 100µL PBS) was administrated immediately after propranolol-BY630/650 injection and images were acquired on the IVIS Lumina II system, by capturing sequential luminescence (open channel, 30 sec exposure time) and fluorescence (Cy5.5 channel 660/20nm bandpass, 5min exposure time) emissions. Sequential images were captured every 6min for a total time of 51min. Mice were kept under 2-3% isoflurane anaesthesia during injections and imaging.

ii) *In vivo* NanoBRET 'dissociation' binding experiments

To monitor fluorescent ligand 'dissociation' over time from Nluc-β_2AR expressed in the primary tumour region, mice were administered with three

different doses of propranolol-BY630/650 (0.01, 0.03 or 0.1 mg/kg). Mice were imaged at 1, 24, 48 and 72h after fluorescent ligand i.t. injection, and 5 min after i.v. injection of furimazine substrate (i.v., 100µL in PBS, *circa* 0.37 mg/kg). Images were acquired using the IVIS lumina II camera system, by capturing sequential luminescence (open channel, 30 sec exposure time) and fluorescence (Cy5.5 channel, 5 min exposure times) images. All mice were imaged on the day before fluorescent ligand injection, 5 min after 100µL i.v. injection with furimazine substrate (1:20 dilution in PBS) to determine luminescence (and BRET) baseline.

iii) Monitoring ligand-receptor engagement of unlabelled β-blockers administered locally in the primary tumour (i.t.) or via intravenous injection (i.v.)

For these experiments, mice were divided into two groups: Group 1 received i.t. injection of 0.1 mg/kg propranolol-BY630 (50µL in PBS), whereas Group 2 received 0.3 mg/kg (i.t.) ICI 118551, 45min prior to injection of 0.1 mg/kg propranolol-BY630 (i.t., 50µL in PBS). 1h after fluorescent ligand injection, luminescence was measured on the IVIS Lumina II system (Nluc donor, using an open channel, 30sec exposure time; BRET acceptor, using a CY5.5 channel, 660nm/20nm band pass, 5min exposure time). After 10 days, when fluorescent ligand was no longer detected by imaging, the treatment schedule was reversed. Group 1 mice were injected with 0.3 mg/kg ICI 118551 plus 0.1 mg/kg propranolol-BY630/650, whereas Group 2 animals were injected with fluorescent ligand. Luminescence and fluorescence emissions were measured as previously described. In each case, mice were also imaged 24h before administration of ligands and 5 min after i.v. furimazine injection to measure baseline BRET ratios. Regions of interest (ROIs) were drawn over the tumour site to obtain luminescence and fluorescence (photons/sec) measurements.

We also investigated the binding of unlabelled drugs administered i.v. to Nluc-β_2AR localised in the primary tumour. For this study, mice received intravenous injection (i.v.) of selective β_2-selective antagonist ICI 118551 (at 1 or 10 mg/kg

dose; 100µL in PBS), or the selective β_1-selective antagonist CGP20712A (at 10 mg/kg dose; 100µL in PBS). The same cross over experimental design was followed, with 0.1 mg/kg propranolol-BY630/650 injected directly into the primary tumour 45min after i.v. administration of ICI 118551 or CGP20712A compounds, or PBS (in animals injected with fluorescent ligand alone). Luminescence/fluorescence images were captured using the IVIS camera system, 5min after furimazine substrate i.v. injection, using the same filter settings and exposure times described earlier. Mice were kept under 2-3% isoflurane anaesthesia during injections and imaging.

2.7.3. In vivo NanoBRET imaging data analysis

In vivo luminescence or fluorescence total flux (photons/sec) measurements were obtained using ROIs positioned on the primary tumour or thorax region, for primary tumour or metastasis measurements, respectively. Raw BRET ratios were calculated as:

$$BRET\ ratio = \frac{Acceptor\ Luminescence\ (CY5.5)}{Donor\ Luminescence\ (open\ channel)},$$

where acceptor emission (Cy5.5 channel) is measured using the CY5.5 emission channel (660nm/20nm bandpass), and luminescence emission (open channel) is measured without using emission filters (open channel).

For association binding data analysis, raw BRET ratios obtained from each individual experiment were fitted using GraphPad Prism 7, using a non-linear regression equation. Total and non-specific binding curves were fitted simultaneously using the following equation:

$$BRET\ Ratio = \frac{B_{max} \times [B]}{[B] + K_D} + \big((M \times [B]) + C\big),$$

where B_{max} corresponds to the maximal binding, K_D is the equilibrium dissociation constant, [B] is the concentration of fluorescent ligand, M is the

slope of the non-specific binding component, and C is the intercept with the Y-axis.

2.8. Statistical analysis

All data analysis was performed using GraphPad Prism 7.02 (San Diego, CA, USA). In Chapter 3, two-way Anova with Sidak's multiple comparison test was used to compare two different condition (i.e. with BSA vs without BSA) at different concentrations. This statistical analysis method was applied for data displayed in table 3.2 and 3.3. Level of significance is described in respective figure legends or tables.

In Chapter 5, two-way Anova with Dunnet's multiple comparison test was used to compare the mean values obtained for different concentrations of BRET acceptor with the mean value obtained for BRET donor alone. This statistical analysis method was applied to all data obtained to investigate receptor-receptor interaction (Fig. 5.1, 5.2, 5.3, 5.4, 5.5 and 5.7 and table 5.1). Level of significance is described in respective figure legends or tables.

In Chapter 6, tumour and metastasis development over time was compared for 11 different mice at different days compared to Day 8 baseline, using two-way Anova with Tukey's multiple comparison test (Fig. 6.1 and 6.2). The effect of different doses of fluorescent tracer on BRET ratio for 6 different mice compared to control at time 0h were compared using two-way Anova and Dunnet's multiple comparison test (Fig. 6.5). Level of significance is described in respective figure legends or tables. Data obtained for 6 different animals receiving reversed treatment of fluorescent tracer in the presence or absence of unlabelled antagonist were analysed using two-way Anova with Tukey's multiple comaprison test (Fig. 6.6 and 6.7). Level of significance is described in respective figure legends.

Chapter 3: Characterisation of a fluorescently labelled $VEGF_{165}a$ ligand in solution using Fluorescence Correlation Spectroscopy

3.1. Introduction

Vascular endothelial growth $factor_{165}a$ ($VEGF_{165}a$) is one of the multiple VEGFa isoforms, derived from alternative gene *Vegfa* splicing, that can be present in cells as a dimer to bind and activate VEGFR2 and VEGFR1 (Peach et al., 2018a; Simons et al., 2016). This activation occurs upon $VEGF_{165}a$ ligand binding, receptor dimerization and a consequential change in conformation of receptor intracellular domains, resulting in an auto- or trans-phosphorylation of specific tyrosine residues. Phosphorylation of tyrosine residues then leads to the recruitment of different adaptor proteins and signalling cascade propagation (Berger and Ballmer-Hofer, 2011; Sarabipour et al., 2016). This VEGF isoform is one of the key drivers of tumour angiogenesis, and is therefore an important target in cancer therapy (Claesson-Welsh and Welsh, 2013; Hilmi et al., 2012; Shibuya, 2014).

A fluorescently-labelled version of $VEGF_{165}a$, consisting of two anti-parallel bound $VEGF_{165}a$ protomers, each labelled at a single N-terminal cysteine residue with a tetramethyl-rhodamine fluorophore ($VEGF_{165}a$-TMR; ~165kDa expressed protein) was generated by Promega (Madison, Wisconsin, USA). $VEGF_{165}a$-TMR ligand has been used in our lab as a pharmacological tool to measure ligand-receptor binding kinetics, using human full-length VEGF receptor-2 (VEGFR2), at real-time in living cells, (Kilpatrick et al., 2017; Stoddart et al., 2018). This fluorescent ligand was also used in Chapters 4 and 5 of this thesis as a pharmacological probe to characterise VEGFR2.

Fluorescence Correlation Spectroscopy is a single-photon counting technique that can detect very small changes in fluorescence intensity from fluorescently labelled molecules diffusing through a small defined detection volume (~0.25

femtoliters) (Gherbi et al., 2018). Changes in fluorescence intensity (fluctuations in intensity), resulting from fluorescently-labelled particles moving in and out of the small confocal volume are measured in a time-correlated manner. Analysis of the time-dependent variations in intensity is performed using an autocorrelation analysis that provides quantitative information on average diffusion (or dwell) time of the fluorescent molecules in the measured volume (τ_D), and on the average number of particles (N) (Briddon et al., 2018). A different analysis can be performed using the same fluctuations in intensity, which is the photon counting histogram (PCH) analysis. PCH analyses fluctuations in intensity in respect to their amplitude, rather than in a time-dependent manner (Briddon et al., 2018). This analysis enables the determination of fluorescent molecules stoichiometry based on their molecular brightness (ε) (Briddon et al., 2018; Kilpatrick et al., 2012).

FCS was applied in this study to: (1) determine the 'real' concentration of free $VEGF_{165}$a-TMR fluorescent ligand in solution in the presence and absence of bovine serum albumin (BSA), and to (2) determine the dimeric and double-labelled structure of $VEGF_{165}$a-TMR. Some of the data presented here has been published in (Kilpatrick et al., 2017).

3.2. Brief materials and methods

Fluorescently-labelled molecules

A fluorescently-labelled version of $VEGF_{165}$a was generated as an anti-parallel bound dimer with two $VEGF_{165}$a protomers, each labelled at a single N-terminal cysteine residue with a tetramethyl-rhodamine fluorophore ($VEGF_{165}$a-TMR). This ligand was generated by Promega (Madison, Wisconsin, USA). Fluorescence ligand synthesis and purification is described in (Kilpatrick et al., 2017). Commercial Rhodamine 6G (R6G) and 5-Carboxy-tetramethylrhodamine N-succinimidyl ester (TAMRA) fluorophores were used for calibration or experimental purposes.

Fluorescence Correlation Spectroscopy (FCS)

Detailed methods about FCS experiments, and data analysis are provided in Chapter 2, section 2.4. FCS experiments were performed using a LSM510 NLO Confocor3 microscope equipped with a c-Apochromat 40x/1.2NA water-immersion objective (Zeiss, Germany). Briefly, this methodology was applied here to investigate the concentration in solution of $VEGF_{165}$a-TMR in the presence or absence of 0.1% protease-free BSA. FCS calibration was performed before all experiments using R6G and TAMRA fluorophores. Calibration with 10nM R6G (with a known diffusion coefficient, D_{R6G} = 2.8 x10^{-6} cm^2s^{-1} allowed the estimation of confocal volume waist radius (w_0 = (4x D_{R6G} x τ_D)$^{1/2}$). The diffusion coefficient for fluorescent species could then be determined using equation 1: D = w_0^2/4 x τ_D, and concentration using details provided in Box 1. Further details are provided in Chapter 2, section 2.4.

Box 1: Data analysis to calculate free fluorescent ligand concentration in solution:

5. **The radius of the detection volume** $(\boldsymbol{w_0}) = \sqrt{\boldsymbol{4 \times \tau_D \times D}}$, where D is the Diffusion Coefficient of a reference fluorophore; D(R6G)= 2.8X$10^{-10}$$m^2s^{-1}$. And τ_D is the diffusion time representing halfway point decay of the autocorrelation function, G(τ).
6. **The half-height of the detection volume** $(\boldsymbol{w_1}) = \boldsymbol{w_0} \times \boldsymbol{SP}$
7. **The detection volume is calculated as:** $\boldsymbol{V = \pi^{3/2} \text{ x } w_0^2 \text{ x } w_1}$.
8. **The concentration of fluorescent particles in solution is then calculated as:**

$\boldsymbol{C(M) = \frac{1}{V} \text{ x } \frac{N}{NA}}$, where N is the particle number, which is equal to the inverse of G(0), as shown in the autocorrelation curve represented above, V is the confocal detection volume, and NA is the Avogadro constant 6x10^{23} mol^{-1}.

Calibration experiments were performed with TAMRA fluorophore to determine PCH analysis first order correction, which is required for the determination of molecular brightness (ε). PCH analysis divides the fluctuations in intensity into a desired binning time. The binning time chosen for these experiments was 20μs, which is shorter than the diffusion time of $VEGF_{165}$a-

TMR, but also long enough to avoid fast photophysical events). Using that specific binning time, PCH describes the resultant frequency distribution of photon counts per bin (k), and particle number (N). PCH analysis uses a 3D Gaussian approximation of the laser bin profile and super-Poisson statistics to predict the molecular brightness (ε) of the fluorescent molecule being measured. Molecular brightness (ε) refers to the counts of photons per molecule per second ($cpms^{-1}$) and is calculated by the following equation 2:

(Equation 2): $\varepsilon = k/N$, where k =photon count rate (in kHz) and N = average number of molecules.

3.3. Results

Using FCS and autocorrelation analysis to determine the concentration of free $VEGF_{165}$a-TMR ligand in buffer solution

Fluorescence correlation spectroscopy (FCS) was applied in this study to measure the concentration of free $VEGF_{165}$a-TMR ligand in 1% HEPES-buffered salt solution (HBSS), in the absence or presence of 0.1% protease-free bovine serum albumin (BSA).

$VEGF_{165}$a-TMR molecules crossing the detection confocal volume due to Brownian motions were excited by a laser (at 560nm, with laser power set to 0.394 kW/cm^2), and fluctuations in fluorescence intensity were recorded in a time-correlated manner generating autocorrelation curves (Figure 3.1.). FCS-detected fluctuations in intensity were measured for a range of $VEGF_{165}$a-TMR concentrations (0.25 to 10nM) prepared in HBSS buffer in the absence of 0.1% BSA, which were placed and measured in an 8-well coverglass plate. These measurements were performed by positioning the confocal volume in buffer solution 200µm above the top of the plate coverslip. All experiments were performed at 22^{o}C. Autocorrelation analysis of these fluctuations in intensity resulted in simple monophasic autocorrelation curves, for all $VEGF_{165}$a-TMR concentrations (Figure 3.1.). Therefore, autocorrelation data were fit to a one-component 3-dimensional (3D) Brownian diffusion model. Two important parameters can be determined from autocorrelation analysis, fluorescent particles diffusion (or dwell) time and particle number. Diffusion time (τ_D) is determined from the mid-decay of the autocorrelation function (in the abscissa). Whereas, particle number (N) is inversely proportional to the amplitude of the autocorrelation function at time zero, ($N = \frac{1}{G(0)}$). Autocorrelation analysis measured for 10nM $VEGF_{165}$a-TMR in solution resulted in an average diffusion time (τ_D) of 233.8 ± 31.5 µs (n=3), in the absence of 0.1% BSA, which corresponds to the diffusion time of $VEGF_{165}$a-TMR homodimer. In all these experiments calibration was first carried out to determine the diffusion time of 10nM Rhodamine 6G, which allowed the

determination of VEGF165a-TMR diffusion coefficient, as explained in the brief methods described above and in more detail in Chapter 2, section 2.4.4. A calculated diffusion coefficient (D) of 74.6 ± 7.0 $\mu m^3 s^{-1}$ (n=3), was determined for 10nM $VEGF_{165}$a-TMR, in the absence of 0.1% BSA.

FCS-detected concentration can be calculated from particle number and confocal volume, which can be calculated as previously described in Box 1, in brief methods and methodology section (and Chapter 2, section 2.4). FCS-detected concentrations measured for a nominal (or added) concentration of 10nM $VEGF_{165}$a-TMR was 3.6 ± 0.2 nM (n=3), in the absence of 0.1% BSA. Therefore, FCS-detected concentration was much less compared to nominal 10nM concentration of $VEGF_{165}$a-TMR. The reduced concentration detected by FCS could result from non-specific binding of $VEGF_{165}$a-TMR to plastic during sample preparation.

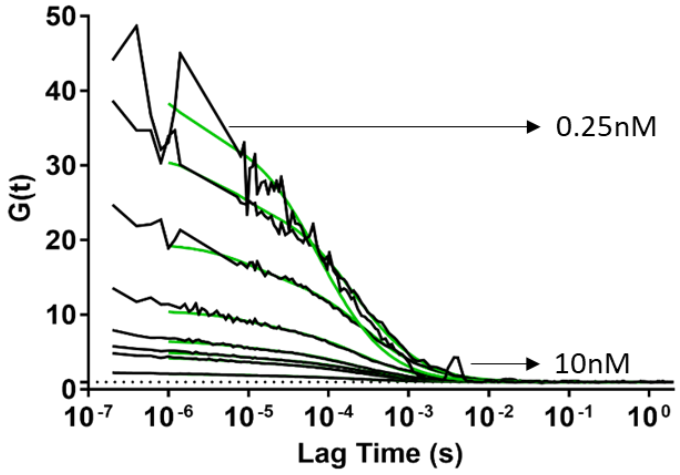

Figure 3.1. Representative autocorrelation curves measured of a range of $VEGF_{165}$a-TMR concentrations (0.25nM to 10nM) in HBSS buffer without 0.1% BSA. FCS-detected fluctuations in intensity measured for different $VEGF_{165}$a-TMR concentrations were analysed using an autocorrelation analysis and fitted to a single-component 3D Brownian diffusion model. Black lines correspond to autocorrelation curves, whereas green lines correspond to curve fitting. Different parameters can be measured from autocorrelation function G(t), which is represented in a logarithmic time scale in seconds (Lag Time). The mid-point decay of the curve (x axis) correspond to the fluorescent particle diffusion or dwell time (τ_D). Whereas the particle

number can be determined from the function amplitude (y axis), which is inversely proportional to the amplitude of the function at time zero ($N = \frac{1}{G(0)}$).

Bovine serum albumin (BSA) is a carrier protein commonly used to block or prevent non-specific protein-surface interactions (Francis, 2010). Therefore, FCS measurements were performed for the same range of $VEGF_{165}$a-TMR nominal concentrations which were prepared in HBSS containing 0.1% protease-free BSA. Autocorrelation analysis of fluctuations in intensity measured for $VEGF_{165}$a-TMR in the presence of 0.1% BSA resulted in monophasic autocorrelation curves, for all $VEGF_{165}$a-TMR concentrations (Figure 3.2.). Interestingly, the autocorrelation curves showed a decrease in amplitude at time zero (y axis), compared to autocorrelation function measured for $VEGF_{165}$a-TMR in the absence of 0.1% BSA, which was observed for all different $VEGF_{165}$a-TMR concentrations (Figure 3.1. and 3.2.). Since particle number is inversely related to the amplitude of the autocorrelation function at time zero, these observations indicate that incorporation of 0.1% BSA in buffer results in the increase in particle number measured. FCS-detected concentration was also increased. Measurement of 10nM nominal $VEGF_{165}$a-TMR in the presence of 0.1% BSA showed a FCS-measured concentration of 8.9 ± 0.8 nM (n=3). Linear regression analysis was used to compare nominal concentration in the absence or presence of 0.1% BSA, which showed a slope = 0.2 (R^2= 0.8; 95% confidence limits 0.2 – 0.3, Figure 3.3.), in the absence of BSA and a slope = 0.8 (R^2= 1; 95% confidence limits 0.7 – 0.9), in the presence of BSA. Autocorrelation analysis resulted in τ_D = 215.8 ± 13.6 μs (n=3) (and D = 74.6 ± 7.0 $\mu m^3 s^{-1}$) for 10nM $VEGF_{165}$a-TMR in buffer containing 0.1% BSA, Diffusion times (τ_D) and calculated diffusion coefficients (D) measured for the range of $VEGF_{165}$a-TMR concentrations, in buffer in the absence and presence of 0.1% BSA, are presented in Table 3.1. No significant differences were observed for both τ_D or D in the absence or presence of 0.1% BSA, which were compared for each individual $VEGF_{165}$a-TMR concentrations.

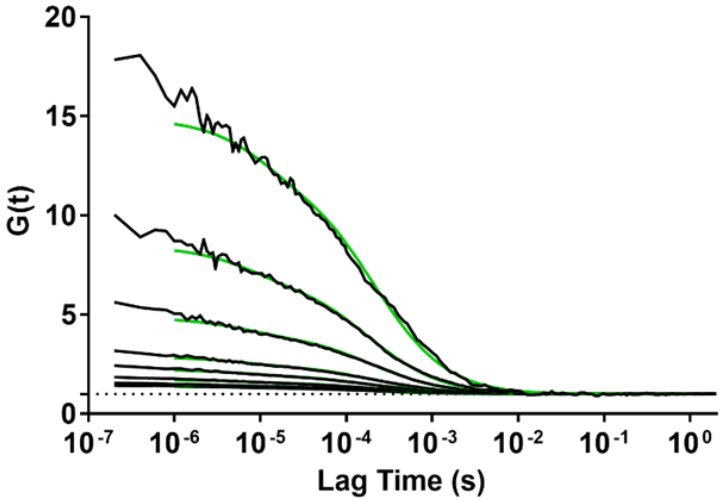

Figure 3.2. Representative autocorrelation curves measured of a range of $VEGF_{165}$a-TMR concentrations (0.25nM to 10nM) in HBSS buffer containing 0.1% BSA. Monophasic autocorrelation curves (black lines) were obtained for the different concentrations of $VEGF_{165}$a-TMR measured in buffer containing 0.1% BSA, which were fitted to a single-component Brownian diffusion model (green lines).

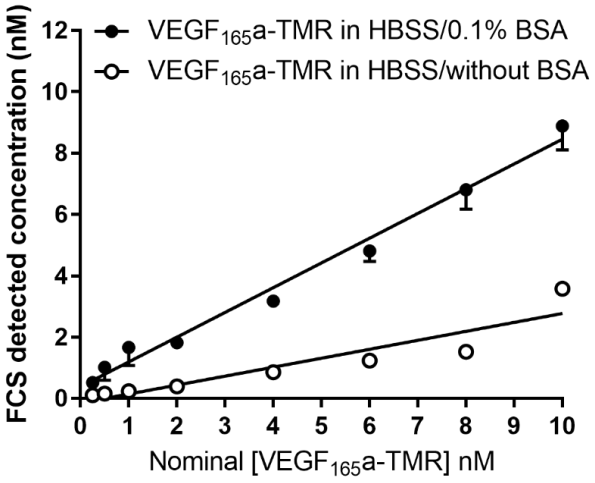

Figure 3.3. Linear regression analysis of a range of nominal $VEGF_{165}$a-TMR concentrations vs FCS-detected concentration in HBSS buffer in the absence or presence of 0.1% BSA. A range of concentrations of $VEGF_{165}$a-TMR (0.25 – 10nM) was used to investigate the effect of BSA on ligand solubility in HBSS buffer solution. FCS-detected $VEGF_{165}$a-TMR concentrations were calculated from particle number, as previously described. Linear regression analysis using PRISM GraphPad 6.0 showed a slope of 0.8 (R^2= 1; 95% confidence limits 0.7 – 0.9) for $VEGF_{165}$a-TMR prepared in buffer containing 0.1% BSA, whereas a slope of 0.20 (R^2= 0.8; 95% confidence limits 0.2 – 0.3), was obtained for VEGF-TMR in buffer without 0.1% BSA. Data are displayed as mean ± SEM from 3 independent experiments.

Table 3.1. Diffusion time (τD, in μs) and calculated diffusion coefficient (D, in μm s^{-1}) measured using autocorrelation analysis for a range of $VEGF_{165}$a-TMR concentrations prepared in HBSS buffer in the absence or presence of 0.1% BSA.

Diffusion time (τ_D)		
[$VEGF_{165}$a-TMR] (nM)	Without 0.1%BSA	With 0.1%BSA
	mean ± SEM (μs)	mean ± SEM (μs)
0.25	186.4 ± 16.7	183.2 ± 9.2
0.5	194.6 ± 19.1	201.3 ± 10.4
1	228.7 ± 17.4	208.4 ± 5.2
2	238.3 ± 25.0	199.5 ± 2.5
4	271.1 ± 29.8	212.3 ± 5.1
6	248.6 ± 10.0	201.2 ± 4.7
8	240.8 ± 13.4	193.4 ± 1.5
10	233.8 ± 31.5	215.8 ± 13.6
Diffusion coefficient (D)		
[VEGF165a-TMR] (nM)	Without 0.1%BSA	With 0.1%BSA
	mean ± SEM ($\mu m^3 s^{-1}$)	mean ± SEM ($\mu m^3 s^{-1}$)
0.25	79.2 ± 12.3	90.8 ± 5.0
0.5	84.8 ± 6.1	83.1 ± 5.6
1	63.3 ± 7.9	78.9 ± 2.4
2	66.8 ± 5.3	82.1 ± 1.2
4	63.3 ± 5.6	77.4 ± 2.1
6	66.3 ± 2.7	81.7 ± 2.4
8	66.9 ± 2.9	84.7 ± 0.6
10	74.6 ± 7.0	77.9 ± 5.4

No significant differences were measured using Two-way ANOVA with Sidak's multiple comparison test for both diffusion times (τ_D) or diffusion coefficients (D) determined for the different concentrations of $VEGF_{165}$a-TMR in the presence or absence of 0.1% BSA.

Investigation of FCS-detected concentration over time for $VEGF_{165}$a-TMR ligand in buffer solution in the absence or presence of 0.1% BSA

FCS-detected concentration for the same range of nominal $VEGF_{165}$a-TMR concentrations was monitored over time for 20 min, to investigate ligand solubility in HBSS buffer without or with 0.1% BSA. 5-Carboxy-tetramethylrhodamine N-succinimidyl ester (TAMRA) fluorophore was used in here as a control. FCS-detected $VEGF_{165}$a-TMR concentration in buffer without the incorporation of 0.1% BSA was reduced, as previously described, with a further decrease over time (Figure 3.4.a). FCS measurements were also performed using TAMRA fluorophore to investigate FCS-detected

concentration in buffer without 0.1% BSA. FCS-detected concentration for 10nM nominal TAMRA concentration was also reduced (4.8 ± 0.1 nM (n=3), measured at time zero). On the other hand, incorporation of 0.1% BSA in buffer resulted in higher FCS-detected concentration for $VEGF_{165}$a-TMR, which were kept constant over time (Figure 3.4.b). A higher concentration was also detected for TAMRA fluorophore, with nominal 10nM TAMRA concentration displaying a FCS-measured concentration of 10.1 ± 0.4 nM (n=3), measured at time zero.

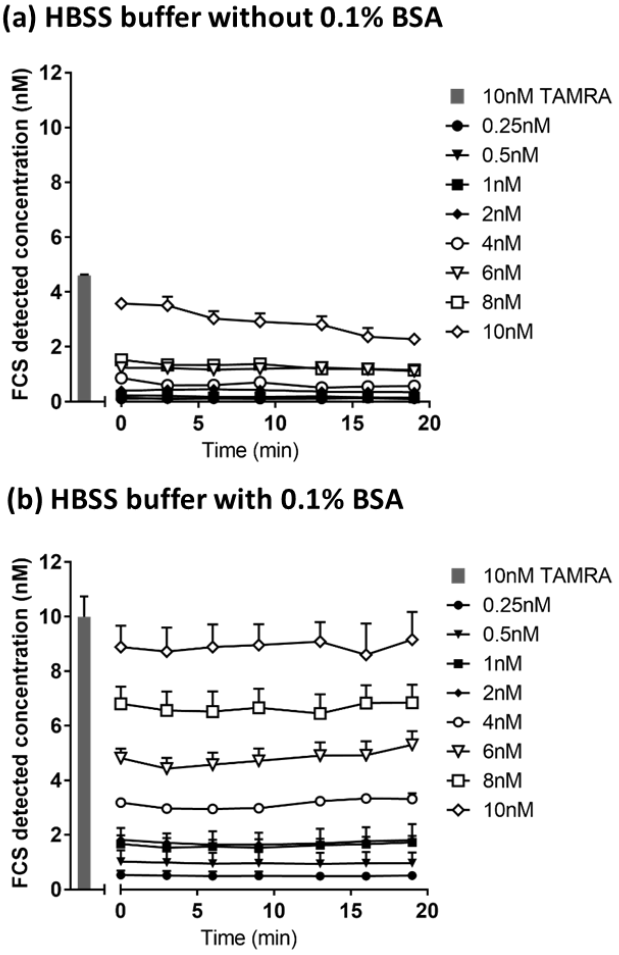

Figure 3.4. Investigation of the effect of BSA in $VEGF_{165}$a-TMR and TAMRA fluorophore solubility in buffer solution. FCS-detected particle number (and calculated concentration) were measured for a range of $VEGF_{165}$a-TMR concentrations prepared in buffer in the absence (a) or presence (b) of 0.1% BSA, which were measured over time for 20 min. 10nM TAMRA fluorophore was used in this study as a control, which FCS-detected concentration was measured at time zero. These data are displayed as mean ± SEM from 3 independent experiments.

Using FCS and autocorrelation analysis to determine $VEGF_{165}$a-TMR homodimeric structure

$VEGF_{165}$a-TMR range of concentrations (0.25nM to 10nM) were calculated assuming homodimeric species. Linear regression analysis showed that FCS-detected concentrations for $VEGF_{165}$a-TMR matched with FCS-detected concentrations measured for TAMRA fluorophore (Figure 3.5.), which were prepared in buffer containing 0.1% BSA. Linear regression for TAMRA displayed a slope = 0.94 (R^2=1; 95% confidence limits 0.8-1.0), whereas linear regression for $VEGF_{165}$a-TMR resulted in a slope = 0.8 (R^2=1; 95% confidence limits 0.7-0.9). These results provide strong evidence that $VEGF_{165}$a-TMR ligand is in fact formed by two protomers, each one labelled with a TMR fluorophore. However, photon counting histogram (PCH) analysis is a better option to determine fluorescent particles stoichiometry (Briddon et al., 2018).

PCH analysis allows the differentiation between species based on their molecular brightness (ε), which is the average count of photons per molecule per second ($cpms^{-1}$) (Briddon et al., 2018). This analysis was used to investigate the homodimeric and the dual-labelled structure of $VEGF_{165}$a-TMR ligand, based on its molecular brightness. TAMRA fluorophore was also used as a control. PCH analysis was performed using the same fluctuations in intensity measured for both $VEGF_{165}$a-TMR and TAMRA fluorophore (using a range of concentrations, 0.25 to 10nM). These data were fit to a single-component PCH model, using a selected binning time of 20µs.

In theory, the brightness of a molecule containing two fluorophores, which seems to be the case for the $VEGF_{165}$a-TMR dimer, would result in a two-fold in brightness compared to a single TAMRA fluorophore. Data analysed for 10nM $VEGF_{165}$a-TMR resulted in ε = 194.2 ± $8.6x10^3$ $cpms^{-1}$(n=3), whereas PCH analysis of 10nM TAMRA showed a ε = 146.5 ± $0.6x10^3$ $cpms^{-1}$ (n=3), which were significantly different at this measured concentration (Table 3.2.), showing a 0.2-fold difference. However, TAMRA and $VEGF_{165}$a-TMR are not totally comparable as their quantum yield is likely to be different.

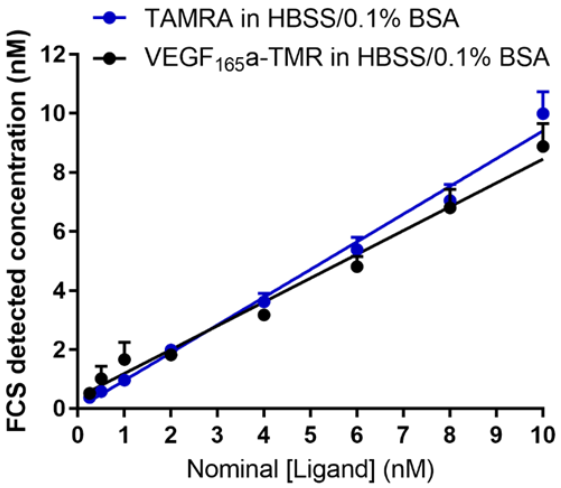

Figure 3.5. Linear regression analysis for nominal vs FCS-detected concentrations for a range of $VEGF_{165}$a-TMR (assuming dimeric species) and TAMRA (0.25 to 10nM) prepared and measured in HBSS buffer in the absence of 0.1% BSA. $VEGF_{165}$a-TMR resulted in a slope of 0.8 (R^2= 1; 95% confidence limits 0.7 – 0.9. Whereas TAMRA measurements showed a slope = 0.8; R^2=1.0; 95% confidence limits 0.7 – 0.8. Data are displayed as mean ± SEM from 3 independent experiments.

Table 3.2. Molecular brightness measured using PCH analysis for a range of $VEGF_{165}$a-TMR and TAMRA in HBSS buffer containing 0.1% BSA.

Molecular brigthness			
Concentration (nM)	$VEGF_{165}$a-TMR mean ± SEM x10^3 ($cpms^{-1}$)	TAMRA mean ± SEM x10^3 ($cpms^{-1}$)	p value
0.25	118.3 ± 4.8	124.0 ± 3.3	ns
0.5	153.6 ± 8.3	139.5 ± 3.4	ns
1	169.8 ± 3.9	144.1 ± 2.1	**
2	178.5 ± 7.2	150.6.3 ± 0.7	**
4	184.3 ± 8.5	167.2 ± 0.6	ns
6	192.2 ± 6.5	164.3 ± 0.7	**
8	192.5 ± 6.7	154.8 ± 0.5	****
10	194.2 ± 8.6	146.5 ± 0.6	****

Molecular brightness data (measured as counts per molecule per second, $cmps^{-1}$) is displayed as mean ± SEM from 3 independent experiments. ****p<0.0001, using Two-way ANOVA with Sidak's multiple comparison test.

Using 2-mercaptoethanol (2-ME) reducing agent to investigate homodimeric structure of $VEGF_{165}$a-TMR fluorescent ligand

$VEGF_{165}$a-TMR was chemically generated as a homodimer formed by two antiparallel disulfide-bridged $VEGF_{165a}$ protomers, each labelled at a single cysteine residue with TMR fluorophore (Kilpatrick et al., 2017; Muller et al., 1997). A different alternative to investigate the homodimers structure of VEGF165a-TMR is the incubation of this ligand under reducing conditions to disrupt the disulphide-bridges connecting the dimer (Figure 3.6.a). For this purpose, $VEGF_{165}$a-TMR ligand was incubated in buffer containing 0.1% BSA and 1mM 2-mercaptoethanol (2-ME, also known as β-mercaptoethanol) reducing agent. 2-ME is a potent reducing agent that denature proteins by irreversibly reducing disulfide linkages, leading to tautomerization and breaking up of the quaternary protein structure (Chang, 1997). Since $VEGF_{165}$a-TMR is formed by two protomers and each labelled with TMR fluorophore, pre-incubation of this fluorescent ligand under reducing conditions should theoretically result in a two-fold increase in particle number (and hence concentration) detected by FCS.

The treatment of 10nM $VEGF_{165}$a-TMR with 1mM 2-ME, pre-incubated for 30min, at 37^{o}C, showed an increase in concentration for $VEGF_{165}$a-TMR fluorescent ligand (Figure 3.6.b), with a τ_D = 350.4 µs (n=2) (and a calculated D = 49.3 $\mu m^3\ s^{-1}$). However, incubation of 10nM TAMRA fluorophore with 1mM 2-ME also resulted in an increase in calculated concentration, which should not have been affected. Similar data was obtained using PCH analysis, which showed a decrease in molecular brightness for both $VEGF_{165}$a-TMR and TAMRA (Figure 3.6.c). Therefore, these data suggest that 2-ME reducing agent may alter the photophysical properties of the fluorescent molecules.

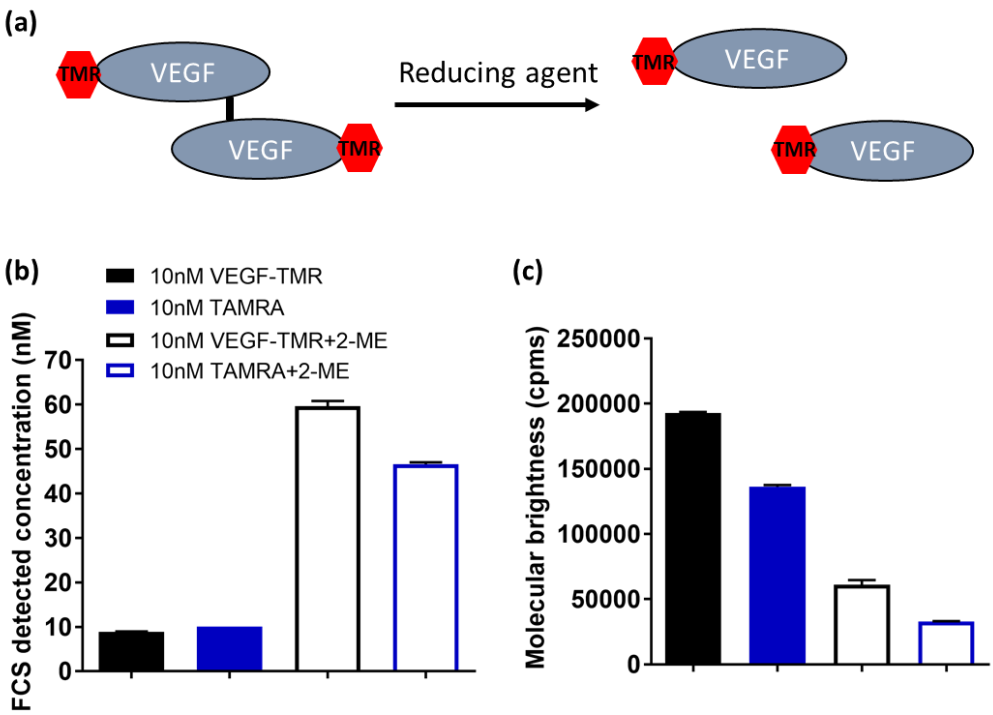

Figure 3.6. Investigation of homodimeric structure of $VEGF_{165}$a-TMR ligand using 2-mercaptoethanol (2-ME) reducing agent. 10nM $VEGF_{165}$a-TMR or 10nM TAMRA fluorophore were prepared in HBSS buffer in the presence of 0.1% BSA, and under non-reducing or reducing conditions, using 1mM 2-ME reducing agent. Incubation with 1mM 2-ME were performed for 30min, at 37°C, before FCS measurements. FCS detected concentrations were calculated from particle number obtained from autocorrelation analysis of fluctuations in intensity. **(a)** Schematic representation of reducing agent effect in separating the disulfide-linked $VEGF_{165}$a-TMR promoters forming the homodimeric ligand. **(b)** FCS-detected concentration for 10nM $VEGF_{165}$a-TMR and 10nM TAMRA measured in buffer under non-reducing or 2-ME-reducing conditions. **(c)** Molecular brightness ($cpms^{-1}$) determined using PCH analysis for 10nM $VEGF_{165}$a-TMR and 10nM TAMRA measured in buffer under non-reducing or 2-ME-reducing conditions. These data are expressed as mean from two independent experiments.

Using dithiothreitol (DTT) reducing agent to investigate homodimeric structure of $VEGF_{165}$a-TMR fluorescent ligand

The next step was to use a different reducing agent, L-(-)-Dithiothreitol (DTT) to confirm the homodimeric nature of $VEGF_{165}$a-TMR ligand. This reducing agent was previously used at a concentration of 100mM to investigate the homodimeric structure of this fluorescent ligand using fluorescent SDS-PAGE

(Kilpatrick et al., 2017). In this study, a range of $VEGF_{165}$a-TMR concentrations (0.25 to 10nM) were prepared in HBSS buffer containing 0.1% BSA and pre-incubated for 30min, at 37^{o}C, with 10mM DTT. $VEGF_{165}$a-TMR DTT-treated showed a significant increase in particle number and, hence in concentration (*$p<0.0001$, Figure 3.7.a). Linear regression analysis showed a slope of 1.61 (n=3, R^2 = 0.97; 95% confidence limits 1.5-1.7), for $VEGF_{165}$a-TMR under reducing conditions. These data suggest a two-fold increase in concentration calculated from particle number for DTT-treated vs non-treated $VEGF_{165}$a-TMR, indicating the successful disruption of homodimers to monomers. The use of 1mM concentration of DTT was not as efficient as 10mM DTT for the disruption of dimeric ligand (Figure 3.7.b). DTT treatment had no significant effect on TAMRA FCS-measured concentration (n=3, slope = 0.8; R^2=1.0; 95% confidence limits 0.7 – 0.8, Figure 3.7.c), indicating that DTT does not affect photophysical properties of the fluorophore. No significant changes were observed in diffusion time (or diffusion coefficients) for $VEGF_{165}$a-TMR DTT-treated or untreated conditions, which is represented in Figure 3.7.d, also determined using Two-way ANOVA with Sidak's multiple comparison test for the different range of $VEGF_{165}$a-TMR concentrations under reducing or non-reducing conditions.

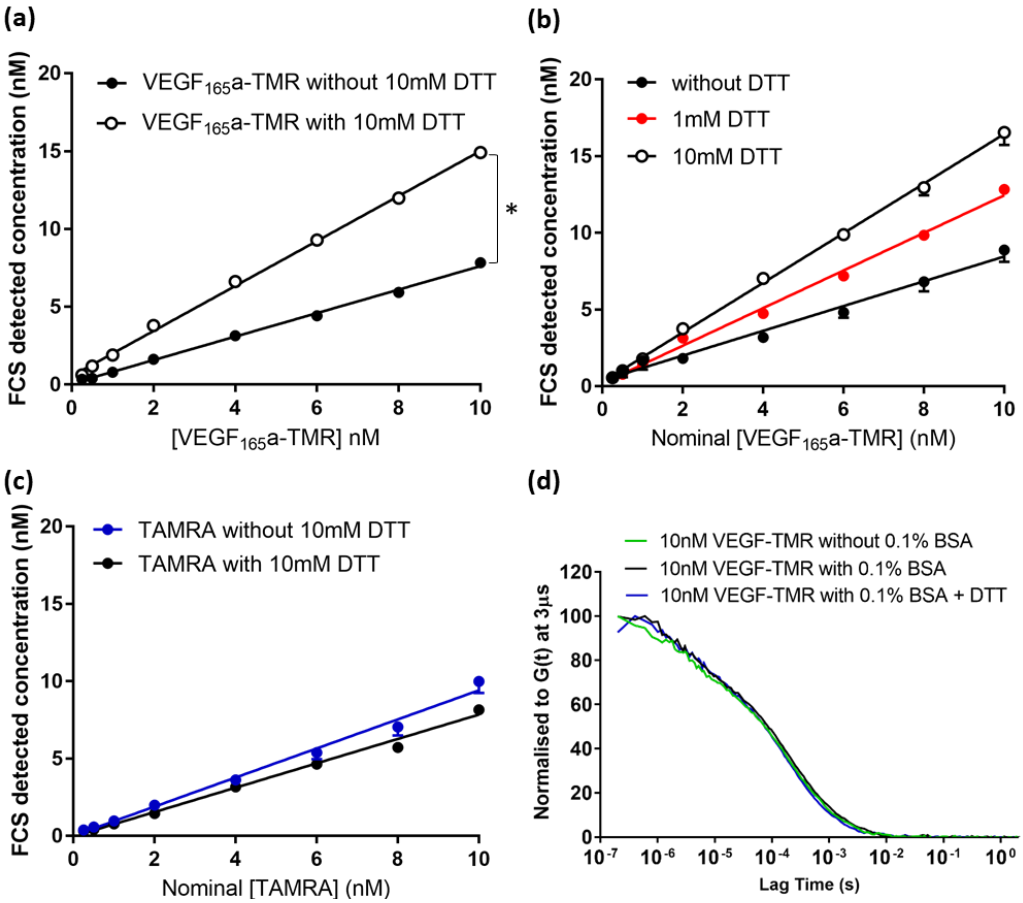

Figure 3.7. Investigation of homodimeric structure of VEGF$_{165}$a-TMR ligand using dithiothreitol (DTT) reducing agent. A range of VEGF$_{165}$a-TMR or TAMRA fluorophore concentrations (0.25 to 10nM) were prepared in HBSS buffer in the presence of 0.1% BSA, and under non-reducing or reducing conditions. These were incubated for 30min, at 37^{o}C with DTT before FCS measurements. FCS detected concentrations was calculated from particle number obtained from autocorrelation analysis of fluctuations in intensity. **(a)** Linear regression to compare nominal vs FCS-detected concentrations for VEGF$_{165}$a-TMR under non-reducing (slope = 0.8) or reducing conditions (slope = 1.61), using 10mM DTT. **(b)** Linear regression comparing nominal vs FCS-detected concentrations for VEGF$_{165}$a-TMR under non-reducing or reducing conditions with 1mM or 10mM DTT. **(c)** Linear regression comparing nominal vs FCS-detected concentrations for TAMRA under non-reducing or reducing conditions using 10mM DTT. **(d)** Representation of autocorrelation functions for 10nM VEGF$_{165}$a-TMR in HBSS buffer in the absence or presence of 0.1% BSA and under non-reducing or reducing conditions (10mM DTT). These autocorrelation curves were normalized considering G(t) at 3µs 100%. Data in (a), (b) and (c) are expressed as mean ± SEM from three independent experiments. Treatment with 1mM DTT is from two individual experiments. * p<0.0001 Two-way ANOVA with Sidak's multiple comparison test.

PCH analysis was also used to compare molecular brightness (ε) measured for DTT-treated and untreated $VEGF_{165}$a-TMR at different concentrations. This analysis showed a significant increase, rather than decrease, in ε for all concentrations of $VEGF_{165}$a-TMR under DTT-treated condition, compared to DTT-untreated condition (Table 3.3). This difference was particularly significant for lower concentrations (with a 1.4-fold difference for 0.25nM $VEGF_{165}$a-TMR concentrations), compared to higher concentrations (with a 0.5-fold difference for 10nM $VEGF_{165}$a-TMR concentrations). Particle number measured using PCH analysis was very similar to particle number measured using autocorrelation analysis.

Table 3.3. Molecular brightness (ε) measured using PCH analysis for a range of $VEGF_{165}$a-TMR concentrations prepared in HBSS containing 0.1% BSA under reducing or non-reducing conditions, using 10mM DTT reducing agent.

Molecular brigthness			
[$VEGF_{165}$a-TMR] (nM)	Without DTT	With DTT	p value
	mean ± SEM x10^3 ($cpms^{-1}$)	mean ± SEM x10^3 ($cpms^{-1}$)	
0.25	118.3 ± 4.8	289.0 ± 5.4	***
0.5	153.6 ± 8.3	345.8 ± 5.2	****
1	169.8 ± 3.9	327.3 ± 4.9	**
2	178.5 ± 7.2	297.4 ± 3.5	*
4	184.3 ± 8.5	299.7 ± 2.6	*
6	192.2 ± 6.5	301.1 ± 2.7	*
8	192.5 ± 6.7	297.8 ± 3.0	*
10	194.2 ± 8.6	294.4 ± 3.2	*

Molecular brightness data is displayed as mean ± SEM from 3 independent experiments. Data analysis was performed using Two-way ANOVA with Sidak's multiple comparison test.

3.4. Discussion and Conclusion

A fluorescently labelled version of $VEGF_{165}$a dimeric ligand ($VEGF_{165}$a-TMR) was developed by Promega and has been used by our lab for the pharmacological characterisation of human full-length VEGFR2, and more recently its co-receptor neuropilin-1 (NRP-1), at the level of ligand binding and function (Kilpatrick et al., 2017; Peach et al., 2018b).

FCS and autocorrelation analysis have been applied to investigate diffusion characteristics of free fluorescent ligands in solution, and fluorescent ligands bound to receptors in membranes and whole-living cells, by positioning the small defined confocal volume on the cell membranes and in the cytosol (Briddon et al., 2018; Gherbi et al., 2018; Herrick-Davis et al., 2012; Kilpatrick et al., 2012). In this study is demonstrated the sensitivity of FCS technique to characterise free $VEGF_{165}$a-TMR fluorescent ligand in solution, by measuring its 'real' concentration in buffer, and to determine its homodimeric structure. FCS measurements of a range of $VEGF_{165}$a-TMR concentrations (considering dimeric species) in buffer without the presence of 0.1% BSA, showed reduced particle number and calculated concentration compared to nominal (or added) concentrations. $VEGF_{165}$a-TMR is a large (~165kDa) and lipophilic peptide ligand that can form non-specific interactions with plastic during sample preparation, and to the plate coverglass during FCS measurements, leading to ligand depletion over time (Figure 3.4.). This is an important observation, since ligand concentration is crucial when performing assays to measure, for example, ligand-receptor binding kinetics or receptor function, using reporter gene assays, where the system is dependent on the concentration of ligand added.

Here is demonstrated that FCS can be used to sensitively monitor ligand depletion over time. The incorporation of 0.1% BSA in buffer restored the concentrations to added values, suggesting that BSA is acting as a blocker to reduce non-specific interactions between ligand and plastic/glass surfaces.

Therefore, incorporation of 0.1% BSA in buffer is important when performing assay measurements using this fluorescent ligand (Kilpatrick et al., 2017; Peach et al., 2018b). Notably, incorporation of 0.1% BSA in buffer also showed to rescue TAMRA fluorophore concentrations, by reducing non-specific binding of this fluorophore to plastic/glass surfaces. These data suggest that the fluorophore moiety has a large contribution to the non-specific binding properties of $VEGF_{165}$a-TMR fluorescent ligand.

No significant differences were observed in diffusion times (or calculated diffusion coefficients) from autocorrelation analysis of $VEGF_{165}$a-TMR in the presence or absence of 0.1% BSA, suggesting that BSA is not binding directly to $VEGF_{165}$a-TMR. However, the autocorrelation analysis is not sensitive enough to detect possible BSA (~66kDa) binding to $VEGF_{165}$a-TMR ligand (~165kDa). This is because only differences of 1.6-fold in diffusion times can be detected, which is equivalent of an approximate six-fold difference in molecular weight (Briddon et al., 2010). Previous reports have demonstrated direct interaction between BSA and fluorescent probes (Ghosh et al., 2016). Therefore, it is likely that BSA may also be interacting with $VEGF_{165}$a-TMR ligand and acting as a protein carrier to reduce non-specific binding to surfaces.

FCS-detected concentrations measured for a range of $VEGF_{165}$a-TMR (assuming dimeric species) matched with the same range of concentrations for TAMRA single fluorophore (Figure 3.5.). These data provided strong evidence for the dimeric structure of $VEGF_{165}$a-TMR. This fluorescent ligand was known to be formed by two antiparallel disulphide-bridged protomers, each labelled with a TMR fluorophore. Therefore, incubation of $VEGF_{165}$a-TMR ligand under reducing conditions, should result in the disruption of $VEGF_{165}$a-TMR promoters, rendering them to a monomeric structure. The use of 1mM 2-mercaptoethanol resulted in an increase in particle number and calculated concentration, using autocorrelation analysis, and a decrease in molecular brightness. However, similar observations were observed for TAMRA fluorophore also pre-incubated under 2-ME reducing conditions, suggesting that 2-ME can change fluorescence quantum yield, possibly due to

fluorescence quenching. Quenching can be defined as a loss of fluorescence signal as a result of short series of interactions between the fluorophore and the local environment (Nagaraja et al., 2015). Fluorescence quenching leads to the decrease in proton emission which greatly decreases the fluorophore quantum yield (Nagaraja et al., 2015). In fact, studies investigating quantum dot fluorescence intermittency and its dependence on 2-ME showed that this reducing agent acts as a blinking suppressant (Hohng and Ha, 2004; Nadeau et al., 2012). Therefore, a different reducing agent, dithiothreitol (DTT) was used which did not change the photophysical properties for the TAMRA fluorophore. Treatment of $VEGF_{165}$a-TMR ligand under DTT-reducing conditions resulted in a two-fold increase in particle number (hence calculated concentration), which was measured using both autocorrelation analysis and PCH analysis. These data show evidence that $VEGF_{165}$a-TMR is formed by two protomers bridges by disulphide bonds. Molecular brightness, measured using PCH analysis, was investigated to access whether both protomers forming the dimer are labelled with a TMR fluorophore. Molecular brightness resulted in an increase, instead of a decrease, in molecular brightness which was particularly significant at lower ligand concentrations (Table 3.3.). These observations can be explained by a phenomenon of self-quenching (Behera et al., 2017), which would alter the quantum yield of monomers compared to homodimers in solution. Therefore, in this case we could not determine ligand stoichiometry based on PCH analysis.

Overall, FCS allowed the precise measurement of concentration in solution for $VEGF_{165}$a-TMR peptide ligand, as well as for a small fluorophore (TAMRA, ~52kDa). Incorporation of 0.1% BSA in buffer is important as it prevents ligand depletion by reducing non-specific binding of $VEGF_{165}$a-TMR to plastic and glass surfaces. Measurements under non-reducing conditions, using DTT reducing agent demonstrated the homodimeric structure of this ligand.

Chapter 4: Characterisation of two different class A GPCRs and VEGFR2 at the level of ligand binding using NanoBRET.

4.1. Introduction

G-protein coupled receptors (GPCRs) and Receptor Tyrosine Kinases (RTK) are two major families of transmembrane receptors in eukaryotic cells (Kamato et al., 2013). These receptors are activated upon agonist ligand binding, which leads to a conformational change of the receptor and consequent activation of different signalling cascades for signalling propagation (Drake et al., 2006; Sarabipour et al., 2016; Simons et al., 2016). Ligand-receptor binding pharmacology has been studied using different methodologies (Stoddart et al., 2016). Traditional methods have applied the use of radiolabelled-ligands (radioligands) to investigate ligand-receptor interactions both *in vitro* (Baker, 2005; Baker et al., 2002; Dionisotti et al., 1997) and *in vivo* (Grachev et al., 2014; van Waarde et al., 2004). Radioligands are not only expensive to manufacture, but also need expensive licencing for their safe disposal and handling. More recently, fluorescently-labelled ligands have been developed as an alternative and successful approach to measure ligand-receptor binding pharmacology for different GPCRs (Arruda et al., 2017; Soave et al., 2016; Stoddart et al., 2015a, 2012), and more recently for VEGFR2 (Kilpatrick et al., 2017) and its co-receptor neuropilin-1 (Peach et al., 2018b). Fluorescent ligands are composed by a pharmacologically active pharmacophore conjugated to a fluorescent dye via a linker region (Middleton and Kellam, 2005). The chemical structure of fluorescent ligands is usually very bulky and highly lipophilic, which can lead to high degree of non-specific binding and intracellular uptake in cells (Baker et al., 2003). To overcome this limitation, our lab has combined the use of fluorescent ligands with a proximity-based technique, NanoBRET (Stoddart et al., 2015a, 2018). NanoBRET technology enables accurate measurement of specific ligand-receptor interactions that occur at a distance <10nm, at real-time in living cells (Stoddart et al., 2015a).

One of the aims of this PhD project was to investigate the molecular interactions between a receptor tyrosine kinase, VEGFR2 and two different class A GPCRs (adenosine or β_2-adrenergic receptors), which been shown to have an intimate relationship to promote tumour angiogenesis and invasion (Ahmad et al., 2009; Barron et al., 2012; Creed et al., 2015; Gessi et al., 2011; Hatfield and Sitkovsky, 2016; Sloan et al., 2010). Receptor-receptor interactions were investigated using NanoBRET methodology, which study is described later in Chapter 5.

This chapter will present the pharmacological characterisation of human full-length receptors (Adenosine A_{2A}, A_3, β_2-adrenergic receptors and VEGFR2) that have been fused at the N-terminus with a NanoLuc luciferase and overexpressed in HEK 293T cells. This chapter will also describe the pharmacological characterisation of NanoLuc-tagged-β_2-adrenoceptors expressed in two different breast cancer cell lines, a highly metastatic human breast cancer cell line (MDA-MB-231^{HM}) and a low metastatic mouse breast cancer cell line (66cl4). The pharmacological characterisation of these receptors was performed using NanoBRET-based assays with a combination of fluorescently labelled and unlabelled ligands.

NanoBRET-based assays to investigate ligand-receptor binding pharmacology

Investigation of ligand binding is an important pharmacological approach to investigate how a certain molecule binds to its receptor (Kenakin and Williams, 2014). Three different NanoBRET assays have been developed to investigate ligand-receptor binding kinetics: saturation and competition binding assays which are performed under equilibrium conditions, and the kinetics binding assay that is performed under non-equilibrium conditions (Stoddart et al., 2018).

i) NanoBRET Saturation binding assay

The NanoBRET saturation binding assay was applied in this study to investigate the ability of different receptors, that have been modified to express a NanoLuc

luciferase tag at the N-terminus, to bind fluorescently-labelled ligands. The strength of the interaction between the ligand and its receptor (binding affinity) is quantified in this assay after whole-cell incubation with increasing concentrations of fluorescently-labelled ligand for 60min at 37^{o}C, to achieve equilibrium (Stoddart et al., 2015a). The concentration of ligand required to bind 50% of available receptors at equilibrium is defined as equilibrium dissociation constant (K_D), which is commonly used to evaluate and rank strengths of molecular interactions between labelled ligands and cognate receptors (Kenakin, 2017; Stoddart et al., 2018). Non-specific binding is determined in the presence of a fixed high concentration of non-fluorescent competitors (Stoddart et al., 2015a). In these experiments, NanoLuc-tagged receptors were used as BRET donors (after treatment with NanoLuc luciferase substrate, furimazine), whereas fluorescent ligands that specifically engage with the Nluc-tagged receptor act as BRET acceptors (Stoddart et al., 2015a).

ii) NanoBRET competition binding assay

A competition binding assay was used to determine the concentration of competing ligand needed to inhibit 50% of the specific binding of a fixed concentration of fluorescent ligand (IC_{50}). Cells were co-treated with a fixed concentration of labelled ligand and increasing concentrations of unlabelled ligands to determine their binding affinities at the Nluc-tagged receptor. Negative log inhibitory dissociation constant (pKi) of unlabelled ligands is calculated from obtained IC_{50} values using the Cheng Prusoff equation, as indicated in the methods Chapter 2, section 2.5.8.

iii) NanoBRET binding kinetics assay

NanoBRET binding kinetics assay can determine real-time association (k_{on}) and dissociation (k_{off}) rates of the fluorescent ligand, as well as, its residence time on the receptor, which is calculated from the k_{off} ($1/k_{off}$) (Guo et al., 2016b; Stoddart et al., 2018). These are important pharmacological parameters to

consider when applying small molecules in an *in vivo* system, where equilibrium is rarely reached (Guo et al., 2016b).

4.2. Brief materials and methods

Cell culture

In this chapter, HEK 293T stably transfected with N-terminally tagged human full-length receptors with NanoLuc luciferase [adenosine A_3 receptor (Nluc-A_3R), β_2-adrenergic receptor (Nluc-β_2AR) and VEGFR2 (Nluc-VEGFR2)] were used. As well as, HEK 293T transiently transfected with Nluc-tagged adenosine A_{2A} receptor (Nluc-A_{2A}AR). Two different breast cancer cell lines were also used, which were transfected with a lentiviral construct (pSIN-Nluc-β_2AR) to stably express human Nluc-tagged-β_2AR, see transfection details in chapter 2, section 2.3.1. The breast cancer cell lines used here were the human triple-negative (or highly metastastic) breast cancer cell line, MDA-MB-231^{HM} (MDA-231; which lack expression of HER2 (human epidermal growth factor receptor 2), progesterone and estrogen receptors (Pon et al., 2016)), and a low metastatic mouse breast cancer cell line 66cl4 (Sloan et al., 2010).

Confocal fluorescence imaging

Confocal imaging was performed using a Leica SP8 inverted microscope to visualise labelling of endogenous and overexpressing Nluc-β_2AR in MDA-231 cells, using a propranolol fluorescent ligand derivative (propranolol-β-Ala-β-Ala-X-BODIPY630/650, here mentioned as propranolol-BY630/650), see further details in Chapter 2, section 2.6.3.

Wide-field luminescence imaging

Bioluminescence imaging was performed using an Olympus LV200 wide-field inverted microscope. Bioluminescence imaging was used to visualise and quantify BRET resulting from resonance energy transfer (RET) between Nluc-

β_2AR and receptor-bound propranolol-BY630/650 (see further details in Chapter 2, section 2.6.4.)

NanoBRET binding assays

NanoBRET saturation, competition and kinetics binding assays were performed using a PHERAstar or CLARIOstar plate-readers, and the whole animal bioluminescence imager (IVIS Lumina II camera system), as described in Chapter 2, section 2.5. NanoBRET binding assays were used to characterise ligand-receptor binding for full-length human receptors labelled at the N-terminus with NanoLuc luciferase, stably or transiently expressed in HEK 293T and in breast cancer cell lines, 66cl4 and MDA-231.

4.3. Results

Pharmacological characterisation of fluorescently-labelled ligand-receptor binding in HEK 293T cell model using a NanoBRET saturation binding assay

A NanoBRET saturation binding assay was used to investigate binding affinity and specificity at the different receptors of interest that have been fused to express NanoLuc luciferase at their N-terminus. A non-selective adenosine fluorescent antagonist, CA200645, was used to investigate its binding affinity at the Nluc-tagged adenosine A_3 and A_{2A} receptors stably or transiently transfected in HEK 293T cells, respectively. CA200645 is a derivative of the adenosine receptor antagonist XAC (xanthine amine congener) linked to BODIPY 630/650 via a β-Ala-β-Ala linker (Stoddart *et al.*, 2015). This fluorescent ligand has been previously used to investigate binding affinity in untagged human adenosine A_1 and A_3 receptors overexpressed in Chinese hamster ovarian (CHO) cells, using high content imaging (Stoddart et al., 2012). This fluorescent ligand displayed high affinity for A_3 receptors with rapid association to the receptor (fast on-rate) and slow dissociation (slow off-rate) (Corriden et al., 2014; Stoddart et al., 2012).

A binding affinity of 7.68 ± 0.08 (n=5), represented as negative log of equilibrium dissociation constant (pK_D), was obtained for Nluc-A_3 adenosine receptor (Figure 4.1.a, Table 4.1.). Whereas, a pK_D of 7.64 ± 0.05 (n=5) was obtained at the Nluc-A_{2A} (Figure 4.1.b, Table 1). These data show similar binding affinities for both receptors. Low level of non-specific binding was determined using a fixed high concentration of a unlabelled selective antagonists, 10μM MRS1220, for Nluc-A_3R (Jacobson et al., 1997), and 10μM SCH58261 for the Nluc-A_{2A}R (Ongini, 1997).

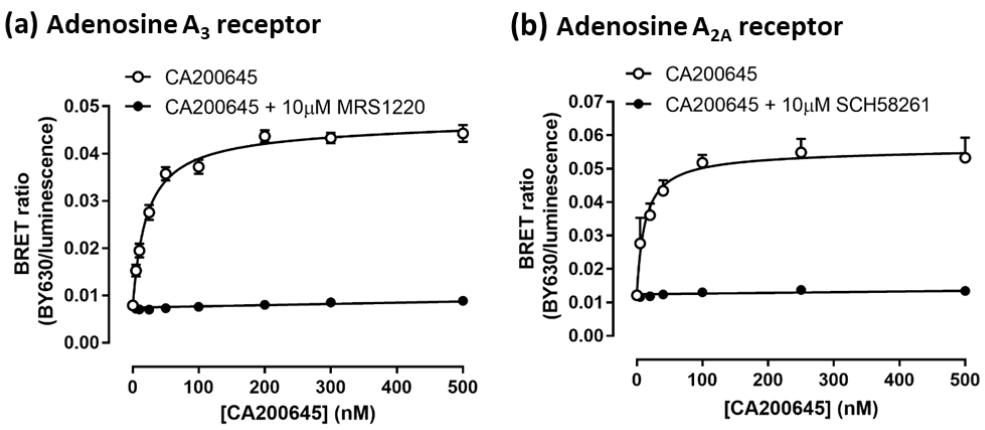

Figure 4.1. NanoBRET saturation binding assay to determine CA200645 fluorescent ligand binding affinity at the Nluc-A_3 (a) and A_{2A} (b) adenosine receptors. HEK 293T cells stably or transiently expressing Nluc-tagged-A_3 or -A_{2A} adenosine receptors, respectively, were treated with increasing concentration of CA200645 fluorescent ligand. Non-specific binding was determined with co-treatment with a fixed high concentration of a specific unlabelled antagonist (MRS1220 for A_3 receptor, and SCH58261 for A_{2A} receptor). Cells were treated with respective ligands for 60min, at 37°C. BRET measurements were performed using a PHERAstar plate-reader, 5min after incubation with furimazine substrate. Data are combined BRET ratios expressed as mean ± SEM of 5 independent experiments, using triplicate measurements per experiment.

Table 4.1. Saturation binding data for Nluc-A_3 and Nluc-A_{2A} adenosine receptors using CA200645 fluorescent ligand and selective unlabelled antagonists to determine non-specific binding.

Saturation Binding				
Receptor	**Fluorescent ligand**	**pK_D ± SEM**	**n**	**Literature pK_D**
Nluc-A_3AR	CA200645	7.68 ± 0.08	5	7.6 (1)
Nluc-A_{2A}AR	CA200645	7.64 ± 0.05	5	-

Data are represented as negative log of equilibrium dissociation constant (pK_D) and expressed as mean ± SEM of n number of individual experiments. Literature pK_D value was obtained from (1) (Stoddart et al., 2015a), who used the same methodology and fluorescent ligand.

Two different antagonist fluorescent ligands (CGP12177-TMR and propranolol-BY630/650) were used to characterise Nluc-tagged-β_2-adrenoceptors stably expressed in HEK 293T cells. The CGP12177-TMR (also known as BODIPY-TMR-CGP) is a bordifluoropyrromethane-tetramethyl-rhodamine derivative of the β_1- and β_2-AR antagonist ligand CGP12177 (Baker et al., 2003). This fluorescent ligand has been characterised at the level of binding and functional properties at the human β_2AR (Baker et al., 2003), and more recently at human β_1AR (Gherbi et al., 2014, 2015) in CHO cells. Upon excitation, this fluorescent ligand emits light at 560nm (Baker et al., 2003). propranolol-β-Ala-β-Ala-X-BODIPY630/650 (mentioned here as propranolol-BY630/650) is a propranolol fluorescent derivative that has been previously characterised in HEK 293T cells (Stoddart et al., 2015a). This is a red-shifted ligand with emission peak at 650nm. Saturation binding data measured at Nluc-β_2AR resulted in a pK_D of 7.98 ± 0.11 (n=5) for CGP12177-TMR, whereas a pK_D of 7.86 ± 0.03 (n=5) was obtained for propranolol-BY630/650 (Figure 4.2. a and b, Table 4.2.). Previous studies have reported that both ligands have high affinity for β_2AR and slow dissociation from the receptor (Baker et al., 2003; Stoddart et al., 2015a). Low level of non-specific binding was observed for both fluorescent ligands, which was determined using an unlabelled selective β_2AR antagonist , ICI 118551 (Baker, 2003, 2005).

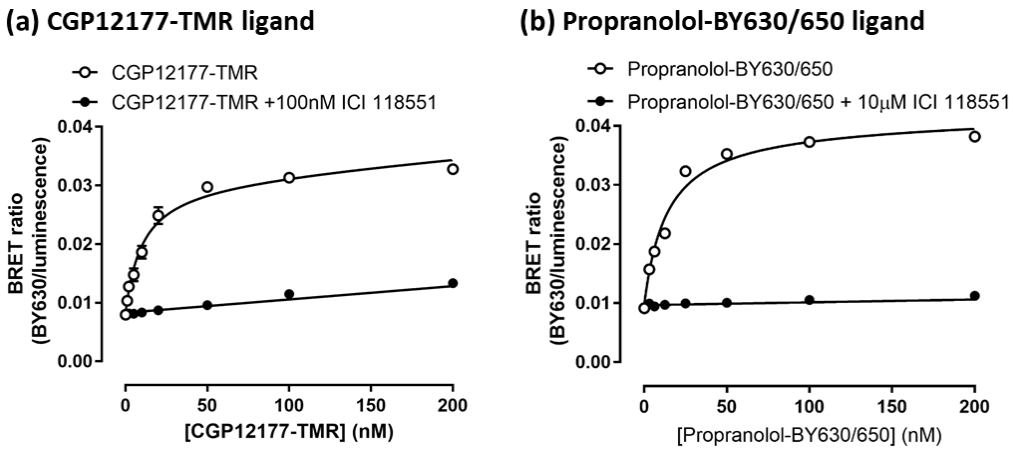

Figure 4.2. NanoBRET saturation binding assay to determine binding affinity for two different fluorescent ligands, CGP12177-TMR and propranolol-BY630/650 at the Nluc-β_2-adrenoceptor

overexpressed in HEK 293T cells. HEK cells stably Nluc-tagged-β_2AR, were treated with increasing concentrations of either CGP12177-TMR (**a**) or propranolol-BY630/650 (**b**) fluorescent ligands. Non-specific binding was determined by co-treatment of cells with a fixed high concentration of a specific unlabelled antagonist ICI 118551 (100nM for experiments using CGP12177-TMR, and 10µM for experiments using propranolol-BY630/650). Cells were treated with respective ligands for 60min, at 37^{o}C. BRET measurements were performed using a PHERAstar plate-reader, 5min after incubation with furimazine substrate. Data are combined BRET ratios expressed as mean ± SEM of 5 independent experiments, using triplicate measurements per experiment.

Table 4.2. Saturation binding data for Nluc-β_2AR using CGP12177-TMR or propranolol-BY630/650 fluorescent ligands, and a selective unlabelled antagonist to determine non-specific binding.

Saturation Binding				
Receptor	**Fluorescent ligand**	**pK_D ± SEM**	**n**	**Literature pK_D**
Nluc-β_2AR	CGP12177-TMR	7.98 ± 0.11	5	7.57 (1)
Nluc-β_2AR	propranolol-BY630/650	7.86 ± 0.03	5	7.72 (2)

Data are represented as negative log of equilibrium dissociation constant (pK_D) and expressed as mean ± SEM of n number of individual experiments. Similar pK_D value was obtained for CGP12177-TMR measured in untagged β_2AR overexpressed in CHO cells, using fluorescent intensity with confocal microscopy (1) (Baker et al., 2003). Similar pK_D value was also obtained for propranolol-BY630/650 at Nluc-β_2AR stably expressed in HEK 293T, measured using the same methodology (1) (Stoddart et al., 2015a).

To investigate the ability of Nluc-tagged VEGFR2 to bind cognate ligands, a tetramethyl-rhodamine-labelled $VEGF_{165}$a agonist ligand ($VEGF_{165}$a-TMR) was used. This fluorescent ligand has been previously characterised in Chapter 3 as an antiparallel bound dimer, with each $VEGF_{165}$a protomer labelled at a single cysteine amino acid with a tetramethyl-rhodamine (TMR) fluorophore. This fluorescent ligand has been previously characterised for its binding and functional properties at Nluc-VEGFR2 (Kilpatrick et al., 2017), and neuropilin-1 (Peach et al., 2018b). In this study, a pK_D of 9.09 ± 0.08 (n=4) was obtained for $VEGF_{165}$a-TMR at the Nluc-VEGFR2 (Figure 4.3., Table 4.3.), which corresponds

to previously reported pK_D (9.04) using the same NanoBRET approach (Kilpatrick et al., 2017). A low level of non-specific binding was also observed across the range of concentrations of fluorescent ligand used, when competing with 10nM unlabelled $VEGF_{165}a$ ligand.

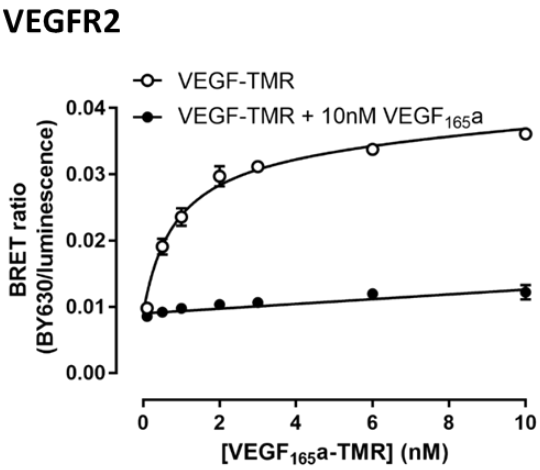

Figure 4.3. NanoBRET saturation binding assay to determine binding affinity for $VEGF_{165}a$-TMR fluorescent ligand at the Nluc-tagged-VEGFR2. HEK 293T cells stably expressing Nluc-tagged-VEGFR2, were treated with increasing concentration of $VEGF_{165}a$-TMR labelled ligand (**a and a1**) Non-specific binding was determined by co-treatment of cells with a fixed high concentration of unlabelled $VEGF_{165}a$ agonist. Cells were treated with respective ligands for 60min, at 37°C. BRET measurements were performed using a PHERAstar plate-reader, 5min after incubation with furimazine substrate. Data are combined BRET ratios expressed as mean ± SEM of 5 independent experiments, using triplicate measurements per experiment.

Table 4.3. Saturation binding data for Nluc-VEGFR2 using $VEGF_{165}a$-TMR fluorescent ligand and an unlabelled $VEGF_{165}a$ ligand to determine non-specific binding.

Saturation Binding				
Receptor	**Fluorescent ligand**	**pK_D ± SEM**	**n**	**Literature pK_D**
Nluc-VEGFR2	$VEGF_{165}a$-TMR	9.09 ± 0.08	4	9.04 (1)

Data are represented as negative log of equilibrium dissociation constant (pK_D) and expressed as mean ± SEM of n number of individual experiments. Similar pK_D value was obtained using the same methodology and fluorescent ligand at Nluc-VEGFR2 stably expressed in HEK 293T cells (1) (Kilpatrick et al., 2017).

Pharmacological characterisation of unlabelled ligand-receptor binding in HEK 293T cell model using a NanoBRET competition binding assay

A NanoBRET competition binding assay was used to investigate binding affinity of unlabelled ligands at the different receptors of interest. Affinities are displayed as negative log inhibitory dissociation constant (pKi). For Nluc-A_3 adenosine receptor, a fixed concentration of 100nM CA200645 fluorescent ligand was used together with increasing concentrations of the adenosine A_3R-selective antagonist MRS1220 (Jacobson et al., 1997), A_1R-selective antagonists DPCPX and PSB36 (Alexander et al., 2013), and the non-selective agonist NECA (Jacobson et al., 1997). Saturation binding data showed pKi values of 7.90 ± 0.10 (n=5) and 6.09 ± 0.07 (n=5) for MRS1220 and for NECA, respectively (Figure 4.4.a, Table 4.4.). As expected, the adenosine A_1R-selective antagonists only showed a small degree of binding at high non-selective concentrations (10µM).

For Nluc-A_{2A} adenosine receptor, a fixed concentration of 25nM CA200645 fluorescent ligand was used together with increasing concentrations of the adenosine A_{2A}R-selective antagonist, SCH58261 (Fredholm et al., 1998). Saturation binding data resulted in a pKi = 7.48 ± 0.13 (n=6) for SCH58261 (Figure 4.4.b, Table 4.4.). This is the first study showing the characterisation of full length human adenosine A_{2A} receptor using NanoBRET. Previous studies using membrane preparations and radioligand antagonists reported pKi values of 8.3 – 9.2 (Table 4.4.).

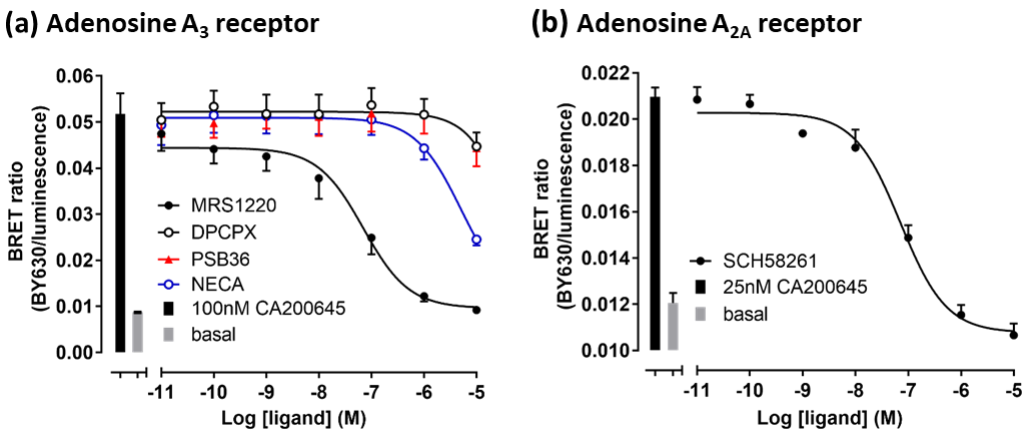

Figure 4.4. NanoBRET competition binding assay to determine binding affinity for different unlabelled ligands at the (a) Nluc-A_3 or (b) Nluc-A_{2A} adenosine receptors. HEK 293T cells stably expressing Nluc-tagged-A_3 or transiently expressing Nluc-A_{2A} receptors, were treated with a fixed concentration of CA200645 fluorescent ligand (100nM used for adenosine Nluc-A_3R and 25nM used for the adenosine Nluc-A_{2A}R) and increasing concentrations of unlabelled ligands. Cells were treated with respective ligands for 60min, at 37^{o}C. BRET measurements were performed using a PHERAstar plate-reader, 5min after incubation with furimazine substrate. Basal represents cells treated with furimazine only (BRET baseline, grey bar). Whereas black bar corresponds to cells treated with fluorescent ligand alone. Data are combined BRET ratios expressed as mean ± SEM of 5 or 6 independent experiments, for adenosine Nluc-A_3 or Nluc-A_{2A}, respectively, using triplicate measurements per experiment.

Table 4.4. Competition binding data for different unlabelled ligands at Nluc-A_3 or Nluc-A_{2A} adenosine receptors, using CA200645 labelled ligand.

Competition Binding					
Receptor	**Fluorescent ligand**	**Unlabelled ligands**	**pKi ± SEM**	**n**	**Literature pKi**
Nluc-A_3AR	CA200645	MRS1220	7.90 ± 0.10	5	8.2 – 9.3 (1-4)
		NECA	6.09 ± 0.07	5	7.5 – 8.4 (2,6)
Nluc-A_{2A}AR	CA200645	SCH58261	7.48 ± 0.13	6	8.3 – 9.2 (5,7,8)

Data are represented as negative log of inhibition dissociation constant (pKi) for unlabelled ligands, expressed as mean ± SEM of n number of individual experiments. pKi values were slightly lower compared to reported pKi values in the literature, using NanoBRET (1), high-content fluorescence imaging (2,3) and radioligand binding assays (4-8).

(1) (Stoddart et al., 2015a)

(2) (Stoddart et al., 2012)

(3) (Arruda et al., 2017)

(4) (Jacobson et al., 1997)

(5) (Yates et al., 2003)

(6) (Bosch et al., 2004)

(7) (Ongini, 1997)

(8) (Dionisotti et al., 1997)

At Nluc-β_2 adrenergic receptor, using CGP12177-TMR as tracer, pKi values of 9.06 ± 0.12 (n=6), 8.96 ± 0.12 (n=6), 9.04 ± 0.15 (n=6) and 6.05 ± 0.22 (n=6) were obtained for ICI 118551, propranolol, CGP12177 and for the β-AR-selective agonist isoprenaline (Baker, 2010), respectively (Figure 4.5a, Table 4.5.). Whereas, pKi values of 8.48 ± 0.11 (n=5), 8.48 ± 0.09 (n=5) and 6.38 ± 0.16 (n=5) were obtained for ICI118551, propranolol and isoprenaline, respectively, to compete with propranolol-BY630/650 labelled ligand (Figure 4.5b, Table 4.5.). The selective-β_1AR antagonist, CGP20712A (Baker, 2005), did not show binding at β_2AR, as it was not able to compete with propranolol-BY630/650 even at high concentrations of 10µM (pKi > 5). Competition binding data obtained was similar to previous studies performed using NanoLuc-tagged (Stoddart et al., 2015a) and untagged receptors (Arruda et al., 2017; Dionisotti et al., 1997; Ongini, 1997; Stoddart et al., 2012) (Table 4.5.).

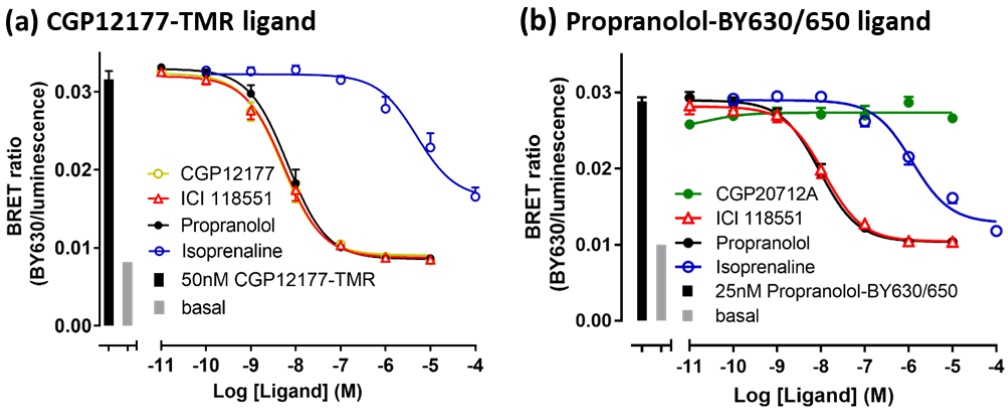

Figure 4.5. NanoBRET competition binding assay to determine binding affinity of different unlabelled ligands at the Nluc-β_2AR. HEK 293T cells stably expressing Nluc-tagged-β_2-adrenoceptors, were treated with a fixed concentration of **(a)** CGP12177-TMR or **(b)** propranolol-BY630/650 fluorescent ligands and increasing concentrations of unlabelled ligands. Cells were treated with respective ligands for 60min, at 37°C. BRET measurements were performed using a PHERAstar plate-reader, 5min after incubation with furimazine substrate. Data are represented as previously described. Data are combined BRET ratios expressed as mean ± SEM of 5 (using propranolol-BY630/650) or 6 (using CGP12177-TMR) independent experiments, using triplicate measurements per experiment.

Table 4.5. Competition binding data for different unlabelled ligands at Nluc-β_2AR, using two different labelled ligands, CGP12177-TMR and propranolol-BY630/650.

Competition Binding					
Receptor	**Fluorescent ligand**	**Unlabelled ligands**	**pKi ± SEM**	**n**	**Literature pKi**
Nluc-β_2AR	CGP12177-TMR	ICI 118551	9.06 ± 0.12	6	9.2 – 9.5 (1-3)
		Isoprenaline	6.05 ± 0.22	6	6.4 – 6.6 (1,3)
		Propranolol	8.96 ± 0.12	6	9.1 – 9.5 (2,3)
		CGP12177	9.04 ± 0.15	6	-
Nluc-β_2AR	Propranolol-BY630/650	ICI 118551	8.48 ± 0.11	5	8.04 (4)
		Isoprenaline	6.38 ± 0.16	5	6.4 – 6.6 (1,3,4)
		Propranolol	8.48 ± 0.09	5	8.1 (4)
		CGP20712A	>5	5	5.68 (2)

Data are represented as negative log of inhibition dissociation constant (pKi) for unlabelled ligands, expressed as mean ± SEM of n number of individual experiments. pKi values obtained were similar to previously published data using radioligand binding (1,2,4,5), fluorescence intensity measurements (3) and NanoBRET (6).

(1) (Baker, 2005)

(2) (Baker, 2010)

(3) (Arruda et al., 2017)

(4) (Alexander et al., 2017)

(5) (Baker et al., 2002)

(6) (Stoddart et al., 2015a)

Competition binding data for Nluc-VEGFR2 resulted in a pKi of 10.17 ± 0.09 (n=7, Figure 4.6., Table 4.6.) for the unlabelled $VEGF_{165}$a agonist, when competing with 3nM $VEGF_{165}$a-TMR fluorescent ligand. These results are in agreement with previous published data using the same NanoBRET approach (Kilpatrick et al., 2017) and radioligand binding studies using untagged VEGFR2 (Leppanen et al., 2010; Simon et al., 1998).

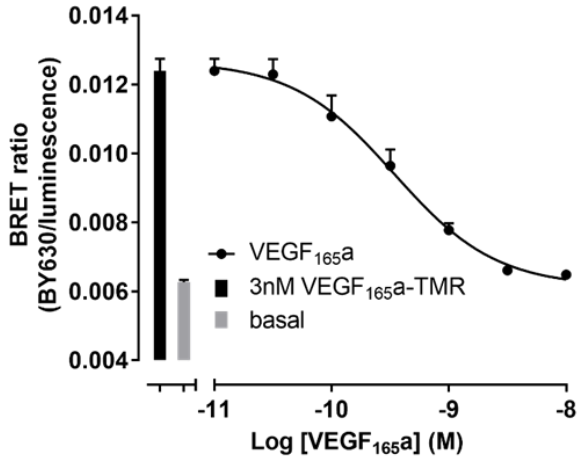

Figure 4.6. NanoBRET competition binding assay to determine binding affinity of unlabelled $VEGF_{165}a$ agonist at the Nluc-VEGFR2. HEK 293T cells stably expressing Nluc-tagged-VEGFR2, were treated with a fixed concentration of $VEGF_{165}a$-TMR fluorescent ligand and increasing concentrations of unlabelled $VEGF_{165}a$ ligand. Cells were treated with ligands for 60min, at 37°C. BRET measurements were performed using a PHERAstar plate-reader, 5min after incubation with furimazine substrate. Basal represents cells treated with furimazine only (BRET baseline). Data are expressed as combined BRET ratios of 7 independent experiments, using triplicate measurements per experiment.

Table 4.6. Competition binding data for unlabelled $VEGF_{165}a$ ligand at Nluc-VEGFR2, using $VEGF_{165}a$-TMR labelled ligand.

Competition Binding				
Receptor	**Unlabelled ligand**	**pKi ± SEM**	**n**	**Literature pKi**
Nluc-VEGFR2	$VEGF_{165}a$	10.17 ± 0.09	7	9.4 – 10.4 (1-3)

Data are represented as negative log of inhibition dissociation constant (pKi) for the unlabelled ligand, expressed as mean ± SEM of n number of individual experiments. Similar pKi value was obtained using the same methodology in previous published data (1), as well as in radioligand binding studies using untagged receptor (2,3).

(1) (Kilpatrick et al., 2017)

(2) (Simon et al., 1998)

(3) (Leppanen et al., 2010)

Pharmacological characterisation of cancer cell lines stably expressing Nluc-β_2-adrenoceptors

NanoBRET technology has shown great potential to investigate ligand-receptor kinetics in living HEK cells (Stoddart et al., 2018). In this study we also demonstrate the use of NanoBRET methodology to measure ligand binding to Nluc-β_2-adrenoceptors in a physiologically relevant whole-cell system.

Targeting β_2-adrenoceptors has shown potential for the treatment of different cancers including breast cancer (Chang et al., 2016; Melhem-Bertrandt et al., 2011; Sloan et al., 2010). In this part of the study we describe the pharmacological characterisation of two different breast cancer cell lines (MDA-231 and 66cl4) that have been transfected with a lentiviral construct to overexpress β_2AR-tagged with NanoLuc at the N-terminus.

The NanoBRET saturation assay was performed using two different fluorescent ligand tracers, propranolol-BY630/650 and CGP12177-TMR, previously used for the characterisation of Nluc-β_2AR overexpressed in HEK 293T cells. Saturation binding experiments performed with 66cl4 Nluc-β_2AR cell line showed a pK_D value of 7.84 ± 0.06 (n=5) for CGP12177-TMR fluorescent antagonist, and a pK_D of 8.21 ± 0.06 (n=5) for propranolol-BY630/650 (Figure 4.7. a and b, Table 4.7.). In MDA-231 Nluc-β_2AR cell line, saturation binding experiments resulted in pK_D = 7.25 ± 0.06 (n=5), for CGP12177-TMR, and pK_D = 7.28 ± 0.07 (n=5) for propranolol-BY630/650 (Figure 4.8. a and b, Table 4.7.). Low level of non-specific binding was observed across the range of concentrations for both fluorescent ligands, in both cell lines.

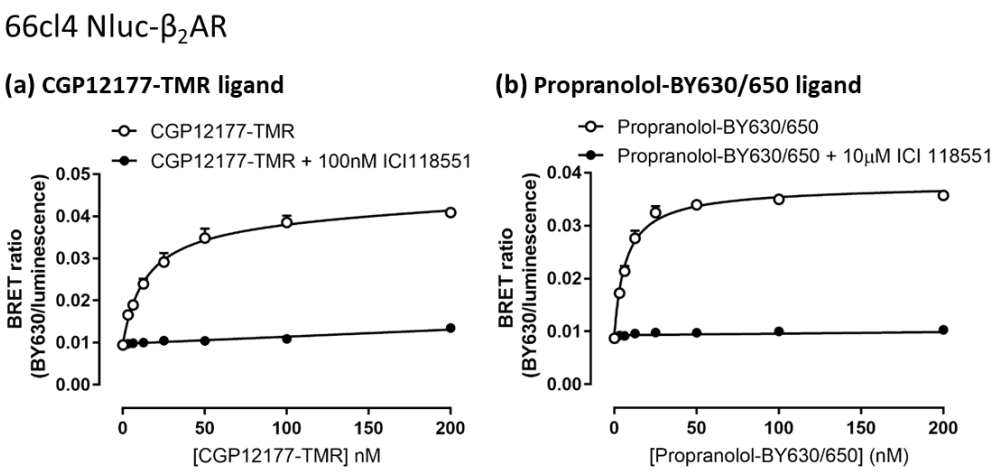

Figure 4.7. NanoBRET saturation binding assay to determine binding affinity of a β-selective fluorescent antagonists CGP12177-TMR and propranolol-BY630/650 at the Nluc-β_2AR overexpressed in 66cl4 cells. 66cl4 cells stably expressing Nluc-tagged-β_2AR were treated with increasing concentration of CGP12177-TMR (**a**) or propranolol-BY630/650 (**b**) fluorescent ligands. Non-specific binding was determined after co-treatment with a fixed high concentration of the specific unlabelled antagonist ICI 118551. Cells were treated with respective ligands for 60min, at 37°C. BRET measurements were performed using a PHERAstar plate-reader, 5min after incubation with furimazine substrate. Data are combined BRET ratios expressed as mean ± SEM of 5 independent experiments, using triplicate measurements per experiment.

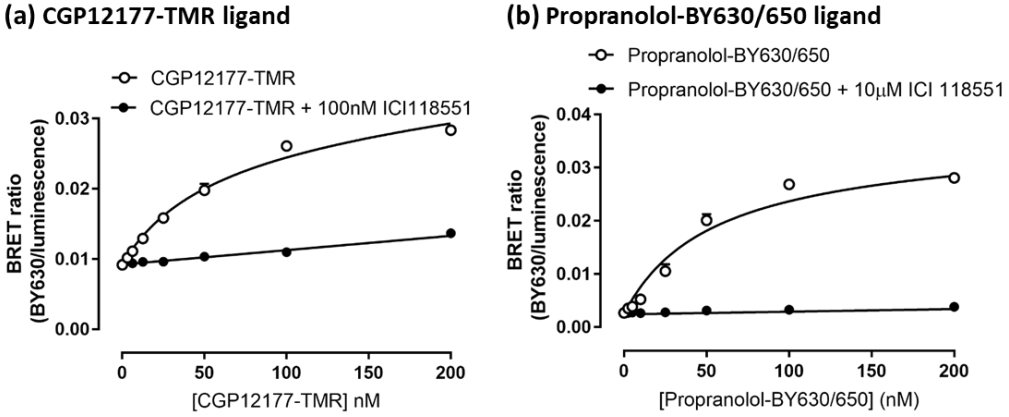

Figure 4.8. NanoBRET saturation binding assay to determine binding affinity of a β-adrenoceptor selective fluorescent antagonists CGP12177-TMR and propranolol-BY630/650 at the Nluc-β_2AR overexpressed in MDA-231 cells. MDA-231 cells stably expressing Nluc-tagged-β_2AR were treated with increasing concentration of CGP12177-TMR (**a**) or propranolol-BY630/650 (**b**) fluorescent ligands. Cells were treated with fluorescent ligand alone or co-treated with a high concentration of unlabelled ICI 118551 for 60min, at 37°C. BRET measurements were performed using a PHERAstar (**a**) or a CLARIOstar (**b**) plate-reader, 5min

after incubation with furimazine substrate. Data are combined BRET ratios expressed as mean ± SEM of 5 independent experiments, using triplicate measurements per experiment.

Table 4.7. Saturation binding data for CGP12177-TMR or propranolol-BY630/650 at the Nluc-β_2AR expressed in 66cl4 and MDA-231 cancer cell lines.

Saturation Binding					
Equipment	**Cell line**	**Fluorescent ligand**	**pK_D ± SEM**	**n**	**pK_D ± SEM (HEK 293T)**
PHERAstar	66cl4 Nluc-β_2AR	CGP12177-TMR	7.84 ± 0.06	5	8.00 ± 0.10
PHERAstar		Propranolol-BY630/650	8.21 ± 0.06	5	7.87 ± 0.04
PHERAstar	MDA-231 Nluc-β_2AR	CGP12177-TMR	7.25 ± 0.06	5	
CLARIOstar		Propranolol-BY630/650	7.28 ± 0.07	5	

Data are represented as negative log of equilibrium dissociation constant (pK_D) and expressed as mean ± SEM of n number of individual experiments. HEK 293T pK_D values displayed are from previous presented data (Figure 4.2, Table 4.2.).

Further pharmacological characterisation of MDA-231 Nluc-β_2AR cells using propranolol-BY630/650 fluorescent ligand

Chapter 6 will describe the novel use of NanoBRET technology to monitor ligand-β_2-adrenoceptor engagement *in vivo*, using a breast cancer mouse model available at Monash University (Alcobia et al., 2018; Sloan et al., 2010). For these studies, the highly metastatic breast cancer cell line (MDA-231 Nluc-β_2AR) was used, together with propranolol-BY630/650 fluorescent probe, which has a red-shifted emission (peak emission at 650nm) reducing tissue absorption, and hence increasing fluorescence emission (Unen et al., 2015).

Fluorescence and bioluminescence imaging of MDA-231 cells with propranolol-BY630/650 fluorescent probe

Standard confocal fluorescence imaging was used to investigate the binding of propranolol-BY630/650 to endogenous β-adrenergic receptor in MDA-231 cells

(Figure 4.9., upper left panel), and to both endogenous βAR and overexpressed Nluc-β_2AR in MDA-231 Nluc-β_2AR cells (Figure 4.9., lower left panel). Both functional β_1- and β_2- adrenergic receptors are known to be expressed in MDA-231 cells, with β_2AR being predominant (Creed et al., 2015; Pon et al., 2016). Specific binding was investigated using a high concentration of the non-selective βAR antagonist propranolol (Figure 4.9., right panels), which can bind to both β_1- and β_2-adrenoceptors. 10μM Propranolol was able to displace binding of propranolol-BY630/650 to β_2AR overexpressed in MDA-231 with localisation on the cell surface. However, a substantial amount of fluorescent ligand was observed inside these cells, which was not displaced by unlabelled propranolol. This intracellular labelling is likely to be a result from non-specific uptake of the fluorescent ligand, which is a common feature of fluorescent ligands due to their bulky and highly lipophilic structure (Baker et al., 2003; Stoddart et al., 2018).

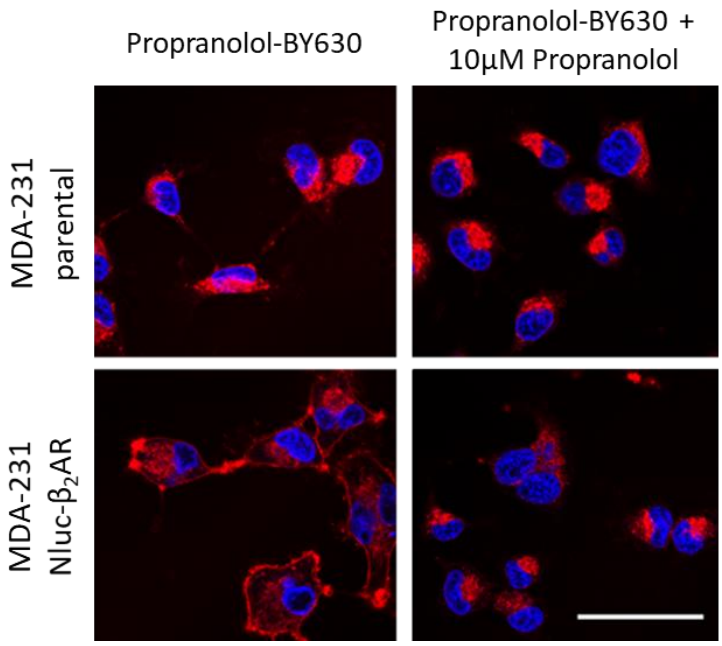

Figure 4.9. Confocal fluorescence imaging of non-transfected (parental) or stably transfected Nluc-β_2AR MDA-231 cells, using propranolol-BY630/650 fluorescent ligand. MDA-231 non-transfected (top panels) or stably transfected with Nluc-β_2AR (bottom panels) were treated with 50nM propranolol-BY630/650. Cells were pre-treated with Hoechst 33342 nuclear stain (2 μg/ml; blue labelling) and then labelled for 30 min with fluorescent ligand (red labelling). 10μM non-selective β-adrenoceptor unlabelled antagonist propranolol was used to investigate

specific binding of propranolol-BY630/650 (right panels). Cells were washed after ligand incubation to remove unbound fluorescent ligand. Data are representative images from 3 independent experiments. Scale bar represent 50μm.

Live cell bioluminescence microscopy was then applied to investigate the location (cytoplasm and/or plasma membrane) of specific interactions between the fluorescent ligand and Nluc-β_2AR, in MDA-231 cells overexpressing Nluc-β_2AR (Figure 4.10.). Bioluminescence imaging was performed by capturing sequential images of the luminescent donor (Nluc-β_2AR, DAPI channel Figure 4.10.a left panels) and the fluorescence emission of the acceptor (fluorescent ligand, Cy5 channel, Figure 4.10.a right panels). Acceptor emission only occurs upon energy transfer from the NanoLuc to the fluorescent ligand at a very close proximity (distance <10nm), detecting specific ligand-receptor interactions (Stoddart et al., 2018). Under basal conditions there was no fluorescent signal detected, only luminescence background (Figure 4.10. a and a_1). In the presence of propranolol-BY630/650 there was a significant increase in BRET signal (Figure 4.10. a_1), which was decreased to nearly basal levels in cells co-treated with the β_2AR-selective unlabelled antagonist ICI 118551. Specific ligand-receptor interactions were mainly observed at the plasma membrane (Cy5 channel, Figure 10a).

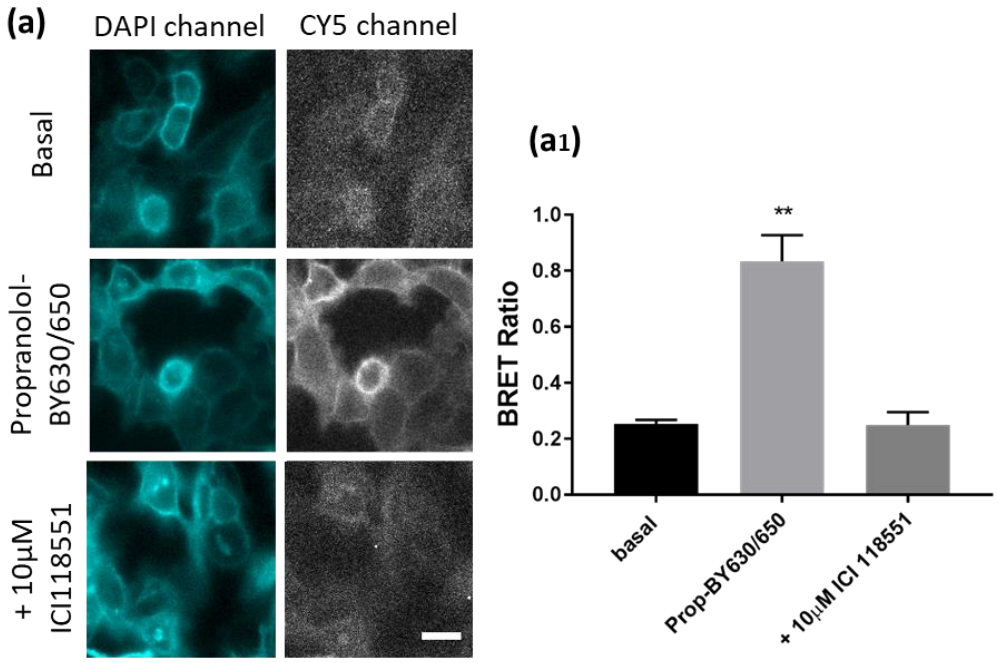

Figure 4.10. Using Bioluminescence imaging to localise (a) and measure (a1) specific ligand-β_2AR interactions in MDA-231 Nluc-β_2AR cells. MDA-231 Nluc-β_2AR cells were treated with 400nM furimazine substrate alone (upper panels) to detect luminescence in the absence of fluorescent ligand, using a DAPI channel (20 sec exposure time; 420nm longpass filter; upper left panel) or a CY5 channel (4 min exposure time; 600/50nm bandpass filter; upper right panel). Middle and lower panels show images from cells treated with 50nM propranolol-BY630/650, in the absence (middle panels) or presence (lower panels) of the unlabelled selective antagonist ICI 118551 (10μM). BRET ratios displayed in (**a1**) were obtained using ROIs positioned on individual cells and quantified acceptor to donor emission ratios using ImageJ time-series analyser. Scale bar represent 50μm. Data show the mean ± SEM obtained in 3 independent experiments. ** $p<0.01$ compared to basal or in the presence of 10μM ICI 118551, using one-way ANOVA with Tukey multiple comparison test.

Characterisation of MDA-231 Nluc-β_2AR using a whole-animal imaging system

Two different systems were used for MDA-231 Nluc-β_2AR *in vitro* cell line characterisation, a CLARIOstar plate-reader and the whole-animal bioluminescence camera system, IVIS Lumina II. Since the IVIS camera system will be used to perform NanoBRET measurements in living animals, it is important to evaluate the dynamic range, spectral resolution and sensitivity of this system for BRET detection, compared to a commonly used plate-reader.

Saturation assay performed using the IVIS camera system showed a pK_D = 7.20 ± 0.06 (n=5), for propranolol-BY630/650 in MDA-231 NLuc-β_2AR cells (Figure 4.11.). These results were very similar to binding affinity data obtained using the CLARIOstar plate-reader (pK_D = 7.16 ± 0.07; Figure 4.8.b, Table 4.8.).

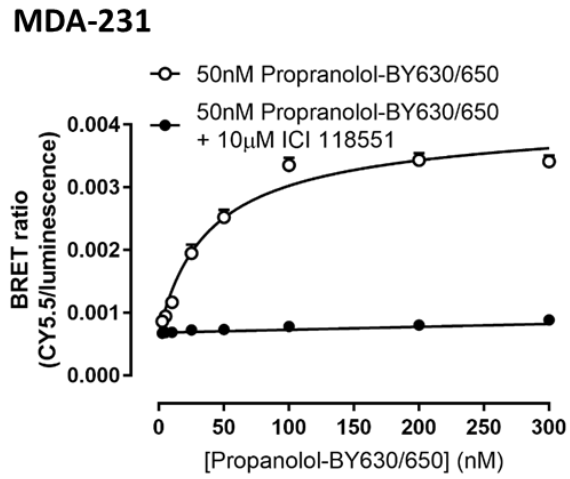

Figure 4.11. NanoBRET saturation binding assay to determine binding affinity of propranolol-BY630/650 at the Nluc-β_2AR overexpressed in MDA-231 cells, using the IVIS Lumina II camera system. MDA-231 cells stably expressing Nluc-tagged-β_2AR were treated with increasing concentrations of propranolol-BY630/650 fluorescent ligand. Non-specific binding was determined after co-treatment with a fixed high concentration (10μM) of the specific unlabelled antagonist ICI 118551. Cells were treated with respective ligands for 60min, at 37°C. BRET measurements were performed using the IVIS system, 5min after incubation with furimazine substrate. Data are combined BRET ratios expressed as mean ± SEM of 5 independent experiments, using triplicate measurements per experiment.

Table 4.8. Saturation binding data for propranolol-BY630/650 at the Nluc-β_2AR expressed in MDA-231 cell lines, measured using a CLARIOstar plate-reader or the IVIS Lumina II system.

Saturation Binding				
Cell line	**Fluorescent ligand**	**Equipment**	**pK_D ± SEM**	**n**
MDA-231 Nluc-β_2AR	Propranolol-BY630/650	CLARIOstar	7.16 ± 0.07	5
		IVIS	7.20 ± 0.06	5

Data are represented as negative log of equilibrium dissociation constant (pK_D) and expressed as mean ± SEM of n number of individual experiments.

Characterisation of MDA-231 Nluc-β_2AR cell line using NanoBRET kinetics binding assay

The propranolol-BY630/650 fluorescent ligand was further characterised to investigate ligand-receptor binding kinetics under non-equilibrium conditions in MDA-231 Nluc-β_2AR cells, using a NanoBRET binding kinetics assay (Stoddart et al., 2018). This assay can determine real-time ligand association (k_{on}) and dissociation (k_{off}) rates, as well as its residence time (RT) on the receptor (Guo et al., 2016b; Stoddart et al., 2018). These pharmacological parameters are important to consider when using in vivo systems, where equilibrium is not usually reached (Guo et al., 2016b).

NanoBRET kinetics binding assay showed a $k_{on} = 5.4x10^5 \pm 2.2x10^5$ M^{-1} min^{-1} and a $k_{off} = 0.025 \pm 0.004$ min^{-1} (n=5), obtained with the CLARIOstar plate-reader. Using the IVIS system, a $k_{on} = 5.6 \pm 0.6$ x10^5 M^{-1} min^{-1} and $k_{off} = 0.039 \pm 0.013$ min^{-1} (n=3) were determined (Table 4.9.). A residence time (RT) of 44.1 ± 6.7 min was obtained using the CLARIOstar plate-reader, whereas a RT = 37.7 ± 18.3 min was determined using the IVIS camera system. Therefore, propranolol-BY630/650 is a slow dissociating ligand at β_2AR, which makes it an ideal probe for *in vivo* application. Binding affinity under non-equilibrium conditions can also be calculated as k_{off}/k_{on} (Pollard, 2010). A $pK_D = 7.24 \pm 0.14$ (n=5) was calculated from data using a CLARIOstar, and a $pK_D = 7.23 \pm 0.24$ (n=3) was determined using the IVIS camera system (Figure 4.12., Table 9). Binding

affinity constants obtained using a kinetics binding assay were similar to binding affinity constants determined under equilibrium conditions using the saturation binding assay (Table 4.7.).

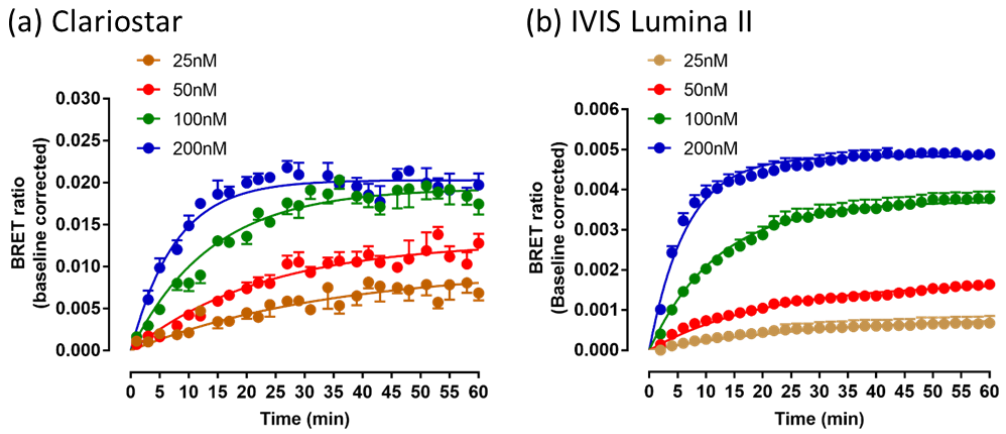

Figure 4.12. NanoBRET kinetics binding assay to measure propranolol-BY630/650 binding to NanoLuc-tagged β_2R, using a CLARIOstar plate-reader or the IVIS camera system. MDA-231 stably expressing Nluc-β_2AR were firstly incubated for 15min with 10µM furimazine substrate, at 37°C. Cells were then rapidly treated with four different concentrations of labelled propranolol in the absence or presence of 10µM ICI 118551, to determine level of non-specific binding. Data displayed has been baseline corrected after subtraction of non-specific component (with 10µM ICI 118551). BRET measurements were obtained using a CLARIOstar plate-reader **(a)** or the IVIS system **(b)**. Sequential acceptor and acceptor emissions were collected every minute for 60min at 37°C. Graphs presented represent a single experiment from 5 (CLARIOstar) or 3 (IVIS) independent experiments, performed in triplicate wells. Data are baseline corrected BRET ratios expressed as mean ± SEM.

Table 4.9. Kinetics binding data for propranolol-BY630/650 at the Nluc-β_2AR expressed in MDA-231 cell lines, measured using a CLARIOstar plate-reader or the IVIS Lumina II system.

Kinetics Binding assay						
Equipment	**Fluorescent ligand**	**k_{on} (M^{-1} min^{-1})**	**k_{off} (min^{-1})**	**pK_D ± SEM**	**RT (min)**	**n**
Clariostar	Propranolol-BY630/650	5.4 ± 2.2 x 10^5	0.025 ± 0.004	7.24 ± 0.14	44.1 ± 6.7	5
IVIS		5.6 ± 0.6 x 10^5	0.039 ± 0.013	7.23 ± 0.24	37.7 ± 18.2	3

Association (k_{on}) and dissociation (k_{off}) rates and dissociation constant calculated as k_{off}/k_{on}, represented as negative log (pK_D), as well as residence time (RT; calculated as $1/k_{off}$) are expressed as mean ± SEM of n number of individual experiments.

Characterisation of MDA-231 Nluc-β_2AR cell line using NanoBRET competition binding assay

A NanoBRET competition binding assay was also used to investigate the ability of unlabelled ligands to displace propranolol-BY630/650 at the Nluc-β_2AR expressed in MDA-231 cells (Figure 4.13. a and b, Table 4.10.). These assays were also performed using a CLARIOstar plate-reader and the IVIS camera system. Data for the selective β_2AR antagonist ICI 118551 showed pKi values of 8.55 ± 0.02 (n=5; CLARIOstar) and 8.59 ± 0.03 (n=4; IVIS system). For the non-selective antagonist carvedilol, pKi values of 8.42 ± 0.15 (n=5; CLARIOstar) and 8.77 ± 0.23 (n=4; IVIS system) were obtained. For the non-selective antagonist propranolol, pKi values of 8.69 ± 0.18 (n=5; CLARIOstar) and 8.44 ± 0.19 (n=4; IVIS system) were determined. The selective β_1AR antagonist CGP20712A showed low level of binding at high non-selective concentrations. pKi values obtained for ICI 118551 and propranolol were consistent to previous published data using HEK 293T cells (Stoddart et al., 2015a). Finally, isoprenaline showed low affinity, with pKi = 5.99 ± 0.04 (n=5; CLARIOstar), and pKi = 6.08 ± 0.03 (n=4; IVIS system), which was expected, since agonists have lower affinity for inactive receptor conformation (May et al., 2011). Binding affinity data obtained for unlabelled ligands in MDA-231 cell line was similar to pKi values obtained in HEK 293T Nluc-β_2AR, using the same fluorescent ligand (Table 4.10.).

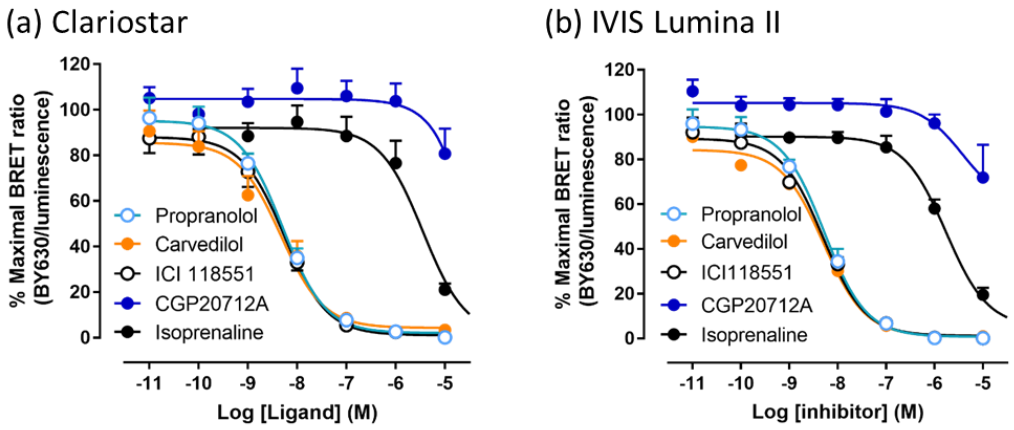

Figure 4.13. NanoBRET competition binding assay was used to determine binding affinity of different unlabelled ligands at the Nluc-β_2AR in MDA-231 cells, using propranolol-BY630/650 fluorescent tracer. MDA-231 cells stably expressing Nluc-tagged-β_2AR, were treated with a

fixed concentration propranolol-BY630/650 fluorescent ligand and increasing concentrations of unlabelled ligands. Cells were treated with respective ligands for 60min, at 37^{o}C. BRET measurements were performed using a CLARIOstar plate-reader (**a**) or the IVIS system (**b**), 5min after incubation with furimazine substrate. Basal represents cells treated with furimazine only (BRET baseline). Data are combined normalised BRET ratios expressed as mean ± SEM of 5 (a, CLARIOstar) or 4 (b, IVIS) independent experiments, using triplicate measurements per experiment.

Table 4.10. Competition binding data for unlabelled ligands at Nluc-β_2AR expressed in MDA-231 cells, using propranolol-BY630/650 fluorescent ligand.

Competition Binding assay				
Equipment	**Unlabelled ligand**	**pKi ± SEM (MDA-231)**	**n**	**pKi ± SEM (HEK 293T)**
Clariostar	ICI118551	8.55 ± 0.02	5	8.48 ± 0.11
	Propranolol	8.69 ± 0.18	5	8.48 ± 0.09
	Carvedilol	8.42 ± 0.15	5	-
	Isoprenaline	5.99 ± 0.04	5	6.38 ± 0.16
IVIS	ICI118551	8.59 ± 0.03	4	
	Propranolol	8.44 ± 0.19	4	
	Carvedilol	8.77 ± 0.23	4	
	Isoprenaline	6.08 ± 0.03	4	

Data are represented as negative log of inhibition dissociation constant (pKi) for unlabelled ligands, expressed as mean ± SEM of n number of individual experiments. pKi values obtained in MDA-231 Nluc-β_2AR cell line were similar to values obtained in HEK 293T Nluc-β_2AR cells, using the same fluorescent ligand.

4.4. Discussion and Conclusion

This chapter described the use of NanoBRET methodology to pharmacologically characterise different GPCRs (adenosine A_3 and A_{2A} receptors, as well as, β_2-adrenoceptors) and VEGFR2, that have been modified to express NanoLuc luciferase-tagged at the N-terminus and expressed in HEK 293T cells. This chapter also demonstrated the successful use of NanoBRET to measure ligand-β_2-adrenoceptor binding kinetics in a breast cancer cell model (MDA-231), which was later used to monitor drug-β_2-adrenoceptors engagement *in vivo* (Chapter 6).

Fluorescent ligands have been recently developed as an alternative to radioligands (Stoddart et al., 2015c). Fluorescent ligands can also be used to visualise and measure ligand-receptor binding in single-cell and cell population using different microscopy approaches (Briddon et al., 2018; Gherbi et al., 2015, 2018; Stoddart et al., 2012). These ligands are composed of a pharmacophore conjugated to a fluorophore via a linker (Middleton and Kellam, 2005). Therefore, the chemical structure of fluorescently-labelled ligands is usually very bulky and highly lipophilic that can lead to high level of non-specific binding in cells and tissues (Baker et al., 2003), which was here shown to be the case for propranolol-BY630/650 compound. Combining the proximity-based NanoBRET technology with fluorescent ligands allows the investigation of specific drug-receptor interaction, which can only be detected at a distance <10nm to allows resonance energy transfer (RET) between the donor and the acceptor. Moreover, NanoBRET methodology allows real-time drug-receptor binding kinetic measurements to be performed in living cells.

Previous published studies have applied NanoBRET technology to measure ligand-receptor binding pharmacology for the adenosine A_3 receptor, β_2-adrenoceptor (Stoddart et al., 2015a) and VEGFR2 (Kilpatrick et al., 2017). These studies have compared binding properties of labelled and unlabelled ligands in Nluc-tagged and untagged receptors. Binding affinities of labelled ligands at the Nluc-A_3, β_2AR and VEGFR2 receptors in HEK 293T were consistent

to previous published data using NanoBRET (Kilpatrick et al., 2017; Stoddart et al., 2015a), high-content imaging fluorescence intensity (Arruda et al., 2017; Stoddart et al., 2012) and radioligand binding assays (Jacobson et al., 1997; Yates et al., 2003). Compared to published data using Nluc-tagged (Stoddart et al., 2015a) and untagged-adenosine A_3R (Alexander et al., 2017; Yates et al., 2003) competition binding data for Nluc-A_3AR showed lower binding affinity for these ligands (lower pKi values, Table 4.4.), compared to a study using the same methodology and fluorescent ligand (Stoddart et al., 2015a). In Stoddart et al. study, a concentration of 25nM CA200645 fluorescent ligand was used for the competition binding assay, with a reported pKi of 9.20 ± 0.08 for MRS1220 (Stoddart et al., 2015a). In this study a pKi = 7.20 ± 0.10 was measured using 100nM CA200645 fluorescent ligand (a concentration that is higher than CA200645 K_D). Previous published data, as well as data showed in Chapter 5 of this thesis, reported evidence for the existence of adenosine A_3R homodimers in HEK 293T and CHO cells (May et al., 2011). Adenosine A_3R homodimers also induce negative cooperativity across their dimer interface (Corriden et al., 2014; May et al., 2011). Negative cooperativity occurs when ligands binding to the first receptor protomer induce faster dissociation (hence, reduced affinity) of ligands binding at the second promoter (Gherbi et al., 2015; May et al., 2011). Therefore, negative cooperativity between A_3R homodimers is likely to explain the observed lower affinity for MRS1220 antagonist, as well as for the other unlabelled ligands, when using a higher concentration of labelled ligand. Binding affinities for unlabelled ligands at the Nluc-β_2AR and Nluc-VEGFR2 were consistent with results obtained in previously published data using radioligands (Alexander et al., 2017; Baker, 2005, 2010; Baker et al., 2003; Simon et al., 1998), fluorescence intensity (Arruda et al., 2017) and NanoBRET (Kilpatrick et al., 2017; Stoddart et al., 2015a).

The second part of the study describes the application of NanoBRET methodology to measure ligand-β_2-adrenoceptor interactions in a physiologically relevant system. β-adrenoceptor antagonists (or beta-blockers) have been widely used in the treatment of cardiovascular disease.

Epidemiologic studies have found a strong correlation for patients under β-blocker usage and reduced breast cancer risk (Barron et al., 2012; Melhem-Bertrandt et al., 2011). Beta-blockers have shown potential therapeutic effect in reducing metastasis, by targeting β_2AR signalling axis in pre-clinical models for different types of cancer (Barron et al., 2012; Creed et al., 2015; Pon et al., 2016; Powe et al., 2010; Sloan et al., 2010). In this study we show the use of NanoBRET for the pharmacological characterisation of two different breast cancer cell lines, that have been transfected to overexpress human full-length β_2-adrenoceptor tagged at the N-terminus with Nanoluc luciferase. Saturation binding experiments revealed similar binding affinities for the two labelled β-selective antagonists, CGP12177-TMR and propranolol-BY630/650, at Nluc-β_2AR expressed in MDA-231 breast cancer cell line. Notably, measured binding affinities for both fluorescent ligands were reduced in MDA-231 Nluc-β_2AR, compared to 66cl4 or HEK 293T cells. One possible explanation for the observed decrease in binding affinity is the higher expression of endogenous β_2AR, compared to 66cl4 or HEK 293T cells (Creed et al., 2015). Another plausible explanation is the different protein environment in these cells, which could result in a negative cooperativity at the level of ligand-receptor binding, with would lead to a decrease in ligand binding affinity (Ferré et al., 2014).

In Chapter 6 the novel use of NanoBRET to monitor beta-blocker-β_2-adrenoceptor engagement in living animals will be demonstrated, using the propranolol-BY630/650 fluorescent ligand as a probe. This chapter described the *in vitro* pharmacological characterisation for the binding of propranolol-BY630/650 at Nluc-β_2AR expressed in MDA-231 cancer cells. Fluorescence imaging of non-transfected or Nluc-β_2AR transfected MDA-231 revealed high-degree of non-specific binding of propranolol-BY630/650 in cells perinuclear region. This is a common feature observed for fluorescently-labelled ligands (Baker et al., 2003). Specific binding was only observed the plasma membrane of these cells, which was determined using wide-field bioluminescence imaging.

MDA-231 Nluc-β_2AR cell line was further characterised using NanoBRET kinetics binding assay to determine propranolol-BY630/650 fluorescent ligand association (k_{on}) and dissociation (k_{off}) rates, as well as its residence time on the receptor (RT). These are important pharmacological parameters to be determined that better predict ligand-receptor binding pharmacology in *in vivo* systems (Guo et al., 2016b). Binding kinetic measurements revealed fast association and slow dissociation rates for this ligand, with a residence time of 44 min. These pharmacological properties, together with the red-shifted emission (with peak emission at 650nm) of this ligand make it an ideal probe for non-invasive *in vivo* imaging (Huynh et al., 2015; Unen et al., 2015). Importantly, binding data measured using a conventional plate-reader or the whole-animal bioluminescence imaging system (IVIS camera system) showed very similar results, indicating that the IVIS camera system is sensitive enough with good spectral resolution to detect BRET.

Overall this chapter demonstrates that Nluc-tagged receptors can retain their pharmacology at the level of ligand binding. It was also demonstrated the successful application of NanoBRET to measure ligand-β_2-adrenoceptor binding kinetics in breast cancer cell lines, demonstrating that propranolol-BY630/650 fluorescent probe has better pharmacological properties, including red-shifted emission, fast on-rate and slow dissociation, for future *in vivo* application. Moreover, the whole-animal bioluminescence imaging system, IVIS Lumina II, displayed good sensitivity and spectral resolution to detect and measure BRET *in vitro*, which is a necessary step before measuring BRET *in vivo*.

Chapter 5: NanoBRET to investigate *in vitro* receptor-receptor interactions and the functional properties of β_2AR-VEGFR2 oligomeric complex in HEK 293T cells.

5.1. Introduction

It is well established that GPCRs can exist as homodimers, heterodimers or as higher-order oligomeric complexes (Calebiro and Sungkaworn, 2017; Ferré et al., 2014). Increasing studies have revealed evidence for the molecular interaction between different GPCRs and the receptor tyrosine kinase (RTK) superfamily of transmembrane receptors (Delcourt et al., 2007; Köse, 2017; Pyne and Pyne, 2011). Some studies reported strong evidence for the formation of a multiprotein functional complex, where the GPCR can transactivate the RTK to promote mitogenic signalling (Borroto-Escuela et al., 2013a; Maudsley, 2000; Tilley et al., 2009; Watson et al., 2016). Fewer studies have also demonstrated bidirectional cross-talk between GPCRs and RTKs, in which GPCR ligands can induce transactivation of RTKs and, reciprocally, RTK ligands can also induce GPCR transactivation (Delcourt et al., 2007; Pyne and Pyne, 2011). This type of cross-talk was observed for VEGFR2 and the GPCR sphingosine phosphate 1 receptor ($S1P_1$) that can oligomerise in myeloid ML1 cells to regulate cell migration (Balthasar et al., 2008; Bergelin et al., 2010).

VEGFR2 is the key mediator of angiogenesis, and aberrant activation of this receptor is associated with tumour angiogenesis and invasion (Niu and Chen, 2010; Peach et al., 2018a). Adenosine A_{2A} receptors and β_2-adrenoceptors activation can induce the release of growth factors, including VEGFa, the endogenous ligand for VEGFR2, to promote angiogenesis (Ahmad et al., 2009; Garg et al., 2017). The activation of β_2-adrenoceptor (via chronic stress or pharmacological activation) has been reported to promote a more invasive breast cancer cell phenotype, and to promote an increase in metastasis in a mouse model of breast cancer (Chang et al., 2016; Creed et al., 2015; Sloan et al., 2010). β_2-adrenoceptor activation can also promote tumour-induced angiogenesis in prostate cancer (Hulsurkar et al., 2017). The non-selective β-

adrenoceptor antagonist, propranolol, is the first line of treatment for Infantile Haemangioma, a benign infant tumour that is characterised by an abnormal increase in proliferation of vascular endothelial cells (Ji et al., 2015; Rotter and de Oliveira, 2017). Adenosine A_{2A} receptor is a key mediator of hypoxia-induced angiogenesis, via the release of VEGFa, and is also involved in hypoxia-induced immunosuppression by the tumour microenvironment (Allard et al., 2017; Gessi et al., 2011). Antagonists for A_{2A} receptor have shown a potential therapeutic effect in reducing tumour-induced immunosuppression (Hatfield and Sitkovsky, 2016). The molecular cross-talk between VEGFR2 and the two Gs-coupled receptors adenosine A_{2A}R and β_2AR was never investigated before. Therefore, the aim of this study was to investigate whether these receptor families could cross-talk via a mechanism involving receptor oligomerisation.

NanoBRET has been successfully used to monitor ligand-receptor interactions at real-time in living cells (Stoddart et al., 2018). Therefore, in this study was proposed the development of a new assay to investigate direct receptor-receptor interactions using the proximity-based assay NanoBRET.

Receptor-receptor interactions were investigated using NanoLuc-tagged receptors as resonance energy transfer (RET) donors, and Halo/SNAP-tagged receptors that were used as RET acceptors. A NanoBRET titration or saturation assay was applied with transiently co-transfected cells, expressing both donor and acceptor. This assay was a good option to check for non-specific (or bystander) BRET, that could potentially occur due to overexpression of receptor in cells (Borroto-Escuela et al., 2013b). In this assay a fixed amount of donor is co-expressed with increasing concentrations of the acceptor. Non-specific BRET signals would increase linearly with increasing concentrations of the acceptor. On the other hand, specific protein-protein interactions result in a BRET signal that increases hyperbolically reaching a plateau level, when all the donor molecules are saturated with acceptor molecules. The use of SNAP/Halo-tag labelling of receptors is ideal, as it allows labelling of active/inhactive receptors localised at the cell membrane with the use of cell impermeable Halo/SNAP-Tag substrates. Moreover, these Tags allow the

covalent binding of substrates with different fluorophores that emit at different wavelengths. More importantly, as previously investigated in Chapter 4, and showed in published studies (Peach et al., 2018b; Soave et al., 2016; Stoddart et al., 2015a), the small (~19kDa) N-terminal Nluc or SNAP/Halo Tags do not interfere with the receptor binding pocket or function. Recent studies have also taken the advantage of SNAP-Tag labelling system to track and measure receptor-receptor interactions at a single-molecule level (Calebiro and Sungkaworn, 2017; Calebiro et al., 2013) .

5.2. Brief materials and methods

Molecular biology

A detailed description of the constructs used in this study is provided in Chapter 2, section 2.2. Briefly, human full-length receptors were used in this study, which were fused with either Nanoluc luciferase (Nluc-receptor) or SNAP/Halo-Tags (SNAP- or Halo-receptor). A lentiviral construct encoding a GFP-tagged single domain nanobody 80 (Nb-80-GFP) and a β_2AR-tagged at the C-terminus with Nluc (in a pF-SNnk vector) were also used for the Nb-80-GFP recruitment assay. Moreover, a β-arrestin-2-tagged with Venus-YFP (β-arrestin-2-YFP) cDNA construct was used for the β-arrestin-2-YFP recruitment assay.

Cell culture

Detailed description of cell transfection is provided in Chapter 2 section 2.3. Briefly, HEK 293T cells were transiently co-transfected with different human full-lenght tagged receptors, depending on the assay performed. All transfections were performed using Fugene^{HM} reagent, using a 3:1 Fugene:DNA ratio. HEK 293T were stably transfected with Nb-80-GFP, and used for the Nb-80-GFP recruitment assay.

NanoBRET saturation assay to measure receptor-receptor interactions

Detailed methods for these experiments are provided in Chapter 2, section 2.5.3. Briefly, HEK 293T were co-transfected with a fixed concentration of Nluc-tagged receptor (0.05µg, RET donor) and increasing concentrations of SNAP/Halo-tagged receptor (0 to 0.2µg, RET acceptor). On the following day, cells were incubated in serum-free media (baseline BRET signal) or treated with 0.2µM Halo- or SNAP- cell impermeable Alexa Fluor 488 (AF488) substrates prepared in serum-free media. After incubation, cells were washed three times with assay buffer to remove unbound substrates. Cells were then incubated with 10µM Furimazine substrate for 5min before BRET measurements. BRET measurements were taken using a PHERAstar FS plate-reader, using sequential luminescence (460/80nm bandpass; Nluc emission) and fluorescence (535/60nm bandpass; AF488 emission) measurements. Raw BRET ratios were calculated as acceptor to donor ratios.

Confocal imaging

Full details for confocal imaging are provided in Chapter 2, section 2.6.1. For these experiments, HEK 293T seeded in an 8-well plate were co-transfected with Halo-VEGFR2 and either SNAP-β_2AR or SNAP-A_{2A}AR cDNA (0.025µg/well each cDNA). 24h after transfection, cells were labelled with 0.5µM cell impermeable Halo AF660 and SNAP AF488 substrates prepared in serum-free media. After incubation, cells were washed three times with assay buffer to remove unbound substrates. Cells were then incubated with vehicle, 10nM $VEGF_{165}$a and either 10µM isoprenaline (β-selective agonist) or 10µM CGS21680 (A_{2A}AR-selective agonist) for 60min, at 37^{o}C. Imaging was performed with a Zeiss 710 confocal microscope, using an Argon488 laser (SNAP AF488; 496-574nm band pass; 3% power) and HeNe excitation (Halo AF660; 621-759nm bandpass; 20% power).

Super Resolution Structured Illumination Microscopy (SIM)

Full details for SIM imaging are provided in Chapter 2, section 2.6.5. HEK 293T cells, seeded in coverslips, were co-transfected with Halo-VEGFR2 and SNAP-β_2AR cDNA (3.3µg total cDNA). 24h after transfection, cells were labelled with 0.5µM cell impermeable Halo AF660 and SNAP AF488 substrates prepared in serum-free media. After incubation, cells were washed three times with assay buffer to remove unbound substrates. Cells were then incubated with vehicle, 10nM $VEGF_{165}$a and 10µM isoprenaline (β-selective agonist) for 60min, at 37^{o}C. After treatment, cells were fixed and mounted onto slides containing ProLong Glass Antifade Mountant. Imaging was performed using a Zeiss ELYRA PS.1 microscope. Z-stack images of SNAP-β_2AR were acquired using bandpass 495-550 plus longpass 750 filter, at 5% laser power with 150ms exposure time (28µm grating). And, images of Halo-VEGFR2 were acquired using a long-pass 655 filter at 8% laser power with 150ms exposure time (42µm grating).

NanoBRET Nb-80-GFP recruitment assay time-course and isoprenaline concentration response curve

Detailed description for the Nb-80-GFP recruitment assay is provided in Chapter 2, section 2.5.7. Briefly, HEK 293T stably expressing Nb-80-GFP were used in these studies, which were seeded onto 96-well plates and co-transfected on the following day with 0.025µg/well β_2AR-Nluc and either 0.025µg/well empty vector or 0.025 Halo-VEGFR2.

For the time-course assay, HEK 293T cells stably expressing Nb-80-GFP and transiently co-expressing β_2AR-Nluc and empty vector (pcDNA3.1) were used. These cells were incubated with 10µM furimazine substrate, incubated for 5min, and sequential luminescence and fluorescence emissions were measured every minute for 5min, using a PHERAstar FS plate reader, with the same filter settings used for the receptor-receptor interaction studies. 5min after first reads, cells were treated with vehicle, or 10µM isoprenaline, and continuous readings were performed using the same settings for a total time

of 45min. Raw BRET ratios were calculated dividing the 535nm emission (acceptor) by the 460nm emission (donor).

For isoprenaline concentration response curve, HEK 293T cells stably expressing Nb-80-GFP and transiently co-expressing β_2AR-Nluc and empty vector or Halo-VEGFR2 were used. These cells were incubated for 30min with vehicle or 10µM isoprenaline and/or 10nM $VEGF_{165}$a before measurements. After ligand incubation, cells were incubated for 5min with 10µM Furimazine substrate and sequential luminescence and fluorescence emission measurements were taken using a PHERAstar FS plate reader, using the same filter settings mentioned above.

NanoBRET β-arrestin 2-YFP recruitment assay

Detailed methods description is provided in Chapter 2, section 2.5.6. HEK 293T cells, seeded onto 96-well plates, were co-transfected with 0.01µg/well β_2AR-Nluc and either 0.04µg/well empty vector or 0.04µg/well Halo-VEGFR2. Cells were incubated with 10µM Furimazine substrate for 5min before sequential luminescence and fluorescence emission measurements using the PHERAstar plate reader and the same filter settings described earlier. Cell were treated with vehicle or 10µM isoprenaline, or/and 10nM $VEGF_{165}$a 4 min after initial reads. Continuous sequential readings were taken for a total time of 45min. Raw BRET ratios were calculated dividing the 535nm emission (acceptor) by the 460nm emission (donor).

5.3. Results

NanoBRET to investigate VEGFR2 dimerization in the presence or absence of $VEGF_{165}a$ agonist

Here we used NanoBRET technology to investigate VEGFR2 dimerization, in the presence or absence of $VEGF_{165}a$ agonist (Figure 5.1.). In this experiment, HEK 293T cells were co-transfected with a fixed concentration of donor (0.05 µg/well Nluc-VEGFR2) and increasing concentrations of acceptor (0 to 0.2 µg/well Halo-VEGFR2). A significant saturable increase in BRET ratio (evidence for specific receptor-receptor interactions) was observed under basal conditions (Figure 5.1.a, open circles). At higher concentrations of acceptor (0.2µg/well Halo-VEGFR2 cDNA), there was a decrease in the BRET signal, probably due to the concentration of expressed protein not corresponding to the added cDNA concentration. Importantly, treatment with 1nM $VEGF_{165}a$ agonist showed to enhance the BRET signal (Figure 1a, closed black circles), suggesting an increase in VEGFR2 homodimerization. Stimulation with 10nM agonist did not result in a further increase in BRET signal (Figure 5.1.a, red circles).

The effect of $VEGF_{165}a$ in promoting VEGFR2 homodimerization was also investigated in HEK 293T cells stably expressing Nluc-VEGFR2 and co-transfected with a fixed concentration of Halo-VEGFR2 cDNA (0.05 µg/well, Figure 5.1.b). A clear saturable increase in BRET was observed with the increase in ligand concentration with a pEC_{50} of 9.40 ± 0.28 (n=4, Figure 5.1.b).

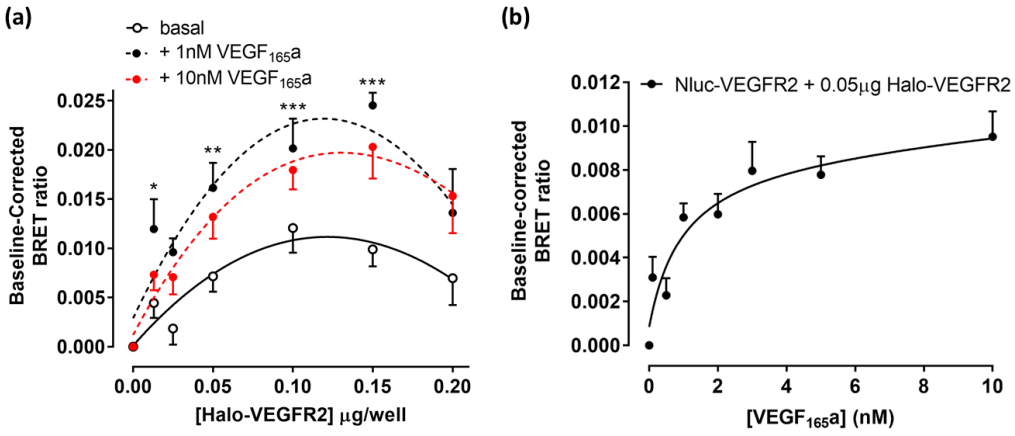

Figure 5.1. Investigation of VEGFR2 dimerization under non-stimulated or $VEGF_{165}a$-stimulated conditions. (a) NanoBRET experiments to investigate constitutive and ligand-induced dimerization of VEGFR2. HEK 293T cells were transiently transfected with a fixed concentration of NLuc-VEGFR2 (0.05 μg/well; donor) and increasing concentrations of Halo-VEGFR2 (0–0.2 μg/well; acceptor), and empty vector (pcDNA3.1) was used to keep same DNA concentration in all wells. Cells were treated with either vehicle (open circles), 1nM $VEGF_{165}a$ (closed black circles), or 10nM $VEGF_{165}a$ (closed red circles), for 60min at 37°C. Data are displayed as baseline-corrected BRET ratios expressed as mean ± SEM obtained from seven separate experiments performed in duplicate wells. **(b)** HEK 293T cells stably expressing NLuc-VEGFR2 and transiently transfected with Halo-VEGFR2 cDNA (0.05μg/well), were treated with increasing concentrations of $VEGF_{165}a$, for 60min at 37°C. Data are displayed as baseline-corrected BRET ratios expressed as mean ± SEM obtained from four separate experiments, performed in triplicate wells. Statistical analysis was performed using two-way ANOVA with Dunnett's multiple comparison test (* p<0.01, ** p<0.005 or ***p<0.001 compared to zero).

NanoBRET to investigate GPCR homodimerization for adenosine A_1, A_{2A}, A_3 receptors and β_2-adrenoceptors

NanoBRET approach was then applied to investigate GPCR homodimers for the different adenosine receptor subtypes (A_1, $A_{2A,}$ A_3) and for β_2-adrenoceptors. All these receptors have been previously reported to exist as dimers or as higher-order oligomers in cell models (Canals et al., 2004; Gracia et al., 2013; Mandic et al., 2014; May et al., 2011). Saturation data resulted in a significant saturation for β_2AR pairs (Figure 5.2.), with a $BRET_{max}$ = 0.088 ± 0.012 (n=5). A significant and saturable increase in BRET ratios was also observed for all adenosine receptor subtypes (Figure 5.3.), with $BRET_{max}$ = 0.013 ± 0.006 (n=7) for A_1R pairs, $BRET_{max}$ = 0.096 ± 0.014 (n=5) for A_{2A}R pairs, and $BRET_{max}$ = 0.021 ± 0.001 (n=5) for A_3R pairs. These data provide evidence for the presence of homodimers under non-stimulation conditions in HEK 293T cells. $BRET_{max}$ data is also displayed below in Table 5.1.

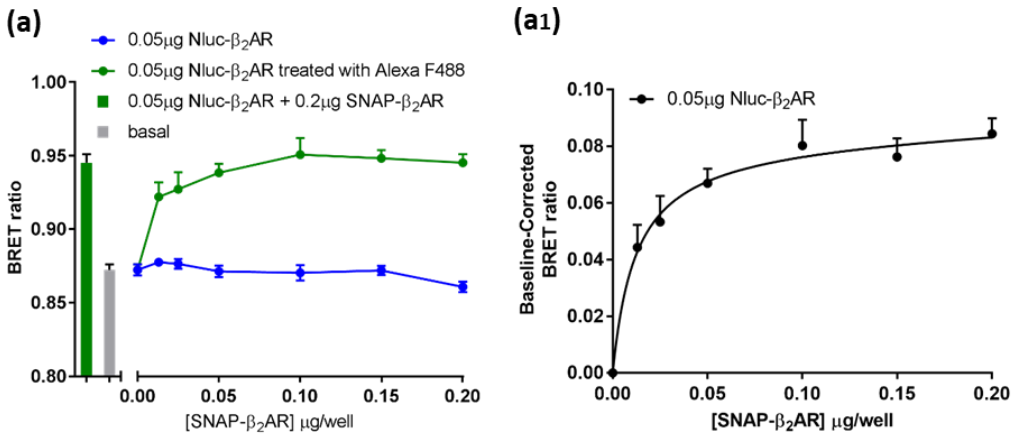

Figure 5.2. Investigation of receptor homodimers for β_2-adrenoceptors, under non-stimulated conditions. β_2-adrenoceptors homodimerization was investigated using transiently co-transfected HEK 293T cells with Nluc-β_2AR cDNA (0.05µg/well) and increasing concentrations of SNAP-tagged- β_2AR cDNA, and empty vector (pcDNA3.1) was used to keep same DNA concentration in all wells. **(a)** Combined NanoBRET raw data obtained from five different experiments. Blue line represents measurements taken from cells treated with furimazine substrate only, whereas green line represents cells pre-treated with SNAP-Tag cell impermeable substrate Alexa Fluor 488 (SNAP AF488). Green bar corresponds to highest concentration of acceptor labelled with both furimazine and SNAP AF488, whereas grey bar represents donor only labelled with furimazine and SNAP AF488 substrates. Saturation binding data was then baseline-corrected by subtracting BRET values obtained from cells treated with furimazine only and displayed in **(a1)**. BRET ratios were calculated by dividing the 535nm emission (acceptor) by the 460nm emission (donor).

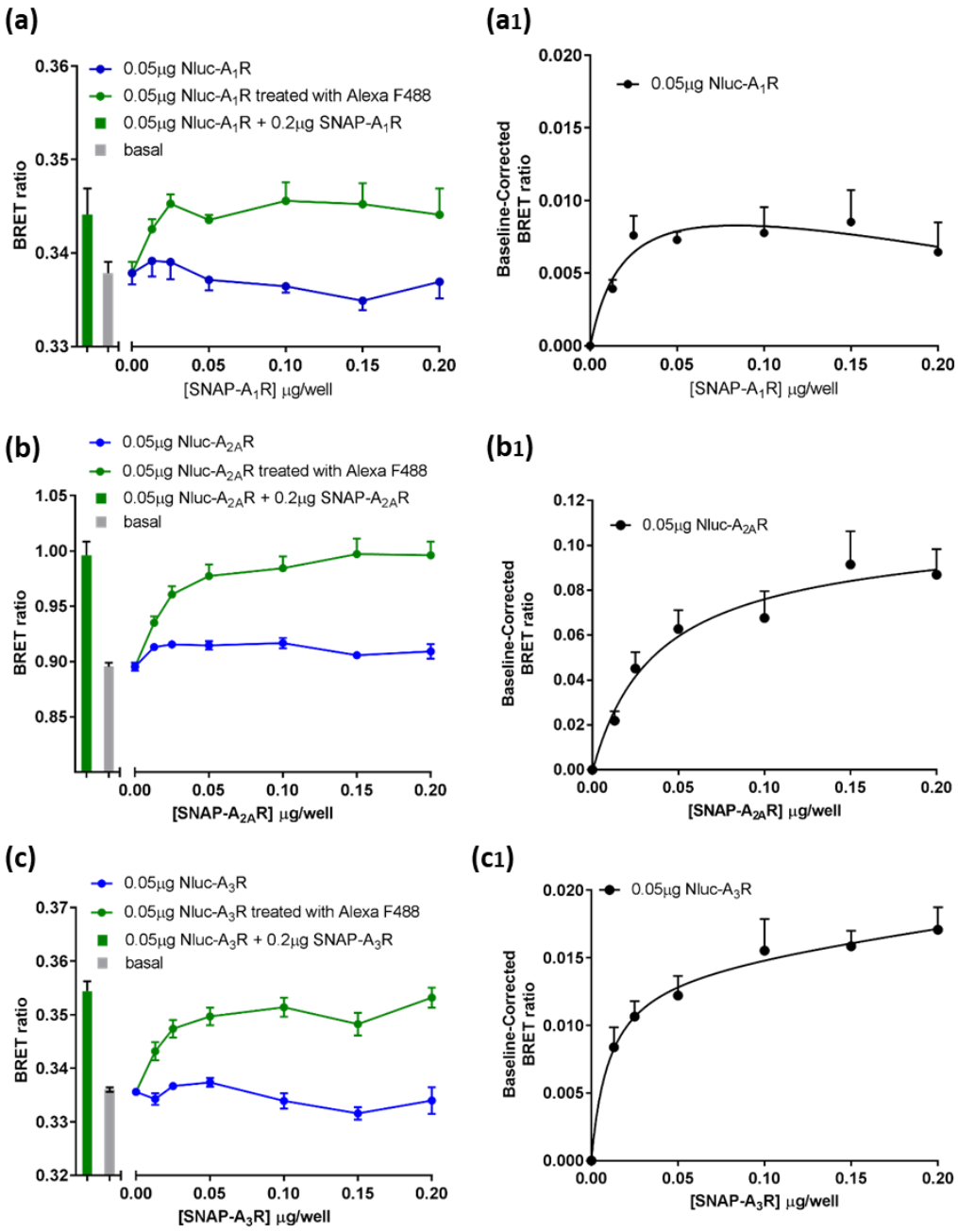

Figure 5.3. Investigation of receptor homodimers for adenosine receptor subtypes A_1, A_{2A} or A_3, under non-stimulated conditions. GPCR homodimerization was investigated and is represented as previously mentioned for β_2AR homodimers. NanoBRET raw saturation data is presented for **(a)** the adenosine A_1 receptor, **(b)** adenosine A_{2A} receptor and **(c)** adenosine A_3 receptor. Baseline-corrected saturation data is represented in **(a1)** for the adenosine A_1R **(b1)** adenosine A_{2A}R and **(c1)** adenosine A_3R. Data are mean ± SEM from five (A_3AR and A_{2A}AR) or seven (A_1AR) separate experiments, each performed in duplicate measurements.

NanoBRET to investigate VEGFR2-GPCR oligomerisation under non-stimulated conditions.

GPCRs and RTKs can cross-talk to regulate downstream signalling via different mechanisms, in some cases, cross-talk requires the physical association between these two receptor families (Köse, 2017; Pyne and Pyne, 2011). A NanoBRET saturation binding assay was used to investigate the molecular interaction between VEGFR2 and the different adenosine receptor subtypes or β_2-adrenoceptor. Data revealed a significant saturable increase in BRET signal for VEGFR2 and adenosine $A_{2A}R$ or β_2-adrenoceptors (Figure 5.4.), which displayed BRETmax of 0.017 ± 0.001 (n=6) and 0.015 ± 0.002 (n=5), respectively. Data obtained for VEGFR2 co-transfected with either A_1 or A_3 receptors, resulted in a linear increase in BRET ratios (Figure 5.5.), consistent with a non-specific interaction caused by Bystander BRET (Borroto-Escuela et al., 2013b). These data indicate that VEGFR2 can associate with adenosine A_{2A} and β_2-adrenergic receptors, but not with adenosine A_1 or A_3 receptors (which were used as negative controls). However, we cannot exclude the possibility that VEGFR2 and adenosine A_1 or A_3 receptors may be present as a complex but in a conformation that does not favour resonance energy transfer (RET) to occur. $BRET_{max}$ values for VEGFR2-GPCR oligomers is displayed in displayed in Table 5.1.

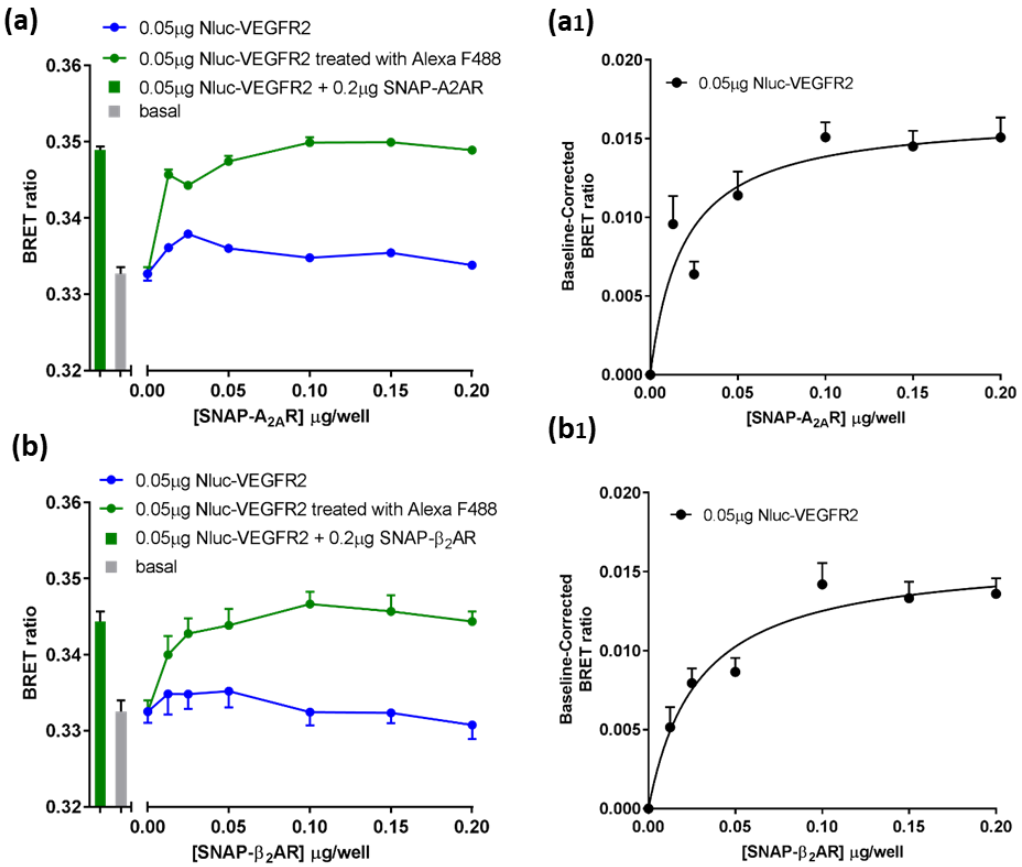

Figure 5.4. Investigation of VEGFR2 oligomerisation with adenosine A_{2A} and β_2-adrenergic receptors. VEGFR2-GPCR oligomerisation was investigated using transiently co-transfected HEK 293T cells with 0.05µg/well Nluc-VEGFR2 cDNA and increasing concentrations of SNAP-tagged-GPCR cDNA. NanoBRET raw saturation data is showed for **(a)** Nluc-VEGFR2/SNAP-A_{2A}R and **(b)** Nluc-VEGFR2/SNAP-β_2AR pairs. BRET ratios were calculated as acceptor to donor ratios. And data is represented as previously mentioned for homodimers investigation. Baseline-corrected saturation data is presented in **(a1)** for Nluc-VEGFR2/SNAP-A_{2A}R oligomeric complexes and **(b1)** Nluc-VEGFR2/SNAP-β_2AR oligomeric complexes. Data are represented as mean ± SEM from five (VEGFR2-β_2AR pairs) or six (VEGFR2-A_{2A}AR pairs) separate experiments, each performed in duplicate measurements.

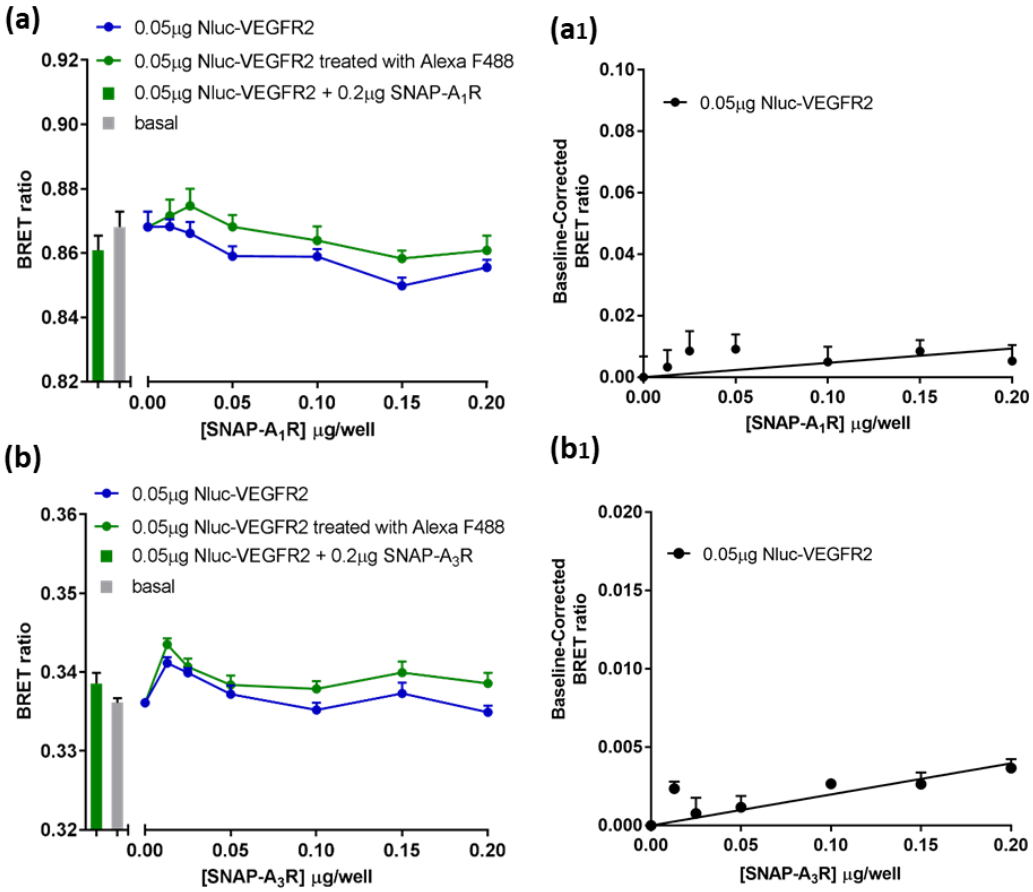

Figure 5.5. Investigation of VEGFR2 oligomerisation with adenosine A_1 and A3 receptors. VEGFR2-GPCR oligomerisation was investigated and is displayed as mentioned above. NanoBRET raw saturation data is showed for **(a)** Nluc-VEGFR2/SNAP-A_1R and **(b)** Nluc-VEGFR2/SNAP-A_3R pairs. BRET ratios were calculated as acceptor to donor ratios. Baseline-corrected saturation data is shown in **(a1)** Nluc-VEGFR2/SNAP-A_1R and **(b1)** Nluc-VEGFR2/SNAP-A_3R pairs. Data are mean ± SEM from five separate experiments, each performed in duplicate measurements.

Table 5.1. $BRET_{max}$ data obtained for homodimers (GPCR-GPCR) and oligomeric complexes (VEGFR2-GPCR).

GPCR Homodimers				
Donor	**Acceptor**	**BRETmax ± SEM**	**p value**	**n**
Nluc-A_1R	SNAP-A_1R	0.013 ± 0.006	< 0.05	7
Nluc-A_3R	SNAP-A_3R	0.021 ± 0.001	< 0.001	5
Nluc-$A_{2A}R$	SNAP-$A_{2A}R$	0.096 ± 0.014	< 0.01	5
Nluc-β_2AR	SNAP-β_2AR	0.088 ± 0.012	< 0.001	5
GPCR-RTK Oligomeric complexes				
Donor	**Acceptor**	**BRETmax ± SEM**	**p value**	**N**
Nluc-VEGFR2	SNAP-A_1R	-	ns	5
	SNAP-A_3R	-	ns	5
	SNAP-$A_{2A}R$	0.017 ± 0.001	< 0.001	6
	SNAP-β_2AR	0.015 ± 0.002	< 0.01	5

Table displays BRETmax values for GPCR homodimers and VEGFR2/GPCR oligomeric complexes taken from individual experiments and expressed as mean ± SEM, from n experiments.using two-way ANOVA with Dunnet's test to compare BRET values obtained for different acceptor concentrations compared to donor alone (baseline BRET signal). . ns = not significant.

Investigation of possible level of cooperativity across dimer interface

Previous studies from our lab reported that dimer formation can lead to negative cooperativity between the ligand binding sites of the different protomers (Gherbi et al., 2015; May et al., 2011). Based on those findings we investigated possible cooperativity across dimer interface for VEGFR2-$A_{2A}R$ or VEGFR2-β_2AR heteromeric complexes. The principle was to use a fluorescent ligand that binds to the Nluc-labelled protomer and investigate whether unlabelled ligands that bind to the receptor pair would interfere with the BRET signal. In other words, whether ligand binding to the second protomer would affect the binding affinity of a ligand to the first protomer.

To investigate any cooperativity across the dimer interface for VEGFR2/$A_{2A}AR$ heteromeric complexes, HEK cells transiently expressing Nluc-$A_{2A}AR$ and Halo-VEGFR2 were treated with 200nM CA200645 (non-selective adenosine fluorescent ligand) and increasing concentrations of $VEGF_{165}a$ (Figure 5.6.a).

Co-treatment with labelled ligand and 10μM SCH58261 (a selective A_{2A}AR antagonist) resulted in nearly full displament of the labelled ligand. However, $VEGF_{165}$a treatment had no effect on CA200645 binding at Nluc-A_{2A}AR. Then, we investigated whether ligands that bind to A_{2A}AR could affect the binding of $VEGF_{165}$a-TMR labelled ligand to Nluc-VEGFR2. For these experiments, HEK 293T were co-transfected with Nluc-VEGFR2 and SNAP-A_{2A}AR. As previously observed, co-treatment with 1nM $VEGF_{165}$a-TMR and 10μM unlabelled $VEGF_{165}$a, resulted in the nearly full displacement of the labelled ligand (Figure 5.6.b). However, co-treatment with the non-selective adenosine agonist NECA or the A_{2A}AR-selective agonist CGS21680 did not result in a significant change in BRET ratios.

Possible cooperative effect across the dimer interface was also investigated for VEGFR2/β_2AR heteromeric complexes, using the same assay format. For Nluc-β_2AR/Halo-VEGFR2, 15nM CGP12177-TMR labelled ligand was displayed by co-treatment with 100nM ICI 118551, but not by increasing concentrations of unlabelled $VEGF_{165}$a agonist (Figure 5.6.c). For Nluc-VEGFR2/SNAP-β_2AR, 2nM $VEGF_{165}$a-TMR were displaced by 10nM unlabelled $VEGF_{165}$a, but not by the following unlabelled ligands, propranolol (non-selective βAR antagonist), isoprenaline (non-selective βAR agonist), CGP12177 (β_1AR and β_2AR-selective antagonist) and ICI 118551 (β_2AR-selective antagonist) (Figure 5.6.d). In these experiments, the SNAP/Halo-tag receptors were not labelled with fluorophores.

Therefore, no cooperativity was observed across the dimer interface of VEGFR2/A_{2A}AR or VEGFR2/β_2AR heteromeric complexes. Eventhough cooperativity was not observed at a ligand-receptor binding level, it is possible that intrinsic cooperativity may occur between these receptors complexes, which can be explored by measuring recruitment of downstream targets, for example, β-arrestins or G-proteins. (Ferré et al., 2014).

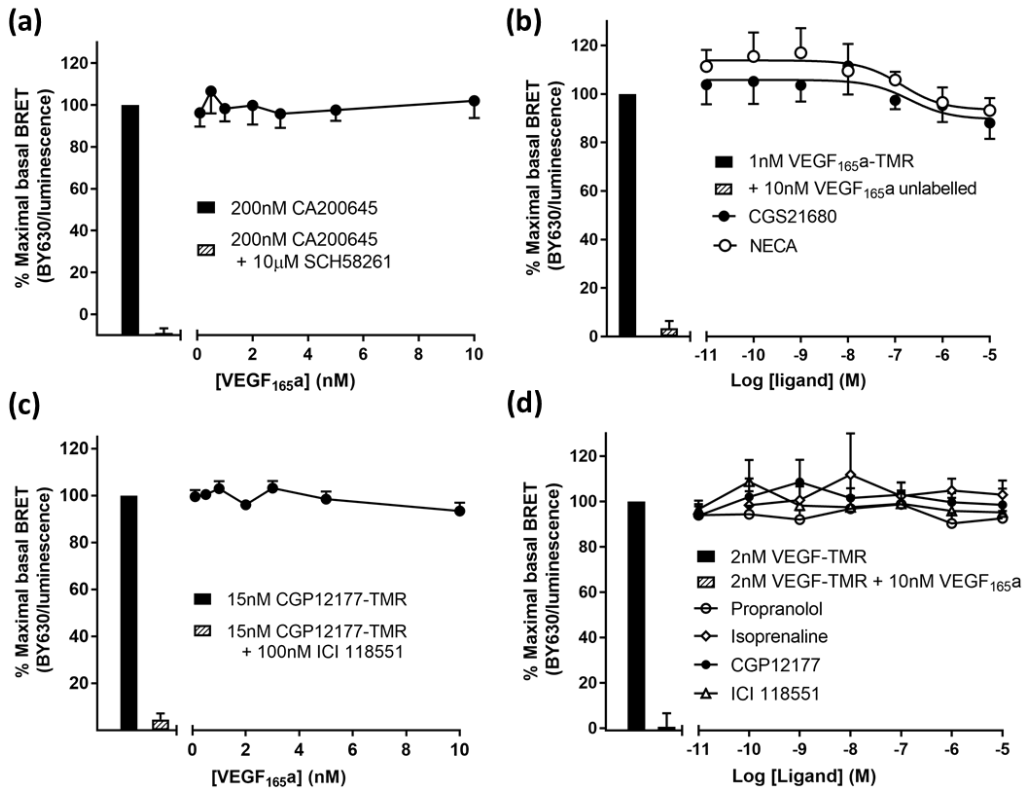

Figure 5.6. Investigation of possible cooperativity across VEGFR2-GPCR dimer interface. (a) HEK 293T cells transiently co-transfected with Nluc-A_{2A}R and Halo-VEGFR2, treated with 200nM CA200645 and increasing concentrations of $VEGF_{165}$a. **(b)** HEK 293 cells transiently co-transfected with Nluc-VEGFR2 and SNAP-A_{2A}R, treated with $VEGF_{165}$a-TMR and increasing concentrations of CGS21680 or NECA. **(c)** Cells transiently co-transfected with Nluc-β_2AR and Halo-VEGFR2, treated with CGP12177-TMR and increasing concentrations of $VEGF_{165}$a. Finally, **(d)** Cells transiently co-transfected with Nluc-VEGFR2 and SNAP-β_2AR, were treated with $VEGF_{165}$a-TMR and increasing concentrations of propranolol, isoprenaline, CGP12177 or ICI 118551. BRET was measured between donor NLuc and acceptor fluorescent ligands with emissions collected using a PHERAstar plate-reader. Data are mean ± SEM from six (a), four (b) or five (c,d) separate experiments, each performed in duplicate.

Investigation of the effect of agonists on VEGFR2-β_2AR and VEGFR2-A_{2A}AR oligomeric complexes

The effect of agonists on VEGFR2-A_{2A}AR or VEGFR2-β_2AR oligomeric complexes was investigated using NanoBRET. For these experiments, HEK 293T cells were transiently co-transfected with 0.05μg Nluc-VEGFR2 and 0.1μg SNAP-GPCR. For VEGFR2-A_{2A}AR oligomers, treatment with 10μM CGS21680, a A_{2A}AR-selective

agonist, resulted in a small but significant increase in BRET ratio, whereas treatment with $VEGF_{165}a$ resulted in a significant decrease in BRET ratio, using 1nM and 10nM $VEGF_{165}a$ (Figure 5.7. a and b). For VEGFR2-β_2AR oligomers, both isoprenaline (a βAR-selective agonist) and $VEGF_{165}a$ agonist treatment resulted in a significant increase in BRET signal, which was concentration-dependent (Figure 5.7. c and d). This increase or decrease in BRET ratio may be associated to a respective increase or decrease in receptors association but, could also result from a change in receptor conformation due to interaction with downstream effectors, such as G proteins or β-arrestin.

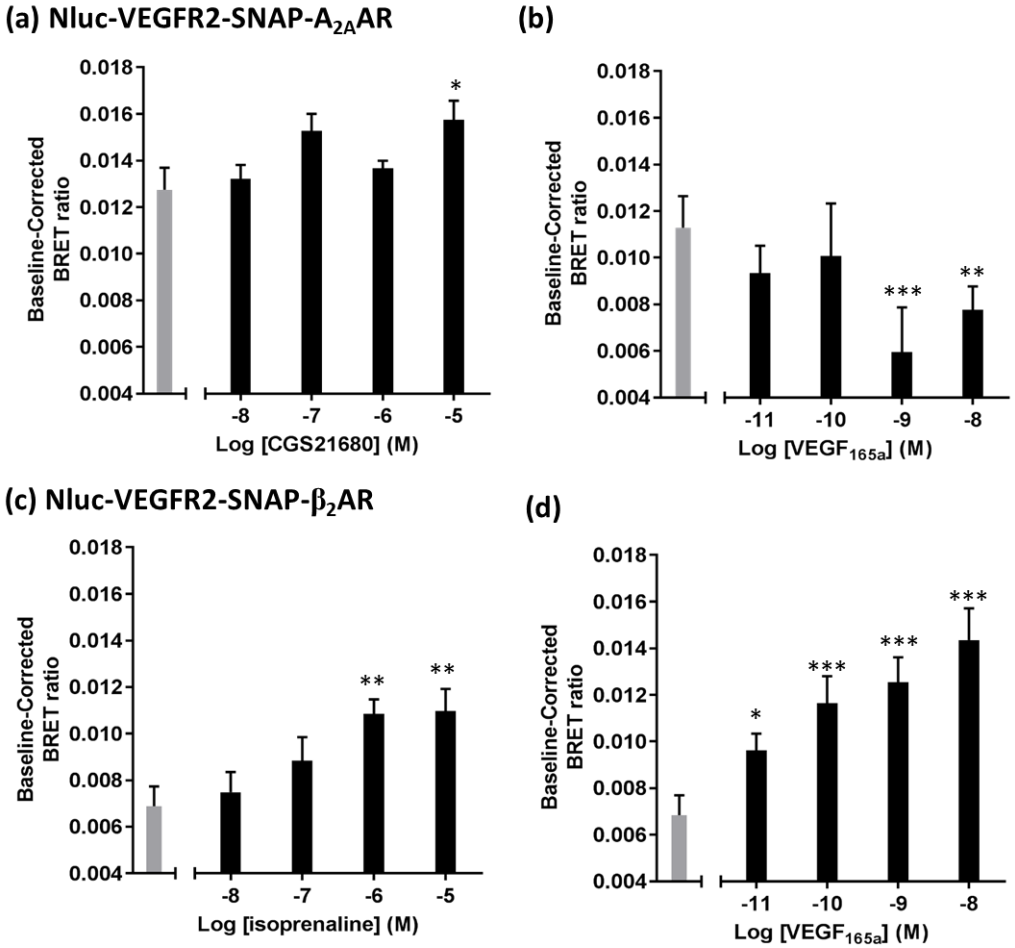

Figure 5.7. Effect of agonist treatment on VEGFR2-A_{2A}R or VEGFR2-β_2AR oligomeric complexes. HEK 293T cells were transiently transfected with 0.05μg/well NLuc VEGFR2 and **(a and b)** 0.1μg/well SNAP-A_{2A}R or **(c and d)** 0.1μg/well SNAP-β_2AR. Cells were labelled with SNAP-AF488 substrate or serum-free media (baseline BRET signal) before ligand treatment. Cells were then treated for 1h, at 37°C with increasing concentrations of **(a)** CGS21680, (c) isoprenaline, or **(b and d)** $VEGF_{165}a$. Grey bar represents co-transfected cells SNAP AF488

substrate-labelled under vehicle conditions. All cells were treated with furimazine substrate 5min before measurements were taken. Data displayed were baseline-corrected by subtracting baseline BRET ratios. BRET ratios were measured by dividing the 535nm emission (acceptor) by the 460nm emission (donor). Data are mean ± SEM from five separate experiments, each performed in quadruplicate. * $p<0.01$, ** $p<0.005$ or *** $p< 0.001$ compared to control, using two-way ANOVA with Dunnett's multiple comparison test.

Conventional confocal imaging to investigate VEGFR2 and GPCR localisation in HEK 293T cells

Confocal imaging was used to investigate receptors localisation under vehicle and agonist treated conditions. For these experiments, cells co-transfected with Halo-VEGFR2 and SNAP-β_2AR or SNAP-A_{2A}AR were labelled with cell impermeable Halo AF660 or SNAP AF488 substrates. Confocal imaging of cells co-transfected with VEGFR2 and β_2AR showed that, under basal conditions, both VEGFR2 and β_2AR are mostly located at the cell surface (Figure 5.8.). However, both receptors display a small degree of constitutive internalisation. Following 10nM $VEGF_{165}$a treatment, VEGFR2 internalisation was markedly increased, and 10μM isoprenaline also induced β_2AR internalisation. Both isoprenaline and $VEGF_{165}$a treatments also resulted in the co-internalisation of VEGFR2 and β_2AR, showed by the overlay of these receptors in the intracellular space (yellow, Figure 5.8.). These data, together with the NanoBRET data, suggest that VEGFR2-β_2AR oligomeric complexes can co-internalise following isoprenaline or $VEGF_{165}$a treatments.

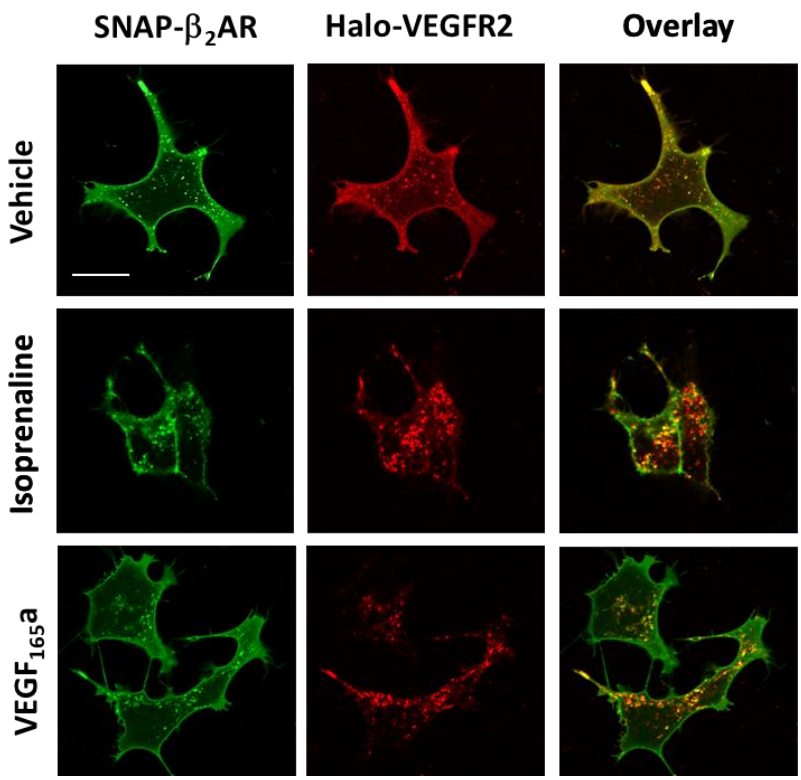

Figure 5.8. Investigation of the effect of agonist treatment on VEGFR2 and β_2AR cellular location using confocal live imaging. (a) Confocal imaging (Zeiss LSM 710) of HEK 293 cells transiently co-transfected with 0.025µg/well Halo-VEGFR2 and 0.025µg/well SNAP-β_2AR. Cells were labelled with cell-impermeable SNAP AF647 and Halo AF660 substrates, and treated for 60min at 37°C with vehicle, 10µM isoprenaline or 10nM $VEGF_{165}$a. Scale bar represents 20µm. These are representative images of 3 independent experiments.

Confocal imaging of cells co-transfected with VEGFR2 and A_{2A}AR showed that, under basal conditions, both VEGFR2 and A_{2A}AR are located at the plasma membrane and also inside the cell (constitutive internalisation). Treatment with CGS21680 increased A_{2A}AR internalisation, whereas $VEGF_{165}$a increased VEGFR2 internalisation. As previously observed for VEGFR2 and β_2AR pair, both $VEGF_{165}$a and CGS12680 treatments seem to induce co-internalisation of VEGFR2 and A_{2A}A receptors to the intracellular space (Figure 5.9.). However, due to the large degree of A_{2A}AR and VEGFR2 constitutive internalisation, it is not clear whether agonists are driving co-internalisation of these receptors.

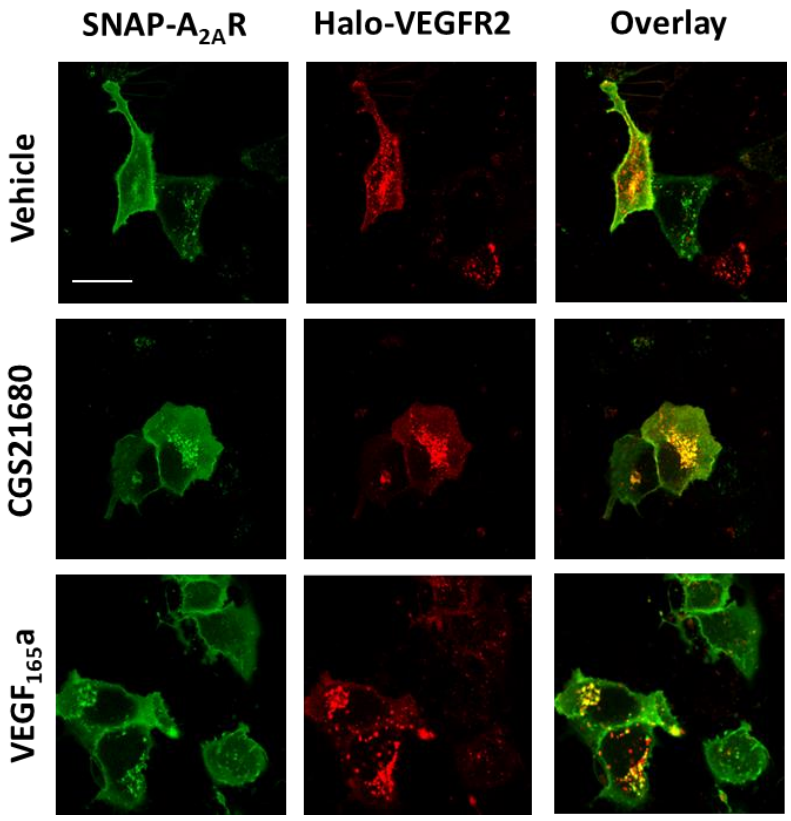

Figure 5.9. Investigation of the effect of agonist treatment on VEGFR2 and A_{2A}AR cellular location using confocal live imaging. (a) Confocal imaging (Zeiss LSM 710) of HEK 293 cells transiently co-transfected with 0.025µg/well Halo-VEGFR2 and 0.025µg/well SNAP-A_{2A}AR. Cells were labelled with cell-impermeable SNAP AF647 and Halo AF660 substrates, and treated for 60min at 37°C with vehicle, 10µM CGS21680 or 10nM $VEGF_{165}$a. Scale bar represents 20µm. These are representative images of 3 independent experiments.

Investigation of receptor co-localisation for VEGFR2 and β_2AR using Super-Resolution Structured Illumination Microscopy (SIM)

NanoBRET data showed evidence for VEGFR2-β_2-adrenergic receptors association under basal non-stimulated conditions, and agonist treatment (isoprenaline or $VEGF_{165}$a) induced further increase in BRET signal, suggesting an increase in interacting partners. Conventional confocal imaging suggested that isoprenaline or $VEGF_{165}$a treatments may induce co-internalisation of VEGFR2 and β_2AR into the intracellular space. However, conventional confocal microscopy has relatively low spatial resolution caused by light diffraction (resolution limit ~200nm), and therefore the lack of resolution does not allow

determination of receptor co-localisation (Wegel et al., 2016). Super-Resolution structured illumination microscopy (SIM) was used to investigate co-localisation of VEGFR2 and β_2AR under basal and agonist treatment conditions. As previously observed with conventional microscopy. Under vehicle conditions, VEGFR2 and β_2AR are co-localised on the plasma membrane and also inside the cell (constitutive internalisation). Isoprenaline treatment induced further internalisation of β_2AR and $VEGF_{165}a$ enhanced internalisation of VEGFR2. As previously observed, both isoprenaline and $VEGF_{165}a$ treatments induced receptor co-internalisation and co-localisation of VEGFR2 and β_2AR in intracellular compartments. Due to lack of time, co-localisation of VEGFR2 with A_{2A}AR was not investigated using SIM. Moreover, the rest of the study was focused on VEGFR2- β_2AR complexes.

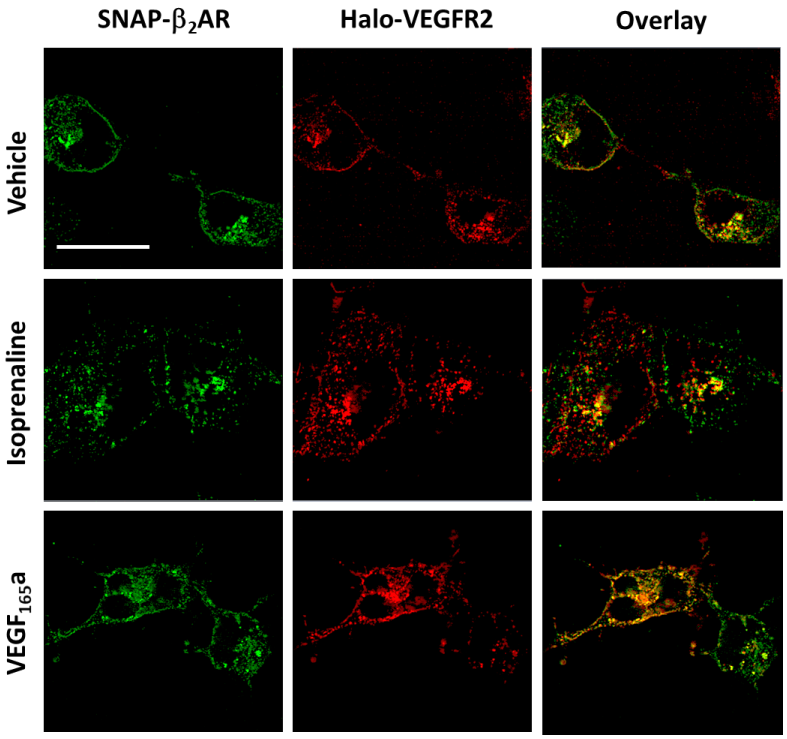

Figure 5.10. Investigation of the effect of agonist treatment on VEGFR2 and β_2AR cellular location using Structured Illumination Microscopy (SIM). HEK 293T cells were transiently co-transfected with equal amounts of SNAP-β_2AR and Halo-VEGFR2 cDNA (3.3 µg total cDNA) in coverslips. Cells were labelled with cell impermeable SNAP AF488 (SNAP-β_2AR) and Halo AF660 (Halo-VEGFR2) substrates. After labelling, cells were treated with vehicle, 10µM isoprenaline or 10nM $VEGF_{165}a$ (60min, at 37°C). Coverslips were imaged using a Zeiss ELYRA PS.1

microscope. Areas of colocalised Halo-VEGFR2 and SNAP-β_2AR labelled receptors are shown in yellow (overlay). These are representative images of three independent experiments.

Investigation of the activation status of β_2AR using the conformational-sensitive single domain nanobody 80, in the presence or absence of active-VEGFR2

A single domain camelid nanobody 80 (Nb-80) was previously used as a G protein surrogate which preferentially binds to the active- β_2AR conformation (Rasmussen et al., 2011a). A GFP-tagged-Nb-80 (Nb-80-GFP) was used as a conformational-sensitive biosensor to measure β_2AR signalling from endosomes (Irannejad et al., 2013).

In this study, Nb-80-GFP was used to investigate whether VEGFR2-β_2AR oligomeric complexes alter the activation status of β_2AR. For this purpose, we investigated the engagement of Nb-80-GFP with β_2AR tagged at the C-terminus with NanoLuc luciferase (β_2AR-Nluc), using NanoBRET. The treatment of HEK293T cells (stably expressing Nb-80-GFP and transiently transfected with 0.025µg β_2AR-Nluc) with 10µM isoprenaline, resulted in a rapid and significant engagement of Nb-80-GFP to β_2AR-Nluc (Figure 5.11.a; $p<0.001$). To investigate the effect of $VEGF_{165}$a-stimulated-VEGFR2 on β_2AR activation status, cells were co-transfected with either Halo-VEGFR2 or an empty control vector. In cells co-transfected with an empty vector, isoprenaline treatment led to the engagement of in a concentration-dependent manner (log EC50 = -7.91 ± 0.11, n=6, Figure 5.11.b). Binding of Nb-80-GFP to β_2AR-Nluc was competitively antagonised by the β_2AR-selective antagonist ICI 118551 (100nM; pKB = 8.6 ± 0.1, n=6). The presence of Halo-VEGFR2 (stimulated with 10nM $VEGF_{165}$a) did not shown an effect (log EC_{50} = -7.87 ± 0.40, n=6, Figure 5.11.b). Therefore, active-VEGFR2 does not affect β_2AR activation status. Expression of Halo-VEGFR2 was confirmed at the end of the experiment after labelling the cells with Halo-Tag substrate and imaging using an ULTRA MetaXpress confocal plate-reader.

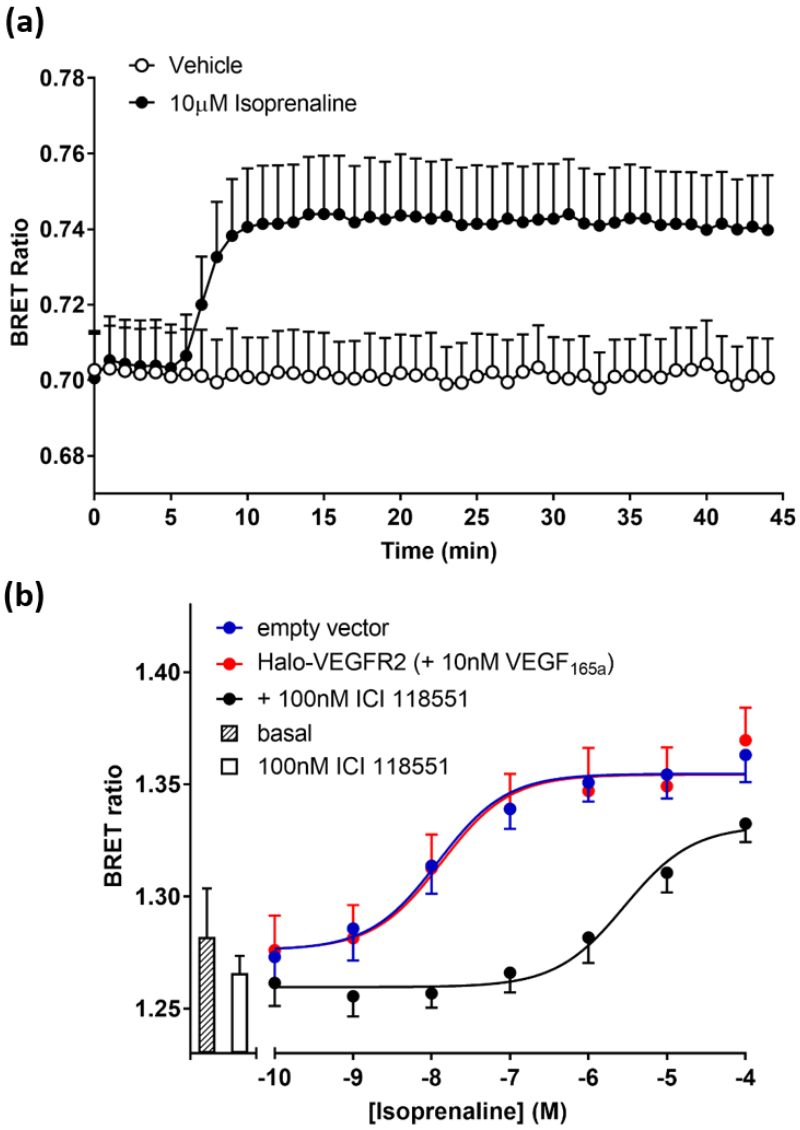

Figure 5.11. Investigation of the activation status of β_2AR using Nb-80-GFP. (a) HEK 293T cells stably expressing Nb-80-GFP were transfected with 0.025μg/well β_2AR-NLuc cDNA and stimulated with 10μM isoprenaline or vehicle added at 5min. A significant increase in BRET ratio was observed with isoprenaline from 8min onwards. Data are expressed as mean ± SEM from five separate experiments each performed in triplicate. Statistical analysis was performed using two-way ANOVA with repeated measures, and Bonferroni's multiple comparison test ($p<0.001$, relative to vehicle treatment). **(b)** HEK 293T cells stably expressing Nb-80-GFP were transiently co-transfected with 0.025μg/well β_2AR-NLuc cDNA and either 0.025μg/well empty vector (pcDNA3.1) or 0.025μg/well Halo-VEGFR2 cDNA. Cells co-transfected with empty vector were treated with increasing concentrations of isoprenaline, in the presence or absence of 100nM ICI 118551, and cells co-transfected with Halo-VEGFR2 were co-stimulated with increasing concentrations of isoprenaline and 10nM $VEGF_{165}$a. Bars correspond to untreated and 100nM ICI 118551 treated controls. Data are mean ± SEM from six separate experiments each performed in triplicate.

Investigation of VEGFR2-β_2AR complexes on β_2AR signalling using a β-arrestin-2-Venus-YFP recruitment assay

β-arrestin-2 is a key scaffold protein that has a major role in GPCR internalisation and signalling from intracellular compartments, such as endosomes (Calebiro et al., 2014; Eichel and von Zastrow, 2018). Some studies have reported that β-arrestin-2 can act as a protein-recruitment platforms to mediate signalling promoted by interacting GPCR-RTK complexes (Delcourt et al., 2007; Köse, 2017; Pyne and Pyne, 2011). A NanoBRET β-arrestin-2-Venus-YFP recruitment assay was used to investigate potential functional effect of VEGFR2-β_2AR interaction on β-arrestin-2 recruitment to β_2AR. For these experiments, HEK 293T cells were transiently co-transfected with 0.04 μg/well YFP-tagged β-arrestin-2-tagged with Venus-YFP (β-arrestin-2-YFP), 0.01 μg/well β_2AR C-terminally tagged with NanoLuc luciferase (β_2AR-Nluc) and either 0.04 μg/well empty vector or 0.04 μg/well Halo-VEGFR2.

β_2AR is a 'Class A' receptor in the way how it interacts with β-arrestins, forming a transient complex with β-arrestin-2, followed by a rapid dissociation and rapid recycling to the plasma membrane (Cahill et al., 2017; Shenoy and Lefkowitz, 2003). Treatment with 10μM isoprenaline induced in rapid recruitment of β-arrestin2-YFP to β_2AR-Nluc, that reached a BRET signal peak between 4 to 6 min after agonist stimulation (in the presence of empty vector Figure 5.12.a black circles). After that, the BRET signal showed a decline over-time, as expected. In cells transfected with both VEGFR2 and β_2A receptors, but stimulated only with isoprenaline, showed a similar profile for β-arrestin2-YFP recruitment (figure 5.12.a, blue circles). However, in matched experiments, under co-treatment conditions with 10nM $VEGF_{165}$a and 10μM isoprenaline, the activation of VEGFR2 appeared to alter the profile of the β_2-adrenoceptor engagement with β-arrestin2 (figure 5.12.a, red circles). Under co-stimulation conditions, the peak response was slightly truncated, and a plateau was observed 9min after agonist treatment, indicating a more sustained β-arrestin-2 engagement with β_2-adrenoceptor. This effect of $VEGF_{165}$a was prevented by

the pre-treatment of cells with the VEGFR2 inhibitor cediranib (Kilpatrick et al., 2017) (Figure 5.12.a, grey circles). These data suggests a change in β-arrestin-2 recruitment profile to a more sustained one, which may have impact on endosomal signalling (Thomsen et al., 2016).

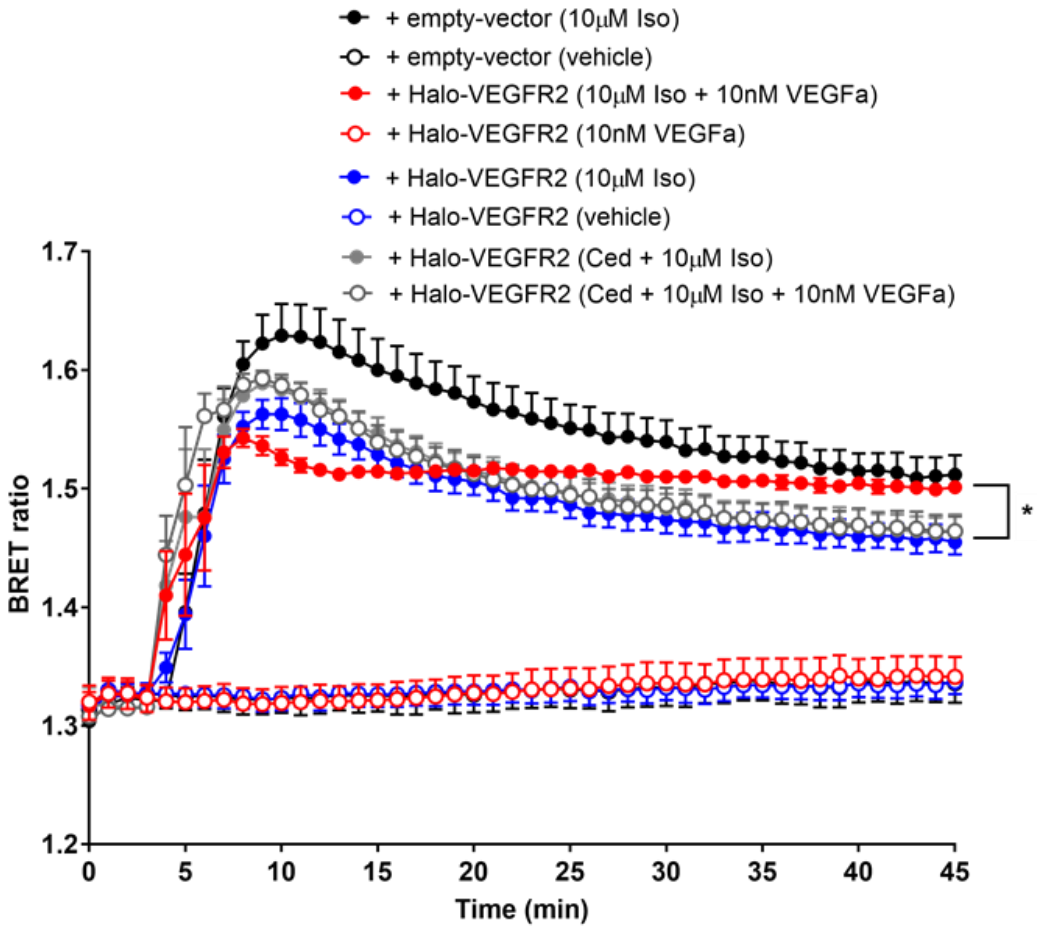

Figure 5.12. Investigation of β-arrestin2 recruitment to β_2AR, using a NanoBRET-based approach. HEK 293T cells were co-transient transfected with 0.01μg/well β_2AR-NLuc, 0.04μg/well β-arrestin2-YFP and either 0.04μg/well Halo-VEGFR2 or empty vector (pcDNA3.1). Cells were treated with vehicle, 10μM isoprenaline, or 10μM isoprenaline (Iso) plus 10nM $VEGF_{165}$a (all added at 4min), in the presence or absence of 1μM cediranib (Ced). Data are expressed as mean ± SEM from five (without cediranib treatment) or four (with cediranib treatment) separate experiments, each performed in triplicate wells. Statistical analysis was performed using 2-Way ANOVA with repeated measures and Bonferroni's multiple comparison's tests, with *p<0.05 between filled red and filled blue, using data points from 20min onwards.

5.3. Discussion and Conclusion

GPCR activation of mitogen-activated protein kinase (MAPK) and extracellular-signal-regulated kinases(ERK) pathway was earlier believed to be G-protein-dependent (Gα or Gβγ) (Rozengurt, 2007). Nowadays, we know that GPCR-induced mitogenic signalling is not exclusively mediated by G-proteins, but can also result from GPCR-induced transactivation of RTK, the key mediators of mitogenic signalling (Borroto-Escuela et al., 2016; Cattaneo et al., 2014; Köse, 2017; Pyne and Pyne, 2011; Werry et al., 2005). Several studies describing different transactivation mechanisms have been identified for different GPCRs and RTK family (Cattaneo et al., 2014; Köse, 2017; Pyne and Pyne, 2011). However, not many studies have explored these molecular interactions, via receptor oligomerisation, for GPCRs and the Vascular Endothelial Growth Factor Receptor 2 (VEGFR2) (Bergelin et al., 2010).

Since cellular environment can affect protein-protein interactions, signalling propagation and physiological response (Vanderheyden and Benachour, 2017), having a technique that preserves the native cell environment is ideal (Stoddart et al., 2018). In this study NanoBRET methodology was used to investigate direct receptor-receptor interactions in living HEK 293T cells, using human full-length receptors. NanoBRET to investigate VEGFR2 dimerization revealed the presence of pre-formed VEGFR2 dimers in HEK293T cells (Figure 5.1.), and stimulation with $VEGF_{165}a$ can induce further VEGFR2 dimerization, as previously reported (Basagiannis and Christoforidis, 2016; Jopling et al., 2011). $VEGF_{165}a$-induced VEGFR2 dimerization showed a pEC_{50} = 9.40 ± 0.28 (n=4), which is similar to the binding affinity of $VEGF_{165}a$ at Nluc-VEGFR2 determined from NanoBRET competition binding assay, pKi = 10.17 ± 0.09, n=7 (Table 4.6., Chapter 4).

NanoBRET assay to investigate VEGFR2-GPCR oligomerisation revealed that VEGFR2 can form oligomeric complexes with the adenosine A_{2A} receptor and β_2-adrenernoceptor (Figure 5.4.). In contrast, and therefore used as negative controls, no association between VEGFR2 and the adenosine A_1 and A_3

receptors was observed. NanoBRET data for VEGFR2-A_1AR and VEGFR2-A_3R pairs resulted in a linear increase in BRET ratios, consistent with non-specific interactions caused by bystander BRET (Borroto-Escuela et al., 2013b). All the adenosine subtypes used in this study, as well as β_2-adrenoceptors showed to form homodimers, as previously reported (Canals et al., 2004; Gracia et al., 2013; May et al., 2011; Wnorowski and Jozwiak, 2014). One caveat of this technique, is that it cannot distinguish between homodimers from higher-order oligomers (Calebiro and Sungkaworn, 2017). Therefore, it is possible that some of these interactions may result from higher-order oligomeric structures, which have been previously reported for adenosine A_{2A} receptors (Vidi et al., 2008) and β_2-adrenoceptors (Calebiro et al., 2013). Due to the propensity for VEGFR2 and GPCRs to form homodimers, it is possible that these receptors interact as higher-order oligomeric complexes that may have an impact in downstream signalling regulation (Petersen et al., 2017; Thomsen et al., 2016).

All these three receptors, VEGFR2, A_{2A}AR and β_2AR, are expressed in endothelial cells, and are active participants in the formation of novel vessels from pre-existing ones (angiogenesis) (Desai et al., 2005; Ferrara, 2009; Park et al., 2011). Blocking the VEGFa-VEGFR2 signalling axis has been widely used in the treatment of several cancer types (Shibuya, 2014). Adenosine A_{2A}R signalling is involved in hypoxia-induced angiogenesis and in the increase in VEGFa-expression (Desai et al., 2005; Hatfield and Sitkovsky, 2016). β_2-adrenoceptor-mediated signalling has shown to play a role in chronic-stress induced metastasis in breast cancer (Chang et al., 2016; Sloan et al., 2010) as well as in tumour angiogenesis in prostate cancer (Hulsurkar et al., 2017). However, the molecular mechanisms behind β_2AR and A_{2A}AR activation and angiogenesis are poorly understood.

This study demonstrated a possible novel mechanism by which β_2AR and VEGFR2 can form oligomeric complexes. Agonist co-treatment showed to increase β_2AR-VEGFR2 complex association, measured by NanoBRET, and to induce receptors co-internalisation to intracellular compartments. Agonist stimulation of β_2AR can result in the phosphorylation of the receptor

intracellular C-terminus by G protein receptor kinases (GRKs) that lead to a rapid recruitment of β-arrestin-2 to the phosphorylated β_2AR (Smith and Rajagopal, 2016). β-arrestin-2 forms a transient complex with GRK-phosphorylated β_2AR, and rapidly dissociates from the receptor for its rapid recycling back to the plasma membrane (Smith and Rajagopal, 2016). On the other hand, 'class B' or slow recyclying GPCRs, such as vasopressin type 2 receptor (V_2R), can form stable interactions with β-arrestin-2 in endocytic compartments, that lead to a sustained signalling response from these endocytic compartments (Cahill et al., 2017; Smith and Rajagopal, 2016). Our study showed that in the presence of active-VEGFR2, β_2AR forms a more sustained interaction with β-arrestin-2, which may have implications in signalling from endosomes (Cahill et al., 2017; Smith and Rajagopal, 2016; Thomsen et al., 2016). Agonist-induced β_2-adrenergic receptor internalisation and endocytosis occurs mainly via a clathrin and dynamin-dependent mechanism (Smith and Rajagopal, 2016). Therefore, it would be interesting to investigate whether clathrin or dynamin inhibitors could prevent ligand-induced increase in VEGFR2-β_2AR association.

Some studies have reported that GPCR-induced RTK transactivation can induce a differential signalling and activation of extracellular signal-regulated kinases 1 and 2 (ERK1/2) (Bergelin et al., 2010; Borroto-Escuela et al., 2012; El-Shewy et al., 2006). It would be important to investigate ERK1/2 activation profile, using ERK1/2 biosensors, to investigate the possible role of VEGFR2-β_2AR oligomerisation in promoting ERK1/2 signalling from endosomes (Halls et al., 2016).

It was also demonstrated that VEGFR2 can form oligomeric complexes with the A_{2A}A receptor. However, due to the high degree of constitutive internalisation, it was unclear whether VEGFR2 A_{2A}A receptors can also co-internalise upon CGS21680 or $VEGF_{165}$a stimulation. Further functional studies, including β-arrestin-2 and Gs-protein recruitment assays should be used to investigate functional impact of VEGFR2-A_{2A}A complexes in downstream signalling.

Chapter 6: Visualising ligand-binding to β_2-adrenergic receptor *in vivo* using NanoBRET.

6.1. Introduction

Signalling promoted via β_2-adrenoceptors (β_2AR) has been intimately implicated in cancer progression and metastasis (Chang et al., 2016; Mulcrone et al., 2017; Sloan et al., 2010; Thaker et al., 2006). Activation of this signalling axis can promote different processes involved in tumour progression and invasion including, angiogenesis, inflammation, cell motility and epithelial–mesenchymal transition (Chang et al., 2016; Creed et al., 2015; Madden et al., 2011; Sloan et al., 2010; Tang et al., 2013). Activation of β_2-adrenoceptors by induced chronic-stress, or via pharmacological activation using selective and non-selective agonists, has also been involved in the progression of other vascularised-cancer types including prostate, pancreatic and ovarian cancers (Braadland et al., 2015; Chang et al., 2016; Hulsurkar et al., 2017). In a mouse model of breast cancer, chronic stress-induced release of adrenaline and noradrenaline from sympathetic nerve endings, which are the endogenous agonists for β_2-adrenoceptors, can switch cancer cells to a more invasive and metastatic phenotype, which can be prevented by propranolol treatment (Chang et al., 2016; Creed et al., 2015; Sloan et al., 2010). Treatment with β-adrenoceptor antagonists also showed to abrogate stress-induced tumour progression and metastasis in mouse models of prostate cancer, malignant melanoma and leukaemia (Inbar et al., 2011; Moretti et al., 2013; Palm et al., 2006). However, in all cancer types treatment with β-blockers had no effect on primary tumour growth *in vivo,* or tumour cell proliferation *in vitro* (Chang et al., 2016; Palm et al., 2006; Sloan et al., 2010). On the other hand, β_2-adrenergic agonists, in the absence of induced-stress, were found to accelerate tumour progression and metastasis (Palm et al., 2006; Sloan et al., 2010; Thaker et al., 2006).

Tumours initiate angiogenesis to form a vascular network that provides a source of oxygen and nutrients for the sustained and rapid growth of tumours (Hanahan and Weinberg, 2011). The vascular network created by solid tumours is leaky and disorganised, which results in insufficient and spatially heterogenous drug delivery, particularly to hypoxic regions including the centre of the tumour (Yonucu et al., 2017). The insufficient and heterogenous drug delivery can result in lack of drug efficacy (Durham and Blanco, 2015).

Clinical drug efficacy depends on multiple factors that should be considered in earlier pre-clinical testing (Durham and Blanco, 2015). Three of the factors that should be considered are: 1) sufficient exposure of drug to the target of interest and in the local of action, 2) evidence of specific target-engagement, and 3) generation of a physiological response, as a consequence of that specific drug-target interaction (Durham and Blanco, 2015). Sensitive methodologies to investigate the relationship between target occupancy by drugs and local concentration *in vivo*, are still lacking (Robers et al., 2015; Simon et al., 2013).

NanoBRET methodology has demonstrated great sensitivity in detecting specific drug-target engagement in whole-living cells (Kilpatrick et al., 2017; Soave et al., 2016; Stoddart et al., 2015a). The aim of this study was to investigate whether this methodology could be applied to monitor β-blocker engagement to the β_2-AR *in vivo*, using a mouse model of breast cancer available at Monash University (Sloan et al., 2010).

Chapter 4 described the successful use of NanoBRET methodology to measure ligand-β_2AR binding kinetics in a highly metastatic breast cancer cell line (MDA-231), that was transfected to stably overexpressed Nluc-β_2AR. Chapter 4 also described experiments that demonstrated the sensitivity and spectral resolution of the whole-animal bioluminescence imaging system, IVIS Lumina II, to detect and measure ligand-receptor binding *in vitro* by NanoBRET. The *in vitro* characterisation of the cancer cell line (Chapter 4) and the *in vivo* study were conducted at Monash University, under the supervision of Dr. Erica Sloan. Where noted, parts of the experiments presented in this chapter were

performed by Dr. Alexandra Ziegler, a postdoctoral fellow from Dr. Erica Sloan's lab.

6.2. Brief materials and methods

Cell culture

Human triple negative (or highly metastatic, HM) breast cancer cells, MDA-MB-231^{HM}, were stably transfected to express human full-length β_2-adrenoceptors (β_2AR) N-terminally tagged with NanoLuc luciferase (MDA-231 Nluc-β_2AR). Transfection of this cell line was performed using a lentiviral construct (pSIN-Nluc-β_2AR). See Chapter 2, sections 2.2. and 2.3. for further details about transfection and cell culture.

Breast cancer *in vivo* model

$5x10^5$ MDA-231 Nluc-β_2AR cancer cells were implanted into the bottom left mammary fat pad of female Balb/c nu/nu mice (7-week-old), see Chapter 2 section 2.7. for further details about the *in vivo* model. These mice have a genetic mutation that causes the deterioration or absence of the thymus, resulting in significantly reduced number of T cells and consequent impairment of an adaptive immune system (Mecklenburg et al., 2001). Since MDA-231 are human cancer cells, these can be administered without being rejected in this mouse strain.

All in vivo procedures were carried out at Monash Institute of Pharmaceutical Sciences according to protocols approved (MIPS.2012.11) by the Monash University Animal Ethics Committee and according to NHMRC guidelines.

Whole-animal Bioluminescence Imaging using IVIS Lumina II system and NanoBRET

The whole-animal bioluminescence imaging system (IVIS Lumina II) was used to monitor tumour and metastasis development over time for 35 days in mice bearing MDA-231 Nluc-β_2AR. Primary tumour development was measured by

capturing images of the whole animal, using an open channel and 30 sec exposure, with the IVIS Lumina II camera system. Whereas, metastasis development was measured only in the thorax region, after covering the primary tumour with a black box to avoid light contamination from the primary tumour (imaged using open channel and 2 min exposure time). Furimazine substrate was administered via tail-vein (i.v., *circa* 3.7 mg/kg) injection 5 min before imaging. Further details are provided in Chapter 2, section 2.7.1.

This system was also used to monitor ligand-β_2AR engagement using NanoBRET. For these experiments, mice with established tumours (size >200mm^3) were used. To monitor ligand-β_2AR engagement by BRET, mice were imaged by capturing sequential luminescence (open channel, 30 sec exposure) and fluorescence (CY5.5 channel, using a 660/20nm bandpass, and 5 min exposure time) images. Further details about NanoBRET-based experiments and data analysis are provided in Chapter 2 sections 2.7.2. and 2.7.3., respectively.

6.3. Results

Monitoring tumour growth and metastasis development by tracking Nluc-β_2AR in a breast cancer xenograft mouse model.

For this study, $5x10^5$ MDA-231 Nluc-β_2AR cells (20µL in PBS) were injected into the fourth bottom left mammary fat pad of female BALB/c immunocompromised (nu/nu) mice.

Previous work by our lab at Monash University has reported the involvement of β_2-adrenoceptor signalling in promoting metastasis induced by chronic stress using the same mouse model (Sloan et al., 2010). In those studies MDA-231 tumour cells, that stably expressed cytosolic firefly luciferase, were used to monitor tumour growth and metastasis development (Chang et al., 2016; Sloan et al., 2010). Other studies have used tumour cells expressing cytosolic NanoLuc luciferase to monitor cancer progression in living mice (Stacer et al., 2013). In contrast to those studies that non-specifically monitored tumour cells, here MDA-231 cells overexpressing β_2-adrenoceptor tagged at the N-terminus with NanoLuc luciferase (MDA-231 Nluc-β_2AR) were used. Since this genetically-modified receptor is only present on tumour cells these can be monitored to measure tumour development by bioluminescence imaging (BLI).

Mice injected in the mammary fat pad with MDA-231 Nluc-β_2AR cells showed a significant increase in fat pad-localised luminescence intensity (measured as photons/sec) from day 8 after tumour cell injection (Figure 6.1.a). Tumour growth, measured as luminescence intensity, correlated with tumour growth measured with a conventional calliper (measured as mm^3, Pearson correlation: $p>0.0001$, $R^2=0.499$; Figure 6.1.a).

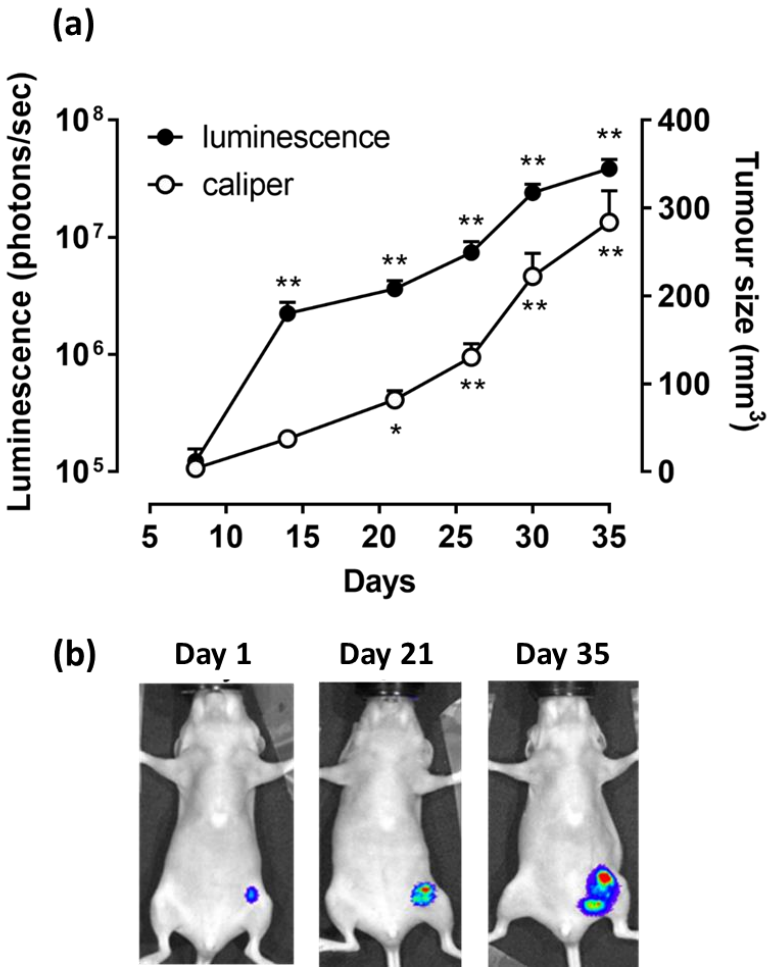

Figure 6.1. Using whole-animal bioluminescence imaging (BLI) to track and monitor primary tumour development of Nluc-β_2AR overexpressed in MDA-231 tumour cells. Female Balb/c nu/nu mice (7-week-old) were injected in the fourth bottom left mammary fat pad with $5x10^5$ MDA-231 cells stably expressing Nluc-β_2AR. **(a)** Tumour development was measured using bioluminescence images (open channel, 30 sec exposure time; measured as photons/sec, left y-axis), or by conventional caliper measurements (mm^3, right y axis), measured over different days after tumour cell injection. These are combined data from 11 different mice expressed as mean ± SEM. *P<0.005 or ** p < 0.0001 (Two-Way ANOVA with Tukey's multiple comparisons with respect to Day 8 baseline). For luminescence measurements, the statistical analysis was applied to the log transformed values. **(b)** Representative images of tumour growth over time.

MDA-231 cells can disseminate to secondary organs including lymph nodes and lungs, where they form metastasis (Chang et al., 2016; Sloan et al., 2010). These studies showed that β_2-adrenoceptor activation can drive invasion of tumour cells into secondary sites (Creed et al., 2015). Therefore, to investigate whether MDA-231 overexpressing Nluc-β_2AR retain the capacity to invade and colonise

secondary sites (metastasis) in lungs and/or lymph nodes, mice transplanted with MDA-231 Nluc-β_2AR cells were imaged over time in the thorax region. Metastasis in lungs and/or axillary lymph nodes were detected at later stages of tumour development, which started to appear 26 days after tumour cell injection (Figure 6.2.). These data showed the capacity of β_2AR-overexpressing MDA-231 cancer cells to invade secondary sites, as well as the successful use of NanoLuc luciferase to track a specific receptor in deeper tissues (lungs).

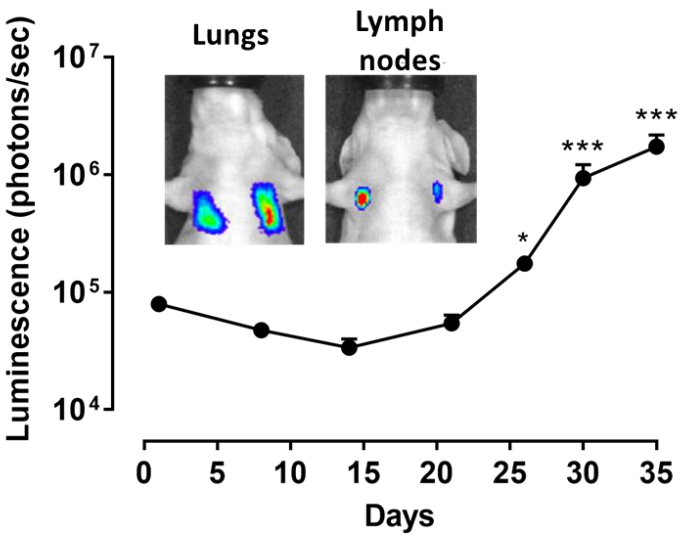

Figure 6.2. Using whole-animal bioluminescence imaging to track Nluc-β_2AR MDA-231 in secondary sites. The same mice were also imaged in the thorax region using bioluminescence imaging (open channel, 2 min exposure time; photons/sec) to monitor metastasis appearance and development over time. Inset: Representative images of mice thorax region displaying metastasis in lungs or axillary lymph nodes. These are combined data from 11 different mice expressed as mean ± SEM. *P<0.05 or *** p < 0.0001 (Two-Way ANOVA with Tukey's multiple comparisons with respect to Day 8 baseline). For luminescence measurements, the statistical analysis was applied to the log transformed values.

Using NanoBRET to monitor and quantify drug-β_2AR engagement in living animals

Previous evidence showed that Nluc-β_2AR expressed in MDA-231 could be visualised in the primary tumour region (Figure 6.1.). In Chapter 4, it was established that NanoBRET can be used to monitor ligand-receptor engagement *in vitro* in MDA-231 Nluc-β_2AR cells, and ligand-receptor binding

kinetics could be quantified using the whole-animal bioluminescence imaging system (IVIS Lumina II camera system). The next step was to investigate whether NanoBRET could be applied to monitor the engagement of propranolol fluorescent ligand derivative, propranolol-β-ala-β-ala--X-BY630/650 (propranolol-BY630/650) to Nluc-β_2AR present in the primary tumour of living mice.

As an attempt to monitor ligand-receptor association *in vivo*, 0.1 mg/kg propranolol-BY630/650 were administered directly into the primary tumour (i.t. injection) of 5 animals with established primary tumours (>200mm^3). After ligand administration, mice were administered with furimazine substrate (*circa* 3.7 mg/kg) via tail-vein injection and imaged for 51 min by capturing sequential luminescence (donor) and fluorescence (acceptor) images every 6 min, using the IVIS camera system (Figure 6.3.). The administration route chosen for the fluorescent ligand was by direct injection into the primary tumour (i.t.) because previous administration of 5 mg/kg propranolol-BY630/650 via tail-vein injection, could not be detected in the primary tumour region by NanoBRET imaging. This is likely to be due to the highly lipophilic properties of this fluorescent ligand and/or due to cleavage by proteases of the dipeptide linker connecting the pharamacophore with fluorophore moieties.

To investigate the degree of specific binding, 4 different animals were administered with the β_2AR-selective antagonist ICI 118551 (0.3 mg/kg, i.t. injection), 45 min before fluorescent ligand administration. Animals injected with fluorescent ligand alone showed a rapid increase in BRET signal, that reached a peak at around 15 min after ligand administration and persisted for the time-course measured (51 min, Figure 6.3., closed circles). On the other hand, animals pre-administered with ICI 118551 did not show an increase in BRET signal, basal BRET levels were observed throughout the time-course measured (Figure 6.3., open circles). These data show that binding of propranolol-BY630/650 to Nluc-β_2AR can be detected using NanoBRET in the primary tumour region. Moreover, administration of a higher dose of the unlabelled competitive antagonist, ICI 118551, resulted in full competition of

propranolol-BY630/650 binding to Nluc-β_2AR, indicating that propranolol-BY630/650 is binding specifically to Nluc-β_2AR overexpressed in the primary tumour.

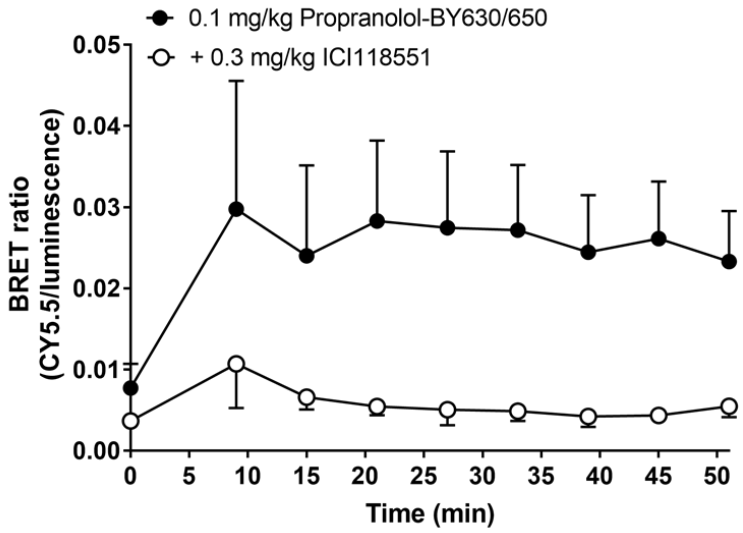

Figure 6.3. NanoBRET was used to investigate real-time association binding of propranolol-BY630/650 to Nluc-β_2AR *in vivo*. Mice bearing MDA-231 Nluc-β_2AR primary tumours (tumour size >200mm^3) were injected directly into the primary tumour (i.t. injection) with 0.1 mg/kg propranolol-BY630/650 alone (n=5 mice, 50µL in PBS), or pre-injected 45 min earlier with 0.3 mg/kg of β_2AR-selective antagonist ICI 118551 (i.t., n=4 mice, 50µL in PBS). Immediately after fluorescent ligand injection, furimazine was injected via the tail-vein (i.v.) and sequential luminescence (30 sec exposure time; open channel, donor emission) and fluorescence (5 min exposure time; Cy5.5 channel with 660/20nm bandpass filter, acceptor emission) images were captured for 51 min. ROIs were positioned on the primary tumour region to measure donor and acceptor intensities (photons/sec), and BRET ratio was calculated as acceptor/donor ratios.

Monitoring propranolol-BY630/650 dissociation/clearance from Nluc-β_2AR over time using NanoBRET

Fluorescent ligand dissociation/clearance was monitored over time after propranolol-BY630/650 injection (i.t.). Two different concentrations of fluorescent ligand (0.1 and 0.01 mg/kg) could be detected up to 72h after administration (Figure 6.4.). Propranolol-BY630/650 showed slow dissociation *in vitro* in isolated cells, with a residence time of ~40 min (Chapter 4, Table 4.9.),

which could explain the extremely slow dissociation observed *in vivo*. However, these tumours are also highly vascularised by a disorganised network of vessels that could result in the fluorescent ligand getting trapped and re-binding to available receptors until being cleared from the primary tumour region.

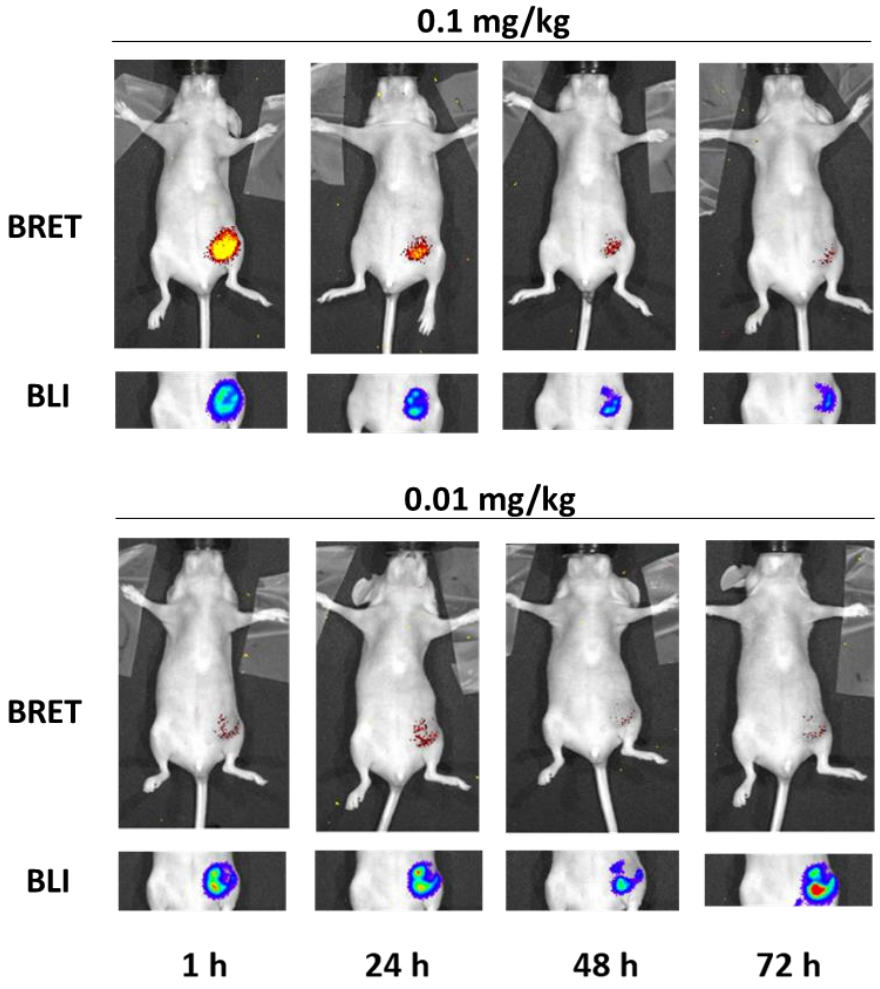

Figure 6.4. *In vivo* imaging of fluorescent ligand dissociation over time for two different doses of propranolol-BY630/650. 0.1 or 0.01 mg/kg of propranolol-BY630/650 (50µL in PBS) were administered directly into the primary tumour (i.t. injection) of two different mice. Sequential luminescence (30 sec exposure time, open channel) and fluorescence (5 min exposure time, Cy5.5 channel) images were taken at 1, 24, 48 or 72h administration of fluorescent ligand, and 5 min after furimazine i.v. injection. Upper panels display BRET signal (Cy5.5 channel, acceptor) and lower panels show bioluminescence imaging (BLI) (open channel, donor). These are representative images of a single qualitative experiment using two different mice.

In a different experiment performed by Dr. Alexandra Ziegler at Monash University after I had returned to Nottingham, these experiments were

repeated with more animals, and using an intermediate concentration of 0.03 mg/kg propranolol-BY630/650 (Figure 6.5.). BRET data confirmed maximal binding at 1h after i.t. injection of propranolol-BY630/650, which persisted for 24h followed by a slow decrease in BRET signal at 48 and 72h. These data confirm the slow dissociation rate and/or clearance of propranolol-BY630/650 from the primary tumour for all concentrations used.

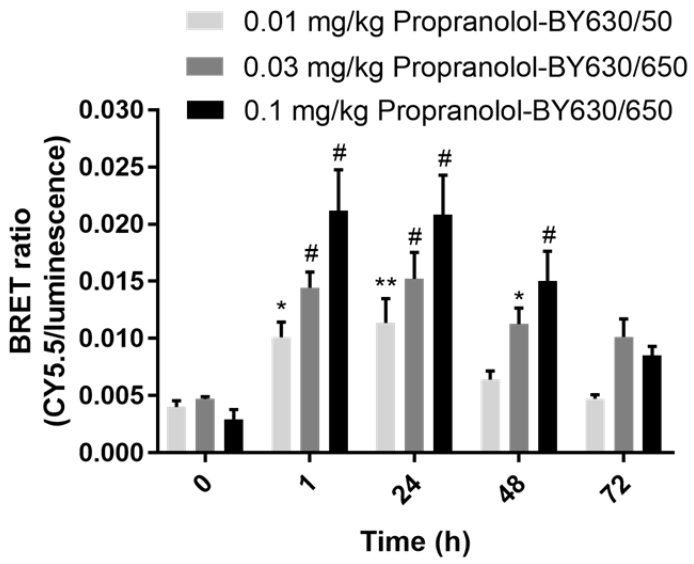

Figure 6.5. NanoBRET measurements of fluorescent ligand dissociation/clearance using three different concentrations of Propranolol-BY630/650 (0.01, 0.03 and 0.1 mg/kg). Different mice with tumour <200mm^3 were administered with three different concentrations of fluorescent ligand. Sequential luminescence (open channel, 30 sec exposure time) and fluorescence (CY5.5 channel, 5 min exposure time) were taken at 1, 24, 48 and 72h after fluorescent ligand administration (i.t.). Time 0h was taken 24h before administration of fluorescent ligand, corresponding to basal BRET levels. Furimazine substrate was administered (i.v.) 5 min before imaging. Data are expressed as mean ± SEM using 6 animals per concentration of fluorescent ligand. *p<0.05. **p<0.01 or # p<0.001 compared to corresponding time zero controls, using Two-way ANOVA with repeated measures and Dunnett multiple comparisons.

Investigation of β-blocker engagement to β_2AR *in vivo* using the propranolol-BY630/650 as a fluorescent tracer.

Having used NanoBRET imaging to monitor and measure specific fluorescent ligand binding to Nluc-β_2AR in the primary tumour of living mice, the next step was to investigate whether propranolol-BY630/650 ligand could be used as a tracer to monitor binding of unlabelled β-blockers to Nluc-β_2AR. Two different β-blockers were used, the β_2AR-selective antagonist ICI 118551 and the β_1AR-selective antagonist CGP20712A. Treatment procedure was performed using a cross-over design using two animal groups: group 1 (3 animals) received an injection of propranolol-BY630/650 on its own (i.t., 0.1 mg/kg), whereas group 2 (3 animals) received injection of ICI 118551 (i.t., 0.3 mg/kg) 45 min prior administration of propranolol-BY630/650 (Figure 6.6.a). After washout of the fluorescent ligand was confirmed (when BRET signal was at basal levels), the treatment was reversed in each mouse (for detailed experimental design see chapter 2, section 2.7.2.).

As previously shown in association binding data, BRET measurements taken from mice injected with propranolol-BY630/650 alone (i.t., 0.1 mg/kg) showed an increase in BRET signal 1h after fluorescent ligand injection (Figure 6.6.a). On the other hand, administration of ICI 118551 (i.t. injection at 0.3 mg/kg) prior to propranolol-BY630, resulted in a significant decrease in BRET signal, nearly to basal levels (Figure 6.6. a and b). These data, as well as binding association data displayed in Figure 6.3., show that propranolol-BY630/650 can be used as a probe to monitor the binding of unlabelled drugs administered i.t. at Nluc-β_2AR, measured by NanoBRET. Moreover, once again it confirms the binding specificity of propranolol-BY630/650 at Nluc-β_2AR expressed in the primary tumour.

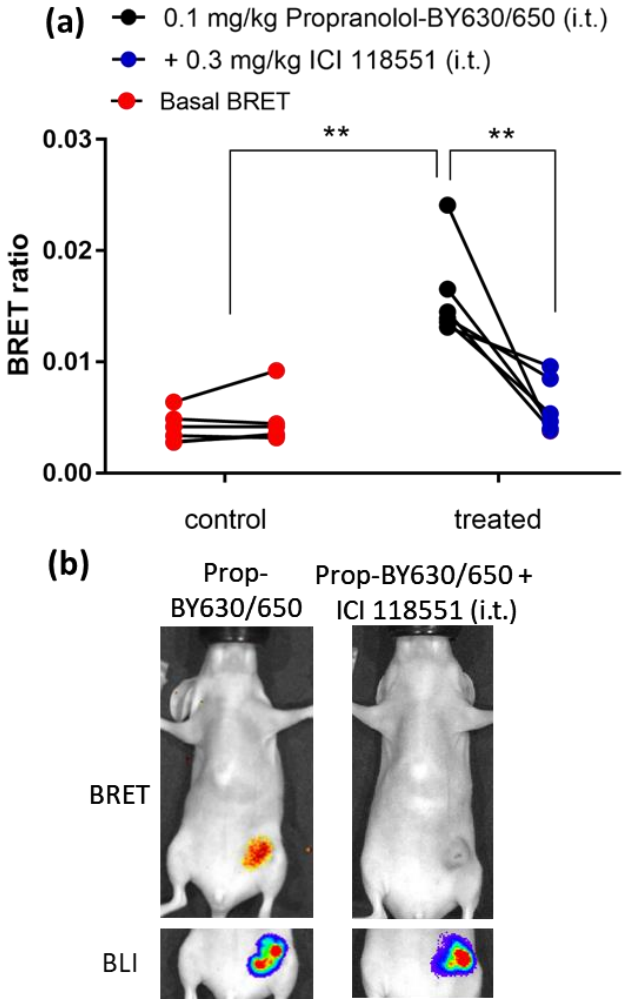

Figure 6.6. Binding of β_2AR-selective antagonist ICI 118551 administered directly into the primary tumour (i.t.), using 0.1 mg/kg propranolol-BY630/650 fluorescent tracer. For these experiments mice were separated into 2 groups: group 1 (3 animals) were administered with 0.1 mg/kg fluorescent ligand (i.t.) alone, whereas mice from group 2 (3 animals) were administered (i.t.) with 0.3 mg/kg ICI 118551, 45 min prior to fluorescent ligand i.t. injection. Once fluorescent ligand was no longer detected in these mice, treatment was reversed. BRET measurements were performed as previously described, 1h after fluorescent ligand injection. Furimazine substrate was injected i.v. 5 min before imaging. Control measurements (red-filled circles) represent BRET basal levels, that were taken 24h prior ligand administration and 5 min after furimazine i.v. injection . Data are displayed as individual BRET ratios for 6 mice with

reversed treatment (connected lines). ** p<0.001 using Two-way ANOVA with Tukey's multiple comparison test. **(b)** Representative images of mice administered (i.t.) with propranolol-BY630/650 alone or pre-administered (i.t.) with 0.3mg/kg ICI 118551, with upper panel displaying BRET (CY5.5 channel, 5 min exposure time) and bottom images displaying bioluminescence (BLI; open channel, 30 sec exposure time).

Administration of a high dose of ICI 118551 ligand via tail vein injection (i.v., 10 mg/kg), 45 min prior administration of fluorescent tracer (0.3 mg/kg, i.t.), also resulted in a significant decrease in BRET signal to nearly basal levels, using the same reversed treatment protocol (Figure 6.7.a). On the other hand, a lower dose of 1 mg/kg ICI 118551 injected also i.v., resulted in a significant decrease in BRET signal for half of the animals (Figure 6.7.b). Notably, this dose of ICI 118551 reduced BRET signal to near basal levels only in mice with smaller tumours (<600mm^3, Figure 6.7.b closed blue circles). In animals with bigger tumour size (>800mm^3, Figure 6.7.b open blue circles) no decrease in BRET was observed. These resultsindicate that in bigger size tumours, 1 mg/kg ICI 118551 i.v. dose may not be sufficient to occupy all the available β_2AR receptors. Another viable explanation is the low level of drug access into bigger tumours which are surrounded by a more complex and disorganised vascular network.

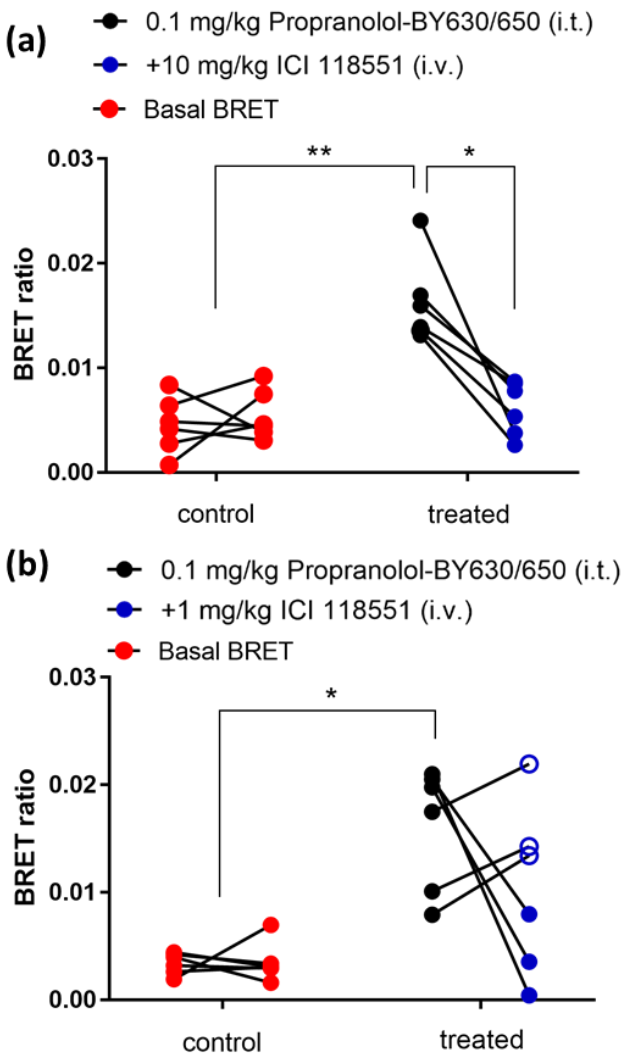

Figure 6.7. Monitoring the engagement of two doses of ICI 118551, administered via tail-vein (i.v.) injection, to Nluc-β_2AR present in primary tumour, using propranolol-BY630/650 as fluorescent tracer. These were performed as mentioned in previous figure, using a reversed treatment design. **(a)** Administration of 0.1 mg/kg propranolol-BY630 (i.t.) alone or pre-administration of 10 mg/kg ICI 118551 (i.v., 100µL in PBS), 45 min prior to fluorescent ligand injection. **(b)** Administration of 0.1 mg/kg ropranolol-BY630 (i.t.) alone or pre-administration of 1 mg/kg ICI 118551 (i.v., 100µL in PBS), 45 min prior to fluorescent ligand injection. Control was measured 24h before ligands injection and 5min after furimazine i.v. injection (basal BRET ratios, red-filled circles). BRET measurements were performed as previously described, 1h after fluorescent ligand injection. Open circles correspond to animals with bigger tumour size (>800mm^3). Data are expressed as individual raw BRET ratios from 6 mice with reverted treatment (connected lines). ** $p<0.001$, * $p<0.01$ using Two-way ANOVA with Tukey's multiple comparison test.

Intravenous administration of a high dose (10 mg/kg) of a selective β_1-adrenoceptor antagonist, CGP20712A, 45min prior to propranolol-BY630/650 i.t. injection did not affect the BRET ratio (Figure 6.8.). These data suggest that this ligand does not bind to Nluc-β_2AR, showing that at the tested concentration (10 mg/kg) this ligand retains its binding selectivity at β_1-adrenoceptors.

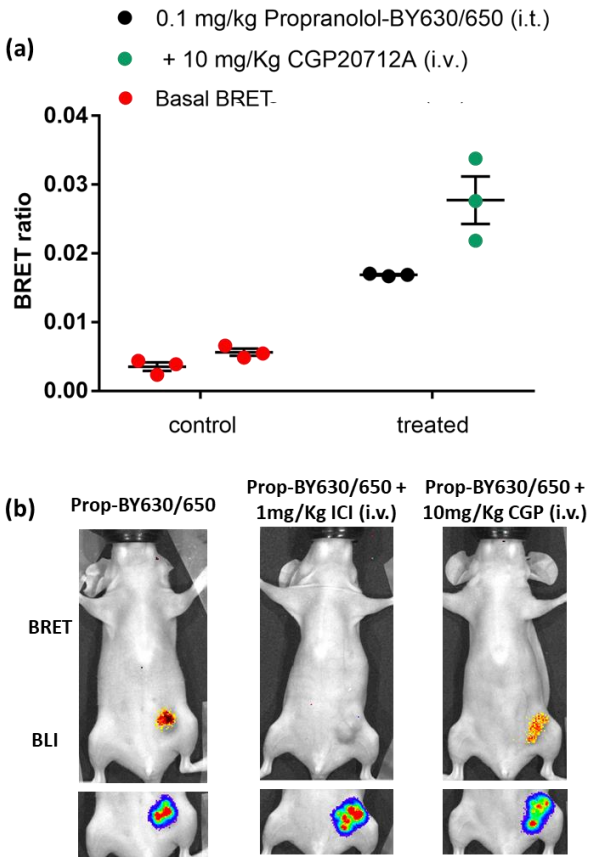

Figure 6.8. Effect of a selective β_1-adrenoceptor antagonist on propranolol-BY630/650 binding to Nluc-β_2AR-expressing tumours *in vivo*. (a) Mice bearing MDA-231 overexpressing Nluc-β_2AR (tumour size >200mm^3) were administered with propranolol-BY630/650 alone (i.t., 0.1 mg/kg) or 45 min after administration of a β_1-selective antagonist CGP20712A (i.v., 10 mg/kg). BRET images were acquired as mentioned previously, 1h after administration of the fluorescent ligand. Images were also acquired 24h prior administration of any ligand for baseline BRET ratio measurements (control). Furimazine substrate was administered i.v. 5 min before imaging. Data are displayed as mean of BRET ratios obtained for 3 animals. **(b)** Representative images of mice receiving the different treatments with upper panel displaying

BRET (acceptor, 5 min exposure time) and bottom images displaying bioluminescence (BLI; acceptor, 30 sec exposure time).

6.4. Discussion and Conclusion

The pharmacological inhibition of β_2-adrenoceptor (β_2AR) signalling represents a potential therapeutic target for the treatment of breast cancer, particularly for the triple-negative variant as these tumours express high levels of β_2AR, and have limited other treatment options (Cole and Sood, 2012; Pasquier et al., 2011; Sloan et al., 2010). Here is reported the novel application of NanoBRET to monitor and measure β-blockers engagement to β_2AR in triple-negative breast cancer tumours of living mice. For this approach, the fluorescently-labelled propranolol analogue (propranolol-β-Ala-β-Ala-X-BODIPY-630/650, propranolol-BY630/650) was used as fluorescent tracer (Soave et al., 2016; Stoddart et al., 2015a), administered locally in the primary tumour.

In vitro characterisation described in Chapter 4, showed that propranolol-BY630/650 has a relatively fast association (k_{on}) and a slow dissociation (k_{off}) rates, with a residence time of ~40 min. *In vivo* studies presented in this chapter showed a fast association of the ligand, with a maximal binding at ~15min (Figure 6.2.), and very slow dissociation and/or clearance of the fluorescent ligand, which could still be detected 72h after administration into the primary tumour (Figure 6.3.). Administration of high doses of the selective β_2AR antagonist ICI 118551, locally in the primary tumour, or via tail-vein injection, resulted in near complete inhibition of propranolol-BY630/650 binding to Nluc-β_2AR, demonstrating binding specificity of the fluorescent ligand at Nluc-β_2AR. A lower dose of ICI 118551 resulted in a significant decrease in fluorescent ligand binding to Nluc-β_2AR in smaller size tumours. In tumours with increased size, this dose of ICI 118551 was not able to displace fluorescent ligand binding, which could be due an increase in receptor density and/or due to an increase in surrounding vascular network that can difficult drug access to tumour cells (Durham and Blanco, 2015; Yonucu et al., 2017). A lack of binding was observed

for the selective β_1AR antagonist, CGP 20712A, suggesting that this compound is selective for β_1AR at a high dose of 10 mg/kg administered i.v., and does not bind to β_2AR.

In this study was also demonstrated the successful use of NanoLuc luciferase to track specifically Nluc-β_2AR expressed in MDA-231 tumour, and to monitor tumour and metastasis development. Metastasis were observed in axillary lymph nodes and in deeper tissues (lungs), at later staged of cancer progression. Notably, MDA-231 cells overexpressing β_2AR have the capacity to invade secondary sites and form metastasis in lungs and/or axillary lymph nodes and would, therefore, be sensitive to treatments using β-blockers.

NanoBRET has been successfully used *in vitro* to rank binding affinities and selectivity for different ligands in whole living cells (Soave et al., 2016; Stoddart et al., 2015a). In this study is reported the successful use of this methodology to monitor and quantify specific drug-target engagement using a pre-clinical model of breast cancer. This methodology has potential to be introduced to the pipeline of drug development, screening and pre-clinical testing. Because NanoBRET is a proximity-based technique that only measures specific ligand-target interaction (at a distance <10nm), it offers greater potential for the measurement of specific drug-target engagement compared to other already available whole-animal imaging techniques that use radioligand tracers, such as Positron Emission Tomography (PET) (Hazari et al., 2017), or fluorescent ligand tracers, such as Fluorescence Emission Computed Tomography (FLECT) flect (Lim et al., 2017).

NanoBRET could also be applied to other *in vivo* models without the need for cell transplantation, with the use of transgenic mice and CRISPR/Cas9 gene-editing to genetically label endogenous target of interest with NanoLuc-luciferase (White et al., 2017). However, as any newly developed technique, this methodology has margin for improvement. For instance, the design and development of better fluorescent tracers with a more water-soluble core, and resistance to protease cleavage and acidic/basic conditions, would enable

intravenous (i.v.) and/or intraperitoneal (i.p.) administration. I.v. or i.p. administration may allow monitoring drug-target engagement at metastatic sites. Moreover, the development of red-shifted NanoLuc substrates should also improve the resonance energy transfer efficiency to far-red fluorescent tracers, which light is less absorbed by tissues.

Overall, this chapter reported the successful use of NanoLuc to specifically track a GPCR in both superficial and deeper tissues of living mice. Most importantly, this study showed the first-time application of NanoBRET methodology to perform real-time read-outs of receptor occupancy and binding selectivity at the tumour site of living animals.

Chapter 7: General Discussion

This study demonstrated the novel application of NanoBRET technology to monitor ligand-receptor interactions in a physiologically relevant system, and to measure direct receptor-receptor interactions in living cells.

Two class A GPCRs, adenosine A_{2A} receptor and β_2-adrenoceptor, which are highly expressed in endothelial cells, have been reported to promote angiogenesis, via a VEGFa-dependent process (Ahmad et al., 2009; Desai et al., 2005; Garg et al., 2017; Lemmens et al., 2017). VEGFa is the key mediator of angiogenesis which exerts its actions by binding and activating its cognate receptor VEGFR2 (Basagiannis et al., 2016; Carter et al., 2015; Peach et al., 2018a).

One of the aims of this study was to investigate cross-talk via receptor oligomerisation between VEGFR2 and adenosine receptor A_{2A} or β_2-adrenoceptors using NanoBRET. These interactions were investigated using a receptor tagged at the N-terminus with NanoLuc luciferase as BRET donor, whereas receptors tagged at the N-terminus with Halo/SNAP-Tag were used as BRET acceptors. NanoBRET-based assays previously established in our lab (Stoddart et al., 2018), were applied in this study for the characterisation of the Nluc-tagged receptors at the level of ligand biding, which displayed similar pharmacological properties to untagged receptors, confirming that these tags do not interfere with receptor function.

Using the novel NanoBRET approach to measure receptor-receptor interactions, it was presented evidence for direct receptor-receptor association between VEGFR2 with the two Gs-coupled receptors, adenosine A_{2A}R and β_2AR, in HEK 293T cells. VEGFR2 did not show to interact with the Gi-coupled adenosine A_1 and A_3 receptors, which were used in this study as negative controls. However, both adenosine A_1 and A_3 receptors, as well as the adenosine A_{2A}R and β_2AR, all showed to form homodimers under non-stimulation conditions, as previously demonstrated by other groups (Briddon et al., 2008; May et al., 2011; Schonenbach et al., 2016; Wnorowski and

Jozwiak, 2014), and used here as positive controls. Given the propensity for these receptors to form homodimers, it is likely that receptor oligomerisation occurs via the formation of higher-order oligomeric structures, which cannot be determined when using NanoBRET alone. Single molecule-based techniques such as total internal reflection fluorescence microscopy (TIRF-M) and fluorescence correlation spectroscopy (FCS), could be applied in future experiments to investigate the oligomeric nature of these interactions in different cellular compartments (Briddon et al., 2018; Calebiro et al., 2013).

Interestingly, co-activation of cells expressing both VEGFR2 and β_2AR, resulted in an increase in receptor-receptor association measured by NanoBRET, and induced receptors co-internalisation into intracellular compartments. This was not as clear for VEGFR2/A_{2A}AR complexes due to their high levels of constitutive internalisation, which have been reported to occur when these receptors are expressed on their own (Basagiannis and Christoforidis, 2016; Mundell and Kelly, 2011).

β-arrestins are key scaffolding proteins involved in GPCR internalisation and endocytosis (Smith and Rajagopal, 2016). These proteins are key players in intracellular signalling promoted from endocytic compartments (Cahill et al., 2017; Ranjan et al., 2017). In this study, a NanoBRET approach was also used to monitor β-arrestin-2-YFP recruitment to isoprenaline-stimulated β_2AR expressing a Nluc-Tag at the intracellular C-terminus (β_2AR-Nluc). β_2AR is known to form a transient complex with β-arrestin-2 (‘class A’ GPCR), which rapidly dissociates from the receptor upon receptor internalisation (Drake et al., 2006; O’Hayre et al., 2017). A transient interaction between β-arrestin-2-YFP and β_2AR-Nluc was observed upon treatment with isoprenaline (peak at 4-6 min followed by a decay over time), which was measured in the presence of unstimulated VEGFR2. Interestingly, co-treatment with isoprenaline and $VEGF_{165}$a agonists resulted in a sustained β-arrestin-2-YFP recruitment to β_2AR-Nluc, which was inhibited in cells pre-treated with the VEGFR2 inhibitor, cediranib. These results suggest that active-VEGFR2 can alter β-arrestin-2 recruitment profile to a more sustained one, which is typically observed for

'class B' receptors, such as vasopressin type 2 receptor (V_2R), which form a sustained complex with β-arrestins to promote intracellular signalling (Thomsen et al., 2016).

A Gs-protein surrogate, nanobody-80 (Nb-80), was previously used in crystallisation studies to stabilise the active β_2AR conformation (Rasmussen et al., 2011a). A version of the Nb-80 tagged with GFP protein (Nb-80-GFP) was used by a different group, who found that β_2AR can be activated in early endosomes to promote signalling (Irannejad et al., 2013). Nb-80-GFP was used in this study to monitor Nb-80-GFP recruitment to isoprenaline-stimulated β_2AR-Nluc, using NanoBRET. This approach was also used to investigate the activation status of β_2AR in the presence of $VEGF_{165}$a-stimulated VEGFR2. Isoprenaline-treatment of cells expressing β_2AR-Nluc alone resulted in a rapid and sustained recruitment of Nb-80-GFP to β_2AR-Nluc (peak at ~5min). Isoprenaline and $VEGF_{165}$a co-treatment of cells co-expressing both β_2AR-Nluc and VEGFR2 did not affect the recruitment of Nb-80-GFP to β_2AR-Nluc (which was measured 30min after co-treatment). Recent structural and functional studies showed evidence that β-arrestin-1-bound to a GPCR chimera (β_2AV_2R) can also bind Gs protein to form a functional super-complex in endosomes (Cahill et al., 2017; Lee et al., 2016; Thomsen et al., 2016). Our findings suggest a novel mechanism in which VEGFR2 can form a complex with β_2AR, and that co-stimulation with agonists can alter the β-arrestin-2 recruitment profile to a more sustained β_2AR/β-arrestin-2 interaction, which may have an impact in intracellular signalling regulation. Further functional studies should be performed to investigate whether theseco-stimulated receptor oligomeric complexes can alter the intracellular signalling profile, compared to receptor complexes stimulated with either isoprenaline or $VEGF_{165}$a. For example, cAMP and ERK1/2 biosensors would be a good option to investigate signalling activation from different cellular compartments, including plasma membrane and endosomes (Halls et al., 2005). Since β_2AR was reported to mediate rapid cAMP and ERK1/2 activation from endosomes localised near the plasma membrane (Irannejad et al., 2013; Lee et al., 2016), it would be interesting to

investigate whether agonist co-stimulated VEGFR2/β_2AR complexes can induce a prolonged activation and/or a later second pool activation of these downstream effectors (Calebiro and Godbole, 2018; Lohse and Calebiro, 2013). Moreover, it would should also be investigated the effect of antagonists and inverse agonists on VEGFR2/β_2AR or VEGFR2/A_{2A}AR complexes. These interactions and functional outcome should also be investigated in a physiologically relevant system including primary endothelial cells and cancer cells. The better understanding of the signalling cascade events that are downstream of the complex formation, as well as, the molecular events that lead to complex formation, may unveil novel and more selective targets for cancer therapy.

This thesis also described the novel application of NanoBRET to monitor specific ligand-β_2AR interaction *in vivo* (Alcobia et al., 2018). These studies were performed at the Monash Institute of Pharmaceutical Sciences (MIPS) at Monash University in Melbourne. The group that I worked with has been using a bioluminescence whole-animal imaging system (IVIS Lumina II camera system) to monitor tumour growth and metastasis development in mice bearing breast cancer tumours expressing a cytosolic firefly luciferase (Chang et al., 2016; Sloan et al., 2010). This *in vivo* model and whole-animal imaging system were ideal to investigate whether NanoBRET could be applied to monitor specific ligand-β_2AR interactions in living animals. Firstly, it was demonstrated that NanoBRET-based *in vitro* assays can be applied to pharmacologically characterise Nluc-β_2AR overexpressed in breast cancer cell lines (the human triple-negative MDA-231, and the low metastatic mouse 66cl4 cell lines). Secondly, it was demonstrated that MDA-231 Nluc-β_2AR cells implanted in the mammary fat pad of mice to develop tumours, can be tracked over time to monitor tumour and metastasis development, using the whole-animal bioluminescence imaging. These findings showed that MDA-231 overexpressing Nluc-β_2AR tumours can invade secondary sites (lungs and axillary lymph nodes). Finally, the *in vivo* study revealed that NanoBRET can be successfully applied to monitor specific binding of a fluorescently-labelled

propranolol analogue, propranolol- BY630/650 (Stoddart et al., 2015a), to Nluc-β_2AR. The specific binding of propranolol-BY630/650 to Nluc-β_2AR was inhibited by pre-injection (intratumoral, i.t., or intravenous, i.v.) of a high dose of the unlabelled β_2AR-selective antagonist ICI 118551, but not by i.v. injection of a high dose of a selective β_1AR antagonist (CGP20712A).

Since NanoBRET measurements only account for specific protein-protein interactions occurring at a distance <10nm, this methodology offers greater potential for the measurement of specific drug-target engagement compared to other already available whole-animal imaging techniques such as PET (which uses radio-labelled probes) (Hazari et al., 2017) and FLECT (which uses fluorescently-labelled probes) (Lim et al., 2017). BRET readouts should not account for probe interaction with endogenous receptors in the same or neighbouring cells, as well as non-specific binding of the probe with membranes and other proteins. This system could potentially be applied to the drug discovery pipeline, as it allows the direct measurement of ligand-target engagement and local concentration (Durham and Blanco, 2015).

NanoBRET may also be applied to monitor protein-protein interaction to endogenous receptors *in vivo*, using CRISPR/Cas9 gene-editing to genetically label endogenous receptors with NanoLuc-luciferase (White et al., 2017).

This *in vivo* NanoBRET methodology could be widely applicable to monitor drug-target engagement in animal models using cell-surface-tagged-receptors, including VEGFR2 and adenosine A_{2A} receptors, and potentially to monitor receptor-receptor or receptor-adaptor protein interactions occurring inside the cell in living animals (Kono et al., 2017; Robers et al., 2015). Moreover, the design and development of better fluorescent tracers with a more water-soluble core and resistance to protease cleavage and acidic/basic conditions, would enable intravenous and/or intraperitoneal administration of these labelled ligands. Another alternative would be the use of nanoparticle-delivery systems to allow systemic administration of fluorescent probes (Chen, 2010).

Overall, this study established the application of NanoBRET to determine receptor-receptor interactions, demonstrating for the first time the formation of oligomeric complexes between VEGFR2 and the two class A GPCRs, adenosine A_{2A} or β_2-adrenergic receptors. This novel mechanism should be investigated further at a functional level to determine the role of VEGFR2-β_2AR-β-arrestin-2 complex in intracellular signalling and biological responses, such as angiogenesis. Finally, it was also demonstrated the novel application of NanoBRET to monitor direct binding of β-blockers to β_2AR *in vivo*, using a pre-clinical model of breast cancer.

References

Abulrob, A., Lu, Z., Baumann, E., Vobornik, D., Taylor, R., Stanimirovic, D., and Johnston, L.J. (2010). Nanoscale imaging of epidermal growth factor receptor clustering: Effects of inhibitors. J. Biol. Chem. *285*, 3145–3156.

Adair, T.H. (2005). Growth regulation of the vascular system: an emerging role for adenosine. Am. J. Physiol. Regul. Integr. Comp. Physiol. *289*, R283–R296.

Ahmad, A., Ahmad, S., Glover, L., Miller, S.M., Shannon, J.M., Guo, X., Franklin, W.A., Bridges, J.P., Schaack, J.B., Colgan, S.P., et al. (2009). Adenosine A2A receptor is a unique angiogenic target of HIF-2alpha in pulmonary endothelial cells. Proc. Natl. Acad. Sci. U. S. A. *106*, 10684–10689.

Alcobia, D.C., Ziegler, A.I., Kondrashov, A., Comeo, E., Mistry, S., Kellam, B., Chang, A., Woolard, J., Hill, S.J., and Sloan, E.K. (2018). Visualising ligand-binding to a GPCR in vivo using nanoBRET. IScience *6*, 280–288.

Alderton, F., Rakhit, S., Kong, K.C., Palmer, T., Sambi, B., Pyne, S., and Pyne, N.J. (2001). Tethering of the platelet-derived growth factor β receptor to G-protein-coupled receptors: A novel platform for integrative signaling by these receptor classes in mammalian cells. J. Biol. Chem. *276*, 28578–28585.

Alexander, S.P., Benson, H.E., Faccenda, E., Pawson, A.J., Sharman, J.L., Spedding, M., Peters, J.A., Harmar, A.J., Collaborators, C., and for correspondence, A. (2013). the concise guide to pharmacology 2013/14: g protein-coupled receptors. Br. J. Pharmacol. *170*, 1459–1581.

Alexander, S.P.H., Christopoulos, A., Davenport, A.P., Kelly, E., Marrion, N. V., Peters, J.A., Faccenda, E., Harding, S.D., Pawson, A.J., Sharman, J.L., et al. (2017). the concise guide to pharmacology 2017/18: g protein-coupled receptors. Br. J. Pharmacol. *174*, S17–S129.

Allard, D., Turcotte, M., and Stagg, J. (2017). Targeting A2 adenosine receptors in cancer. Immunol. Cell Biol. 1–34.

Angers, S., Salahpour, a, Joly, E., Hilairet, S., Chelsky, D., Dennis, M., and Bouvier, M. (2000). Detection of beta 2-adrenergic receptor dimerization in living cells using bioluminescence resonance energy transfer (BRET). Proc. Natl. Acad. Sci. U. S. A. *97*, 3684–3689.

Antonioli, L., Fornai, M., Colucci, R., Ghisu, N., Tuccori, M., Del Tacca, M., and Blandizzi, C. (2008). Regulation of enteric functions by adenosine: Pathophysiological and pharmacological implications. Pharmacol. Ther. *120*, 233–253.

Antonioli, L., Blandizzi, C., Pacher, P., and Haskó, G. (2013). Immunity, inflammation and cancer: a leading role for adenosine. Nat. Rev. Cancer *13*, 842–857.

Antonioli, L., Csóka, B., Fornai, M., Colucci, R., Kókai, E., Blandizzi, C., and Haskó, G. (2014). Adenosine and inflammation: What's new on the horizon? Drug Discov. Today *19*, 1051–1068.

Arruda, M.A., Stoddart, L.A., Gherbi, K., Briddon, S.J., Kellam, B., and Hill, S.J. (2017). A Non-imaging High Throughput Approach to Chemical Library Screening at the Unmodified Adenosine-A3 Receptor in Living Cells. Front. Pharmacol. *8*, 1–13.

Attramadal, H., Arriza, J.L., Aoki, C., Dawson, T.M., Codina, J., Kwatra, M.M., Snyder, S.H., Caron, M.G., and Lefkowitz, R.J. (1992). Beta-arrestin2, a novel member of the arrestin/beta-arrestin gene family. J Biol Chem *267*, 17882–17890.

Auchampach, J. a (2007). Adenosine receptors and angiogenesis. Circ. Res. *101*, 1075–1077.

Baker, J.G. (2003). Influence of Agonist Efficacy and Receptor Phosphorylation on Antagonist Affinity Measurements: Differences between Second Messenger and Reporter Gene Responses. Mol. Pharmacol. *64*, 679–688.

Baker, J.G. (2005). The selectivity of beta-adrenoceptor antagonists at the human beta1, beta2 and beta3 adrenoceptors. Br. J. Pharmacol. *144*, 317–322.

Baker, J.G. (2010). The selectivity of beta-adrenoceptor agonists at human beta1-, beta2- and beta3-adrenoceptors. Br. J. Pharmacol. *160*, 1048–1061.

Baker, J.G., Hall, I.P., and Hill, S.J. (2002). Pharmacological characterization of CGP 12177 at the human β2-adrenoceptor. Br. J. Pharmacol. *137*, 400–408.

Baker, J.G., Hall, I.P., and Hill, S.J. (2003). Pharmacology and direct visualisation of BODIPY-TMR-CGP: a long-acting fluorescent beta2-adrenoceptor agonist. Br. J. Pharmacol. *139*, 232–242.

Balthasar, S., Bergelin, N., Löf, C., Vainio, M., Andersson, S., and Törnquist, K. (2008). Interactions between sphingosine-1-phosphate and vascular endothelial growth factor signalling in ML-1 follicular thyroid carcinoma cells. Endocr. Relat. Cancer *15*, 521–534.

Bang, I., and Choi, H. J. (2015). Structural Features of beta2 Adrenergic Receptor: Crystal Structures and Beyond. Mol. Cells *38*, 105–111.

Barnes, P.J. (2006). Receptor heterodimerization: A new level of cross-talk. J.

Clin. Invest. *116*, 1210–1212.

Barron, T.I., Sharp, L., and Visvanathan, K. (2012). Beta-adrenergic blocking drugs in breast cancer: A perspective review. Ther. Adv. Med. Oncol. *4*, 113–125.

Basagiannis, D., and Christoforidis, S. (2016). Constitutive endocytosis of VEGFR2 protects the receptor against shedding. J. Biol. Chem. *291*, 16892–16903.

Basagiannis, D., Zografou, S., Murphy, C., Fotsis, T., Morbidelli, L., Ziche, M., Bleck, C., Mercer, J., and Christoforidis, S. (2016). VEGF induces signalling and angiogenesis by directing VEGFR2 internalisation via macropinocytosis. J. Cell Sci. jcs.188219.

Bates, D., Beazley-Long, N., Benest, A.V., Ye, X., Ved, N., Hulse, R.P., Barratt, S., Machado, M.J., Donaldson, L.F., Harper, S.J., Peiris-Pages, M., Tortonese, D.J., Oltean, S. and Foster, R.R. (2018). Physiological role of vascular endothelial growth factors as homeostatic regulators. Comprehensive Physiology. *8*, 955-979.

Behera, S.K., Murkherjee, A., Sadhuragiri, G., Elumalai, P., Sathiyendiran, M., Kumar, M., Mandal, B.B., and Krishnamoorthy, G. (2017). Aggregation induced enhanced and exclusively highly Stokes shifted emission from an excited state intramolecular proton transfer exhibiting molecule. Faraday Discuss. *196*, 71–90.

Bergelin, N., Löf, C., Balthasar, S., Kalhori, V., and Törnquist, K. (2010). S1P1 and VEGFR-2 form a signaling complex with extracellularly regulated kinase 1/2 and protein kinase C-alpha regulating ML-1 thyroid carcinoma cell migration. Endocrinology *151*, 2994–3005.

Berger, P., and Ballmer-Hofer, K. (2011). The reception and the party after: How vascular endothelial growth factor receptor 2 explores cytoplasmic space. Swiss Med. Wkly. *141*, 2–9.

Bers, D.M., and Despa, S. (2009). Na/K-ATPase-An Integral Player in the Adrenergic Fight-or-Flight Response. Trends Cardiovasc. Med. *19*, 111–118.

Bologna, Z., Teoh, J., Bayoumi, A.S., Tang, Y., and Kim, I. (2017). Biased G Protein-Coupled Receptor Signaling: New Player in Modulating Physiology and Pathology. Biomol. Ther. (Seoul). *25*, 12–25.

Borea, P.A., Gessi, S., Merighi, S., and Varani, K. (2016). Adenosine as a Multi-Signalling Guardian Angel in Human Diseases: When, Where and How Does it Exert its Protective Effects? Trends Pharmacol. Sci. *37*, 419–434.

Borea, P.A., Gessi, S., Merighi, S., Vincenzi, F., and Varani, K. (2017).

Pathological overproduction: the bad side of adenosine. Br. J. Pharmacol. *174*, 1945–1960.

Borland, G., Smith, B.O., and Yarwood, S.J. (2009). EPAC proteins transduce diverse cellular actions of cAMP. Br. J. Pharmacol. *158*, 70–86.

Borroto-escuela, D.O., Narvaez, M., Pérez-alea, M., Tarakanov, A.O., Jiménez-beristain, A., Mudó, G., Agnati, L.F., Ciruela, F., Belluardo, N., and Fuxe, K. (2015). Biochemical and Biophysical Research Communications Evidence for the existence of FGFR1 – 5-HT1A heteroreceptor complexes in the midbrain raphe 5-HT system. Biochem. Biophys. Res. Commun. *456*, 489–493.

Borroto-Escuela, D.O., Romero-Fernandez, W., Pérez-Alea, M., Narvaez, M., Tarakanov, A.O., Mudó, G., Agnati, L.F., Ciruela, F., Belluardo, N., and Fuxe, K. (2012). Cellular/Molecular The Existence of FGFR1–5-HT1A Receptor Heterocomplexes in Midbrain 5-HT Neurons of the Rat: Relevance for Neuroplasticity. J. Neurosci. *32*, 6295–6303.

Borroto-Escuela, D.O., Corrales, F., Narvaez, M., Oflijan, J., Agnati, L.F., Palkovits, M., and Fuxe, K. (2013a). Dynamic modulation of FGFR1-5-HT1A heteroreceptor complexes. Agonist treatment enhances participation of FGFR1 and 5-HT1A homodimers and recruitment of β-arrestin2. Biochem. Biophys. Res. Commun. *441*, 387–392.

Borroto-Escuela, D.O., Flajolet, M., Agnati, L.F., Greengard, P., and Fuxe, K. (2013b). bioluminiscence resonance energy transfer (bret) methods to study g protein-coupled receptor - receptor tyrosine kinase heteroreceptor complexes. methods cell biol. *117*, 141–164.

Borroto-Escuela, D.O., Tarakanov, A.O., and Fuxe, K. (2016). FGFR1-5-HT1A Heteroreceptor Complexes: Implications for Understanding and Treating Major Depression. Trends Neurosci. *39*, 5–15.

Bosch, M.P., Campos, F., Niubó, I., Rosell, G., Díaz, J.L., Brea, J., Loza, M.I., and Guerrero, A. (2004). Synthesis and biological activity of new potential agonists for the human adenosine A2A receptor. J. Med. Chem. *47*, 4041–4053.

Braadland, P.R., Ramberg, H., Grytli, H.H., and Tasken, A. (2015). beta2-Adrenergic Receptor Signaling in Prostate Cancer. Front. Oncol. *4*, 1–11.

Briddon, S.J., and Hill, S.J. (2007). Pharmacology under the microscope: the use of fluorescence correlation spectroscopy to determine the properties of ligand-receptor complexes. Trends Pharmacol. Sci. *28*, 637–645.

Briddon, S.J., Gandía, J., Amaral, O.B., Ferré, S., Lluís, C., Franco, R., Hill, S.J., and

Ciruela, F. (2008). Plasma membrane diffusion of G protein-coupled receptor oligomers. Biochim. Biophys. Acta *1783*, 2262–2268.

Briddon, S.J., Hern, J.A., and Hill, S.J. (2010). Use of Fluorescence Correlation Spectroscopy to Study the Diffusion of G Protein-coupled Receptors. In G Protein-Coupled Receptors - Essential Methods, M. Poyner, David R and Wheatley, ed. (Sussex, UK: Wiley-Blackwell), pp. 169–191.

Briddon, S.J., Kilpatrick, L.E., and Hill, S.J. (2018). Studying GPCR Pharmacology in Membrane Microdomains: Fluorescence Correlation Spectroscopy Comes of Age. Trends Pharmacol. Sci. *39*, 158–174.

Cahill, T.J., Thomsen, A.R.B., Tarrasch, J.T., Plouffe, B., Nguyen, A.H., Yang, F., Huang, L.Y., Kahsai, A.W., Bassoni, D.L., Gavino, B.J., et al. (2017). Distinct conformations of GPCR–β-arrestin complexes mediate desensitization, signaling, and endocytosis. Proc. Natl. Acad. Sci. *114*, 2562–2567.

Calebiro, D., and Godbole, A. (2018). Internalization of G-protein-coupled receptors: Implication in receptor function, physiology and diseases. Best Pract. Res. Clin. Endocrinol. Metab. *32*, 83–91.

Calebiro, D., and Sungkaworn, T. (2017). Single-Molecule Imaging of GPCR Interactions. Trends Pharmacol. Sci. *39*, 109–122.

Calebiro, D., Rieken, F., Wagner, J., Sungkaworn, T., Zabel, U., Borzi, A., Cocucci, E., Zürn, A., and Lohse, M.J. (2013). Single-molecule analysis of fluorescently labeled G-protein-coupled receptors reveals complexes with distinct dynamics and organization. Proc. Natl. Acad. Sci. U. S. A. *110*, 743–748.

Calebiro, D., Sungkaworn, T., Maiellaro, I., and Biomedicine, E. (2014). Real-Time Monitoring of GPCR / cAMP Signalling by FRET and Single-Molecule Microscopy. Horm Metab Res *46*, 827–832.

Canals, M., Burgueño, J., Marcellino, D., Cabello, N., Canela, E.I., Mallol, J., Agnati, L., Ferré, S., Bouvier, M., Fuxe, K., et al. (2004). Homodimerization of adenosine A2A receptors: Qualitative and quantitative assessment by fluorescence and bioluminescence energy transfer. J. Neurochem. *88*, 726–734.

Capote, L. a., Mendez Perez, R., and Lymperopoulos, A. (2015). GPCR signaling and cardiac function. Eur. J. Pharmacol. 1–6.

Carmeliet, P., and Jain, R.K. (2011). Molecular mechanisms and clinical applications of angiogenesis. Nature *473*, 298–307.

Carpenter, B., and Lebon, G. (2017). Human adenosine A2Areceptor: Molecular mechanism of ligand binding and activation. Front. Pharmacol. *8*, 1–15.

Carpenter, B., Nehmé, R., Warne, T., Leslie, A.G.W., and Tate, C.G. (2016). Structure of the adenosine A2A receptor bound to an engineered G protein. Nature *536*, 104–107.

Carter, J.J., Wheal, A.J., Hill, S.J., and Woolard, J. (2015). Characterisation of $VEGF_{165}a$ and $VEGF_{165}b$ - stimulated NFAT-mediated gene transcription in HEK-293 cells expressing the human vascular endothelial growth factor receptor 2 (VEGFR2): Influence o. Br. J. Pharmacol. *172,* 3141-50

Casaletto, J.B., and McClatchey, A.I. (2013). Spatial regulation of receptor tyrosine kinases in development and cancer. Nat Rev Cancer *12*, 387–400.

Cattaneo, F., Guerra, G., Parisi, M., De Marinis, M., Tafuri, D., Cinelli, M., and Ammendola, R. (2014). Cell-surface receptors transactivation mediated by g protein-coupled receptors. Int. J. Mol. Sci. *15*, 19700–19728.

Chang, J. (1997). A two step-stage mechanism for the reductive unfolding of disulfide-containing proteins. J. Biol. Chem. *272*, 69–75.

Chang, A., Kim-Fuchs, C., Le, C., Hollande, F., and Sloan, E. (2015). Neural Regulation of Pancreatic Cancer: A Novel Target for Intervention. Cancers (Basel). *7*, 1292–1312.

Chang, A., Le, C.P., Walker, A.K., Creed, S.J., Pon, C.K., Albold, S., Carroll, D., Halls, M.L., Lane, J.R., Riedel, B., et al. (2016). Beta2-Adrenoceptors on tumor cells play a critical role in stress-enhanced metastasis in a mouse model of breast cancer. Brain. Behav. Immun. *57*, 106–115.

Chaplin, R., Thach, L., Hollenberg, M.D., Cao, Y., Little, P.J., and Kamato, D. (2017). Insights into cellular signalling by G protein coupled receptor transactivation of cell surface protein kinase receptors. J. Cell Commun. Signal. *11*, 117–125.

Chen, Z.G. (2010). Small-molecule delivery by nanoparticles for anticancer therapy. Trends Mol. Med. *16*, 594–602.

Chen, H., Liu, D., Yang, Z., Sun, L., Deng, Q., Yang, S., Qian, L., Guo, L., Yu, M., Hu, M., et al. (2014). Adrenergic signaling promotes angiogenesis through endothelial cell–tumor cell crosstalk. Endocr. Relat. Cancer *21*, 783–795.

Cheng, R.K.Y., Segala, E., Robertson, N., Deflorian, F., Doré, A.S., Errey, J.C., Fiez-Vandal, C., Marshall, F.H., and Cooke, R.M. (2017). Structures of Human A1 and A2A Adenosine Receptors with Xanthines Reveal Determinants of Selectivity. Structure *25*, 1275–1285.e4.

Cherezov, V., Rosenbaum, D.M., Hanson, M.A., Rasmussen, S.G.F., Thian, F.S., Kobilka, T.S., Choi, H.-J., Kuhn, P., Weis, W.I., Kobilka, B.K., et al. (2007). High-Resolution Crystal Structure of an Engineered Human beta2-

Adrenergic G Protein-Coupled Receptor. Science. *318*, 1258–1265.

Chow, W., Amaya, C.N., Rains, S., Chow, M., Dickerson, E.B., and Bryan, B.A. (2015). Growth attenuation of cutaneous angiosarcoma with propranolol-mediated β-blockade. JAMA Dermatology *151*, 1226–1229.

Ciruela, F., Casadó, V., Mallol, J., Canela, E.I., Lluis, C., and Franco, R. (1995). Immunological identification of A1 adenosine receptors in brain cortex. J. Neurosci. Res. *42*, 818–828.

Claesson-Welsh, L., and Welsh, M. (2013). VEGFA and tumour angiogenesis. J. Intern. Med. *273*, 114–127.

Clark, A.N., Youkey, R., Liu, X., Jia, L., Blatt, R., Day, Y.-J.J., Sullivan, G.W., Linden, J., and Tucker, A.L. (2007). A1 adenosine receptor activation promotes angiogenesis and release of VEGF from monocytes. Circ. Res. *101*, 1130–1138.

Cole, S.W., and Sood, A.K. (2012). Molecular Pathways: Beta-Adrenergic Signalling in Cancer. Clin. Cancer Res. *18*, 1201–1206.

Corriden, R., Kilpatrick, L.E., Kellam, B., Briddon, S.J., and Hill, S.J. (2014). Kinetic analysis of antagonist-occupied adenosine-A3 receptors within membrane microdomains of individual cells provides evidence of receptor dimerization and allosterism. FASEB J. *28*, 4211–4222.

Creed, S.J., Le, C.P., Hassan, M., Pon, C.K., Albold, S., Chan, K.T., Berginski, M.E., Huang, Z., Bear, J.E., Lane, J.R., et al. (2015). Beta2-Adrenoceptor Signaling Regulates Invadopodia Formation To Enhance Tumor Cell Invasion. Breast Cancer Res. *17*, 145.

Dacres, H., Michie, M., Wang, J., Pfleger, K.D.G., and Trowell, S.C. (2012). Effect of enhanced Renilla luciferase and fluorescent protein variants on the Förster distance of Bioluminescence resonance energy transfer (BRET). Biochem. Biophys. Res. Commun. *425*, 625–629.

Datta, S.R., Brunet, A., and Greenberg, M.E. (1999). Cellular survival: A play in three akts. Genes Dev. *13*, 2905–2927.

Daub, H. (1996). Role of transactivation of the EGF receptor in signalling by G-protein-coupled receptors. Nat. Commun.

Daub, H., Wallasch, C., Lankenau, a, Herrlich, a, and Ullrich, a (1997). Signal characteristics of G protein-transactivated EGF receptor. EMBO J. *16*, 7032–7044.

Delcourt, N., Bockaert, J., and Marin, P. (2007). GPCR-jacking: from a new route in RTK signalling to a new concept in GPCR activation. Trends Pharmacol. Sci. *28*, 602–607.

Desai, A., Victor-vega, C., Gadangi, S., Montesinos, M.C., Chu, C.C., and Cronstein, B.N. (2005). Adenosine A2A Receptor Stimulation Increases Angiogenesis by Down-Regulating Production of the Antiangiogenic Matrix Protein Thrombospondin 1. System *67*, 1406–1413.

Dionisotti, S., Ongini, E., Zocchi, C., Kull, È., Arslan, G., and Fredholm, B.B. (1997). Characterization of human A 2A adenosine receptors with the antagonist radioligand [3 H] -SCH 58261. 353–360.

Doherty, G.J., and McMahon, H.T. (2009). Mechanisms of Endocytosis. Annu. Rev. Biochem. *78*, 857–902.

Domigan, C.K., Ziyad, S., and Iruela-Arispe, M.L. (2014). Canonical and Noncanonical Vascular Endothelial Growth Factor Pathways: New Developments in Biology and Signal Transduction. Arterioscler. Thromb. Vasc. Biol. *35*, 30–39.

Doré, A.S., Robertson, N., Errey, J.C., Ng, I., Hollenstein, K., Tehan, B., Hurrell, E., Bennett, K., Congreve, M., Magnani, F., et al. (2011). Structure of the adenosine A2A receptor in complex with ZM241385 and the xanthines XAC and caffeine. Structure *19*, 1283–1293.

Drake, M.T., Shenoy, S.K., and Lefkowitz, R.J. (2006). Trafficking of G protein-coupled receptors. Circ. Res. *99*, 570–582.

Du, X., Ou, X., Song, T., Zhang, W., Cong, F., Zhang, S., and Xiong, Y. (2015). Adenosine A2B receptor stimulates angiogenesis by inducing VEGF and eNOS in human microvascular endothelial cells. Exp. Biol. Med. *0*, 1–8.

Durham, T.B., and Blanco, M. (2015). Target Engagement in Lead Generation. Bioorg. Med. Chem. Lett. *25*, 998–1008.

Eichel, K., and von Zastrow, M. (2018). Subcellular Organization of GPCR Signaling. Trends Pharmacol. Sci. *39*, 200–208.

Eichel, K., Jullié, D., and Von Zastrow, M. (2016). β-Arrestin drives MAP kinase signalling from clathrin-coated structures after GPCR dissociation. Nat. Cell Biol. *18*, 303–310.

Eichel, K., Jullié, D., Barsi-rhyne, B., Latorraca, N.R., and Masureel, M. (2018). Catalytic activation of β-arrestin by GPCRs. Nature *557*, 381–386.

El-Shewy, H.M., Johnson, K.R., Lee, M.H., Jaffa, A. a., Obeid, L.M., and Luttrell, L.M. (2006). Insulin-like growth factors mediate heterotrimeric G protein-dependent ERK1/2 activation by transactivating sphingosine 1-phosphate receptors. J. Biol. Chem. *281*, 31399–31407.

Ellisdon, A.M., and Halls, M.L. (2016). Compartmentalization of GPCR signalling controls unique cellular responses. Biochem. Soc. Trans. *44*, 562–567.

England, C.G., Ehlerding, E.B., and Cai, W. (2016). NanoLuc: A Small Luciferase Is Brightening Up the Field of Bioluminescence. Bioconjug. Chem. *27*, 1175–1187.

Fearnley, G.W., Smith, G.A., Abdul-Zani, I., Yuldasheva, N., Mughal, N.A., Homer-Vanniasinkam, S., Kearney, M.T., Zachary, I.C., Tomlinson, D.C., Harrison, M.A., et al. (2016). VEGF-A isoforms program differential VEGFR2 signal transduction, trafficking and proteolysis. Biol. Open 1–13.

Feoktistov, I., Goldstein, A.E., Ryzhov, S., Zeng, D., Belardinelli, L., Voyno-Yasenetskaya, T., and Biaggioni, I. (2002). Differential expression of adenosine receptors in human endothelial cells: Role of A2B receptors in angiogenic factor regulation. Circ. Res. *90*, 531–538.

Feoktistov, I., Ryzhov, S., Zhong, H., Goldstein, A.E., Matafonov, A., Zeng, D., and Biaggioni, I. (2004). Hypoxia modulates adenosine receptors in human endothelial and smooth muscle cells toward an A2B angiogenic phenotype. Hypertension *44*, 649–654.

Ferrara, N. (2009). VEGF-A: A critical regulator of blood vessel growth. Eur Cytokine Netw *20*, 158–163.

Ferrara, N., Gerber, H.P., and LeCouter, J. (2003). The biology of VEGF and its receptors. Nat. Med. *9*, 669–676.

Ferré, S., Casadó, V., Devi, L.A., Filizola, M., Jockers, R., Lohse, M.J., Milligan, G., Pin, J.-P., and Guitart, X. (2014). G Protein–Coupled Receptor Oligomerization Revisited: Functional and Pharmacological Perspectives. Pharmacol. Rev. *66*, 413–434.

Ferreira, F., Foley, M., Cooke, A., Cunningham, M., Smith, G., Woolley, R., Henderson, G., Kelly, E., Mundell, S., and Smythe, E. (2012). Endocytosis of G protein-coupled receptors is regulated by clathrin light chain phosphorylation. Curr. Biol. *22*, 1361–1370.

Firouzabadi, N., Raeesi, R., Zomorrodian, K., Bahramali, E., and Yavarian, I. (2017). Beta adrenoceptor polymorphism and clinical response to sertraline in major depressive patients. J. Pharm. Pharm. Sci. *20*, 1–7.

Flajolet, M., Wang, Z., Futter, M., Shen, W., Nuangchamnong, N., Bendor, J., Wallach, I., Nairn, A.C., Surmeier, D.J., Greengard, P., et al. (2008). FGF acts as a co-transmitter through Adenosine A2A receptor to regulate morphological and physiological synaptic plasticity. Nat Neurosci *11*, 1402–1409.

Fontanella, C., Ongaro, E., Bolzonello, S., Guardascione, M., Fasola, G., and Aprile, G. (2014). Clinical advances in the development of novel VEGFR2

inhibitors. Ann. Transl. Med. *2*, 123.

Francis, G.L. (2010). Albumin and mammalian cell culture: Implications for biotechnology applications. Cytotechnology *62*, 1–16.

Franco, R., Martínez-Pinilla, E., Lanciego, J.L., and Navarro, G. (2016). Basic pharmacological and structural evidence for class A G-protein-coupled receptor heteromerization. Front. Pharmacol.

Fraser, C.M., Kerlavage, A.R., Mariani, A.P., and Venter, J.C. (1987). Structural analysis of purified beta-adrenergic receptors. Proteins Struct. Funct. Bioinforma. *2*, 34–41.

Fredholm, B.B., Lindström, K., Dionisotti, S., and Ongini, E. (1998). [3H]SCH 58261, a selective adenosine A2A receptor antagonist, is a useful ligand in autoradiographic studies. J. Neurochem. *70*, 1210–1216.

Fredholm, B.B., Ijzerman, A.P., Jacobson, K.A., Linden, J., and Müller, C.E. (2011). International Union of Basic and Clinical Pharmacology . LXXXI . Nomenclature and Classification of Adenosine Receptors — An Update. Pharmacol. Rev *63*, 1–34.

Fu, Q., Xu, B., Liu, Y., Parikh, D., Li, J., Li, Y., Zhang, Y., Riehle, C., Zhu, Y., Rawlings, T., et al. (2014). Insulin inhibits cardiac contractility by inducing a Gi-Biased β2-adrenergic signaling in hearts. Diabetes *63*, 2676–2689.

Fung, J.J., Deupi, X., Pardo, L., Yao, X.J., Velez-Ruiz, G.A., Devree, B.T., Sunahara, R.K., and Kobilka, B.K. (2009). Ligand-regulated oligomerization of beta-2-adrenoceptors in a model lipid bilayer. EMBO J. *28*, 3315–3328.

Galperin, E., and Sorkin, A. (2008). Endosomal Targeting of MEK2 Requires RAF, MEK Kinase Activity and Clathrin-Dependent Endocytosis. Traffic *9*, 1776–1790.

Gampel, A., Moss, L., Jones, M.C., Brunton, V., Norman, J.C., and Mellor, H. (2006). VEGF regulates the mobilization of VEGFR2/KDR from an intracellular endothelial storage compartment. Blood *108*, 2624–2631.

Gandía, J., Lluís, C., Ferré, S., Franco, R., and Ciruela, F. (2008). Light resonance energy transfer-based methods in the study of G protein-coupled receptor oligomerization. BioEssays *30*, 82–89.

Gao, Z.G., Mamedova, L.K., Chen, P., and Jacobson, K. a. (2004). 2-Substituted adenosine derivatives: Affinity and efficacy at four subtypes of human adenosine receptors. Biochem. Pharmacol. *68*, 1985–1993.

García-Nafría, J., Lee, Y., Bai, X., Carpenter, B., and Tate, C.G. (2018). Cryo-EM structure of the adenosine A2A receptor coupled to an engineered heterotrimeric G protein. Elife *7*, e35946.

Garg, J., Feng, Y.-X., Jansen, S.R., Friedrich, J., Lezoualc'h, F., Schmidt, M., and Wieland, T. (2017). Catecholamines facilitate VEGF-dependent angiogenesis via Beta2-adrenoceptor-induced Epac1 and PKA activation. Oncotarget *8*, 44732–44748.

Gavard, J., and Gutkind, J.S. (2006). VEGF controls endothelial-cell permeability by promoting the β-arrestin-dependent endocytosis of VE-cadherin. Nat. Cell Biol. *8*, 1223–1234.

George, A.J., Hannan, R.D., and Thomas, W.G. (2013). Unravelling the molecular complexity of GPCR-mediated EGFR transactivation using functional genomics approaches. FEBS J. *280*, 5258–5268.

George, S., Furness, B., Liang, Y., Nowell, C.J., Christopoulos, A., Wootten, D., G (2016). Ligand-Dependent Modulation of G Protein Article Ligand-Dependent Modulation of G Protein Conformation Alters Drug Efficacy. Cell *167*, 1–11.

Gessi, S. et al. (2009). Adenosine Receptors in Health and Disease. Handbook of Experimental Pharmacology. *193*, 1–25.

Gessi, S., Merighi, S., Sacchetto, V., Simioni, C., and Borea, P.A. (2011). Adenosine receptors and cancer. Biochim. Biophys. Acta *1808*, 1400–1412.

Gessi, S., Bencivenni, S., Battistello, E., Vincenzi, F., Colotta, V., Catarzi, D., Varano, F., Merighi, S., Borea, P.A., and Varani, K. (2017). Inhibition of A2A Adenosine Receptor Signaling in Cancer Cells Proliferation by the Novel Antagonist TP455. Front. Pharmacol. *8*, 1–13.

Gherbi, K., Briddon, S.J., and Hill, S.J. (2014). Detection of the secondary, low-affinity β1-adrenoceptor site in living cells using the fluorescent CGP 12177 derivative BODIPY-TMR-CGP. Br. J. Pharmacol. *171*, 5431–5445.

Gherbi, K., May, L.T., Baker, J.G., Briddon, S.J., and Hill, S.J. (2015). Negative cooperativity across β1-adrenoceptor homodimers provides insights into the nature of the secondary low-affinity CGP 12177 β1-adrenoceptor binding conformation. FASEB J. *29*, 2859–2871.

Gherbi, K., Briddon, S.J., and Charlton, S.J. (2018). Micro-pharmacokinetics: Quantifying local drug concentration at live cell membranes. Sci. Rep. *8*, 3479.

Ghosh, K., Rathi, S., and Arora, D. (2016). Fluorescence spectral studies on interaction of fluorescent probes with Bovine Serum Albumin (BSA). J. Lumin. *175*, 135–140.

Gilmour, A.M., Abdulkhalek, S., Cheng, T.S.W., Alghamdi, F., Jayanth, P., O'Shea, L.K., Geen, O., Arvizu, L. a, and Szewczuk, M.R. (2013). A novel

epidermal growth factor receptor-signaling platform and its targeted translation in pancreatic cancer. Cell. Signal. *25*, 2587–2603.

Glukhova, A., Thal, D.M., Nguyen, A.T., Vecchio, E.A., Jörg, M., Scammells, P.J., May, L.T., Sexton, P.M., and Christopoulos, A. (2017). Structure of the Adenosine A1 Receptor Reveals the Basis for Subtype Selectivity. Cell *168*, 867–877.e13.

Godbole, A., Lyga, S., Lohse, M.J., and Calebiro, D. (2017). Internalized TSH receptors en route to the TGN induce local Gs-protein signaling and gene transcription. Nat. Commun. *8*.

Goh, L.K., and Sorkin, A. (2013). Endocytosis of receptor tyrosine kinases. Cold Spring Harb. Perspect. Biol. *5*, a017459.

Gomes, C. V., Kaster, M.P., Tomé, A.R., Agostinho, P.M., and Cunha, R.A. (2011). Adenosine receptors and brain diseases: Neuroprotection and neurodegeneration. Biochim. Biophys. Acta - Biomembr. *1808*, 1380–1399.

Grachev, I.D., Doder, M., Brooks, D.J., and Hinz, R. (2014). Quantitative in vivo Imaging of Adenosine A 2A Receptors in the Human Brain Using 11 C-SCH442416 PET : A Pilot Study. J. Diagnostic Imaging Ther. *1*, 1–19.

Gracia, E., Moreno, E., Cortés, A., Lluís, C., Mallol, J., McCormick, P.J., Canela, E.I., and Casadó, V. (2013). Homodimerization of adenosine A1 receptors in brain cortex explains the biphasic effects of caffeine. Neuropharmacology *71*, 56–69.

Grant, M.B., Tarnuzzer, R.W., Caballero, S., Ozeck, M.J., Davis, M.I., Spoerri, P.E., Feoktistov, I., Biaggioni, I., Shryock, J.C., and Belardinelli, L. (1999). Adenosine receptor activation induces vascular endothelial growth factor in human retinal endothelial cells. Circ. Res. *85*, 699–706.

Gschwind, A., Fischer, O.M., and Ullrich, A. (2004). The discovery of receptor tyrosine kinases: targets for cancer therapy Andreas. Nat. Rev. Cancer *4*, 361–367.

Guo, D., Heitman, L.H., and IJzerman, A.P. (2016a). Kinetic Aspects of the Interaction between Ligand and G Protein-Coupled Receptor: The Case of the Adenosine Receptors. Chem. Rev. *117*, acs.chemrev.6b00025.

Guo, D., Heitman, L.H., and Ijzerman, A.P. (2016b). The Added Value of Assessing Ligand-Receptor Binding Kinetics in Drug Discovery. ACS Med. Chem. Lett. *7*, 819–821.

Guo, H., An, S., Ward, R., Yang, Y., Liu, Y., Guo, X.X., Hao, Q., and Xu, T. (2017). Methods used to study the oligomeric structure of G-protein-coupled

receptors. Biosci. Rep. *37*, 1–20.

Gupte, T.M., Malik, R.U., Sommese, R.F., Ritt, M., and Sivaramakrishnan, S. (2017). Priming GPCR signaling through the synergistic effect of two G proteins. Proc. Natl. Acad. Sci. *114*, 3756–3761.

Gurevich, V. V., and Gurevich, E. V. (2008). How and why do GPCRs dimerize? Trends Pharmacol. Sci. *29*, 234–240.

Gutkind, J.S., and Kostenis, E. (2018). Arrestins as rheostats of GPCR signalling. Nat. Rev. Mol. Cell Biol. 2–3.

Hall, M.P., Unch, J., Binkowski, B.F., Valley, M.P., Butler, B.L., Wood, M.G., Otto, P., Zimmerman, K., Vidugiris, G., MacHleidt, T., et al. (2012). Engineered luciferase reporter from a deep sea shrimp utilizing a novel imidazopyrazinone substrate. ACS Chem. Biol. *7*, 1848–1857.

Hallak, H., Seiler, A.E.M., Green, J.S., Ross, B.N., and Rubin, R. (2000). Association of Heterotrimeric Gi with the Insulin-like Growth Factor-I Receptor. J. Biol. Chem. *275*, 2255–2259.

Halls, M.L., Poole, D.P., Ellisdon, A.M., Nowell, C.J., and Canals, M. (2005). Detection and Quantification of Intracellular Signaling Using FRET-Based Biosensors and High Content Imaging. In G Protein-Coupled Receptors in Drug Discovery Methods and Protocols, M. Filizola, ed. (Hatfield: Springer), p. 376.

Halls, M.L., Yeatman, H.R., Nowell, C.J., Thompson, G.L., Gondin, A.B., Civciristov, S., Bunnett, N.W., Lambert, N.A., Poole, D.P., and Canals, M. (2016). Plasma membrane localization of the m -opioid receptor controls spatiotemporal signaling. *9*, 1–14.

Hamm, H.E. (1998). The Many Faces of G Protein Signaling *. J. Biol. Chem. *273*, 5–8.

Hanahan, D., and Weinberg, R.A. (2011). Hallmarks of cancer: The next generation. Cell *144*, 646–674.

Hanson, M.A., Cherezov, V., Griffith, M.T., Roth, C.B., Jaakola, V.P., Chien, E.Y.T., Velasquez, J., Kuhn, P., and Stevens, R.C. (2008). A Specific Cholesterol Binding Site Is Established by the 2.8 Å Structure of the Human β2-Adrenergic Receptor. Structure *16*, 897–905.

Harms, H., Zaagsma, J., and B, V.D.W. (1974). β-Adrenoceptor studies. III. On the β-adrenoceptors in rat adipose tissue. Eur. J. Heart Fail. *25*, 87–91.

Hatfield, S.M., and Sitkovsky, M. (2016). A2A adenosine receptor antagonists to weaken the hypoxia-HIF-1α driven immunosuppression and improve immunotherapies of cancer. Curr. Opin. Pharmacol. *29*, 90–96.

Hazari, P.P., Pandey, A., Chaturvedi, S., and Mishra, A.K. (2017). New Trends and Current Status of Positron-Emission Tomography and Single-Photon-Emission Computerized Tomography Radioligands for Neuronal Serotonin Receptors and Serotonin Transporter. Bioconjug. Chem. *28*, 2647–2672.

Hebert, T.E., Moffett, S., Morello, J.P., Loisel, T.P., Bichet, D.G., Barret, C., and Bouvier, M. (1996). A peptide derived from a beta2-adrenergic receptor transmembrane domain inhibits both receptor dimerization and activation. J. Biol. Chem. *271*, 16384–16392.

Herrick-Davis, K., Grinde, E., Lindsley, T., Cowan, A., and Mazurkiewicz, J.E. (2012). Oligomer size of the serotonin 5-hydroxytryptamine 2C (5-HT2C) receptor revealed by fluorescence correlation spectroscopy with photon counting histogram analysis: Evidence for homodimers without monomers or tetramers. J. Biol. Chem. *287*, 23604–23614.

Hildebrandt, J. (1983). Stimulation and inhibition of adenylyl cyclases mediated by distincr regulatory proteins. Nature *302*, 706–709.

Hilmi, C., Guyot, M., and Pagès, G. (2012). VEGF spliced variants: Possible role of anti-angiogenesis therapy. J. Nucleic Acids.

Hohng, S., and Ha, T. (2004). Near-Complete Suppression of Quantum Dot Blinking in Ambient Conditions. Society *126*, 1324–1325.

Holmqvist, K., Cross, M.J., Rolny, C., Hägerkvist, R., Rahimi, N., Matsumoto, T., Claesson-Welsh, L., and Welsh, M. (2004). The adaptor protein Shb binds to tyrosine 1175 in vascular endothelial growth factor (VEGF) receptor-2 and regulates VEGF-dependent cellular migration. J. Biol. Chem. *279*, 22267–22275.

Howell, R.E., Albelda, S.M., Daise, M.L., and Levine, E.M. (1988). Characterization of beta-adrenergic receptors in cultured human and bovine endothelial cells. J Appl Physiol. *65*, 1251–1257.

Hubbard, S.R., and Miller, W.T. (2008). Receptor tyrosine kinases: mechanisms of activation and signaling. Curr OpiniCell Biol *19*, 117–123.

Hulsurkar, M., Li, Z., Zhang, Y., Li, X., Zheng, D., and Li, W. (2017). Beta-adrenergic signaling promotes tumor angiogenesis and prostate cancer progression through HDAC2-mediated suppression of thrombospondin-1. Oncogene *36*, 1525–1536.

Huynh, A.S., Estrella, V., Stark, V.E., Cohen, A.S., Chen, T., Casagni, T.J., Josan, J.S., Lloyd, M.C., Johnson, J., and Kim, J. (2015). Tumor Targeting and Pharmacokinetics of a Near Infrared Fluorescent-labeled δ-Opioid Receptor Antagonist Agent, Dmt-Tic-Cy5. Mol. Pharm.

Inbar, S., Neeman, E., Avraham, R., Benish, M., Rosenne, E., and Ben-Eliyahu, S. (2011). Do stress responses promote leukemia progression? an animal study suggesting a role for epinephrine and prostaglandin-e2 through reduced nk activity. PLoS One *6*.

Irannejad, R., Tomshine, J.C., Tomshine, J.R., Chevalier, M., Mahoney, J.P., Steyaert, J., Rasmussen, S.G.F., Sunahara, R.K., El-Samad, H., Huang, B., et al. (2013). Conformational biosensors reveal GPCR signalling from endosomes. Nature *495*, 534–538.

Irannejad, R., Pessino, V., Mika, D., Huang, B., Wedegaertner, P.B., Conti, M., and Von Zastrow, M. (2017). Functional selectivity of GPCR-directed drug action through location bias. Nat. Chem. Biol. *13*, 799–806.

Jacobson, K.A., Park, K.-S.S., Jiang, J.L., Kim, Y.C.C., Olah, M.E., Stiles, G.L., Ji, X.D.D., Jliang, J.L., Kim, Y.C.C., Olah, M.E., et al. (1997). Pharmacological Characterization of Novel A3 adenosine Receptor-selective antagonists. Neuropharmacology *36*, 1157–1165.

Jakobsson, L. (2006). Heparan Sulfate in trans Potentiates VEGFR-Mediated Angiogenesis. Dev. Cell *10*, 625–634.

Jean-Charles, P.Y., Kaur, S., and Shenoy, S.K. (2017). GPCR signaling via β-arrestin-dependent mechanisms. J Cardiovasc Pharmacol. *70*, 29–39.

Jespers, W., Schiedel, A.C., Heitman, L.H., Cooke, R.M., Kleene, L., van Westen, G.J.P., Gloriam, D.E., Müller, C.E., Sotelo, E., and Gutiérrez-de-Terán, H. (2018). Structural Mapping of Adenosine Receptor Mutations: Ligand Binding and Signaling Mechanisms. Trends Pharmacol. Sci. *39*, 75–89.

Ji, Y., Chen, S., Xu, C., Li, L., and Xiang, B. (2015). The use of propranolol in the treatment of infantile haemangiomas: An update on potential mechanisms of action. Br. J. Dermatol. *172*, 24–32.

Jones, M.C., Caswell, P.T., and Norman, J.C. (2006). Endocytic recycling pathways: emerging regulators of cell migration. Curr. Opin. Cell Biol. *18*, 549–557.

Jopling, H.M., Howell, G.J., Gamper, N., and Ponnambalam, S. (2011). The VEGFR2 receptor tyrosine kinase undergoes constitutive endosome-to-plasma membrane recycling. Biochem. Biophys. Res. Commun. *410*, 170–176.

Kallifatidis, G., Munoz, D., Singh, R.K., Salazar, N., Hoy, J.J., and Lokeshwar, B.L. (2016). Beta-Arrestin-2 Counters CXCR7-Mediated EGFR Transactivation and Proliferation. Mol. Cancer Res. *14*, 493–503.

Kamato, D., Burch, M.L., Osman, N., Zheng, W., and Little, P.J. (2013).

Therapeutic implications of endothelin and thrombin G-protein-coupled receptor transactivation of tyrosine and serine/threonine kinase cell surface receptors. J. Pharm. Pharmacol. *65*, 465–473.

Kelly, E., Bailey, C.P., and Henderson, G. (2008). Agonist-selective mechanisms of GPCR desensitization. Br. J. Pharmacol. *153*, S379–S388.

Kenakin, T. (2017). Theoretical Aspects of GPCR–Ligand Complex Pharmacology. Chem. Rev. *117*, 4–20.

Kenakin, T., and Williams, M. (2014). Defining and characterizing drug/compound function. Biochem. Pharmacol. *87*, 40–63.

Khan, S.M., Sleno, R., Gora, S., Zylbergold, P., Laverdure, J., Labbé, J., and Miller, G.J. (2013). The Expanding Roles of G-beta/gama Subunits in G Protein – Coupled Receptor Signaling and Drug Action. Pharmacol. Rev. *65*, 545–577.

Kharmate, G., Rajput, P.S., Watt, H.L., Somvanshi, R.K., Chaudhari, N., Qiu, X., and Kumar, U. (2011). Dissociation of epidermal growth factor receptor and ErbB2 heterodimers in the presence of somatostatin receptor 5 modulate signaling pathways. Endocrinology *152*, 931–945.

Kilpatrick, L.E., Briddon, S.J., and Holliday, N.D. (2012). Fluorescence correlation spectroscopy, combined with bimolecular fluorescence complementation, reveals the effects of beta-arrestin complexes and endocytic targeting on the membrane mobility of neuropeptide Y receptors. Biochim. Biophys. Acta - Mol. Cell Res. *1823*, 1068–1081.

Kilpatrick, L.E., Friedman-Ohana, R., Alcobia, D.C., Riching, K., Peach, C.J., Wheal, A.J., Briddon, S.J., Robers, M.B., Zimmerman, K., Machleidt, T., et al. (2017). Real-time analysis of the binding of fluorescent $VEGF_{165}$a to VEGFR2 in living cells: effect of receptor tyrosine kinase inhibitors and fate of internalized agonist-receptor complexes. Biochem. Pharmacol. *136*, 62–75.

Kim, J., and Grailhe, R. (2016). Nanoluciferase signal brightness using furimazine substrates opens bioluminescence resonance energy transfer to widefield microscopy. Cytom. Part A *89*, 742–746.

Kim, G.D., Oh, J., Jeong, L.S., and Lee, S.K. (2013). Thio-Cl-IB-MECA, a novel A_3 adenosine receptor agonist, suppresses angiogenesis by regulating PI3K/AKT/mTOR and ERK signaling in endothelial cells. Biochem. Biophys. Res. Commun. *437*, 79–86.

Kim, I.M., Tilley, D.G., Chen, J., Salazar, N.C., Whalen, E.J., Violin, J.D., and Rockman, H. a (2008). Beta-blockers alprenolol and carvedilol stimulate beta-arrestin-mediated EGFR transactivation. Proc. Natl. Acad. Sci. U. S. A.

105, 14555–14560.

Kimple, A.J., Bosch, D.E., Giguère, P.M., and Siderovski, D.P. (2011). Regulators of G-protein signaling and their Gα substrates: promises and challenges in their use as drug discovery targets. Pharmacol. Rev. *63*, 728–749.

Klaasse, E.C., IJzerman, A.P., de Grip, W.J., and Beukers, M.W. (2008). Internalization and desensitization of adenosine receptors. Purinergic Signal. *4*, 21–37.

Klinger, M., Freissmuth, M., and Nanoff, C. (2002). Adenosine receptors: G protein-mediated signalling and the role of accessory proteins. Cell. Signal. *14*, 99–108.

Kocan, M., See, H.B., Seeber, R.M., Eidne, K.A., and Pfleger, K.D.G. (2008). Demonstration of improvements to the bioluminescence resonance energy transfer (BRET) technology for the monitoring of g protein-coupled receptors in live cells. J. Biomol. Screen. *13*, 888–898.

Koch, S., Tugues, S., Li, X., Gualandi, L., and Claesson-Welsh, L. (2011). Signal transduction by vascular endothelial growth factor receptors. Biochem. J. *437*, 169–183.

Komolov, K.E., and Benovic, J.L. (2018). G protein-coupled receptor kinases: Past, present and future. Cell. Signal. *41*, 17–24.

Kono, M., Conlon, E.G., Lux, S.Y., Yanagida, K., Hla, T., and Proia, R.L. (2017). Bioluminescence imaging of G protein-coupled receptor activation in living mice. Nat. Commun. *8*, 1163.

Köse, M. (2017). GPCRs and EGFR – Cross-talk of membrane receptors in cancer. Bioorganic Med. Chem. Lett. *27*, 3611–3620.

Krasel, C., Zabel, U., Lorenz, K., Reiner, S., Al-Sabah, S., and Lohse, M.J. (2008). Dual role of the β2-adrenergic receptor C terminus for the binding of β-arrestin and receptor internalization. J. Biol. Chem. *283*, 31840–31848.

Krilleke, D., Ng, Y.S.E., and Shima, D.T. (2009). The heparin-binding domain confers diverse functions of VEGF-A in development and disease: a structure-function study. Biochem. Soc. Trans. *37*, 1201–1206.

Kroll, J., and Waltenberger, J. (1997). The vascular endothelial growth factor receptor KDR activates multiple signal transduction pathways in porcine aortic endothelial cells. J. Biol. Chem. *272*, 32521–32527.

Kumari, P., Srivastava, A., Banerjee, R., Ghosh, E., Gupta, P., Ranjan, R., Chen, X., Gupta, B., Gupta, C., Jaiman, D., et al. (2016). Functional competence of a partially engaged GPCR-β-arrestin complex. Nat. Commun. *7*, 1–16.

Lamalice, L., Houle, F., and Huot, J. (2006). Phosphorylation of Tyr1214 within VEGFR-2 triggers the recruitment of Nck and activation of Fyn leading to SAPK2/p38 activation and endothelial cell migration in response to VEGF. J. Biol. Chem. *281*, 34009–34020.

Lanahan, A.A., Lech, D., Dubrac, A., Zhang, J., Zhuang, Z.W., Eichmann, A., and Simons, M. (2014). PTP1b is a physiologic regulator of vascular endothelial growth factor signaling in endothelial cells. Circulation *130*, 902–909.

Lane, J.R., May, L.T., Parton, R.G., Sexton, P.M., and Christopoulos, A. (2017). A kinetic view of GPCR allostery and biased agonism. Nat. Chem. Biol. *13*, 929–937.

Laporte, S. a, Oakley, R.H., Zhang, J., Holt, J. a, Ferguson, S.S., Caron, M.G., and Barak, L.S. (1999). The beta2-adrenergic receptor/betaarrestin complex recruits the clathrin adaptor AP-2 during endocytosis. Proc. Natl. Acad. Sci. U. S. A. *96*, 3712–3717.

Laramé, M., Chabot, C., Cloutier, M., Stenne, R., Holgado-Madruga, M., Wong, A.J., and Royal, I. (2007). The scaffolding adapter Gab1 mediates vascular endothelial growth factor signaling and is required for endothelial cell migration and capillary formation. J. Biol. Chem. *282*, 7758–7769.

Le, C.P., Nowell, C.J., Kim-Fuchs, C., Botteri, E., Hiller, J.G., Ismail, H., Pimentel, M.A., Chai, M.G., Karnezis, T., Rotmensz, N., et al. (2016). Chronic stress in mice remodels lymph vasculature to promote tumour cell dissemination. Nat. Commun. *7*, 10634.

Lebman, D. a, and Spiegel, S. (2008). Cross-talk at the crossroads of sphingosine-1-phosphate, growth factors, and cytokine signaling. J. Lipid Res. *49*, 1388–1394.

Lebon, G., Warne, T., and Tate, C.G. (2012). Agonist-bound structures of G protein-coupled receptors. Curr. Opin. Struct. Biol. *22*, 482–490.

Lebon, G., Edwards, P.C., Leslie, A.G.W., and Tate, C.G. (2015). Molecular Determinants of CGS21680 Binding to the Human Adenosine A2A Receptor. Mol. Pharmacol. *87*, 907–915.

Lee, MH., Appleton, K.M., Strungs, E.G., Kwon, J.Y., Morinelli, T.A., Peterson, Y.K., Laporte, S.A., and Luttrell, L.M. (2016). The conformational signature of β-arrestin2 predicts its trafficking and signalling functions. Nature *531*, 665–668.

Lefkowitz, R.J. (2007). Seven transmembrane receptors-A brief personal retrospective. Biochim. Biophys. Acta - Biomembr. *1768*, 748–755.

Lemmens, S., Kusters, L., Bronckaers, A., Geurts, N., and Hendrix, S. (2017). The

β2-Adrenoceptor Agonist Terbutaline Stimulates Angiogenesis via Akt and ERK Signaling. J. Cell. Physiol. *232*, 298–308.

Lemmon, M.A., and Schlessinger, J. (2010). Cell signaling by receptor tyrosine kinases. Cell *141*, 1117–1134.

Leppanen, V.-M., Prota, A.E., Jeltsch, M., Anisimov, A., Kalkkinen, N., Strandin, T., Lankinen, H., Goldman, A., Ballmer-Hofer, K., and Alitalo, K. (2010). Structural determinants of growth factor binding and specificity by VEGF receptor 2. Proc. Natl. Acad. Sci. *107*, 2425–2430.

Li, H., Hu, D., Fan, H., Zhang, Y., LeSage, G.D., Caudle, Y., Stuart, C., Liu, Z., and Yin, D. (2014). β-Arrestin 2 negatively regulates Toll-like receptor 4 (TLR4)-triggered inflammatory signaling via targeting p38 MAPK and interleukin 10. J. Biol. Chem. *289*, 23075–23085.

Di Liberto, V., Borroto-Escuela, D.O., Frinchi, M., Verdi, V., Fuxe, K., Belluardo, N., and Mudò, G. (2017). Existence of muscarinic acetylcholine receptor (mAChR) and fibroblast growth factor receptor (FGFR) heteroreceptor complexes and their enhancement of neurite outgrowth in neural hippocampal cultures. Biochim. Biophys. Acta - Gen. Subj. *1861*, 235–245.

Liebmann, C. (2011). EGF receptor activation by GPCRs: An universal pathway reveals different versions. Mol. Cell. Endocrinol. *331*, 222–231.

Liebmann, C., and Böhmer, F.D. (2000). Signal transduction pathways of G protein-coupled receptors and their cross-talk with receptor tyrosine kinases: lessons from bradykinin signaling. Curr. Med. Chem. *7*, 911–943.

Lim, B., Yao, Y., Huang, A.L. i., Yap, M.L., Flierl, U., Palasubramaniam, J., Zaldivia, M.T.K., Wang, X., and Peter, K. (2017). A unique recombinant fluoroprobe targeting activated platelets allows in vivo detection of arterial thrombosis and pulmonary embolism using a novel three-dimensional fluorescence emission computed tomography (FLECT) technology. Theranostics *7*, 1047–1061.

Lohse, M.J., and Calebiro, D. (2013). Receptor signals come in waves. Nature *495*, 457–458.

Lohse, M.J., Benovic, J.L., Codina, J., Caron, M.G., and Lefkowitz, R.J. (1990). Beta-Arrestin : A Protein That Regulates beta-Adrenergic Receptor Funcation. Science (80-.). *248*, 1547–1550.

Long, J.S., Natarajan, V., Tigyi, G., Pyne, S., and Pyne, N.J. (2006). The functional PDGF receptor-S1P1 receptor signaling complex is involved in regulating migration of mouse embryonic fibroblasts in response to platelet derived growth factor. Prostaglandins Other Lipid Mediat. *80*, 74–80.

Di Lorenzo, A., Lin, M.I., Murata, T., Landskroner-Eiger, S., Schleicher, M., Kothiya, M., Iwakiri, Y., Yu, J., Huang, P.L., and Sessa, W.C. (2014). eNOS-derived nitric oxide regulates endothelial barrier function through VE-cadherin and Rho GTPases. J. Cell Sci. *127*, 2120–2120.

Luttrell, T. (2006). Transmembrane signalling by G protein-coupled receptors. Transmembrane signalling Protocols.

Luttrell, L.M., and Lefkowitz, R.J. (2002). The role of beta-arrestins in the termination and transduction of G-protein-coupled receptor signals. J. Cell Sci. *115*, 455–465.

Luttrell, L.M., Ferguson, S.S., Daaka, Y., Miller, W.E., Maudsley, S., Della Rocca, G.J., Lin, F., Kawakatsu, H., Owada, K., Luttrell, D.K., et al. (1999). Beta-arrestin-dependent formation of beta2 adrenergic receptor-Src protein kinase complexes. Science *283*, 655–661.

Luttrell, L.M., Roudabush, F.L., Choy, E.W., Miller, W.E., Field, M.E., Pierce, K.L., and Lefkowitz, R.J. (2001). Activation and targeting of extracellular signal-regulated kinases by beta-arrestin scaffolds. Proc. Natl. Acad. Sci. U. S. A. *98*, 2449–2454.

Lymperopoulos, A., and Negussie, S. (2013). beta-arrestins in cardiac G protein-coupled receptor signaling and function: Partners in crime or “good cop, bad cop”? Int. J. Mol. Sci. *14*, 24726–24741.

Madden, K.S., Szpunar, M.J., and Brown, E.B. (2011). Beta-Adrenergic receptors (beta-AR) regulate VEGF and IL-6 production by divergent pathways in high beta-AR-expressing breast cancer cell lines. Breast Cancer Res. Treat. *130*, 747–758.

Magalhaes, A.C., Dunn, H., and Ferguson, S.S.G. (2012). Regulation of GPCR activity, trafficking and localization by GPCR-interacting proteins. Br. J. Pharmacol. *165*, 1717–1736.

Mandic, M., Drinovec, L., Glisic, S., Veljkovic, N., Nohr, J., and Vrecl, M. (2014). Demonstration of a direct interaction between&beta2- Adrenergic receptor and insulin receptor by BRET and bioinformatics. PLoS One *9*.

Manni, S., Kisko, K., Schleier, T., Missimer, J., and Ballmer-Hofer, K. (2014a). Functional and structural characterization of the kinase insert and the carboxy terminal domain in VEGF receptor 2 activation. FASEB J. *28*, 4914–4923.

Manni, S., Mineev, K.S., Usmanova, D., Lyukmanova, E.N., Shulepko, M.A., Kirpichnikov, M.P., Winter, J., Matkovic, M., Deupi, X., Arseniev, A.S., et al. (2014b). Structural and functional characterization of alternative

transmembrane domain conformations in VEGF receptor 2 activation. Cell Press *22*, 1077–1089.

Maruyama, I.N. (2014). Mechanisms of activation of receptor tyrosine kinases: monomers or dimers. Cells *3*, 304–330.

Matsumoto, T., Bohman, S., Dixelius, J., Berge, T., Dimberg, A., Magnusson, P., Wang, L., Wikner, C., Qi, J.H., Wernstedt, C., et al. (2005). VEGF receptor-2 Y951 signaling and a role for the adapter molecule TSAd in tumor angiogenesis. EMBO J. *24*, 2342–2353.

Maudsley, S. (2000). The beta 2-Adrenergic Receptor Mediates Extracellular Signal-regulated Kinase Activation via Assembly of a Multi-receptor Complex with the Epidermal Growth Factor Receptor. J. Biol. Chem. *275*, 9572–9580.

May, L.T., Bridge, L.J., Stoddart, L. a, Briddon, S.J., and Hill, S.J. (2011). Allosteric interactions across native adenosine-A3 receptor homodimers: quantification using single-cell ligand-binding kinetics. FASEB J. *25*, 3465–3476.

McCudden, C.R., Hains, M.D., Kimple, R.J., Siderovski, D.P., and Willard, F.S. (2005). G-protein signaling: Back to the future. Cell. Mol. Life Sci. *62*, 551–577.

Mcgraw, D.W., Mihlbachler, K.A., Schwarb, M.R., Rahman, F.F., Small, K.M., Almoosa, K.F., and Liggett, S.B. (2006). Airway smooth muscle prostaglandin-EP 1 receptors directly modulate β 2 –adrenergic receptors within a unique heterodimeric complex. J. Clin. Invest. *116*.

Meadows, K.N., Bryant, P., and Pumiglia, K. (2001). Vascular Endothelial Growth Factor Induction of the Angiogenic Phenotype Requires Ras Activation. J. Biol. Chem. *276*, 49289–49298.

Mecklenburg, L., Nakamura, M., Paus, R., Mecklenburg, L., and Sundberg, J.P. (2001). The nude mouse skin phenotype: The role of Foxn1 in hair follicle development and cycling. Exp. Mol. Pathol. *71*, 171–178.

Melhem-Bertrandt, A., Chavez-MacGregor, M., Lei, X., Brown, E.N., Lee, R.T., Meric-Bernstam, F., Sood, A.K., Conzen, S.D., Hortobagyi, G.N., and Gonzalez-Angulo, A.M. (2011). Beta-blocker use is associated with improved relapse-free survival in patients with triple-negative breast cancer. J. Clin. Oncol. *29*, 2645–2652.

Mercier, J.F., Salahpour, A., Angers, S., Breit, A., and Bouvier, M. (2002). Quantitative assessment of beta1- and beta2-adrenergic receptor homo- and heterodimerization by bioluminescence resonance energy transfer. J.

Biol. Chem. *277*, 44925–44931.

Merighi, S., Varani, K., Gessi, S., Cattabriga, E., Iannotta, V., Ulouglu, C., Leung, E., and Borea, P. a (2001). Pharmacological and biochemical characterization of adenosine receptors in the human malignant melanoma A375 cell line. Br. J. Pharmacol. *134*, 1215–1226.

Merighi, S., Benini, A., Mirandola, P., Gessi, S., Varani, K., Leung, E., Maclennan, S., and Borea, P.A. (2006). Adenosine modulates vascular endothelial growth factor expression via hypoxia-inducible factor-1 in human glioblastoma cells. Biochem. Pharmacol. *72*, 19–31.

Miaczynska, M. (2013). Effects of membrane trafficking on signaling by receptor tyrosine kinases. Cold Spring Harb. Perspect. Biol. *5*, a009035.

Middleton, R.J., and Kellam, B. (2005). Fluorophore-tagged GPCR ligands. Curr. Opin. Chem. Biol. *9*, 517–525.

Miller, L.J., Sexton, P.M., Dong, M., and Harikumar, K.G. (2014). The class B G-protein-coupled GLP-1 receptor: an important target for the treatment of type-2 diabetes mellitus. Int. J. Obes. Suppl. *4*, S9–S13.

Milligan, G., and Kostenis, E. (2006). Heterotrimeric G-proteins: A short history. Br. J. Pharmacol. *147*.

Mira, E., Lacalle, R.A., González, M. a., Gómez-Moutón, C., Abad, J.L., Bernad, A., Martínez-A., C., and Mañes, S. (2001). A role for chemokine receptor transactivation in growth factor signaling. EMBO Rep. *2*, 151–156.

Montesinos, M.C., Desai, A., Chen, J.F., Yee, H., Schwarzschild, M.A., Fink, J.S., and Cronstein, B.N. (2002). Adenosine promotes wound healing and mediates angiogenesis in response to tissue injury via occupancy of A2Areceptors. Am. J. Pathol. *160*, 2009–2018.

Montesinos, M.C., Desai-Merchant, A., and Cronstein, B.N. (2015). Promotion of Wound Healing by an Agonist of Adenosine A2A Receptor Is Dependent on Tissue Plasminogen Activator. Inflammation *38*, 2036–2041.

Moretti, S., Massi, D., Farini, V., Baroni, G., Parri, M., Innocenti, S., Cecchi, R., and Chiarugi, P. (2013). B-Adrenoceptors Are Upregulated in Human Melanoma and Their Activation Releases Pro-Tumorigenic Cytokines and Metalloproteases in Melanoma Cell Lines. Lab. Investig. *93*, 279–290.

Moughal, N.A., Waters, C.M., Valentine, W.J., Connell, M., Richardson, J.C., Tigyi, G., Pyne, S., and Pyne, N.J. (2006). Protean agonism of the lysophosphatidic acid receptor-1 with Ki16425 reduces nerve growth factor-induced neurite outgrowth in pheochromocytoma 12 cells. J. Neurochem. *98*, 1920–1929.

Mulcrone, P.L., Campbell, J.P., Clément-Demange, L., Anbinder, A.L., Merkel, A.R., Brekken, R.A., Sterling, J.A., and Elefteriou, F. (2017). Skeletal Colonization by Breast Cancer Cells Is Stimulated by an Osteoblast and β2AR-Dependent Neo-Angiogenic Switch. J. Bone Miner. Res. *32*, 1442–1454.

Muller, Y.A., Li, B., Christinger, H.W., Wells, J. a, Cunningham, B.C., and de Vos, a M. (1997). Vascular endothelial growth factor: crystal structure and functional mapping of the kinase domain receptor binding site. Proc. Natl. Acad. Sci. U. S. A. *94*, 7192–7197.

Mundell, S., and Kelly, E. (2011). Adenosine receptor desensitization and trafficking. Biochim. Biophys. Acta *1808*, 1319–1328.

Nadeau, J.L., Carlini, L., Suffern, D., Ivanova, O., and Bradforth, S.E. (2012). Effects of β-mercaptoethanol on quantum dot emission evaluated from photoluminescence decays. J. Phys. Chem. C *116*, 2728–2739.

Nagai, T., Ibata, K., Park, E.S., Kubota, M., Mikoshiba, K., and Miyawaki, A. (2002). A variant of YFP with fast and efficient maturation for cell-biological applications. Nature *20*, 1585–1588.

Nagaraja, D., Melavanki, R.M., Patil, N.R., Geethanjali, H.S., and Kusanur, R.A. (2015). Solvent effect on the relative quantum yield and fluorescence quenching of a newly synthesized coumarin derivative. Luminescence *30*, 495–502.

Nan, L., Wei, J., Jacko, A.M., Culley, M.K., Zhao, J., Natarajan, V., Ma, H., and Zhao, Y. (2016). Cross-talk between lysophosphatidic acid receptor 1 and tropomyosin receptor kinase A promotes lung epithelial cell migration. Biochim. Biophys. Acta - Mol. Cell Res. *1863*, 229–235.

Negro, A., Brar, B.K., Gu, Y., Peterson, K.L., Vale, W., and Lee, K.F. (2006). erbB2 is required for G protein-coupled receptor signaling in the heart. PNAS *103*, 15889–15893.

Niu, G., and Chen, X. (2010). Vascular endothelial growth factor as an anti-angiogenic target for cancer therapy. Curr. Drug Targets *11*, 1000–1017.

Nobles, K.N., Xiao, K., Ahn, S., Shukla, A.K., Christopher, M., Rajagopal, S., Strachan, R.T., Huang, T., Bressler, E.A., Hara, M.R., et al. (2012). Distinct Phosphorylation Sites on the β2-Adrenergic Receptor Establish a Barcode That Encodes Differential Functions of β-Arrestin. Sci Signal *4*.

Nowak, D.G., Woolard, J., Amin, E.M., Konopatskaya, O., Saleem, M.A., Churchill, A.J., Ladomery, M.R., Harper, S.J., and Bates, D.O. (2008). Expression of pro- and anti-angiogenic isoforms of VEGF is differentially

regulated by splicing and growth factors. J. Cell Sci. *121*, 3487–3495.

Nuber, S., Zabel, U., Lorenz, K., Nuber, A., Milligan, G., Tobin, A.B., Lohse, M.J., and Hoffmann, C. (2016). β-Arrestin biosensors reveal a rapid, receptor-dependent activation/deactivation cycle. Nature *531*, 661–664.

O'Hayre, M.O., Eichel, K., Avino, S., Zhao, X., Steffen, D.J., Feng, X., Kawakami, K., Aoki, J., Messer, K., Sunahara, R., et al. (2017). Genetic evidence that beta-arrestins are dispensable for the initiation of beta2 -adrenergic receptor signaling to ERK. Sci. Signal. *10*, eaal3395.

O'Leary, A.P., Fox, J.M., and Pullar, C.E. (2015). Beta-adrenoceptor activation reduces both dermal microvascular endothelial cell migration via a cAMP-dependent mechanism and wound angiogenesis. J. Cell. Physiol. *230*, 356–365.

Ohta, A., Gorelik, E., Prasad, S.J., Ronchese, F., Lukashev, D., Wong, M.K.K., Huang, X., Caldwell, S., Liu, K., Smith, P., et al. (2006). A2A adenosine receptor protects tumors from antitumor T cells. Proc. Natl. Acad. Sci. *103*, 13132–13137.

Oligny-Longpre, G., Corbani, M., Zhou, J., Hogue, M., Guillon, G., and Bouvier, M. (2012). Engagement of beta-arrestin by transactivated insulin-like growth factor receptor is needed for V2 vasopressin receptor-stimulated ERK1/2 activation. Proc. Natl. Acad. Sci. *109*, E1028–E1037.

Olsson, A.-K., Dimberg, A., Kreuger, J., and Claesson-Welsh, L. (2006). VEGF receptor signalling - in control of vascular function. Nat. Rev. Mol. Cell Biol. *7*, 359–371.

Ongini, E. (1997). SCH 58261 : A Selective A2A Adenosine Receptor Antagonist. Drug Dev. Res. *42*, 63–70.

Palm, D., Lang, K., Niggemann, B., Drell IV, T.L., Masur, K., Zaenker, K.S., and Entschladen, F. (2006). The norepinephrine-driven metastasis development of PC-3 human prostate cancer cells in BALB/c nude mice is inhibited by β-blockers. Int. J. Cancer *118*, 2744–2749.

Pan, W.K., Li, P., Zheng-Tuan, G., Qiang, H., and Gao, Y. (2015). Propranolol Induces Regression of Hemangioma Cells via the Down-Regulation of the PI3K/Akt/eNOS/VEGF Pathway. Pediatr Blood Cancer *62*, 1414–1420.

Park, J.Y., Lee, S.Y., Kim, H.R., Seo, M.-D., and Chung, K.Y. (2016). Structural mechanism of GPCR-arrestin interaction: recent breakthroughs. Arch. Pharm. Res. *39*, 293–301.

Park, S.Y., Kang, J.H., Jeong, K.J., Lee, J., Han, J.W., Choi, W.S., Kim, Y.K., Kang, J., Park, C.G., and Lee, H.Y. (2011). Norepinephrine induces VEGF

expression and angiogenesis by a hypoxia-inducible factor-1α protein-dependent mechanism. Int. J. Cancer *128*, 2306–2316.

Pasquier, E., Ciccolini, J., Carre, M., Giacometti, S., Fanciullino, R., Pouchy, C., Montero, M.-P., Serdjebi, C., Kavallaris, M., Andre, N., et al. (2011). Propranolol potentiates the anti-angiogenic effects and anti-tumor efficacy of chemotherapy agents: implication in breast cancer treatment. Oncotarget *2*, 797–809.

Peach, C.J., Mignone, V.W., Arruda, M.A., Alcobia, D.C., Hill, S.J., Kilpatrick, L.E., and Woolard, J. (2018a). Molecular pharmacology of VEGF-A isoforms: Binding and signalling at VEGFR2. Int. J. Mol. Sci. *19*.

Peach, C.J., Kilpatrick, L.E., Friedman-Ohana, R., Zimmerman, K., Robers, M.B., Wood, K. V., Woolard, J., and Hill, S.J. (2018b). Real-Time Ligand Binding of Fluorescent VEGF-A Isoforms that Discriminate between VEGFR2 and NRP1 in Living Cells. Cell Chem. Biol. *25*, 1–11.

Petersen, J., Wright, S.C., Rodríguez, D., Matricon, P., Lahav, N., Vromen, A., Friedler, A., Strömqvist, J., Wennmalm, S., Carlsson, J., et al. (2017). Agonist-induced dimer dissociation as a macromolecular step in G protein-coupled receptor signaling. Nat. Commun. *8*, 1–15.

Pollard, T.D. (2010). A Guide to Simple and Informative Binding Assays. Mol. Biol. Cell *21*, 4061–4067.

Pon, C.K., Lane, J.R., Sloan, E.K., and Halls, M.L. (2016). The Beta2-adrenoceptor activates a positive cAMP-calcium feedforward loop to drive breast cancer cell invasion. FASEB J. *30*, 1144–1154.

Poppleton, H., Sun, H., Fulgham, D., Bertics, P., and Patel, T.B. (1996). Activation of Gsα by the epidermal growth factor receptor involves phosphorylation. J. Biol. Chem. *271*, 6947–6951.

Porzionato, A., Stocco, E., Guidolin, D., Agnati, L., Macchi, V., and De Caro, R. (2018). Receptor-receptor interactions of G protein-coupled receptors in the carotid body: A working hypothesis. Front. Physiol. *9*, 1–17.

Poulsen, S. a, and Quinn, R.J. (1998). Adenosine receptors: new opportunities for future drugs. Bioorg. Med. Chem. *6*, 619–641.

Povsic, T.J., Kohout, T.A., and Lefkowitz, R.J. (2003). β-Arrestin1 Mediates Insulin-like Growth Factor 1 (IGF-1) Activation of Phosphatidylinositol 3-Kinase (PI3K) and Anti-apoptosis. J. Biol. Chem. *278*, 51334–51339.

Powe, D.G., Voss, M.J., Zänker, K.S., Habashy, H.O., Green, A.R., Ellis, I.O., and Entschladen, F. (2010). Beta-blocker drug therapy reduces secondary cancer formation in breast cancer and improves cancer specific survival.

Oncotarget *1*, 628–638.

Prenzel, N., Zwick, E., Daub, H., Leserer, M., Abraham, R., Wallasch, C., and Ullrich, A. (1999). EGF receptor transactivation by G-protein-coupled receptors requires metalloproteinase cleavage of proHB-EGF. *402*.

Pyne, N.J., and Pyne, S. (2011). Receptor tyrosine kinase-G-protein-coupled receptor signalling platforms: out of the shadow? Trends Pharmacol. Sci. *32*, 443–450.

Ranganathan, A., Stoddart, L.A., Hill, S.J., and Carlsson, J. (2015). Fragment-Based Discovery of Subtype-Selective Adenosine Receptor Ligands from Homology Models. J. Med. Chem. *58*, 9578–9590.

Ranjan, R., Gupta, P., and Shukla, A.K. (2016). GPCR Signaling: β-arrestins Kiss and Remember. Curr. Biol. *26*, R285–R288.

Ranjan, R., Dwivedi, H., Baidya, M., Kumar, M., and Shukla, A.K. (2017). Novel Structural Insights into GPCR – β-Arrestin Interaction and Signaling. Trends Cell Biol. *27*, 851–862.

Rasmussen, S.G.F., Choi, H.-J., Rosenbaum, D.M., Kobilka, T.S., Thian, F.S., Edwards, P.C., Burghammer, M., Ratnala, V.R.P., Sanishvili, R., Fischetti, R.F., et al. (2007). Crystal structure of the human β2 adrenergic G-protein-coupled receptor. Nature *450*, 383–387.

Rasmussen, S.G.F., Choi, H.J., Fung, J.J., Pardon, E., Casarosa, P., Chae, P.S., DeVree, B.T., Rosenbaum, D.M., Thian, F.S., Kobilka, T.S., et al. (2011a). Structure of a nanobody-stabilized active state of the β2 adrenoceptor. Nature *469*, 175–180.

Rasmussen, S.G.F., DeVree, B.T., Zou, Y., Kruse, A.C., Chung, K.Y., Kobilka, T.S., Thian, F.S., Chae, P.S., Pardon, E., Calinski, D., et al. (2011b). Crystal structure of the β2 adrenergic receptor–Gs protein complex. Nature *477*, 549–555.

Reiter, E., and Lefkowitz, R.J. (2006). GRKs and β-arrestins: roles in receptor silencing, trafficking and signaling. Trends Endocrinol. Metab. *17*, 159–165.

Ribas, C., Penela, P., Murga, C., Salcedo, A., García-Hoz, C., Jurado-Pueyo, M., Aymerich, I., and Mayor, F. (2007). The G protein-coupled receptor kinase (GRK) interactome: Role of GRKs in GPCR regulation and signaling. Biochim. Biophys. Acta - Biomembr. *1768*, 913–922.

Rink, J., Ghigo, E., Kalaidzidis, Y., and Zerial, M. (2005). Rab conversion as a mechanism of progression from early to late endosomes. Cell *122*, 735–749.

Robers, M.B., Dart, M.L., Woodroofe, C.C., Zimprich, C.A., Kirkland, T.A.,

Machleidt, T., Kupcho, K.R., Levin, S., Hartnett, J.R., Zimmerman, K., et al. (2015). Target engagement and drug residence time can be observed in living cells with BRET. Nat. Commun. 1–10.

Rominger, D.H., Cowan, C.L., Gowen-Macdonald, W., and Violin, J.D. (2014). Biased ligands: Pathway validation for novel GPCR therapeutics. Curr. Opin. Pharmacol. *16*, 108–115.

Rotter, A., and de Oliveira, Z.N.P. (2017). Infantile hemangioma: pathogenesis and mechanisms of action of propranolol. JDDG J. Der Dtsch. Dermatologischen Gesellschaft *15*, 1185–1190.

Rozengurt, E. (2007). Mitogenic signaling pathways induced by G protein-coupled receptors. J. Cell. Physiol. *213*, 589–602.

Ryu, J.M., Baek, Y. Bin, Shin, M.S., Park, J.H., and Park, S.H. (2014). Sphingosine-1-phosphate-induced Flk-1 transactivation stimulates mouse embryonic stem cell proliferation through S1P1/S1P3-dependent β-arrestin/c-Src pathways. Stem Cell Res. *12*, 69–85.

Ryzhov, S., Zaynagetdinov, R., Goldstein, A.E., Matafonov, A., Biaggioni, I., and Feoktistov, I. (2009). Differential role of the carboxy-terminus of the A2B adenosine receptor in stimulation of adenylate cyclase, phospholipase Cβ, and interleukin-8. Purinergic Signal. *5*, 289–298.

Sarabipour, S., Ballmer-Hofer, K., and Hristova, K. (2016). VEGFR-2 conformational switch in response to ligand binding. Elife *5*, 1–23.

Schäfer, B., Gschwind, A., and Ullrich, A. (2004a). Multiple G-protein-coupled receptor signals converge on the epidermal growth factor receptor to promote migration and invasion. Oncogene *23*, 991–999.

Schäfer, B., Marg, B., Gschwind, A., and Ullrich, A. (2004b). Distinct ADAM metalloproteinases regulate G protein-coupled receptor-induced cell proliferation and survival. J. Biol. Chem. *279*, 47929–47938.

Schlessinger, J. (2014). Receptor tyrosine kinases: Legacy of the first two decades. Cold Spring Harb. Perspect. Biol. *6*.

Schonenbach, N.S., Rieth, M.D., Han, S., and O'Malley, M.A. (2016). Adenosine A2a receptors form distinct oligomers in protein detergent complexes. FEBS Lett. *590*, 3295–3306.

Schulte, G., and Fredholm, B.B. (2000). Human adenosine A(1), A(2A), A(2B), and A(3) receptors expressed in Chinese hamster ovary cells all mediate the phosphorylation of extracellular-regulated kinase 1/2. Mol. Pharmacol. *58*, 477–482.

Schulte, G., and Fredholm, B.B. (2003). Signalling from adenosine receptors to

mitogen-activated protein kinases. Cell. Signal. *15*, 813–827.

Schweighofer, B., Testori, J., Sturtzel, C., Sattler, S., Mayer, H., Wagner, O., Bilban, M., and Hofer, E. (2009). The VEGF-induced transcriptional response comprises gene clusters at the crossroad of angiogenesis and inflammation. Thromb. Haemost. *102*, 544–554.

Sepúlveda, C., Palomo, I., and Fuentes, E. (2016). Role of adenosine A2b receptor overexpression in tumor progression. Life Sci. *166*, 92–99.

Shenoy, S.K., and Lefkowitz, R.J. (2003). Trafficking patterns of β-arrestin and G protein-coupled receptors determined by the kinetics of β-arrestin deubiquitination. J. Biol. Chem. *278*, 14498–14506.

Shenoy, S.K., Drake, M.T., Nelson, C.D., Houtz, D. a., Xiao, K., Madabushi, S., Reiter, E., Premont, R.T., Lichtarge, O., and Lefkowitz, R.J. (2006). β-arrestin-dependent, G protein-independent ERK1/2 activation by the β2 adrenergic receptor. J. Biol. Chem. *281*, 1261–1273.

Sheth, S., Brito, R., Mukherjea, D., Rybak, L.P., and Ramkumar, V. (2014). Adenosine receptors: expression, function and regulation. Int. J. Mol. Sci. *15*, 2024–2052.

Shibuya, M. (2013). Vascular endothelial growth factor and its receptor system: Physiological functions in angiogenesis and pathological roles in various diseases. J. Biochem. *153*, 13–19.

Shibuya, M. (2014). Vegf-vegfr signals in health and disease. Biomol. Ther. *22*, 1–9.

Siddiqui, S., Cong, W.N., Daimon, C.M., Martin, B., and Maudsley, S. (2013). BRET biosensor analysis of receptor tyrosine kinase functionality. Front. Endocrinol. (Lausanne). *4*, 1–11.

Simon, G.M., Niphakis, M.J., and Cravatt, B.F. (2013). Determining target engagement in living systems. Nat. Chem. Biol. *9*, 200–205.

Simon, M., Rockl, W., Hornig, C., Grone, E., Theis, H., Weich, H., and Fuchs, E. (1998). Receptors of Vascular Endothelial Growth Factor / Vascular Permeability Factor (VEGF/VPF) in Fetal and Adult Human Kidney : Localization and [125I] VEGF Binding. J. Am. Soc. Nephrol. *9*, 1032–1044.

Simons, M. (2012). An Inside View: VEGF Receptor Trafficking and Signaling. Physiol. *27*.

Simons, M., Gordon, E., and Claesson-Welsh, L. (2016). Mechanisms and regulation of endothelial VEGF receptor signalling. Nat. Rev. Mol. Cell Biol. *17*, 611–625.

Sitkovsky, M. V., Kjaergaard, J., Lukashev, D., and Ohta, A. (2008). Hypoxia-adenosinergic immunosuppression: Tumor protection by T regulatory cells and cancerous tissue hypoxia. Clin. Cancer Res. *14*, 5947–5952.

Sloan, E.K., Priceman, S.J., Cox, B.F., Yu, S., Pimentel, M.A., Tangkanangnukul, V., Arevalo, J.M.G., Morizono, K., Karanikolas, B.D.W., Wu, L., et al. (2010). The sympathetic nervous system induces a metastatic switch in primary breast cancer. Cancer Res. *70*, 7042–7052.

Smith, J.S., and Rajagopal, S. (2016). The β-Arrestins: Multifunctional regulators of G protein-coupled receptors. J. Biol. Chem. *291*, 8969–8977.

Smith, N.J., and Milligan, G. (2010). Allostery at G protein-coupled receptor homo- and heteromers: uncharted pharmacological landscapes. Pharmacol. Rev. *62*, 701–725.

Smrcka, A. V. (2008). G protein βγ subunits: Central mediators of G protein-coupled receptor signaling. Cell. Mol. Life Sci. *65*, 2191–2214.

Soave, M., Stoddart, L.A., Brown, A., Woolard, J., and Hill, S.J. (2016). Use of a new proximity assay (NanoBRET) to investigate the ligand-binding characteristics of three fluorescent ligands to the human β_1-adrenoceptor expressed in HEK-293 cells. Pharmacol. Res. Perspect. *4*, e00250.

Sorkin, A., and Von Zastrow, M. (2002). Signal transduction and endocytosis: Close encounters of many kinds. Nat. Rev. Mol. Cell Biol. *3*, 600–614.

Sorkin, A., and Von Zastrow, M. (2009). Endocytosis and signalling: Intertwining molecular networks. Nat. Rev. Mol. Cell Biol. *10*, 609–622.

Spychala, J. (2000). Tumor-promoting functions of adenosine. Pharmacol. Ther. *87*, 161–173.

Stacer, A.C., Nyati, S., Moudgil, P., Iyengar, R., Luker, K.E., Rehemtulla, A., and Luker, G.D. (2013). NanoLuc reporter for dual luciferase imaging in living animals. Mol. Imaging *12*, 1–13.

Stoddart, L., Johnstone, E.K.M., Wheal, A.J., Goulding, J., Robers, M.B., Machleidt, T., Wood, K. V, Hill, S.J., and Pfleger, K.D.G. (2015a). Application of BRET to monitor ligand binding to GPCRs. Nat. Methods *12*, 661–663.

Stoddart, L. a., Vernall, A.J., Denman, J.L., Briddon, S.J., Kellam, B., and Hill, S.J. (2012). Fragment screening at adenosine-A3 receptors in living cells using a fluorescence-based binding assay. Chem. Biol. *19*, 1105–1115.

Stoddart, L. a., Kellam, B., Briddon, S.J., and Hill, S.J. (2014). Effect of a toggle switch mutation in TM6 of the human adenosine A_3 receptor on Gi protein-dependent signalling and Gi-independent receptor internalization. Br. J. Pharmacol. *171*, 3827–3844.

Stoddart, L. a, White, C.W., Nguyen, K., Hill, S.J., and Pfleger, K.D.G. (2016). Fluorescence- and bioluminescence-based approaches to study GPCR ligand binding. Br. J. Pharmacol. *173*, 3028–3037.

Stoddart, L.A., Vernall, A.J., Briddon, S.J., Kellam, B., and Hill, S.J. (2015b). Direct visualisation of internalization of the adenosine A3receptor and localization with arrestin3 using a fluorescent agonist. Neuropharmacology *98*, 68–77.

Stoddart, L.A., Kilpatrick, L.E., Briddon, S.J., and Hill, S.J. (2015c). Probing the pharmacology of G protein-coupled receptors with fluorescent ligands. Neuropharmacology *98*, 48–57.

Stoddart, L.A., Kilpatrick, L.E., and Hill, S.J. (2018). NanoBRET Approaches to Study Ligand Binding to GPCRs and RTKs. Trends Pharmacol. Sci. *39*, 136–147.

Stuttfeld, E., and Ballmer-Hofer, K. (2009). Structure and function of VEGF receptors. IUBMB Life *61*, 915–922.

Sun, B., Bachhawat, P., Chu, M.L.H., Wood, M., Ceska, T., Sands, Z.A., Mercier, J., Lebon, F., Kobilka, T.S., and Kobilka, B.K. (2017). Crystal structure of the adenosine A2A receptor bound to an antagonist reveals a potential allosteric pocket. Proc. Natl. Acad. Sci. *114*, 2066–2071.

Sun, C., Zhong, H., Mohsenin, A., Morschl, E., Chunn, J.L., Molina, J.G., Belardinelli, L., Zeng, D., and Blackburn, M.R. (2006). Role of A2B adenosine receptor signaling in adenosine-dependent pulmonary inflammation and injury. J. Clin. Invest. *116*, 2173–2182.

Sysa-Shah, P., Tocchetti, C.G., Gupta, M., Rainer, P.P., Shen, X., Kang, B.H., Belmonte, F., Li, J., Xu, Y., Guo, X., et al. (2016). Bidirectional cross-regulation between ErbB2 and β-adrenergic signalling pathways. Cardiovasc. Res. *109*, 358–373.

Szabó, Á., Szöllosl, J., and Nagy, P. (2010). Coclustering of ErbB1 and ErbB2 revealed by FRET-sensitized acceptor bleaching. Biophys. J. *99*, 105–114.

Tang, J., Li, Z., Lu, L., and Cho, C.H. (2013). β-Adrenergic system, a backstage manipulator regulating tumour progression and drug target in cancer therapy. Semin. Cancer Biol.

Thaker, P.H., Han, L.Y., Kamat, A.A., Arevalo, J.M., Takahashi, R., Lu, C., Jennings, N.B., Armaiz-Pena, G., Bankson, J.A., Ravoori, M., et al. (2006). Chronic stress promotes tumor growth and angiogenesis in a mouse model of ovarian carcinoma. Nat. Med. *12*, 939–944.

Thomsen, A.R.B., Plouffe, B., Cahill, T.J., Shukla, A.K., Tarrasch, J.T., Dosey, A.M.,

Kahsai, A.W., Strachan, R.T., Pani, B., Mahoney, J.P., et al. (2016). GPCR-G Protein-β-Arrestin Super-Complex Mediates Sustained G Protein Signaling. Cell *166*, 907–919.

Tilley, D.G., Kim, I.M., Patel, P.A., Violin, J.D., and Rockman, H.A. (2009). Beta-Arrestin Mediates beta1-Adrenergic Receptor-Epidermal Growth Factor Receptor Interaction and Downstream Signaling. J. Biol. Chem. *284*, 20375–20386.

Trincavelli, M.L., Tuscano, D., Cecchetti, P., Falleni, A., Benzi, L., Klotz, K.N., Gremigni, V., Cattabeni, F., Lucacchini, A., and Martini, C. (2000). Agonist-induced internalization and recycling of the human A3 adenosine receptors: Role in receptor desensitization and resensitization. J. Neurochem. *75*, 1493–1501.

Unen, J. Van, Woolard, J., Rinken, A., Hoffmann, C., Hill, S.J., Goedhart, J., Bruchas, M.R., Bouvier, M., and Adjobo-hermans, M.J.W. (2015). minireview — exploring the biology of gpcr s : from in vitro to in vivo a perspective on studying g-protein – coupled receptor signaling with Resonance Energy Transfer Biosensors in Living Organisms. Mol. Pharmacol. *88*, 589–595.

Vanderheyden, P.M.L., and Benachour, N. (2017). Influence of the cellular environment on ligand binding kinetics at membrane-bound targets. Bioorganic Med. Chem. Lett. *27*, 3621–3628.

Verzijl, D., and IJzerman, A.P. (2011). Functional selectivity of adenosine receptor ligands. Purinergic Signal. *7*, 171–192.

Vidi, P.A., Chen, J., Irudayaraj, J.M.K., and Watts, V.J. (2008). Adenosine A2A receptors assemble into higher-order oligomers at the plasma membrane. FEBS Lett. *582*, 3985–3990.

Van Waarde, A., Vaalburg, W., Doze, P., Bosker, F.J., and Elsinga, P.H. (2004). PET imaging of beta-adrenoceptors in human brain: a realistic goal or a mirage? Curr. Pharm. Des. *10*, 1519–1536.

Wacker, D., Fenalti, G., Brown, M.A., Katritch, V., Abagyan, R., Cherezov, V., and Stevens, R.C. (2010). Conserved Binding Mode of Human β_2 Adrenergic Receptor Inverse Agonists and Antagonist Revealed by X-ray Crystallography. J. Am. Chem. Soc. *132*, 11443–11445.

Wang, W., Qiao, Y., and Li, Z. (2018). New Insights into Modes of GPCR Activation. Trends Pharmacol. Sci. *39*, 367–386.

Waters, C., Sambi, B., Kong, K.C., Thompson, D., Pitson, S.M., Pyne, S., and Pyne, N.J. (2003). Sphingosine 1-phosphate and platelet-derived growth

factor (PDGF) act via PDGFβ receptor-sphingosine 1-phosphate receptor complexes in airway smooth muscle cells. J. Biol. Chem. *278*, 6282–6290.

Waters, C.M., Connell, M.C., Pyne, S., and Pyne, N.J. (2005). c-Src is involved in regulating signal transmission from PDGFβ receptor–GPCR(s) complexes in mammalian cells. Cell. Signal. *17*, 263–277.

Waters, C.M., Long, J., Gorshkova, I., Fujiwara, Y., Connell, M., Belmonte, K.E., Tigyi, G., Natarajan, V., Pyne, S., and Pyne, N.J. (2006). Cell migration activated by platelet-derived growth factor receptor is blocked by an inverse agonist of the sphingosine 1-phosphate receptor-1. FASEB J. *20*, 509–511.

Watkins, J.L., Thaker, P.H., Nick, A.M., Ramondetta, L.M., Kumar, S., Urbauer, D.L., Matsuo, K., Squires, K.C., Coleman, R.L., Lutgendorf, S.K., et al. (2015). Clinical impact of selective and nonselective beta-blockers on survival in patients with ovarian cancer. Cancer *121*, 3444–3451.

Watson, L.J., Alexander, K.M., Mohan, M.L., Bowman, A.L., Mangmool, S., Xiao, K., Prasad, S.V.N., and Rockman, H.A. (2016). Phosphorylation of Src by phosphoinositide 3-kinase regulates beta-adrenergic receptor-mediated EGFR transactivation. Cell. Signal. *28*, 1580–1592.

Watt, H.L., Kharmate, G.D., and Kumar, U. (2009). Somatostatin receptors 1 and 5 heterodimerize with epidermal growth factor receptor: Agonist-dependent modulation of the downstream MAPK signalling pathway in breast cancer cells. Cell. Signal. *21*, 428–439.

Wegel, E., Göhler, A., Lagerholm, B.C., Wainman, A., Uphoff, S., Kaufmann, R., and Dobbie, I.M. (2016). Imaging cellular structures in super-resolution with SIM, STED and Localisation Microscopy: A practical comparison. Sci. Rep. *6*, 1–13.

Weis, W.I., and Kobilka, B.K. (2018). The Molecular Basis of G Protein-Coupled Receptor Activation. Annu. Rev. Biochem.

Werry, T.D., Sexton, P.M., and Christopoulos, A. (2005). “Ins and outs” of seven-transmembrane receptor signalling to ERK. Trends Endocrinol. Metab. *16*, 26–33.

Wetzker, R., and Böhmer, F.-D. (2003). Transactivation joins multiple tracks to the ERK/MAPK cascade. Nat. Rev. Mol. Cell Biol. *4*, 651–657.

White, C.W., Vanyai, H.K., See, H.B., Johnstone, E.K.M., and Pfleger, K.D.G. (2017). Using nanoBRET and CRISPR/Cas9 to monitor proximity to a genome-edited protein in real-time. Sci. Rep. *7*, 3187.

Wnorowski, A., and Jozwiak, K. (2014). Homo- and hetero-oligomerization of

β2-adrenergic receptor in receptor trafficking, signaling pathways and receptor pharmacology. Cell. Signal. *26*, 2259–2265.

Woolard, J., Wang, W., Bevan, H.S., Qiu, Y., Morbidelli, L., Pritchard-jones, R.O., Cui, T., Sugiono, M., Waine, E., Perrin, R., et al. (2004). VEGF 165 b, an Inhibitory Vascular Endothelial Growth Factor Splice Variant: Mechanism of Action,. Cancer Res. *8*, 7822–7835.

Wootten, D., Christopoulos, A., Marti-Solano, M., Babu, M.M., and Sexton, P.M. (2018). Mechanisms of signalling and biased agonism in G protein-coupled receptors. Nat. Rev. Mol. Cell Biol.

Wu, H., Wang, C., Gregory, K.J., Han, G.W., Cho, H., Xia, Y., and Stevens, R.C. (2014). Structure of a Class C GPCR Metabotropic Glutamate Receptor 1 Bound to an Allosteric Modulator. Science (80-.). *344*, 58–64.

Xie, K.Q., Zhang, L.-M., Cao, Y., Zhu, J., and Feng, L.-Y. (2009). Adenosine A(1) receptor-mediated transactivation of the EGF receptor produces a neuroprotective effect on cortical neurons in vitro. Acta Pharmacol. Sin. *30*, 889–898.

Yates, L., Clark, J.H., Martin, T.J., James, S., Broadley, K.J., and Kidd, E.J. (2003). Radioligand binding and functional responses of ligands for human recombinant adenosine A 3 receptors. 191–200.

Ye, X., Abou-Rayyah, Y., Bischoff, J., Ritchie, A., Sebire, N.J., Watts, P., Churchill, A.J., and Bates, D.O. (2016). Altered ratios of pro- and anti-angiogenic VEGF-A variants and pericyte expression of DLL4 disrupt vascular maturation in infantile haemangioma. J. Pathol. *239*, 139–151.

Yonucu, S., Defne, Y., Phipps, C., Unlu, M.B., and Kohandel, M. (2017). Quantifying the effects of antiangiogenic and chemotherapy drug combinations on drug delivery and treatment efficacy. PLOS Comput. Biol. *13*, e1005724.

Young, A., Ngiow, S.F., Barkauskas, D.S., Sult, E., Hay, C., Blake, S.J., Huang, Q., Liu, J., Takeda, K., Teng, M.W.L., et al. (2016). Co-inhibition of CD73 and A2AR Adenosine Signaling Improves Anti-tumor Immune Responses. Cancer Cell *30*, 391–403.

Yuan, N., Friedman, J., Whaley, S., and Clark, R.B. (1994). CAMP-dependent Protein Kinase and Protein Kinase C Consensus Site Mutations. J. Biol. Chem. *269*, 23032–23038.

Zajac, M., Law, J., Cvetkovic, D.D., Pampillo, M., McColl, L., Pape, C., Guglielmo, G.M., Postovit, L.M., Babwah, A. V., and Bhattacharya, M. (2011). GPR54 (KISS1R) transactivates EGFR to promote breast cancer cell invasiveness.

PLoS One *6*, e21599–e21599.

Zeng, H., Sanyal, S., and Mukhopadhyay, D. (2001). Tyrosine Residues 951 and 1059 of Vascular Endothelial Growth Factor Receptor-2 (KDR) Are Essential for Vascular Permeability Factor/Vascular Endothelial Growth Factor-induced Endothelium Migration and Proliferation, Respectively. J. Biol. Chem. *276*, 32714–32719.

Zhou, X., Teng, B., Tilley, S., and Mustafa, S.J. (2013). A1 adenosine receptor negatively modulates coronary reactive hyperemia via counteracting A2A -mediated H 2 O 2 production and K ATP opening in isolated mouse hearts. Am. J. Physiol. Circ. Physiol. *305*, H1668–H1679.

Zhou, X.E., Melcher, K., and Xu, H.E. (2017). Understanding the GPCR biased signaling through G protein and arrestin complex structures. Curr. Opin. Struct. Biol. *45*, 150–159.